THE BEHAVIOUR OF GROUND ANCHORS IN SAND

by

Stelios Nicolaou Tsangarides

Thesis submitted for the Degree of Doctor of Philosophy in the Faculty of Engineering,

University of London
Queen Mary College

January, 1978

CONTAINS

PULLOUTS

To

Nicolas

and

Athena

'Πάντα ρεῖ'

Heraclitus (c 540 - c 475 BC)

ABSTRACT

This thesis includes experimental and theoretical work performed to investigate the behaviour of ground anchors in sand. The anchor footing used was a circular plate connected to a tie rod.

The experimental work was carried out by installing the anchor in a 1830mm x 1830mm x 1220mm deep tank containing dry sand. The sand sample was prepared by using a vibrator fixed to the bottom of the tank. The anchor was pulled out at a constant rate of strain and the load-displacement curve was recorded on a plotter.

The vibration of the tank was defined by determining the acceleration and amplitude of the motion in the horizontal and vertical directions.

A density tube and a hydraulic gauge were designed to investigate the distribution of stresses in sand.

The variation of the vibration time, the constant rate of strain, the shaft/plate diameter, the plate thickness/plate diameter, and the boundary distance with the load-displacement curve were also investigated.

The load-displacement curve of different diameter plates embedded at various depths for different times of vibration were recorded.

To investigate the behaviour of ground anchors theoretically, the finite element technique was used and a computer program developed.

A linear stress-strain relationship was used to predict and investigate the behaviour of the anchor.

A non-linear stress-strain relationship and a failure criterion were also used to predict the load-displacement curve of the vertical anchor. The effect of the parameters which were investigated experimentally were also examined. The distribution of the load on the anchor plate and the extent of the failure zone were plotted.

The predicted and experimental results in this thesis were compared with laboratory and field results obtained by previous researchers.

ACKNOWLEDGEMENTS

The author is eternally grateful to his supervisor, Dr. R.C. Harvey B.Sc., Ph.D, M.I.C.E., for his constant encouragement and valuable guidance throughout the research programme.

The author also wishes to express his thanks to all the staff of the Civil Engineering Department, and to Mr. C. Lodge of the Mechanical Engineering Department, for their technical assistance.

The author also extends his thanks to his parents and his brother, Mr. C.N. Tsangarides B.Sc., for their continued support and encouragement throughout the years.

Last but not least, the author's sincere thanks go to his friends Mrs. M. Christofides B.A. for typing this thesis, and to Mr. A.G. Christofides B.Sc., for all his help.

LIST OF CONTENTS

LIST OF PLATES

LIST OF FIGURES

LIST OF TABLES

NOTATION

P_m	Ultimate load of an anchor
H	Depth of anchor plate below soil surface
D	Diameter of anchor plate
γ	Unit weight of soil
ϕ	Angle of internal friction of soil
α	Angle of inclination to vertical of the side face of the cone of rupture
C_u	Undrained cohesive strength of soil
t	Thickness of anchor plate
W_1	Dead weight of anchor
W	Weight of soil in failure surface
T	Vertical component of shearing resistance along failure surface
r	Radius of circle - failure surface
F_1	Function of ϕ, H, t, D
K	Constant
A	Area of anchor plate
D_s	Diameter of anchor shaft
C'	"Appropriate" undistrubed soil strength
p	Pressure on the anchor plate at ultimate load
C_i	Function of ϕ and I_r
I_r	Rigidity index
E	Modulus of elasticity of soil
ν	Poisson's ratio of soil
G	Shear modulus
z	Anchor plate movement
R_1, R_2	Radius of cylindrical cavity
P_p	Ultimate load transmitted to the soil by an anchor plate
P_r	"Useless" work expended to overcome friction between the surface of wedge and surrounding soil
q	Radial pressure under which cavity expands
2θ	Angle of cone at the apex
L	Working length of anchor shaft
f	Specific friction resistance or frequency

H'	Height of restricted failure surface
B	Breadth of anchor plate
K_u	Experimental coefficient
s	Shape factor
H/D	Relative depth
T	Time of vibration of soil or Period
V_m	Maximum acceleration
a	Amplitude
ω	Angular velocity
g	Acceleration due to gravity
σ_z	Vertical stress
σ	Circumferential stress
σ_r	Radial stress
τ_{rz}	Shear stress in r, z plane
x, y, z	Cartesian coordinates
r, z, θ	Polar coordinates
u	Displacement component in the r direction
w	Displacement component in the z direction
$\{U\}$	Assumed displacement function
$[M]$	Function of r, θ, and z only
$[A]$	Vector of undetermined constants defining U
$[\delta_e]$	Vector of extremity displacements
$[C]$	Primary matrix, nodal coordinates
ε_r	Strain within the element in r direction
ε_z	Strain within the element in z direction
ε_θ	Strain within the element in θ direction
γ_{rz}	Shear strain in the (r,z) plane
dvol, dv	Increment of volume
$[L]$	$[\varepsilon_e] = [L]\{A\}$
$[\varepsilon_e]$	Strains within the element
$[B]$	Relationship between strain and stress
$[D]$	Stress-strain relationship
$[H]$	$[L][C]$
$[K_e]$	$[C]^T[S][C]$

$[S]$	$\int_{vol} [L]^T [D] [L] \, dv$
k, m, n	Experimental constants
$\sigma_x, \sigma_y, \sigma_z$	Stresses in x, y, z directions respectively
K_r	Rankine ratio
$\delta\sigma_x, \delta\sigma_y, \delta\sigma_z$	Increments of stresses in x, y, z, directions respectively
$\delta\varepsilon_x, \delta\varepsilon_y, \delta\varepsilon_z$	Increments of strains in x, y, z directions respectively
K_1, K_2	Experimental constants
r_1, r_2, r_3	Ratios of maximum stress to total stress
f_1, f_2, g'	Experimental constants
$[K]$	Overall stiffness matrix
$\{\delta\}$	Displacement matrix
$\{F\}$	Load matrix
[SS]	Element stiffness matrix
K_o	Coefficient of earth pressure at rest
h	Depth of centroid of element from soil surface
NNOD	Number of nodes
NCONS	Number of constraints
NLAYERS	Number of layers
NSQUARE	Number of columns
NELC	Number of elements
NNODESL	Number of nodes in a horizontal plane
NVLC	Number of degrees of freedom
NOTP	Number of nodes on anchor plate
NEP	Number of elements in an anchor plate
NSM	Number of increments of displacement
SPW	γ
NABOVE	Number of first node on the anchor plate
NDOWN	Number of first node at the bottom of the anchor plate
AF2	f_2
AF1	f_1
ACG	g
AK1	K_1
AKR	K_r
AK2	K_2
AKRES	K_o
H	Height of soil in continuum - computer program
GN	g'

CHAPTER I

INTRODUCTION

1.1 General

In recent years, the range of applications of anchors has widened due to the increasing tendency to design structures of a more unusual nature, which may show a less familiar response to physical forces, i.e. wind, snow, buoyancy.

In special cases, i.e. tall slender towers required to resist a large wind force, the uplift loads can be very high. The method of increasing the footing dimensions, i.e. depth and width, of the tower in order to provide adequate resistance, by bearing and uplift, may not provide an attractive solution to the problem. In such cases the resistance to uplift may be obtained using deep anchors.

An increasing demand for methods of securing various components, both temporary and permanent, when constructing buildings with one or more basement floors, exist in the Civil Engineering industry. The necessity to carry out excavations of considerable depth, often below the water table, or below the foundations of nearby structures, makes the use of anchors a favourable method, since the working space available is often limited.

With the increase in capacity of augering equipment, the method of providing the necessary uplift resistance by the use of anchors becomes attractive, in terms of economics, when compared to other methods e.g. large dead weights (Ref. 15 & 16). In future, anchors will become a common construction technique.

1.2 Classification of Anchors

Several ways of classifying anchors are to be found in published papers. Most of the classifications follow the construction techniques, i.e. manner in which the anchors

are placed into the soil. The anchors can be divided into three main groups:-

1. Rock anchors.

2. Ground anchors.

3. Marine anchors.

In the present review however, the first two of the above groups of anchors will be considered.

1.2.1 Rock anchors, used in mines and tunnels, are usually tension rods or cables fixed in place by various methods e.g. grouting, or by wedging action. They are used to stabilize rocks which are fractured or fissured due to the stress relief when openings are formed i.e. tunnels, holes.

The rock anchors were divided by Price (1970, Ref. 22) into the following three groups:-

a) Mechanical types. The uplift resistance is taken by the frictional resistance between anchor and rock and it is achieved mechanically by the following types of anchor:-

(i) Slot and wedge type, Fig. 1.1 (a).

(ii) Rawlplug type or "Duplex", Fig. 1.1 (b).

(b) Bonded type. The bolt or cable is bonded to the rock by using cement grout, polyster or epoxy-resin grout, Fig. 1.1 (c). Since the uplift resistance depends on the length of the grouted zone, this can be increased by under-reaming the drilled hole.

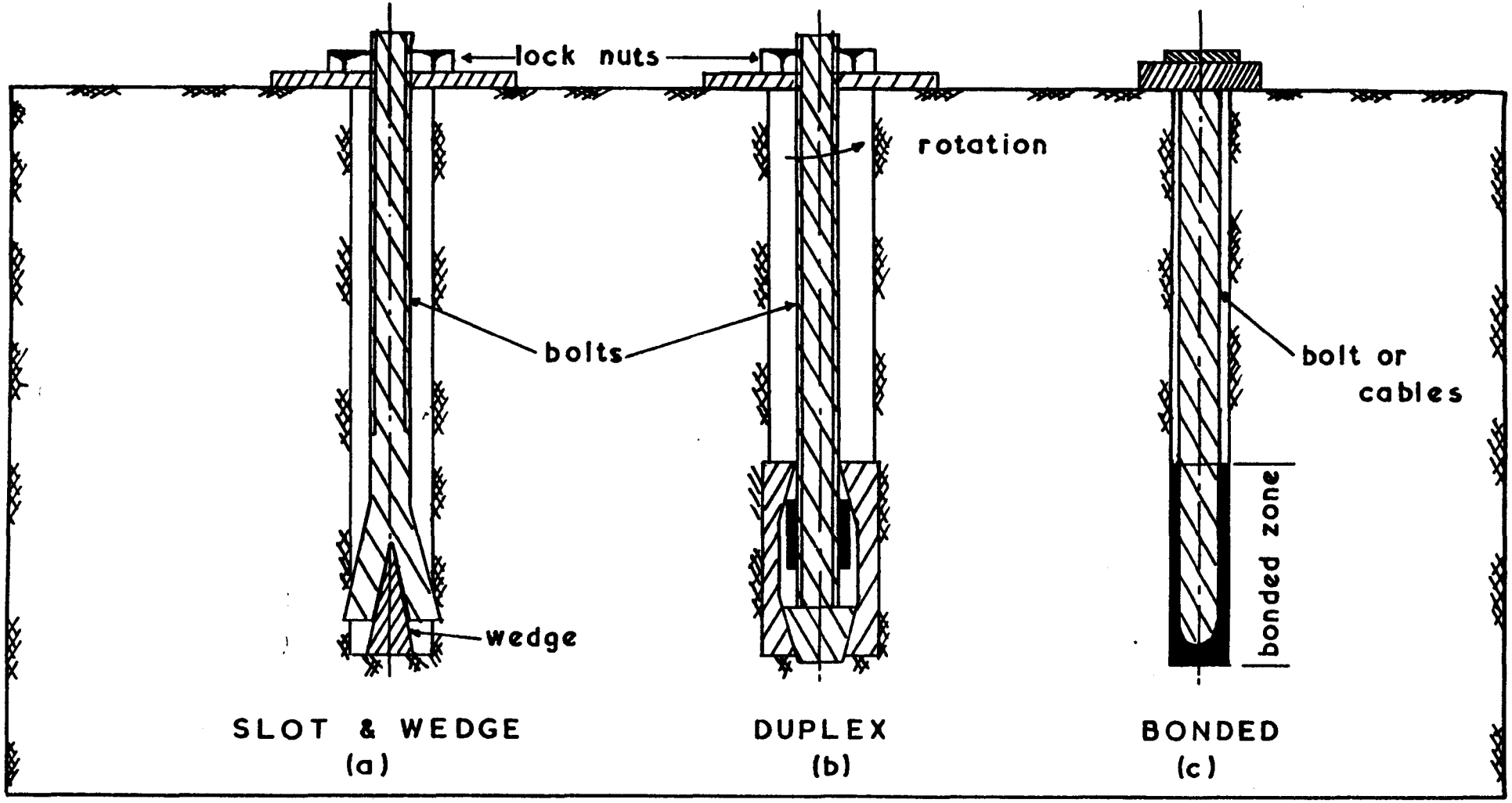

Fig.1.1 TYPES OF ROCK ANCHORS

1.2.2 Ground anchors are used in soils such as clay, granular material or soft rock and can be suitably raked in order to resist uplift loads. They may be divided into the following types:-

(a) Grouted anchor.

(b) Gravity anchor.

(c) Plate or slab anchor.

(a) The grouted anchor, useful when the safety of the entire structure requires the anchorage zone to be situated away from any surface of potential failure, is used in sand and clay soils. A bore hole of fixed diameter is drilled to a certain depth and the base of the hole is enlarged mechanically, or by pressure grouting Fig. 1.2 (a). The hole is filled with reinforcing bars and concrete. A series of multiple underreams, Fig. 1.2 (b), can be formed by enlarging the drilled hole at different depths. The uplift resistance depends on the strength of the soil and the number of underreams.

(b) The gravity anchor, the oldest type of anchor in use, is placed into soils ranging from soft silt to gravel, Fig. 1.2 (c). Their design needs no substantial knowledge of soil mechanics. The uplift forces are resisted by the self-weight of the anchor and therefore heavy foundations must be constructed. The safety factors vary according to the direction of the force on the anchor; between 1.5 and 3.0.

(c) The plate or slab anchor, which is usually square or circular, is made of concrete or steel. A steel rod fixed to the plate, transmits the load from the structure to the foundation, Fig. 1.2 (d). This type of anchor has the following disadvantages:-

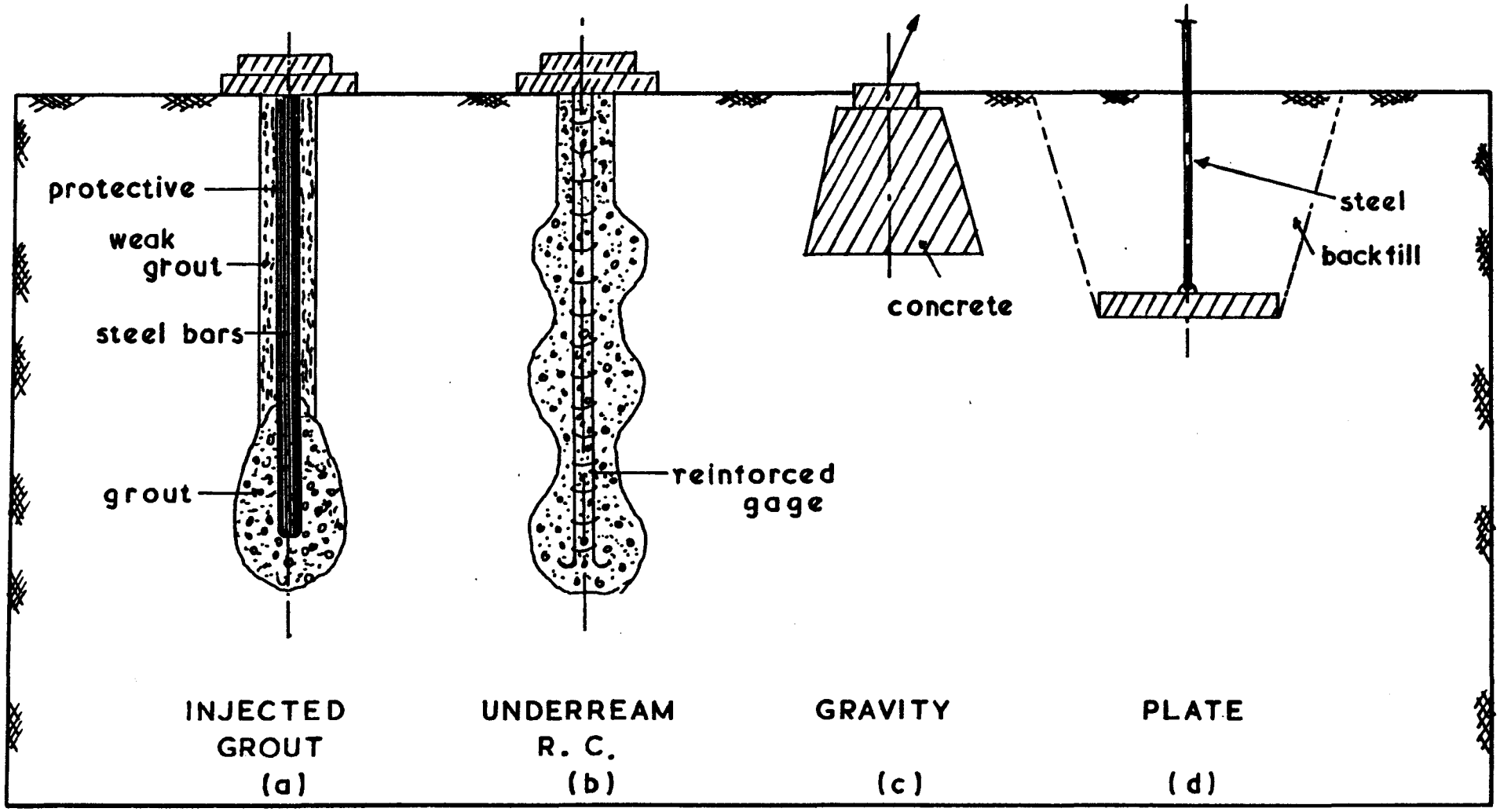

Fig. 1.2 TYPES OF GROUND ANCHORS

(i) The excavation of a trench or a pit requires labour and machinery and the backfill must be compacted in order to restore original soil strength and density.

(ii) The excavated soil can cause obstructions to the general running of the site.

(iii) The depth of embedding the plate is limited by the pit excavation which depends on the ground and water conditions present.

1.3 Application of Anchors

The application of anchors in Civil engineering practice is now common throughout the world and anchorages have been constructed in a wide variety of soil beds. The object of this section is therefore to describe some of the main applications where anchors are successfully used.

(a) Retaining Walls

Retaining walls, often constructed by using sheet steel piles driven into undisturbed ground and suitably anchored, are used to retain soil in road cuttings, Fig. 1.3 (a), deep excavations and other constructions. Cotrill (1969, Ref. 30) reported that one row of anchors was installed in the London Clay and one row in the overlying terrace gravel to retain the rigid wall at Lambeth, London, which enclosed a 12.2m deep excavation. The substantial propping in excavations for the construction of the permanent retaining walls for bridge abutments, used for many years, has now been substantially replaced by anchors. Numerous examples, where retaining walls for bridge abutments were secured using permanent anchors, have been reported in technical journals.

(b) Dams

Anchors are used to improve the foundations of dams, and to

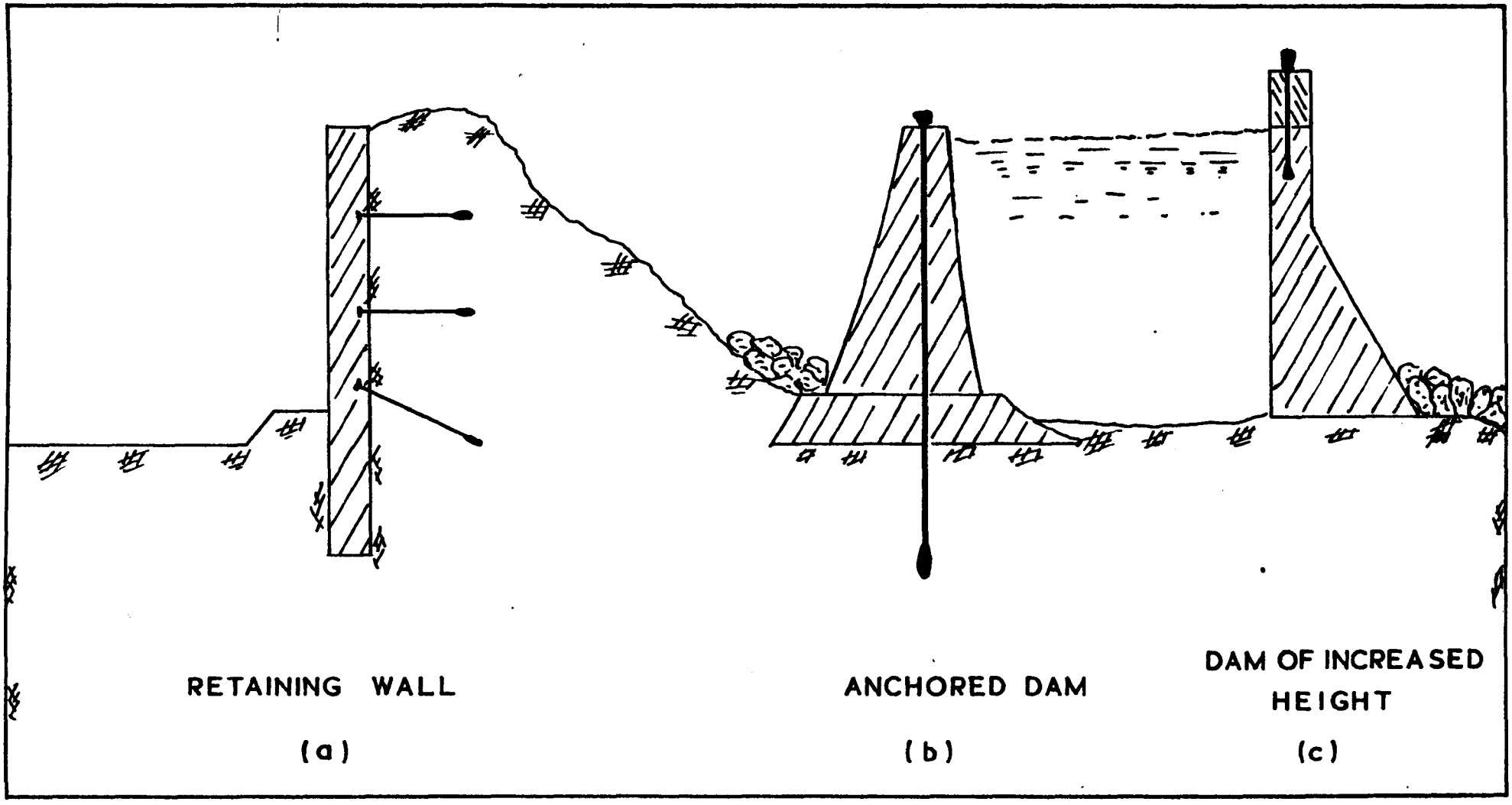

Fig. 1.3 USES OF ANCHORS

strengthen or increase the height of existing dams Fig. 1.3 (b, c).

The stability of dams can be threatened by many phenomena, such as the passage of water through fissures and joints, slipping of rock masses, weathering of faults and dykes. Parry Davies (1967, Ref. 25) reported that at the Kariba Dam, Zambia, the side wall of the power house excavation had moved 40mm inwards due to a fault which had caused local deposition of the rock, i.e. gneiss. Anchors were installed across the fault to prevent any further movement.

The technique, employing anchors to increase the height of dams, has now been applied many times to existing dams all over the world. Crivelli (1970, Ref. 21) reported that the height of the El-Kansera Dam in Morocco was increased by 5.50m.

(c) Bridges

Anchors have been used to resist both uplift and lateral forces on bridges, Fig. 1.4 (a). In suspension bridges, anchors might be used to pre-stress the cable anchorage as an alternative to the method of anchoring the main cable in a large mass of concrete base. Anderson (1965, Ref. 33) reported that anchorages were pre-stressed to give a load of 171,000KN to counteract a main cable force.

Towers of bridges can now be founded on sloping floors, and sliding is prevented using anchors.

(d) Vertical and Horizontal cantilevered structures

Cantilevered structures, i.e. tall buildings and transmission towers, Fig. 1.4 (b), are usually subjected to strong winds, snow and ice. The foundations of such structures

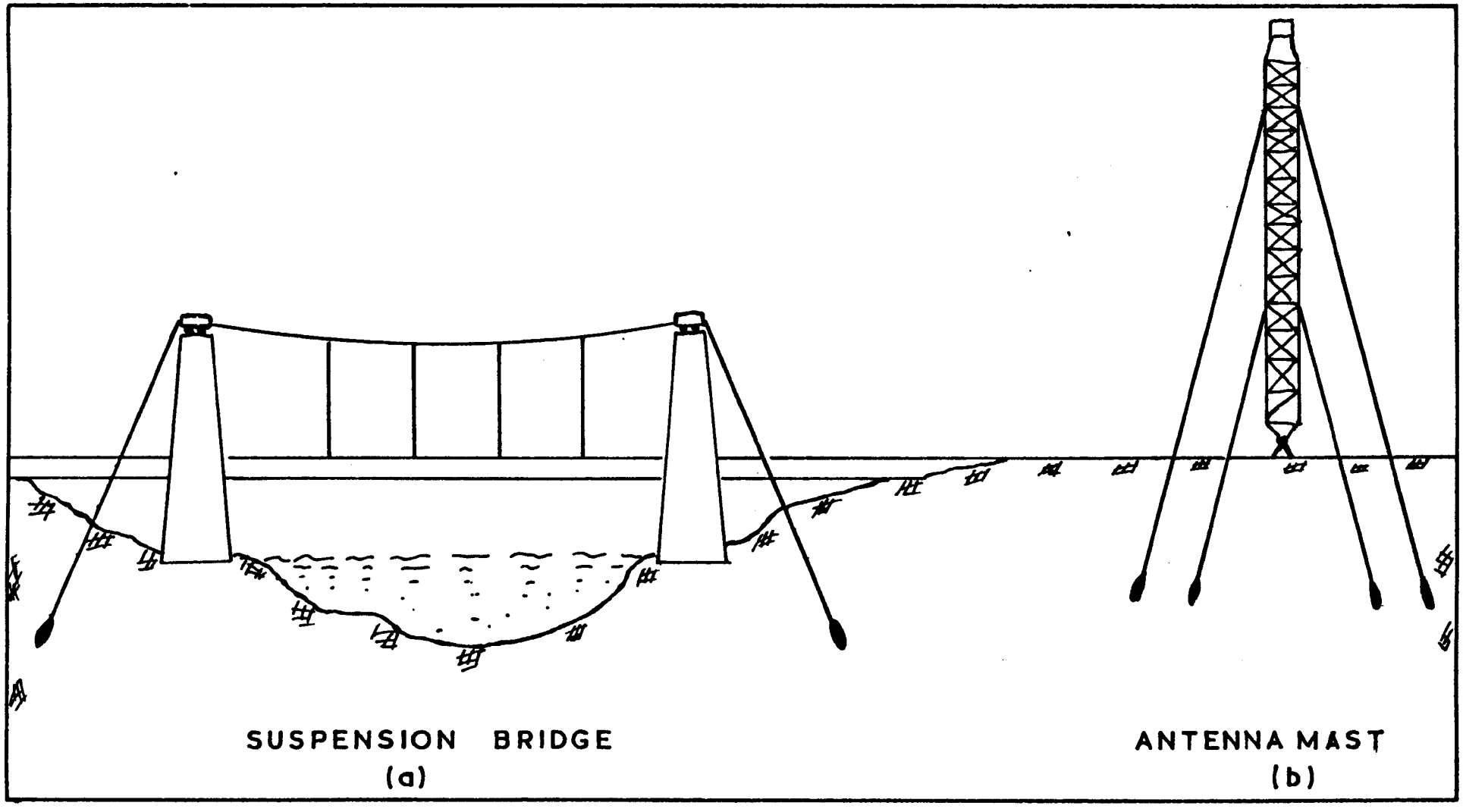

Fig. 1.4 USES OF ANCHORS

must be capable of resisting large overturning moments.

Adams and Klym (1972, Ref. 34) reported that the guyed tower which has been used on the Ontario Hydro Extra High Voltage lines is supported on a central footing and the unbalanced loads, i.e. forces due to wind and ice, are resisted by four-angle guy anchors.

Other structures, such as chimneys and precast concrete roofs, have also been partially supported by anchored guys. Bauer (1965, Ref. 35) reported that anchors were used to prevent the tilting of a pair of chimneys 50.0m high.

(f) Buoyant Structures, Fig. 1.5

Large and deep excavations, often required for the construction of buildings, dry docks, and storage tanks, can subject such structures to buoyancy forces. In recent years the heavy concrete floor, used to neutralise the hydrostatic pressure on the base, has often been replaced by a less substantial floor held down by anchors.

Anchors are also used during the construction of tunnels beneath wide rivers. Poland (1960, Ref. 36) reported that during the installation of a tunnel beneath a river in Florida, a cofferdam was constructed, and anchors were used to prevent flotation of the 1.30m thick concrete base slab designed to resist an uplift force of 15.25m head of water.

1.4 Definitions

ANCHOR: A member that transmits an uplift force from a structure to a medium is called an anchor. The anchor consists of the anchor plate and shaft.

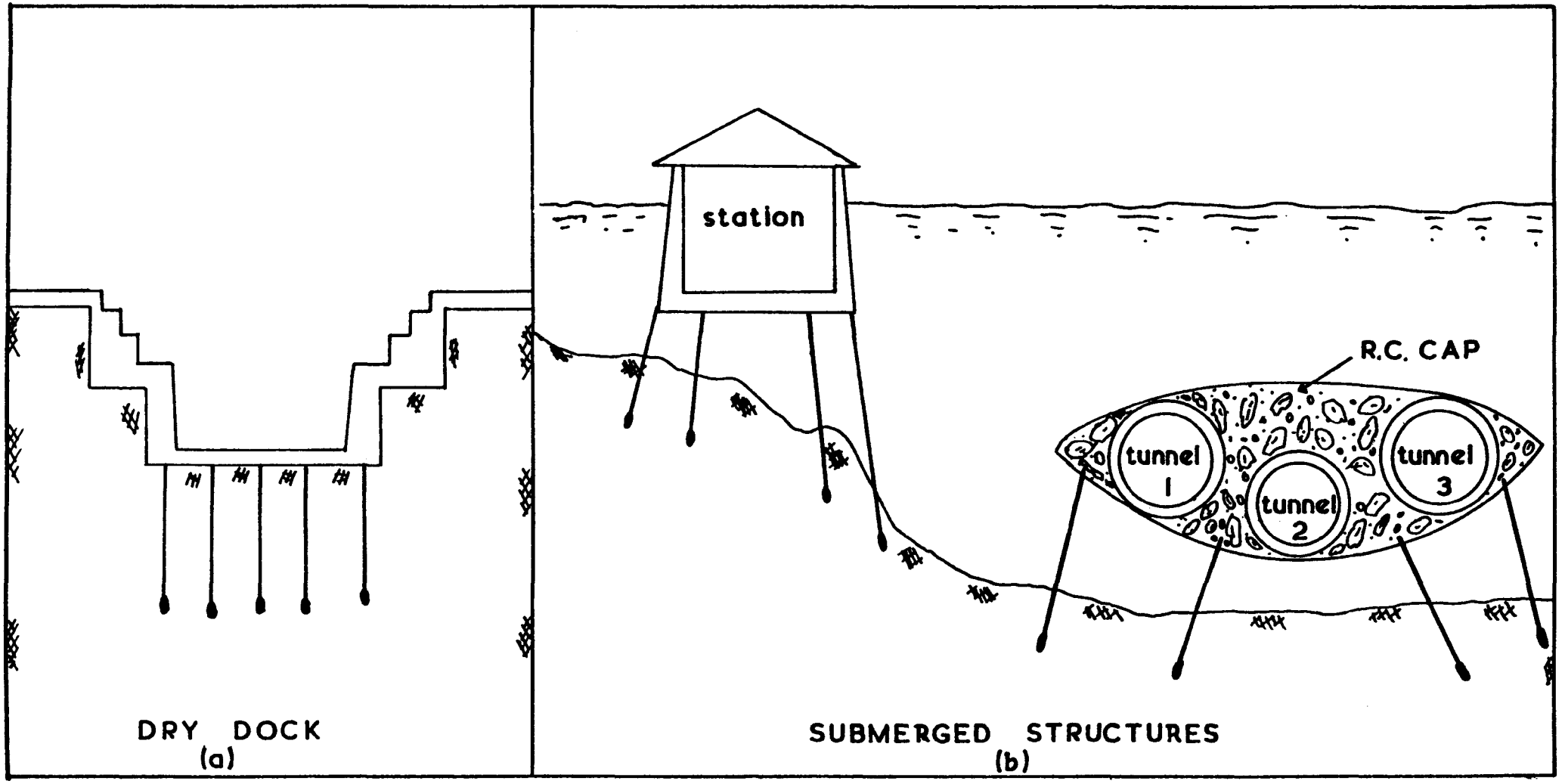

Fig. 1.5 USES OF ANCHORS

SHALLOW ANCHOR: Failure of the anchor occurs when the soil above the anchor plate is lifted, forming a curvilinear surface, with radial and circumferential cracks appearing on the surface of the soil.

DEEP ANCHOR: Failure of the anchor occurs with the anchor plate "tunnelling" through the soil with little or no displacement of the surrounding soil mass.

ULTIMATE LOAD: The maximum uplift force an anchor can sustain is called the ultimate load.

RELATIVE DEPTH: The ratio of the depth of the anchor plate to the diameter of the plate is called the relative depth. The transition point, in terms of the relative depth, from shallow to deep anchor behaviour is called the critical depth.

CHAPTER II

REVIEW OF PREVIOUS WORK ON ANCHORS

2.1 THEORETICAL WORK

2.1.1 Shallow Anchors

The earliest method of calculating the uplift resistance relied on the self weight of the foundation, ignoring the uplift resistance offered by shearing in the soil. The first theoretical analysis was proposed by Dorr in 1924, (Ref. 38). He produced a theory, earth weight method, that took into account the weight of the soil, Fig. 1.1 (a).

Muller (1932, Ref. 17) introduced into the existing theories the friction in the soil. In calculating the ultimate load of a foundation, he proposed a friction cylinder method, Fig. 2.1 (b). Ignoring the effect of soil cohesion and assuming the coefficient of earth pressure equal to unity, Muller obtained the following expression:-

$$P_m = \frac{\pi \gamma H^2 D \tan\phi}{2} + \frac{\pi \gamma H D^2}{4}$$

where,

P_m = Ultimate load.

H = Depth of the anchor plate below ground surface.

D = Diameter of the anchor plate.

γ = Unit weight of the soil above the anchor plate.

ϕ = Angle of internal friction of the soil.

Killer (1953, Ref.39) assuming an angle of inclination of $\alpha = 30^\circ$ i.e. the failure surface rises at 30° to the vertical, he evaluated the ultimate load, P_m, using the

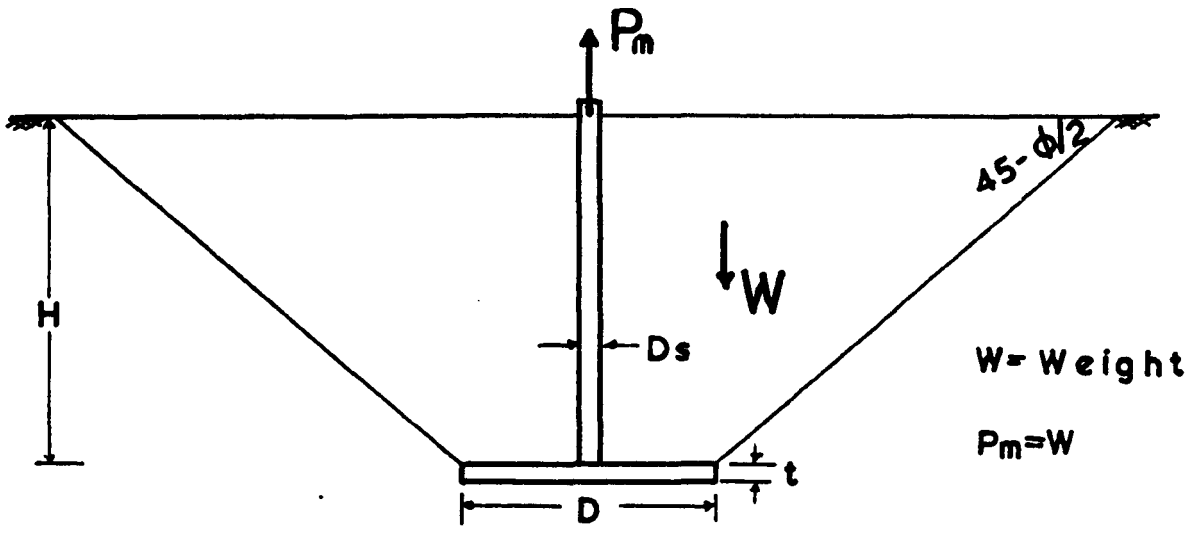

Soil cone method

(a)

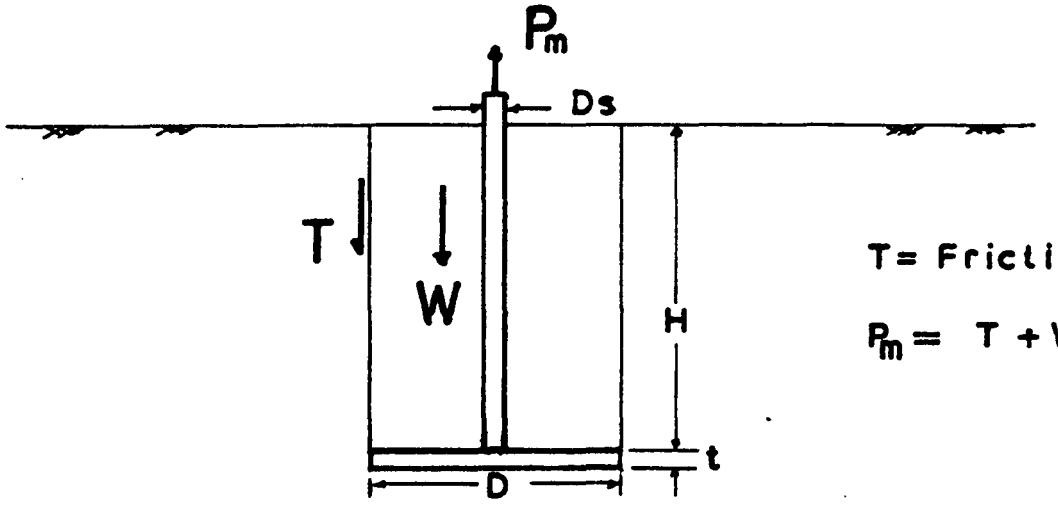

Friction cylinder method

(b)

Fig. 2.1

earth weight method, to be:-

$$P_m = \pi \gamma \left(\frac{H D^2}{4} + \frac{H^2 D}{2} \tan \alpha + \frac{H^3}{3} \tan^2 \alpha \right)$$

where,

$$\alpha = 30^\circ$$

Comparing his ultimate loads with those obtained from the friction cylinder method (Ref. 17), Killer found that the earth weight method gave lower values.

Mors (Appendix A) using the same method but a different shape of failure surface, also produced an equation for the ultimate load of an anchor.

Until 1956, all the theoretical work was limited to evaluation of the ultimate load using either the friction cylinder or the earth weight method.

Jyoey (1956, Ref. 37) introduced a cohesion component into the existing methods and stated that an ultimate load equation should take into account the following:

(a) Weight of soil in the assumed failure surface.

(b) Internal friction along failure surface.

(c) Cohesion along failure surface.

He produced the equation:

$$P_m = \left(\frac{\pi \gamma H^2 \tan \alpha}{2}\right)\left(D + \frac{2H \tan \alpha}{3}\right)(\sin \alpha \tan \phi + 1) + \frac{\pi D^2 \gamma H}{4} + \frac{\pi H C_u (D + H \tan \alpha)}{\cos \alpha}$$

where,

α = Angle of inclination to vertical of the side face of the cone of rupture.

C_u = Undrained cohesive strength of the soil.

Later on, researchers based their theories on failure surfaces observed during small scale anchor tests.

Balla (1961, Ref. 40) assumed a curvilinear surface, and approximated the three dimensional failure surface to an arc of a circle, which originates from the edge of the anchor plate with a vertical tangent and intersects the ground surface at an angle of $(45 - \frac{\phi}{2})$, Fig. 2.2. He assumed that the ultimate load is made up of:

(a) The dead weight of the anchor, W_1.

(b) The weight of the soil in the failure surface, W.

(c) The vertical component of the shearing resistance along the failure surface, T.

He gave the radius of the circle, r, as:

$$r = \frac{H - t}{\sin (45 + \frac{\phi}{2})}$$

where,

t = Thickness of the anchor plate.

He also gave the weight of the soil, W, as:

$$W = (H - t)^3 \gamma F_1 (\phi, \frac{H - t}{D})$$

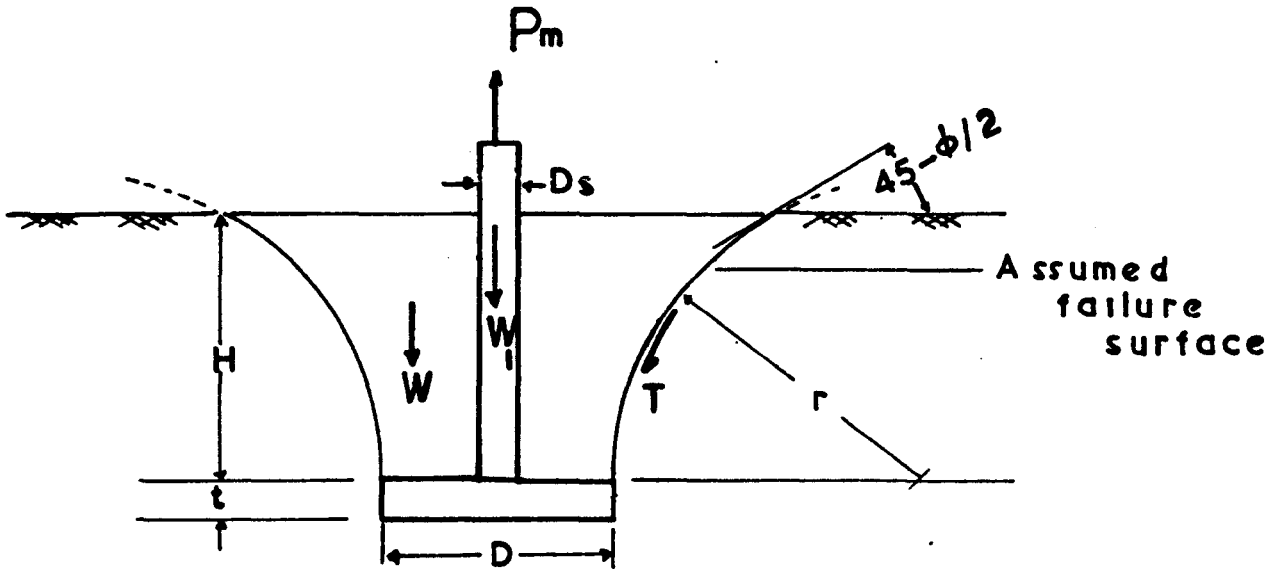

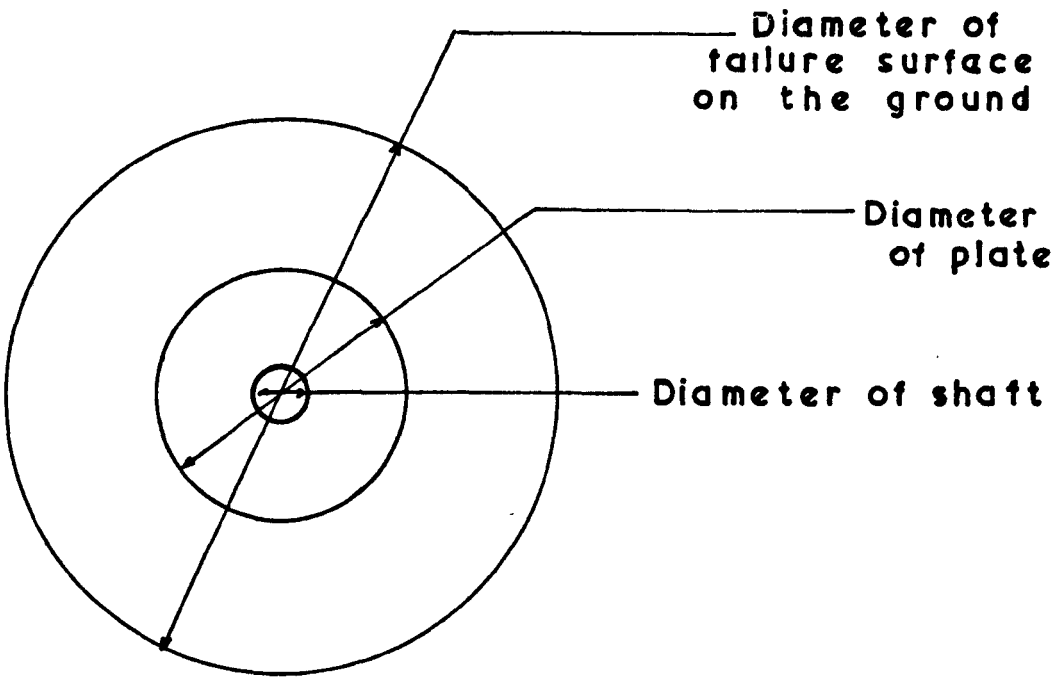

Balla's method

Fig. 2.2

Where F_1 is a function of ϕ, H, t and D.

Using Kotter's equation, valid only for plane stress and therefore not applicable in this case, Balla was able to obtain an expression for the vertical component of the shearing resistance, T, along the failure surface. This was expressed as:

$$T = (H - t)^3 \left[\frac{C_u}{\gamma} \left(\frac{1}{H - t}\right) F_2 \left(\phi, \frac{H - t}{D}\right) + F_3 \left(\phi, \frac{H - t}{D}\right) \right]$$

where F_2 and F_3 are functions found experimentally.

Although there was a good correlation between his experimental and theoretical results, his theory did not correlate with any other researcher's results, (Ref. 18).

Matsuo (1967, Ref. 28) and Howat (1969, Ref. 7) used the principle followed by Balla (1961), but different failure surfaces in order to obtain their ultimate load equations. (Appendix A).

Mariupolskii (1965, Ref. 19) and later Meyerhof - Adams (1968, Ref. 31) who worked on both shallow and deep anchors, produced their own ultimate load equations using the failure surface technique. Mariupolskii stated that since the uplift force was acting against the force of gravity, the weakness of the soil in tension should be taken into account. Meyerhof and Adams replaced the frictional and cohesive components of uplift resistance on the assumed curved failure surface, by the cohesion and passive earth pressure acting on the vertical plane through the edge of the anchor plate, (Appendix A).

Researchers, in order to provide a rational method of design for various structures, turned to empirical methods for which the values of constants were found from laboratory and field scale tests.

Turner (1962, Ref. 41) assumed that the ultimate load is given by the equation:

$P_m = K\ Cu\ A$

where,

K = Constant

A = Projected area equal to $\frac{\pi}{4}\ (D^2 - D_s^2)$

D_s = Diameter of the anchor shaft

From his experimental results, Turner proposed the following equations:

For $\frac{H}{D} < 1.5$ $\qquad P_m = 2.1\ C_u^{\frac{1}{2}}\ (\frac{H}{D})^2\ (D^2 - D_s^2)$

For $\frac{H}{D} > 1.5$ $\qquad P_m = 5.8\ C_u\ (D^2 - D_s^2)$

For $D = O$ $\qquad P_m = \pi\ C'\ D_s\ H$

where C' = "appropriate" undisturbed soil strength corresponding to depth H.

For grillage footings $P_m = 0.69\ C_u\ H\ D.$

Trofimenkov and Mariupolskii (1965, Ref. 26) using the empirical method, produced a formula for calculating the ultimate load of an anchor in the form of a bearing capacity equation (Appendix A).

Another approach to the uplift problem was the use of dimensional analysis techniques to develop empirical relationships

involving the dimensions of the anchor and the ultimate load.

Baker and Kondner (1965, Ref. 20) used the technique to develop relationships involving the plate diameter, the depth of embedment and the ultimate load of an anchor buried in a dense uniform sand. They obtained two equations involving the above mentioned variables i.e.

$$P_m = H D^2 \gamma \left\{ g_1 \left(\frac{H^2}{D^2}, \frac{D}{t} \right) \right\}$$

$$P_m = D^3 \gamma \left\{ g_2 \left(\frac{H}{D}, \frac{D}{t} \right) \right\}$$

By carrying out experiments, they were able to produce two complete equations for the ultimate load of a single vertical anchor.

For shallow conditions, i.e. $\frac{H}{D} < 6$

$$P_m = H D^2 \gamma \left(3.0 + 0.67 \frac{H^2}{D^2} \right)$$

For deep conditions, i.e. $\frac{H}{D} > 6$

$$P_m = D \gamma \left(170 D^2 + 2{,}800 D t + 470 H \gamma \right)$$

Sutherland (1965 Ref.18) using a similar dimensional analysis to Baker and Kondner (1965), obtained the following relationship

$$p = \gamma H f \left\{ \left(\frac{H}{D}, \phi \right) \right\}$$

where p = the pressure on the anchor plate at ultimate load.

He plotted $\frac{p}{\gamma H}$ against $\frac{H}{D}$ for $\phi = 31^{\circ}$ and $\phi = 45^{\circ}$

Laboratory and field scale tests were performed, and experimental and theoretical results showed a reasonable agreement between them.

This dimensional analysis technique was also used by El-Rayes (1965, Ref. 42) to calculate his own results, and compare these with the findings of other researchers.

A recent approach to the anchor problem involves a theory of the expansion of a cavity. This theory was also one of the first to attempt a deep anchor solution.

Vesic (1965, Ref. 43) considered the anchor problem as being analogous to the expansion of a cavity near the surface of a semi-infinite solid. He applied this theory to the ultimate load of the anchors and suggested the following equation:

$$p = C_u F_c + \gamma H F_q$$

where,

$$F_c = \frac{2H}{D} (C_3 + C_4)$$

$$F_q = \frac{2H}{D} (C_1 + C_2) + 1$$

C_i = Functions of ϕ and I_r where i = 1, 2, 3, 4

$$I_r = \text{Rigidity index} = \frac{E}{(1 + \nu)(C_u + \gamma \tan\phi)}$$

E = Modulus of elasticity of the soil

ν = Poisson's ratio of the soil

Diaz (1967, Ref. 44) used Vesic's theory but he added to his ultimate load equation the weight of the soil which filled the upper half of the spherical cavity. He also stated that the compressibility and frictional properties of the soil should also be considered when calculating the ultimate load.

The latest step taken in finding a solution to the anchor problem, is the use of the finite elements technique.

Ashbee (1969, Ref. 45) being one of the first to use this technique in anchors, assumed the following conditions:-

(a) Soil is displaced in one direction only, i.e. along the shaft of the anchor.

(b) Horizontal stress is ignored.

(c) Plastic flow around the anchor plate is neglected, i.e. analysis applicable to shallow anchors only.

(d) Elastic soil parameters are used.

This analysis is limited and also its credibility is questionable due to the introduction of the many assumptions. There is no experimental confirmation.

McMullan (1975, Ref. 24) used the finite element method in order to investigate the elastic load/displacement curve for a single deep vertical anchor. The following programs, the first three written by the author, were used.

(a) An elastic plane strain/stress.

(b) An elastic axisymmetric.

(c) An elastic "no-tension" approach based on the elastic plane strain/stress.

(d) An elastic/plastic plane strain/stress.

In his programs, McMullan applied load to find the displacement and his prediction showed that a purely elastic finite element approach cannot predict the classic behaviour of a single deep vertical anchor. He also showed that having enough computer time and a representative stress-strain curve for the soil, the shape of the sliding failure surface and the displacement at ultimate load could be predicted.

2.1.2 Deep Anchors

More of the theoretical and experimental programmes have involved shallow rather than deep anchors. A local failure surface method and the cavitation expansion approaches were both used to determine the ultimate load of deep anchors.

Mariupolskii (1965, Ref. 19) assumed that a conical wedge is formed above the anchor plate which moves together with the anchor and forces the sand lying above to the sides, Fig. 2.3 (a). He also assumed that on reaching the ultimate load, the anchor starts to tunnel at a substantially constant load.

From his assumption, that the work done in pulling the anchor plate through a distance z is equal to the work done in expanding a cylindrical cavity in the soil from a certain radius R_1 and height z to a radius R_2, Mariupolskii gave the following equation:-

$$P_p \; z - P_f = \frac{q \; z \; \pi}{4} \; (D^2 - D_s^2)$$

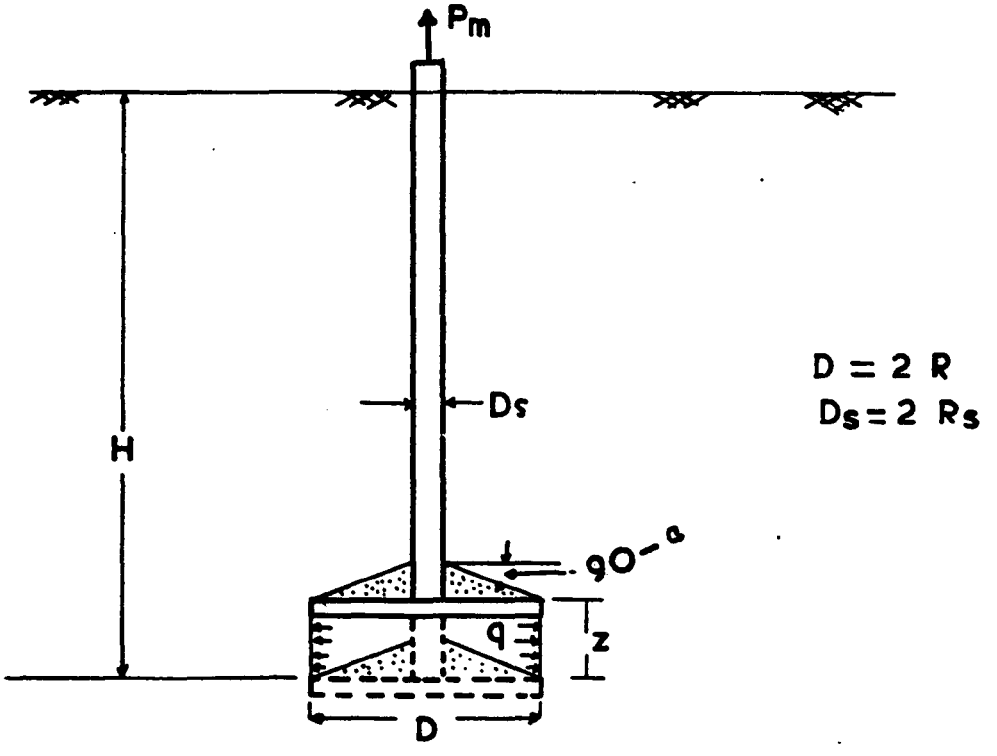

Mariupol'skii s method

(a)

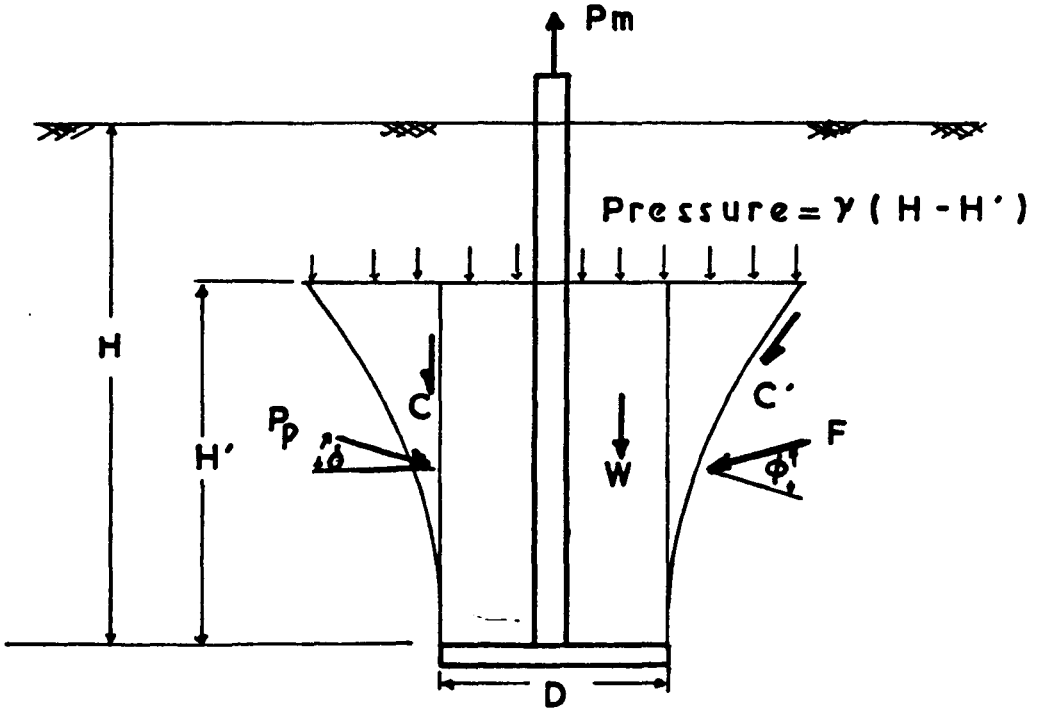

Meyerhof & Adams method

(b)

Fig. 2.3

Where,

P_p = The ultimate load transmitted to the soil by the anchor plate.

P_f = "Useless" work expended to overcome friction between the surface of the wedge and surrounding soil.

q = Radial pressure under which the cavity expands.

By considering the frictional force, T, along the surface of the cone.

$$T = P_p \sin\theta \tan\phi$$

where,

2θ = Angle of the cone at the apex.

but,

$$P_f = T \, z \cos\theta$$

$$P_f = P_p \, z \sin\theta \tan\phi \cos\theta$$

$$P_f = P_p \, z \frac{\sin 2\theta}{2} \tan\phi$$

for,

$$2\theta = 90^{o}$$

$$P_f = \frac{P_p \, z \tan\phi}{2}$$

$$\therefore \; P_p \, z - \frac{P_p \, z \tan\phi}{2} = \frac{q \, z \, \pi}{4} (D^2 - D_s^2)$$

$$P_p = \frac{q \, \pi}{4} \left(\frac{D^2 - D_s^2}{1 - 0.5 \tan\phi}\right)$$

Missing pages are unavailable

He expressed the ultimate pressure, p, on the anchor plate to be:-

$$p = \frac{q}{1 - 0.5 \tan \phi}$$

Where q is the ultimate pressure of the cavity and this was calculated assuming elastic behaviour of the soil. The equations involved are complex and not easily derivable. (Ref. 19).

To calculate this value Mariupolskii using one of his expressions, produced charts of a factor N for cohesionless and cohesive soils;

Where,

$$N = \frac{p}{\gamma H}$$

$$\therefore \quad q = N \gamma H \ (1 - 0.5 \tan \phi)$$

and,

$$P_p = \frac{N \gamma H \pi}{4} \ (D^2 - D_s^2)$$

The ultimate load of the anchor was then given by

$$P_m = W_1 + P_p + L \pi f D_s$$

where,

$L \pi f D_s$ = The force due to the friction on the shaft.

L = The working length of the anchor shaft.

f = The specific friction resistance.

Meyerhof and Adams (1968, Ref.31) restricted the application of their assumed failure surface to a height H' above the anchor plate, Fig. 2.3 (b). They modified their equation for a shallow anchor and obtained the following expression for the ultimate load of deep strip anchor:-

$$P_m = 2 C_u H' + \gamma (2 H - H') H' K_u \tan \phi + W$$

where,

H' = Function of B, ϕ, stress history of soil, relative density and method of compaction.

B = Breadth of anchor plate.

K_u = Experimental coefficient.

From observed failure surfaces, Meyerhof and Adams estimated values of H' and tabulated $\frac{H'}{B}$ against ϕ.

To obtain an equation for the ultimate load of a deep anchor with circular plate, Meyerhof and Adams introduced to their equation a shape factor, S.

Thus for circular plate:

$$P_m = \pi C_u D H' + S \frac{\pi}{2} \gamma D (2 H - H') H' K_u \tan \phi + W$$

2.2 Experimental work on small scale tests

The following conclusions have been drawn by a study of published papers reporting on laboratory scale tests on ground anchors.

(a) Most of the tests were performed using circular discs,

with the force applied to a thin tie-rod connected to the plate. The thickness of the plate varied from 6mm to 25mm, whilst the diameter of the plate varied between 12mm and 152mm, (Ref. 15, 18, 20, 23, & 24).

(b) Not many researchers have carried out work on deep anchors, but from the few tests available it appears that the transition from shallow to deep anchor varies between $\frac{H}{D} = 5$ and $\frac{H}{D} = 10$, (Ref. 7 & 26).

(c) Most of the experimental work was performed by applying increments of load until the ultimate load was reached (Ref. 23, 27, & 28). Few researchers have applied a constant rate of strain to the anchor, (Ref. 24 & 28).

(d) Nearly all the tests were carried out in small tanks, (Ref. 23 & 29).

(e) Researchers have found that the ultimate load increases as the following parameters increase.

(i) Depth of embedment, (Ref. 18, 19, 23 & 28).

(ii) Diameter of anchor plate, (Ref. 23).

(iii) Perimeter of anchor plate, (Ref. 28 & 32).

(iv) Effective depth, (Ref. 7, 23 & 32).

(f) Experiments showed that the critical depth increases with the density, (Ref. 29).

2.3 Comments on the theoretical and experimental work

2.3.1 Theoretical Work

From the theoretical work on shallow and deep anchors the

following points are clear:-

(a) The earth weight method, although not consistent, could ensure reasonable correlation with experimental results, if the angle of failure surface to the horizontal is assumed correctly and the method is limited to shallow anchors.

(b) The friction cylinder method can also be employed for shallow anchors if the coefficient of earth pressure is given a suitable value.

(c) The empirical method could only predict the ultimate load of the anchor, under the same conditions of testing for that particular anchor type.

(d) The assumed failure surface method provides a solution, for shallow anchors, which is based on an approximate failure surface observed during experiments. The following assumptions are generally made:

(i) Shear stresses within the failure surface are ignored.

(ii) Shear stresses along the failure surface are calculated from two dimensioanl stress equations, although the problem is three dimensional.

(iii) Shear stresses along the failure surface vary due to the pressure applied by the anchor plate.

(iv) Part of the weight of the lifted soil is taken by the soil outside the failure surface.

(e) The cavity expansion method generally gives an unsatisfactory solution. Complicated expressions involving elastic parameters are used in calculating the cavity pressure.

(f) The finite element method as used by Ashbee, assumes elastic behaviour and introduces many assumptions which tend to oversimplify the problem. Although McMullan used a series of finite element programs, he only investigated the elastic load/displacement curve in which loads were applied to calculate the displacements.

(g) The load-displacement curve of an anchor has not yet been satisfactorily predicted.

2.3.2 Experimental Work

From the experimental work on shallow and deep anchors the following points are clear:-

(a) There is no information on the soil parameters, i.e. distribution of density and coefficient of earth pressure at rest prior to the test. Therefore the initial state of the sample has not yet been defined.

(b) The effect of the following parameters on the behaviour of the anchor has not been fully investigated.

(i) Boundaries.

(ii) Diameter of shaft.

(iii) Thickness of shaft.

2.3.3 Summary

It is considered that the above theories fail to take into account all the parameters present in the anchor problem. The theories are not based on proper physical assumptions but on failure surfaces, and in the finite element methods the stress-strain relationship may not represent the

behaviour of the soil. It is important that the load-displacement behaviour of the anchor is obtained by using a method in which the properties of the soil are properly taken into consideration. The finite element method could provide a reasonable assessment of the anchor problem when a correct stress-strain relationship of the soil is used and the load-displacement behaviour is predicted by controlling the displacement instead of the load.

CHAPTER III

APPARATUS

3.1 General

The aim of this chapter is to give a detailed description of the experimental set-up and the difficulties met during the construction of the apparatus. The apparatus will be divided into the following individual units:-

(a) Frames.

(b) Sand tank.

(c) Pullout unit.

(d) Suction unit.

(e) Vibration unit.

(f) Anchor unit.

The calibration of the pullout unit and the recording unit will be described and the corresponding charts will be plotted.

Figure 3.1 is a schematic drawing showing the general lay-out of the apparatus. The X-Y plotter and other electrical instruments were placed in a tent, shown in Plate 1, in order to protect them from the dust produced during the preparation of the experiment.

3.2 Frames

Figure 3.2 and Figure 3.3 are drawings showing various frames forming the apparatus.

The main frame was constructed using hollow steel sections of 102mm x 102mm x 4.8mm. Three columns, placed at about

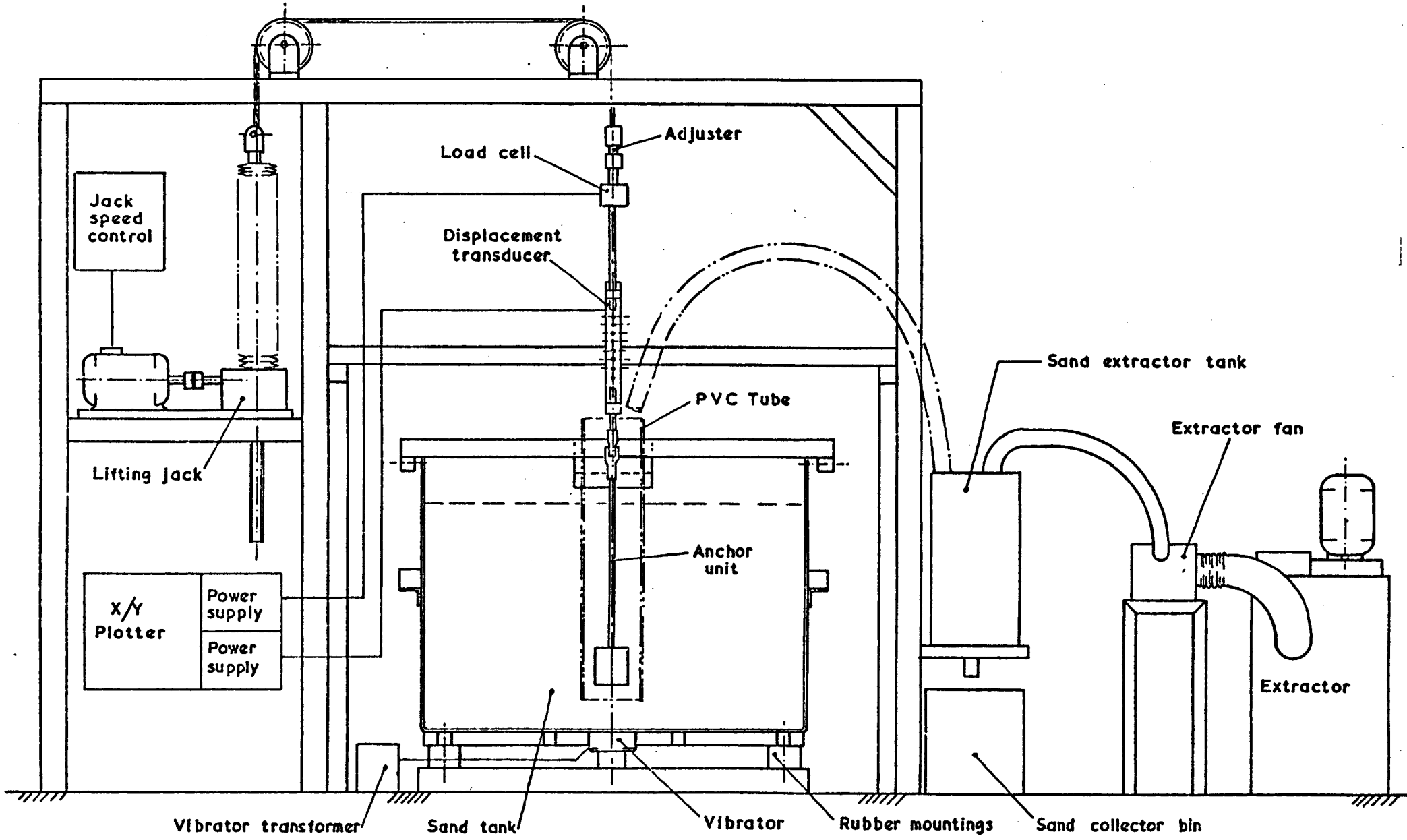

Fig. 3.1 Schematic Layout of Apparatus

1200mm and 2700mm apart, were welded to the horizontal beam to which the pulleys were fixed. The maximum load expected to be obtained by using the largest anchor plate in the experimental programme was used in designing the frame.

The electric motor and jack were supported by two hollow sections 102mm square, 4.8mm thick and 1300mm long, which in turn were welded to the main frame.

The displacement transducer was fixed to a horizontal beam 76mm square, 3.2mm thick and 2600mm long. The beam was supported by two portal frames, made from a hollow section 76mm square and 3.2mm thick, which in turn were welded to the main frame as well as bolted to the floor, Fig. 3.2.

A frame to support the fan was also constructed from a hollow section 76mm square and 3.2mm thick, Fig. 3.3.

3.3 Sand tank

The tank which sits on the vibrator table, has internal dimensions of 1800mm x 1800mm x 1200mm deep and is made of mild steel.

A square frame, made from 102mm x 102mm x 14mm steel angle, was used to provide reinforcement to the walls of the tank. The frame surrounding the tank, was hung from the top of the tank by four steel rods, one at each corner of the tank. The size of the tank was decided on the following factors.

(a) The boundaries should be far enough away from the anchor, so that interference between the anchor failure surface and the walls of the tank is avoided. At the time of design it was thought that the distance of 18 anchor diameters was far enough. This assumption was obtained from the work performed on group anchors, (Ref. 24, 32, 46).

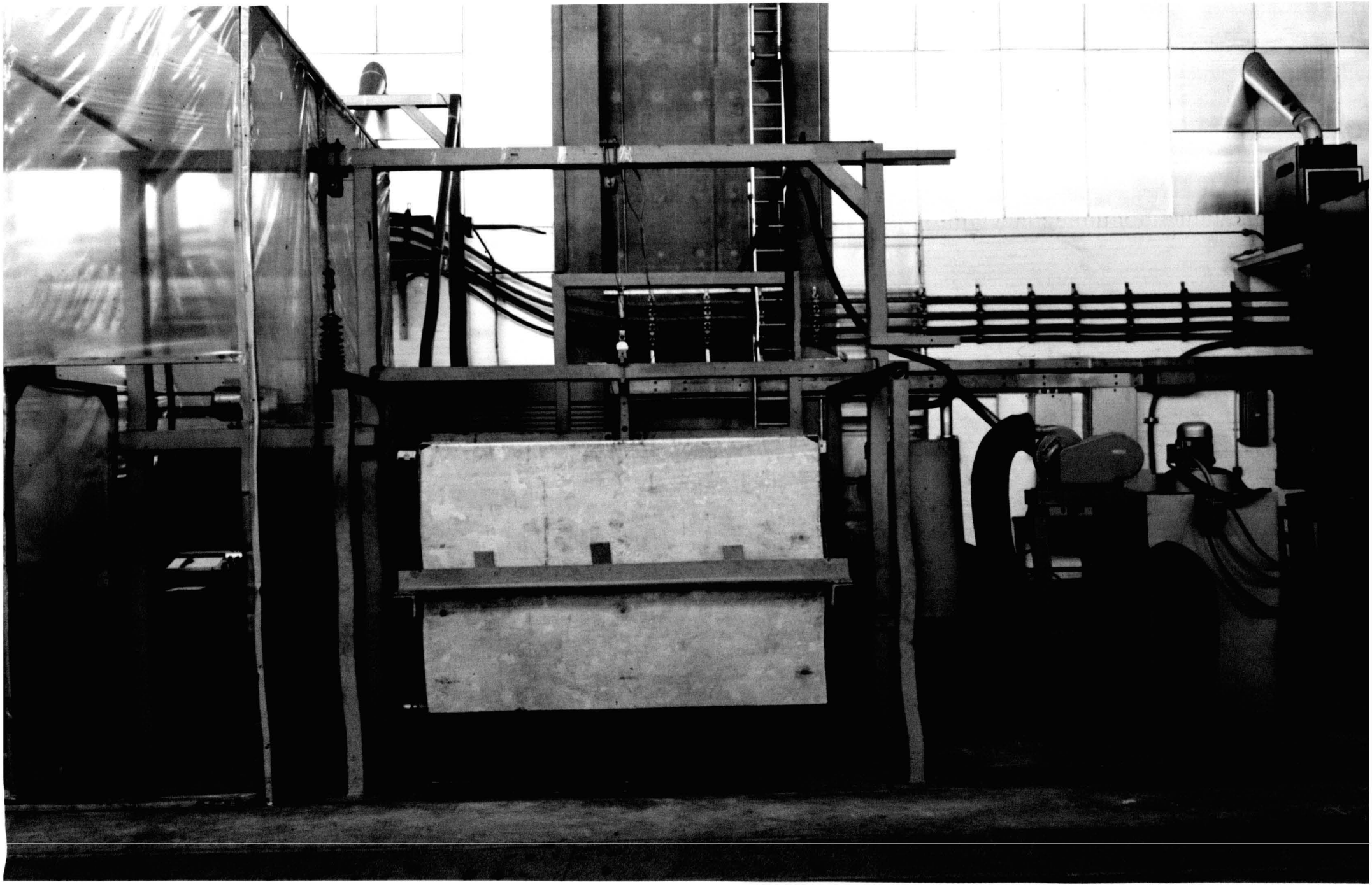

Plate 1

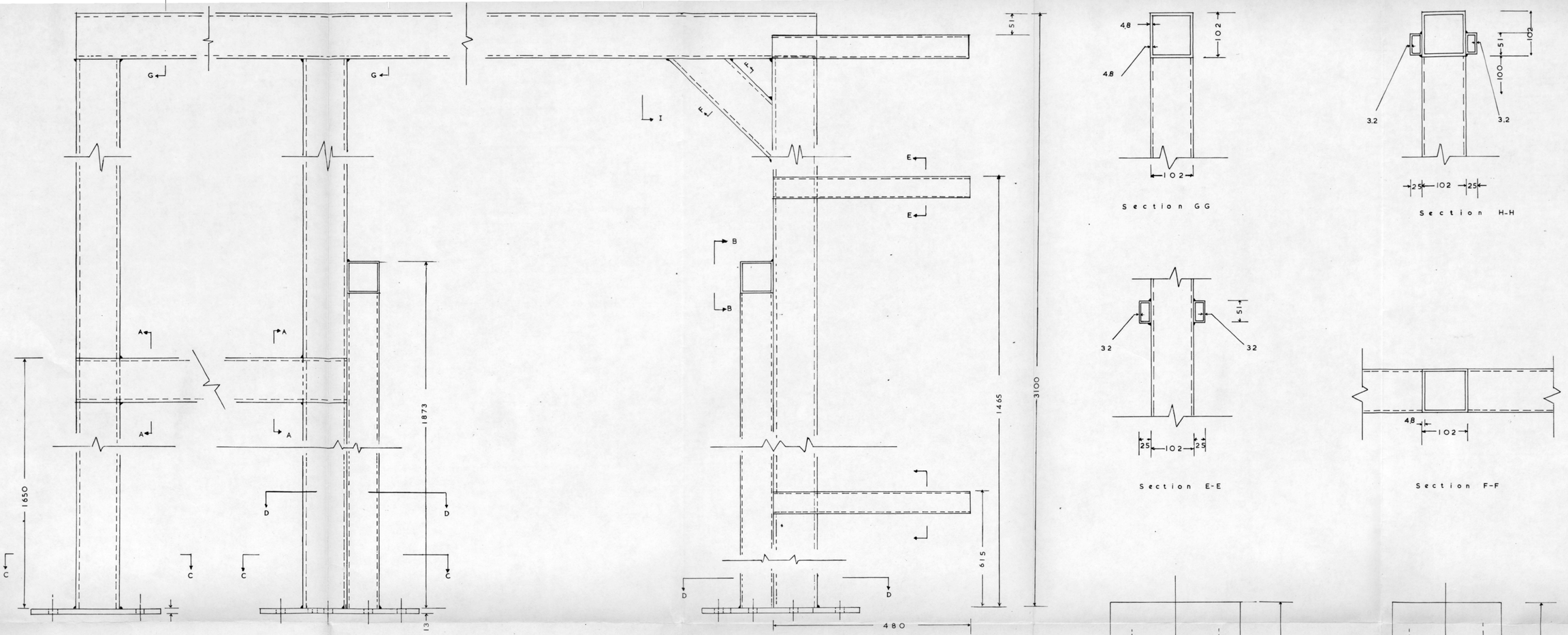

ELEVATION

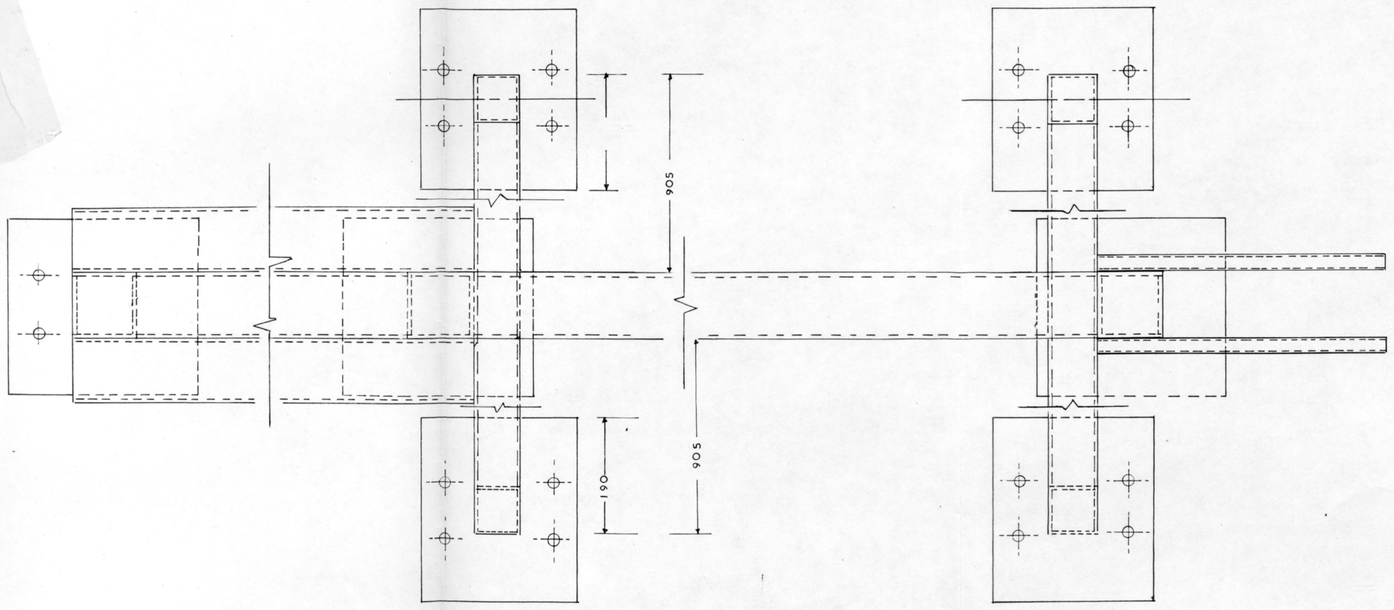

PLAN

Section GG

Section H-H

Section E-E

Section F-F

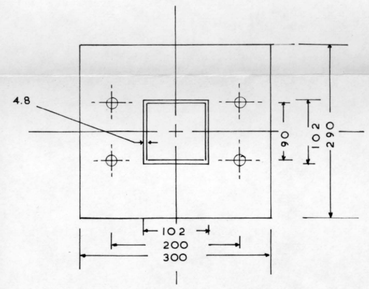

Section C-C

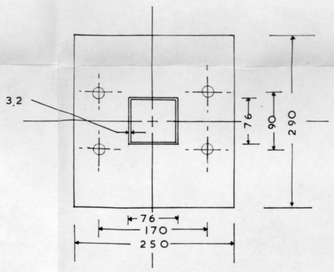

Section D-D

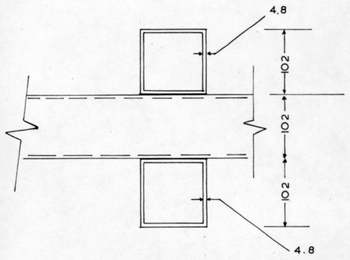

Section A-A

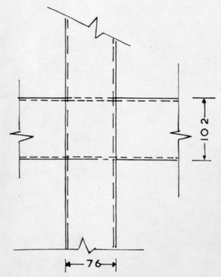

Section B-B

MAIN FRAME OF APPARATUS			
SCALES : AS SHOWN	QUEEN MARY COLLEGE		FIGURE 3.2
DRAWN BY:- S. N. TSANGARIDES	DIMENSIONS:- MILLIMETRES	MATERIAL:- MILD STEEL	

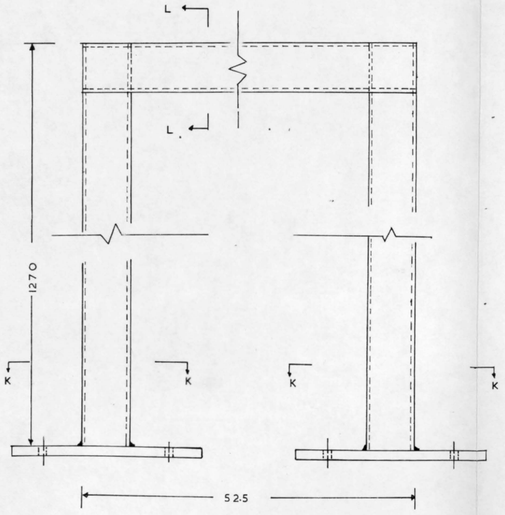

Elevation

scale 1:5

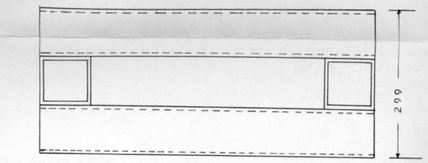

Plan

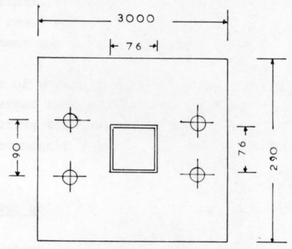

Section K-K

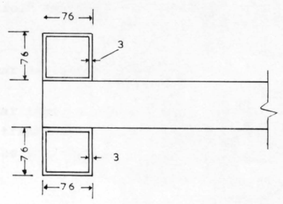

Section L-L

Fan support frame
(a)

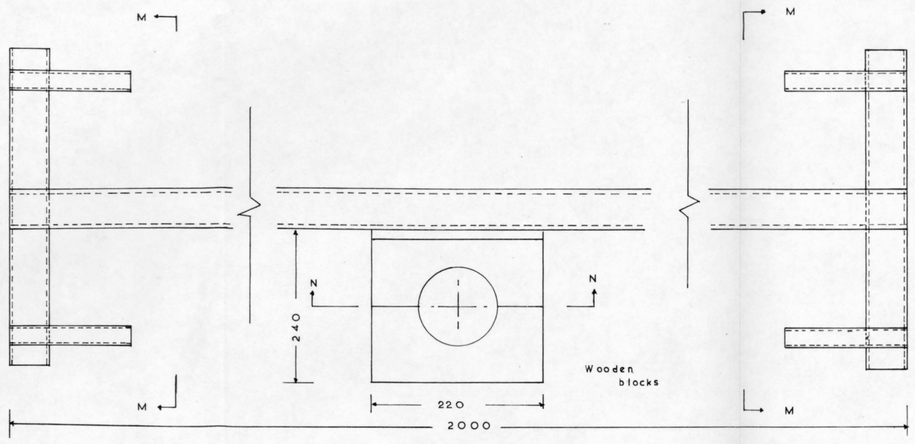

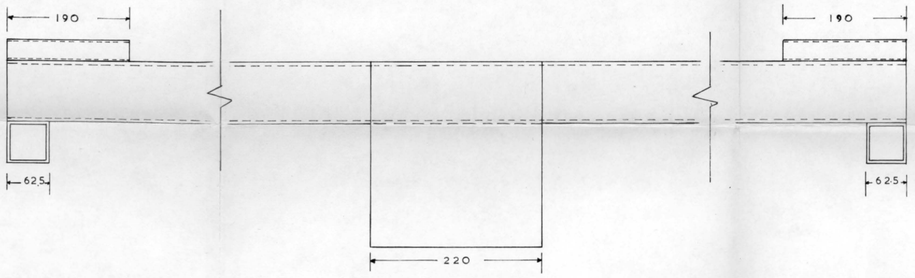

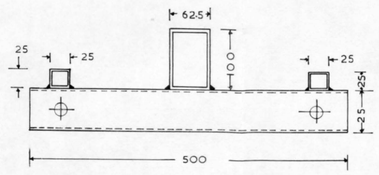

Section M-M

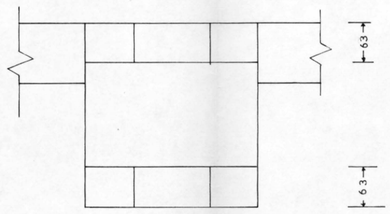

scale 1:5

Section N-N

Guide
(b)

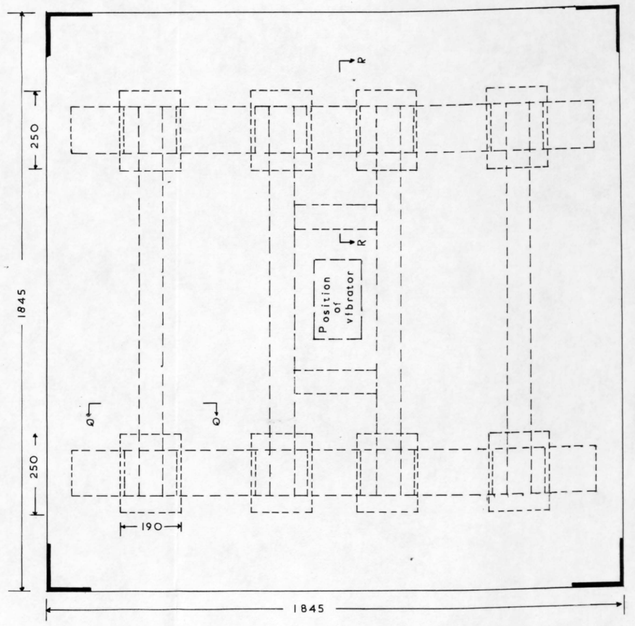

Plan

scale 1:10

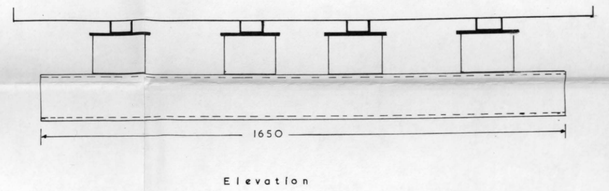

Elevation

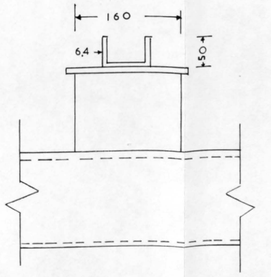

Section Q-Q

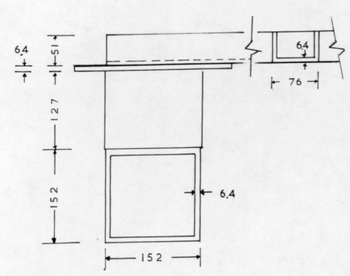

scale 1:5

Section R-R

Vibrating table
(c)

FAN SUPPORT FRAME , GUIDE , VIBRATING TABLE			
SCALES:- AS SHOWN	QUEEN MARY COLLEGE		FIGURE
DRAWN BY:- S. N. TSANGARIDES	DIMENSIONS:- MILLIMETRES	MATERIAL:- MILD STEEL	3.3

(b) The depth of the tank was chosen due to the fact that the anchor was to be buried in deep conditions, i.e. relative depth greater than 6.

(c) The amount of work and time needed to empty and fill the tank. This was due to the fact that the tank had to be emptied later on for the insertion of the smaller boxes to investigate the boundary conditions.

(d) The vibrational intensity of the vibrator, since the sample had to reach a state where reproducibility of the load-displacement curve could be obtained.

(e) The amount of work and time needed to set up a single test. A larger tank would be more difficult to handle i.e. connecting the load cell to the pullout unit, placing the displacement transducer without disturbing the sample.

3.4 Pullout unit

The pullout unit, shown in Plates 1, 2 and 4, was made up of the following major items of equipment.

(a) A Neco geared motor, type DS.

(b) A "Necontrol" thyristor speed control system, type 2AF 25.

(c) A Worm Gear Jactuator, type 1802.

A number of smaller items e.g. pulleys, adjustor, connectors and displacement transducer plate were also used in the construction of the equipment.

Plate 2

3.4.1 Geared motor

The geared motor, Plate 1, which has output speed based on a motor input speed of 2,000 r.p.m. gives a final shaft speed of 23.7 r.p.m. The motor, suitable for a control unit, is specified as follows:-

Horse power = $\frac{1}{4}$

Windings = DC shunt wound to suit control unit detailed below.

Final shaft speed = 23.7 r.p.m.

Output torque = 13.83 Kgf.m. (100lbf. ft.)

Final shaft = 15cm. long.

3.4.2 Thyristor speed control unit

The unit was purchased with due regard to accommodating motors of up to $\frac{1}{2}$ H.P. over a minimum range of 20:1 at constant torque. The range of the speed of the geared motor is controlled in 10 divisions, see Plate 2.

3.4.3 Worm Gear Jactuator

The unit could be operated manually or by geared electronic motors to raise or pull loads. The jactuator is self-locking and can hold a heavy load in position indefinitely without creep of the system. The upright screw, with its end being clevis, is keyed so rotation is prevented and a translating motion results. The length of the lifting screw is about 1 metre. Bellow boots were used to cover the screw, due to

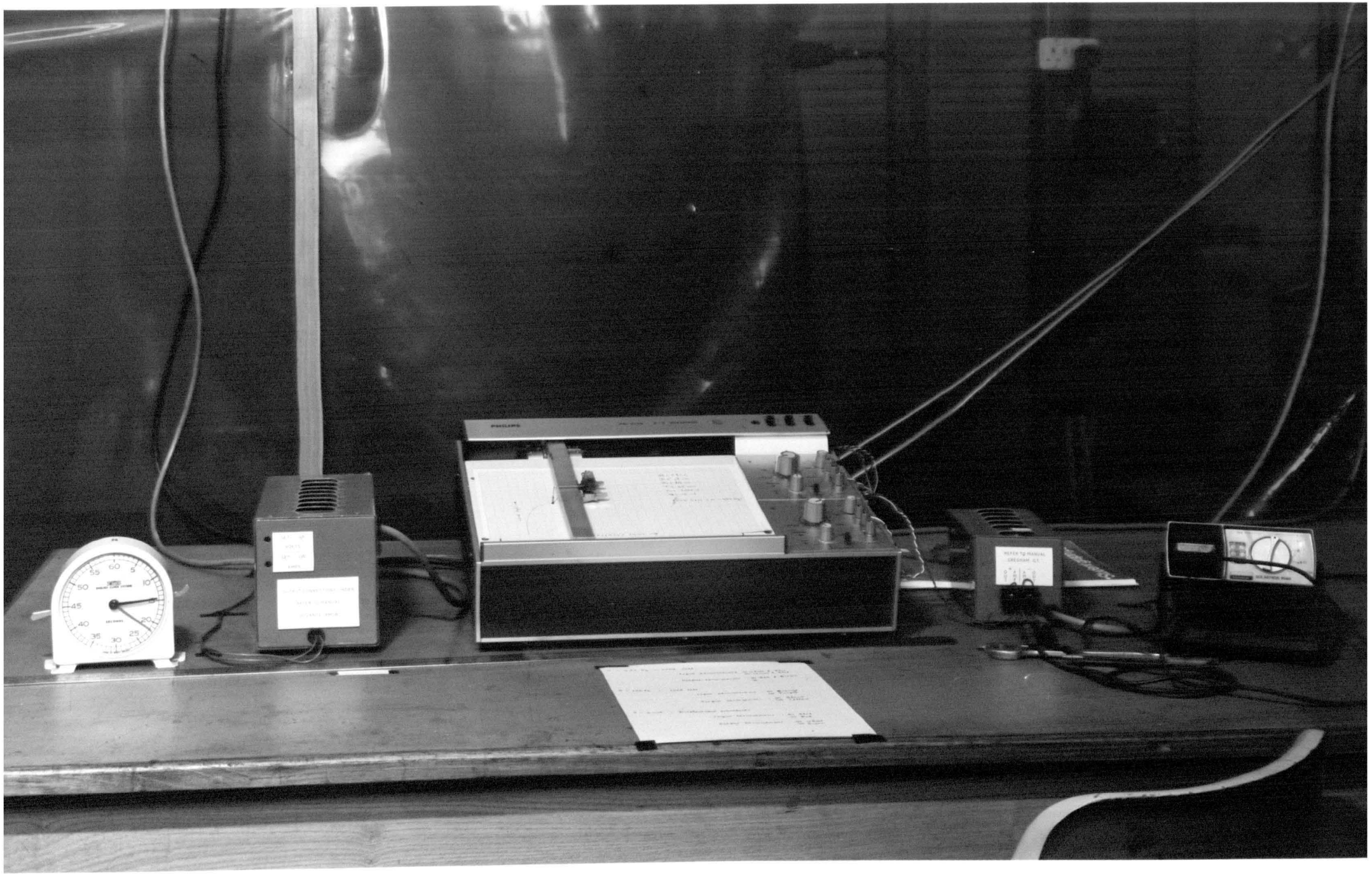

Plate 3

the dirty conditions existing. The jactuator is specified, as follows, in the following imperial units:-

Capacity = 2 tons.

Maximum Horse Power = 1.

Torque at full load = 120 lbs.ins.

Worm gear ratio = 6:1.

Turns of worm for 1" raise = 24.

Diameter of the lifting screw = 1 in.

Pitch - Acme = 0.25 in.

Total weight of jack = 25 lbs.

Base size = $\frac{7}{2}$ in. x 7 in. , height = $\frac{7}{2}$ in.

The lifting torque was chosen with due consideration of the load, the worm gear ratio and the pitch of the lifting screw.

The following points should be considered when the jactuator is to be used:-

(a) The Horse power is directly proportional to the speed and the motor could be out of proportion to the jack if the speed becomes too high.

(b) The maximum worm speed of this jack is 500 r.p.m.

3.4.4 Pulleys

These were used in the pullout system, as shown in Fig. 3.1 and Plate 1. Their purpose was to connect the anchor unit with the jactuator.

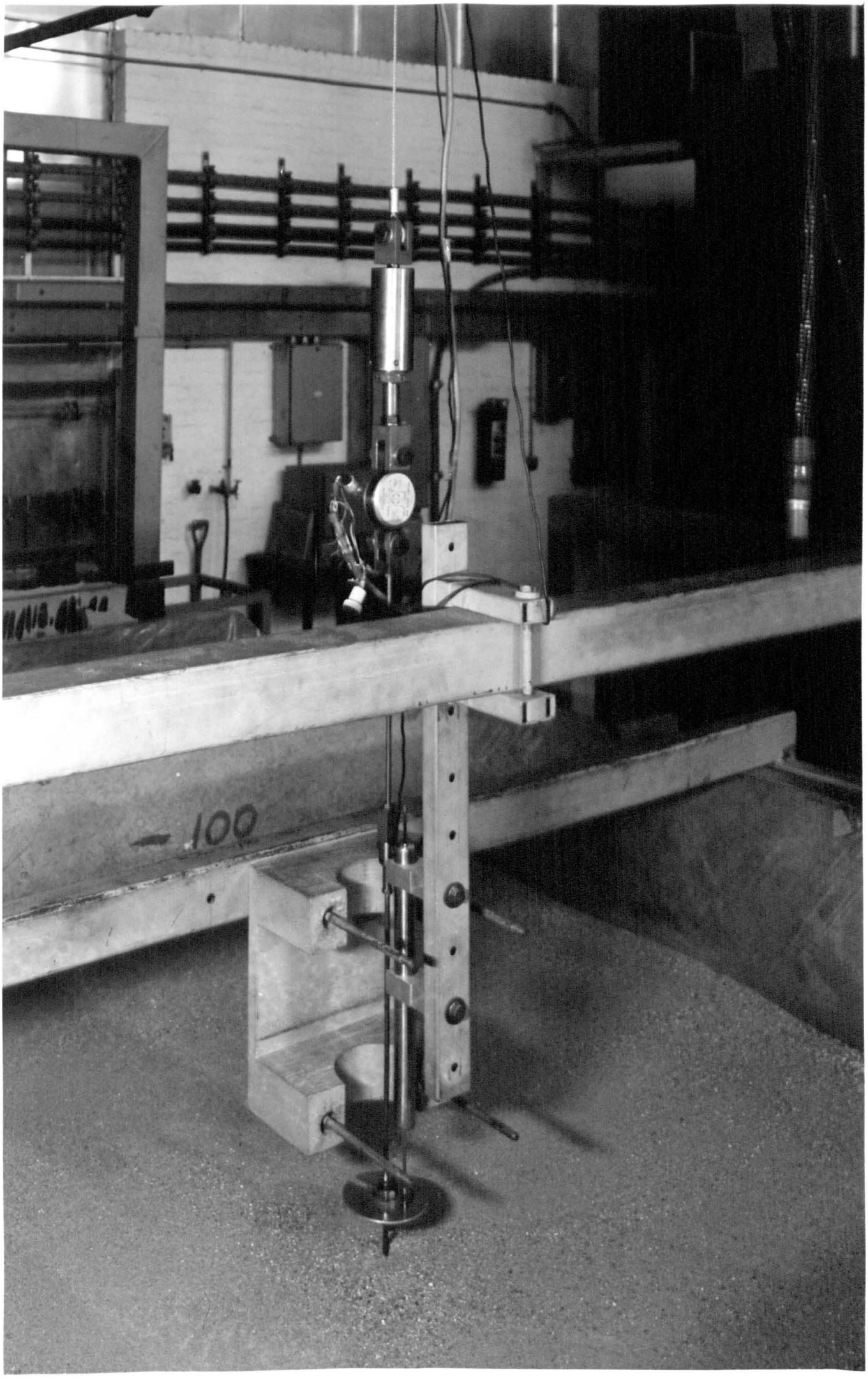

Plate 4

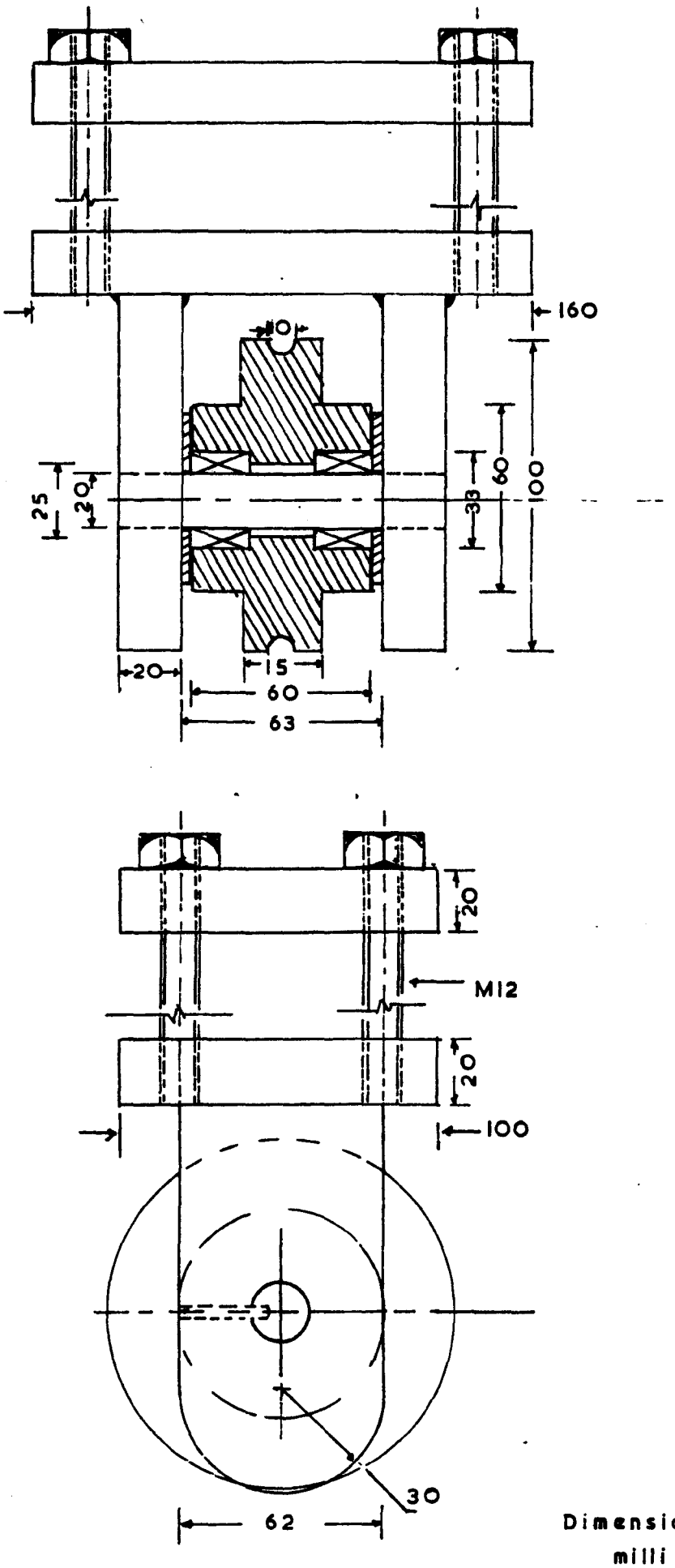

Dimensions are in millimetres

Fig. 3.4 Pulley

The friction in the pulleys does not affect the recorded load, due to the fact that the load cell was placed between the first pulley and the anchor unit. The pulleys were designed to have as little as possible friction, so that the full capacity of the jactuator can be used by the resistance of the anchor if the need arises.

The pulley, designed and manufactured in the laboratory, is shown in Fig. 3.4. Two steel plates, originally rectangular of dimensions 100mm x 62mm x 20mm, were welded to a rectangular steel plate of dimensions 160mm x 100mm x 20mm. Between the two vertical steel plates, a shaft of 20mm diameter and 103mm long was fitted and a pin was used to prevent it from rotating. A pulley wheel, shown in Fig. 3.4, rotates on the two bearings fitted to the shaft. The pulley was clamped to the hollow section of the main frame using an identical steel plate to the horizontal plate, and 12.5mm diameter bolts.

The pulleys were designed to take loads of up to 40000 N.

3.4.5 Adjustor

The adjustor, shown in Fig. 3.5, was connected between the steel cable and the load cell, Plate 4. It was designed to reduce the twisting in the steel cable and also to adjust small distances, i.e. by expanding or shortening the adjustor the pullout unit can be connected to the anchor unit. Later on it was found that the cable could be adjusted even quicker and with less difficulty by using the electric motor at a very low speed. Therefore the adjustor was set to a constant length and its only purpose, in this experimental programme, was to cope with the twisting of the cable.

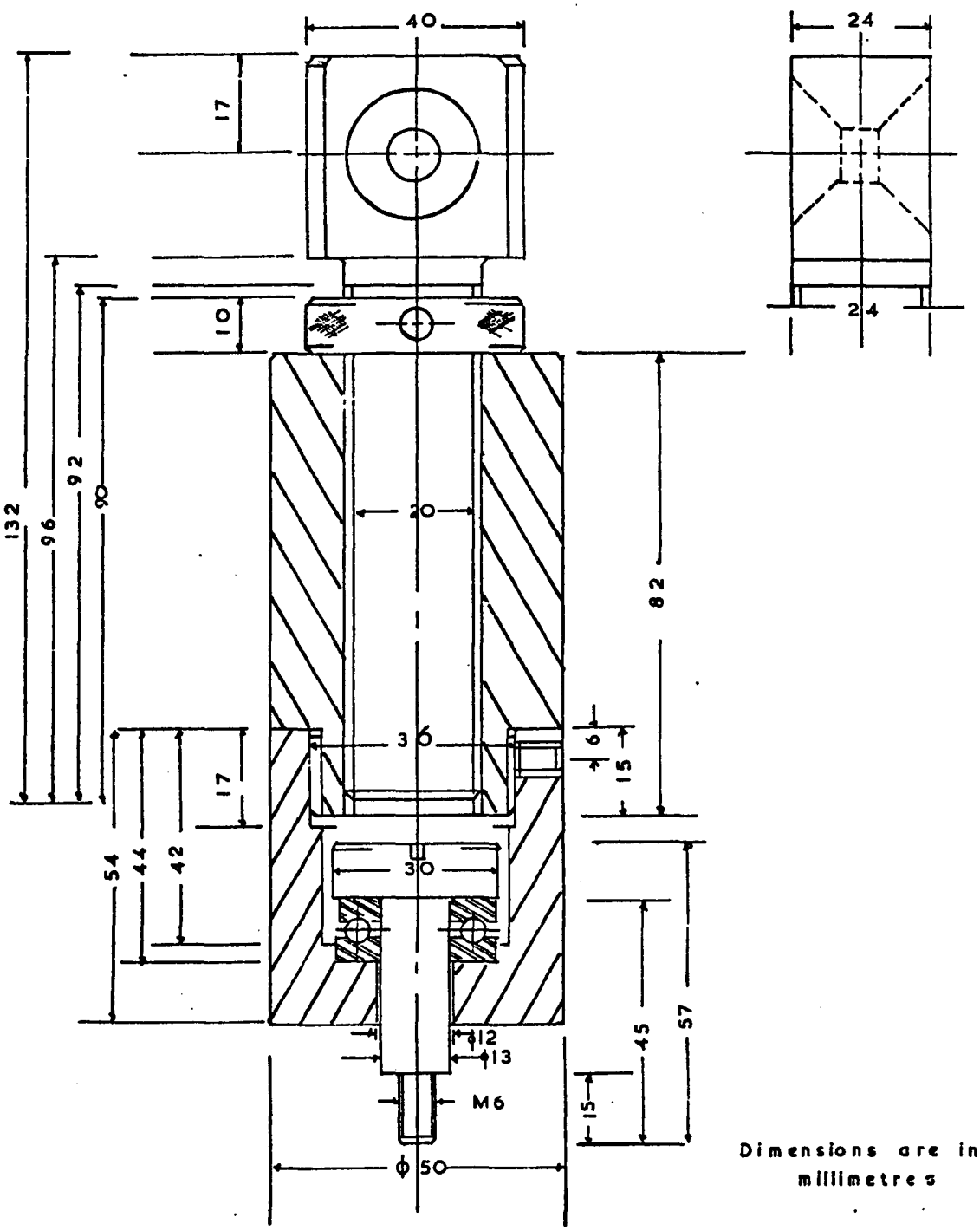

Fig. 3.5 Adjustor

The adjustor was made from a mild steel rod. The rod, 50mm diameter and 140mm long, was machined to form the main part of the unit. Adjustment was achieved by turning the threaded rod fitted inside the upper end of the main part of the body. To reduce the twisting in the cable in a very short time, a thrust bearing was fitted to the unit.

Observations during tests, showed that this mechanism was very effective in avoiding twisting in the steel cable.

3.4.6 Connectors

The electric motor was connected to the jactuator by a coupling. One side of the coupling fits to the shaft of the jactuator, diameter $\frac{1}{2}$ in. (127mm), and the other side fits to the shaft of the geared motor, diameter $\frac{7}{8}$ in. (22.2mm). In the Key-way of the motor shaft a piece of metal was inserted, while in that of the shaft of the jactuator a piece of wood was used, so that when the capacity of the jactuator is exceeded the safety of the pullout unit is ensured.

Two wire rope eyes, Fig. 3.6, were used to connect the ends of the steel cable to the clevis end of the jactuator, and to the adjustor. The loops in the cable were placed in the grooves of the wire rope eyes and these were fixed to the corresponding units using suitable attachments.

The adjustor was screwed to the load cell and held in position by a locking nut.

The connection between the load cell and the anchor unit was made by a mild steel rod, the length of which varies according to the anchor depth. A mild steel plate was machined down to fit the anchor head, and connected with the mild steel rod, Fig. 3.6.

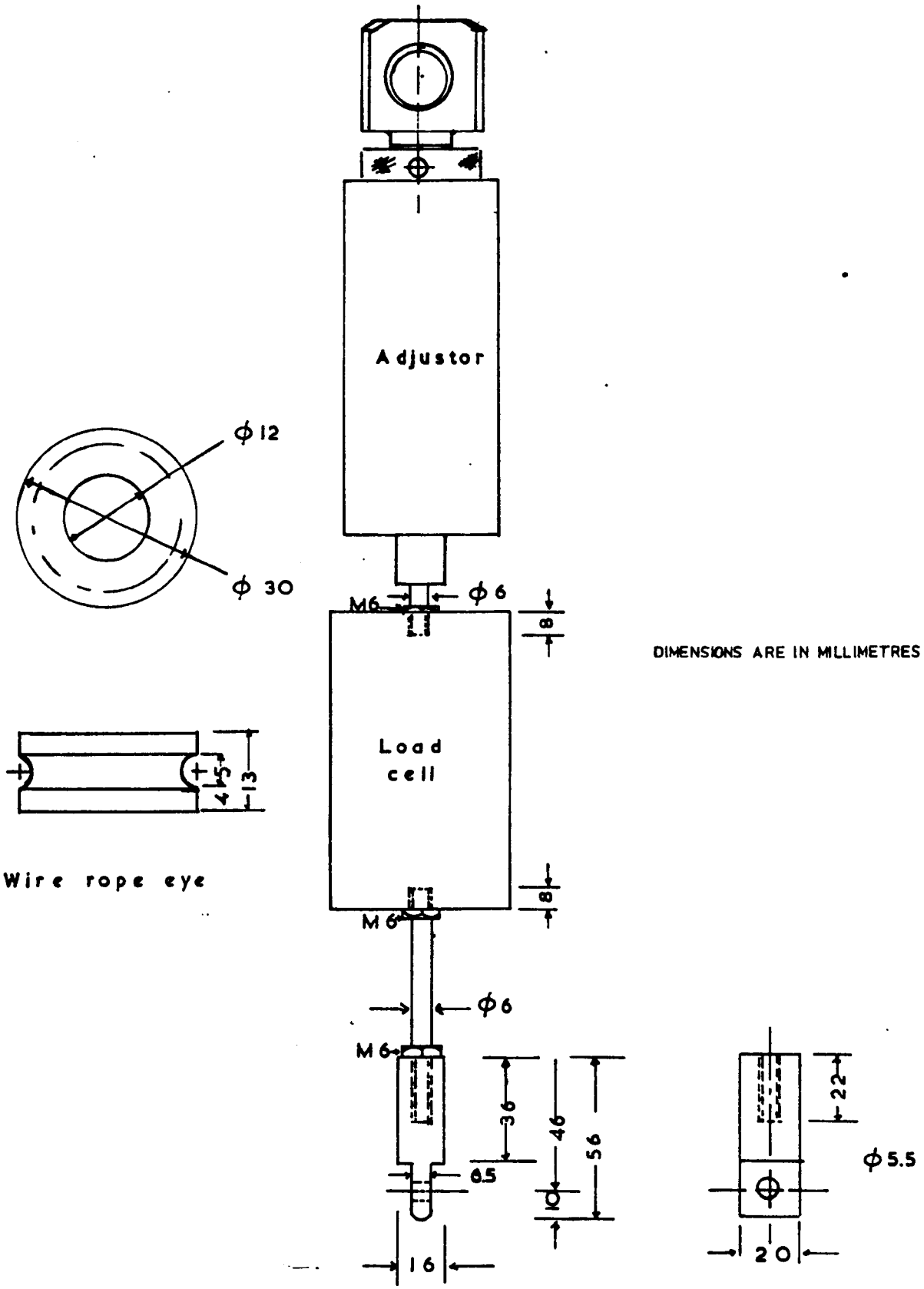

Connecting assembly between anchor & wire rope

Fig. 3.6

3.4.7 Displacement transducer plate

Originally the plate was welded to a 50mm long mild steel rod with a hole in the middle. The rod was able to slide along the length of the anchor shaft. A plate of about 100mm in diameter was needed to accommodate the rod of the displacement transducer. Since the diameter of the pvc tube used to extract the sand was smaller than that of the plate, the plate had to be removed for each test. The dismantling of the anchor unit to reposition the plate produced new problems, e.g. the anchor would be disturbed after placement in the sand, and time would be wasted. A plate with a diameter smaller than that of the pvc tube was then used but this caused new problems. The anchor unit was unable to take a vertical position in the pvc tube due to the plate limiting the movement of the anchor plate.

After trying different shapes of plate, i.e. semicircular - triangular, the fitting shown in Fig. 3.7 was eventually designed and manufactured. The plate was made of aluminium and has 2.5mm thickness and 100mm diameter. A 25mm diameter mild steel rod was machined down to form a clamp for the plate and the anchor shaft. The upper part of the rod was threaded down to 12.5mm diameter, and the lower part was machined down to 15mm diameter. A tapped hole was formed on the side of the rod. The middle part of the fitting, 25mm diameter and 6.5mm thickness, provided a seat for the plate when placed in position and the nut tightened, (See Plate 4). The fitting without the plate, was kept on the anchor shaft throughout the experimental programme.

3.5 Recording unit

The unit recorded the load-displacement curve of an anchor when pullout took place at constant rate of strain. The following instruments were connected together to produce

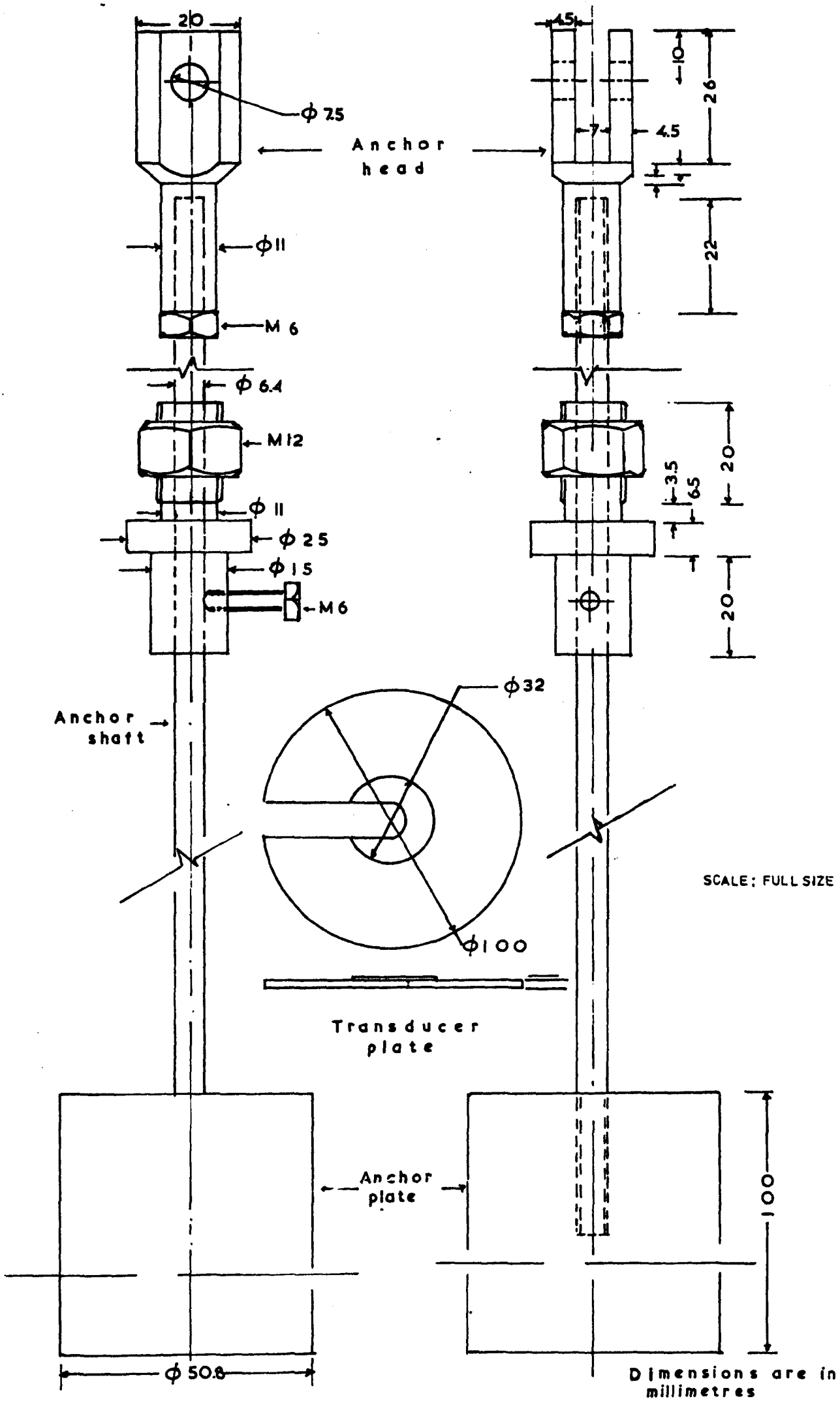

Fig. 3.7 Anchor unit

the recording unit.

(a) Load cells:-

(i) Strain gauge transducer, type UF2, 0-500 lb. tension.

(ii) Strain gauge transducer, type BT2, 0-450Kg tension.

(b) Displacement transducer, type D400.

(c) X-Y flat-bed recorder, PM8120/01.

(d) Power supplies:-

(i) Modular Stabilised Power supply, PM18

(ii) Miniature Stabilised Power supply, GT9/1

3.5.1 Load cells

Two tension load cells were used throughout the experimental programme. The purpose of using two load cells with different ranges instead of one with a large range, was due to the fact that the anchor pullout load could be matched to the range of the load cell.

The 0-500 lb.(0-2220 N) tension load cell was used for both small anchor plates, and for all the anchor plates at shallow depths. The bigger load cell 0-4500 N was used for large sizes of anchor plates, i.e. 38mm (1.5 in.) and 51mm (2 in.), at greater depths.

3.5.2 Displacement transducer

The transducer was able to record displacements of the anchor of up to 101mm. A voltage of about 10 Volts supplied by a power supply was needed for this particular displacement transducer.

It has dimensions as follows:-

Total length = 406mm

Body diameter = 21mm

Rod diameter = 3mm

3.5.3 X-Y recorder

The X-Y recorder, Plate 3, was chosen as the best instrument to obtain the results, due to its suitability of producing a load-displacement curve at different scales. The quantities to be recorded are fed to the instrument in the form of d.c. voltage. The accuracy of the recorder is about 0.25% of the full scale deflection. The axes have different deflections, with the X - axis deflecting from 0 to 250mm and with the Y - axis from 0 to 180mm.

3.5.4 Power supplies

Two power supplies, Plate 3, were used in the circuit. The 9 Volt power supply provided a stabilised voltage to the displacement transducer while the 4 Volt power supply was connected to the input of the load-cell. The supplies can provide voltages of up to 10 Volts, but when set during calibration they were kept constant. The supplies were checked before and after each test, since changes in voltage would result in error in the recorded values.

3.5.5 Cable

A 16 lead cable was connected to the recording unit. Although an 8 lead cable was sufficient, 4 for the displacement and 4 for the load-cell, it was considered wise to provide extra services for future work. Later all the leads in the cable were used, i.e. to connect the second load-cell and

the pressure gauge. The cable was screened to avoid a variation of the voltage.

3.6 Suction unit

The purpose of the suction unit was to obtain an empty cylindrical column in the sand. The following instruments and materials, shown in Plate 1, make up the unit.

(a) Centrifugal fan, model 428F.

(b) Dust extractor.

(c) PVC tubes, 101mm and 127mm diameter.

(d) Hoses, 51mm and 180mm diameter.

(e) Sand extractor tank, 380mm diameter and 760mm height.

(f) PVC tube guide.

The fan removed the sand from the pvc tube and deposited it in the cylindrical tank, while the dust blown out by the fan, was collected by the extractor and fed to a rectangular drawer.

3.6.1 Fan

The size of the fan was based on tests performed using an industrial vacuum cleaner, borrowed for these tests. A vacuum cleaner could have been purchased, but since there was a dust extractor already in the laboratory, by fabricating a tank and purchasing a centrifugal fan it was possible to assemble the complete unit economically.

Specifications of the fan:-

Motor H.P. = 2

Phase = 3

Weight = 33Kg.

3.6.2 Dust extractor

The dust extractor was added to the suction unit for the following reasons:-

(a) To collect the dust, which was then taken and mixed with the sand in the cylindrical tank, keeping the same sample of sand throughout the experimental programme.

(b) To collect the dust and escaped particles for health and safety reasons, i.e. particles were blown out at a very high speed and if not collected could cause injuries to personnel.

3.6.3 PVC tubes

Four different sizes of tubes were used during the preliminary investigation, and these had diameters of 76mm, 101mm, 127mm and 203mm. During the experimental programme the 101mm and 127mm diameter tubes were used for placing the anchor unit and the pressure gauge respectively. Although the 76mm diameter tube was big enough for the insertion of the anchor plates, a vertical anchor embedded in sand could not be obtained i.e. if the pvc tube is off centre by a few centimetres the anchor plate would be touching the wall of the tube.

To facilitate installation, the embedded end of each tube was sharpened. On the other end a flange was fitted. This was made from pieces taken from the 203mm diameter tube and glued together. The flange was to assist in pushing and pulling the tube in and out of the sand.

3.6.4 Hoses

The various individual units, i.e. fan, dust extractor, and pvc tube, were connected together by using different sizes and types of hoses. The cylindrical tank was connected to the inlet of the fan by 51mm diameter hose. The outlet of the fan was connected to the inlet of the dust extractor using a 180mm diameter hose with larger flexibility.

The two diameters the outlet of the fan and the inlet of the dust extractor, were of different dimensions. A cylindrical tube with one end closed and with the other open, was made using a thin steel plate. In the closed end of the tube a 51mm diameter hole was drilled to fit the outlet of the fan to which the tube was fixed, (See Plate 1).

A third hose was needed to remove the sand from the pvc tube, into the cylindrical tank. At first, a hose similar to the one connecting the fan with the cylindrical tank was used. It was found that this was heavy and not flexible enough thus causing problems, i.e. not easy to handle when it was to be placed in the pvc tube. Therefore a more flexible and lighter hose was purchased.

3.6.5 Sand extractor tank (Cylindrical tank)

The tank, 380mm internal diameter and 760mm high, was made from a 2.5mm thick mild steel plate. Outlet and inlet pipes were welded to the tank, Fig. 3.8. The inlet pipe of 38mm diameter was connected to the hose, used for extracting the sand from the pvc tube. The inlet, made of a steel pipe, was bent inside the tank so that its end faced the wall of the tank. The 300mm height (See Fig. 3.8) of the pipe end from the bottom of the tank, was controlled by the size of the pvc tube. The outlet pipe, welded to

the top surface of the tank, was connected to the inlet of the fan. The bottom outlet, which had to be kept blocked during the extraction of the sand, was used to empty the sand into the bin.

3.6.6 Guide

The guide, made of timber, was fixed to a steel hollow section, Fig. 3.3. Different guides were made to accommodate the different sizes of pvc tubes used during the experimental programme. The guide, which provides a cylindrical gap, was made up of two sections bolted together. During the first few experiments it was found that the pvc tube could also be placed vertically in the soil by using part of the guide, shown in Plate 4. In order to save time in performing an experiment, the complementary section of the guide was not used for the rest of the experimental programme. The steel hollow section was secured from moving by bolts acting against the walls of the tank.

3.7 Anchor unit

The unit, shown in Fig. 3.7, consists of the anchor plate, shaft and head, and it was made from mild steel rods. The shaft was screwed both to the plate and the head of the anchor. The anchor unit was connected to the pullout unit using a mild steel pin, (See Plate 4.).

The following anchor plates, shown in Plate 5, were used during the experimental programme:

(a) 25mm diameter plate of 6mm, 13mm, 19mm, 25mm, 51mm, 76mm and 102mm thickness.

(b) 102mm thickness plate of 13mm, 19mm, 25mm, 38mm and 51mm diameter.

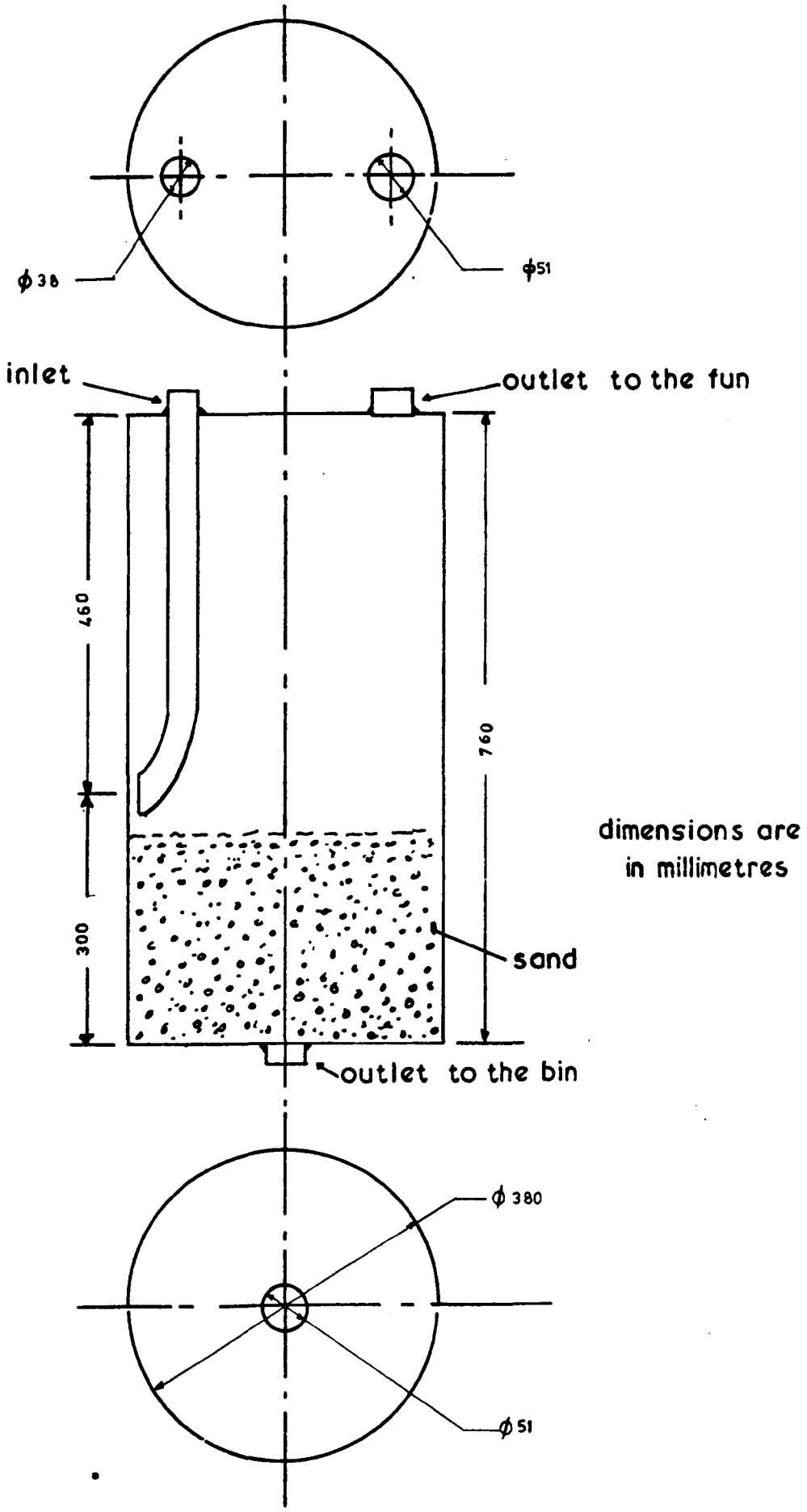

Fig. 3.8 SAND EXTRACTOR TANK

The following shafts, shown in Plate 5, which are mild steel rods of 1050mm in length with both ends threaded were also used.

3mm, 5mm, 6mm, 13mm, 19mm and 25mm diameter.

For the main part of the experimental programme the 5mm diameter shaft was used for the 13mm, 19mm and 25mm diameter plates, and for the plates of 38mm and 51mm diameter the 6mm diameter shaft. The reason for using these shafts is given in a following chapter.

The anchor head, shown in Fig. 3.7, was made using a 25mm diameter mild steel rod, which was machined down to this shape. To avoid any problems, i.e. bending of shaft, caused by the weight of the anchor head, this was designed to be as light as possible. The shaft was screwed to the anchor head and a locking nut was used.

The connection of the anchor unit to the pullout unit was secured by using a mild steel pin of 5mm diameter. Both ends of the pin were threaded to take the corresponding nuts.

3.8 Vibrating unit

The unit was made up of the vibrating table and the vibrator. The purpose of the unit was to compact the soil in the tank.

3.8.1 Vibrating table

The vibrating table, shown in Fig. 3.3, is a modification of the original table which was made by four hollow steel sections. In order to be able to reach the vibrator, should this break down, two opposite sides of the table were removed.

Plate 5

The hollow steel sections, 152mm square and 64mm long, formed the base of the table. On the top of the hollow sections flexible mountings (Tico pads) were glued. A steel plate, 1845mm square and 10mm thick, formed the top of the vibrating table. To increase the stiffness of the plate, channel sections 76mm x 50mm x 6.4mm of different lengths were welded underneath it.

Mild steel plates, 250mm x 190mm x 6.4mm, arranged to sit on the flexible mountings, were bolted to the channel sections.

3.8.2 Vibrator

The vibrator shown in Plate 6 , 3 phase 50 cycles current, has the following specifications:-

Frequency = 2850 vibrations/min.

Power consumption = 500 W

Weight = 31.3 Kg.

Maximum flyweight torque = 6 Kg. cm.

Centrifugal force at 6 Kg. cm. = 570 Kg (1250 lbs)

Maximum current for 220V = 1.9A

Maximum current for 380V = 1.1A

A vibrator with a quick-release holder was chosen rather than a vibrator with a permanent installation. The holder was welded to the 1845mm x 1845mm x 10mm plate of the vibrating table. A footplate is bolted to the vibrator, which in turn is fitted and clamped into the holder.

Plate 6

The flyweight torque of the unit is adjustable from 6 Kg. cm. down to a minimum of 3 Kg. cm. in 5 steps. The adjustment is made by rotating the two movable off-centre weights placed outside the bearings. A few experiments were performed using 80% of the maximum torque, but then it was decided to work on full torque, i.e. 100% in order to obtain the required compaction quickly.

The main advantages of the vibrator are:-

(a) Vibrations are spread over a wide area, so no local overload can occur.

(b) Vibrator can be switched on for a long period of time.

The only disadvantage of the vibrator, is that the bolts of the quick-release holder should be securely tightened, checked and retightened after a running period of 2-3 hours. Failure to do so would result in the vibrator becoming detached from the holder.

3.9 Calibration

Before setting up the apparatus, the recording and pullout units were calibrated.

The recording unit, which includes the load cells and displacement transducers, produced three calibration graphs.

The displacement transducer, connected to the X-axis of the recorder and to the power supply. was fixed to a lathe. Using a magnetic stand, a dial gauge of 50mm maximum deflection was placed touching the moving part of the lathe. The transducer, having a 100mm displacement, was calibrated in two parts, 50mm each part. With the X-Y recorder set on 0.2 V/cm and the power supply giving 9.033V, the graph in Fig. 3.9 was obtained by plotting the displacement on the

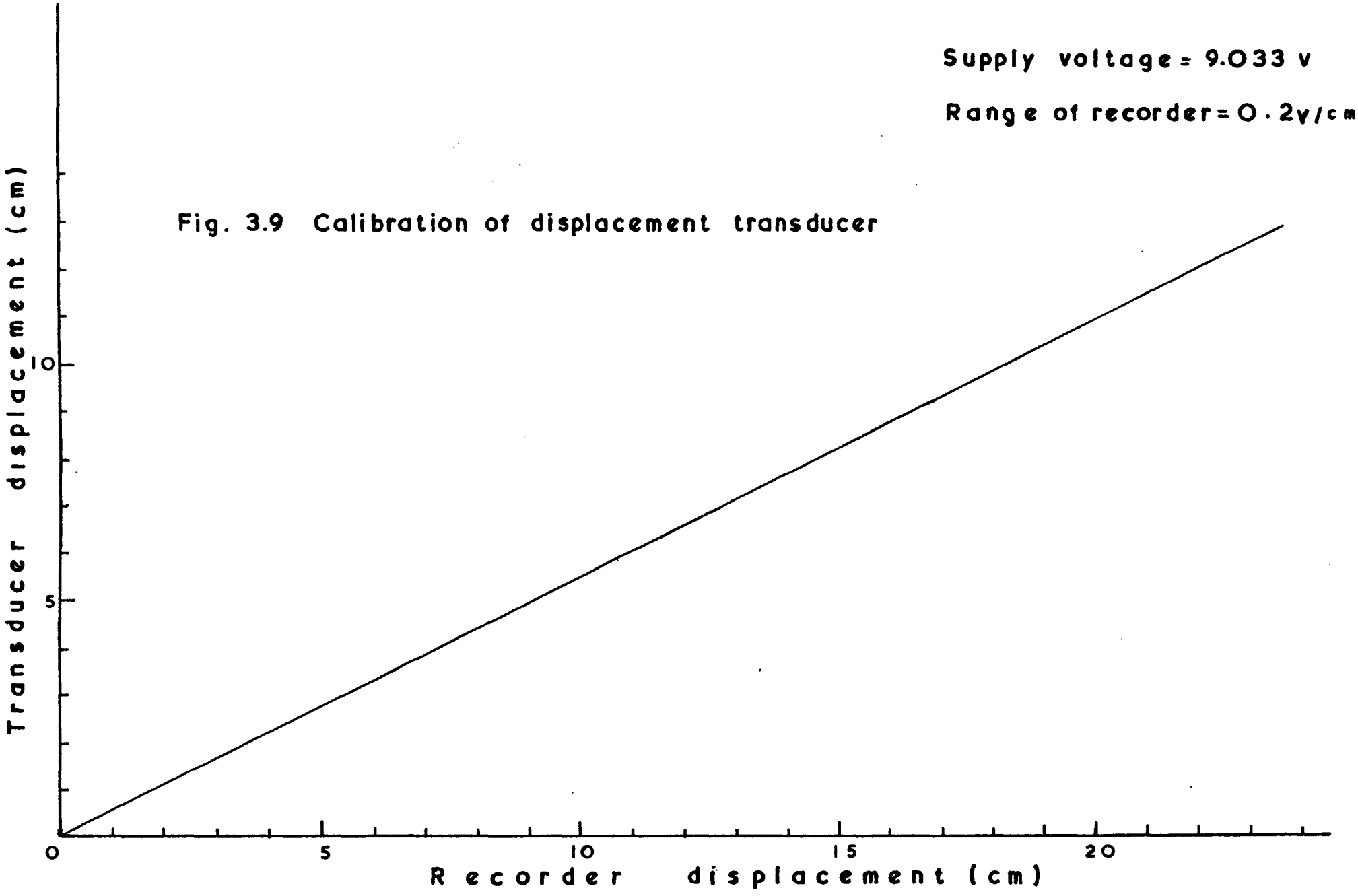

Fig. 3.9 Calibration of displacement transducer

recorder against the dial gauge reading. The graph shows that the voltage-displacement characteristic of the transducer is linear. With the above specified values, i.e. 9.033V and 0.2V/cm, remaining constant, a 5.52mm displacement of the anchor would be represented by 10mm on the X-Y recorder.

For measuring the load on the anchors during the entire experimental programme, two load-cells were needed. These were calibrated in turn by connecting them to the Y-axis of the recorder and to the second power supply.

The load cell with a maximum tension of 2220 N was connected to a universal testing machine. Setting the Y-axis of the recorder on 0.5mV/cm and the power supply on 4.063V, loads of 250 N were applied until the entire range of the load cell was covered. The total load at each step was plotted against the displacement on the recorder and the straight line in Fig. 3.10 was obtained.

The small load cell was removed and the 4500 N load-cell was connected to the testing machine. With the power supply on 4.063V but with Y-axis of the recorder on 1mV/cm, the load cell was calibrated in increments of 500 N, Fig. 3.11.

The load cells and the displacement transducer were checked regularly. Three known loads were applied to the load cells covering the entire range, and the readings on the recorder were compared with the calibration curves. The displacement transducer was checked against a vernier fixed to a stand. A daily check was also done by comparing the ultimate loads and displacements of the anchors.

The voltages of the power supplies were recorded before and after each test. These were found to vary between 0 and 0.2%.

Supply voltage = 4.063v

Range of recorder = 1.0 mv/cm

Range of cell = 500 lbf

Fig. 3.10 Calibration of load cell

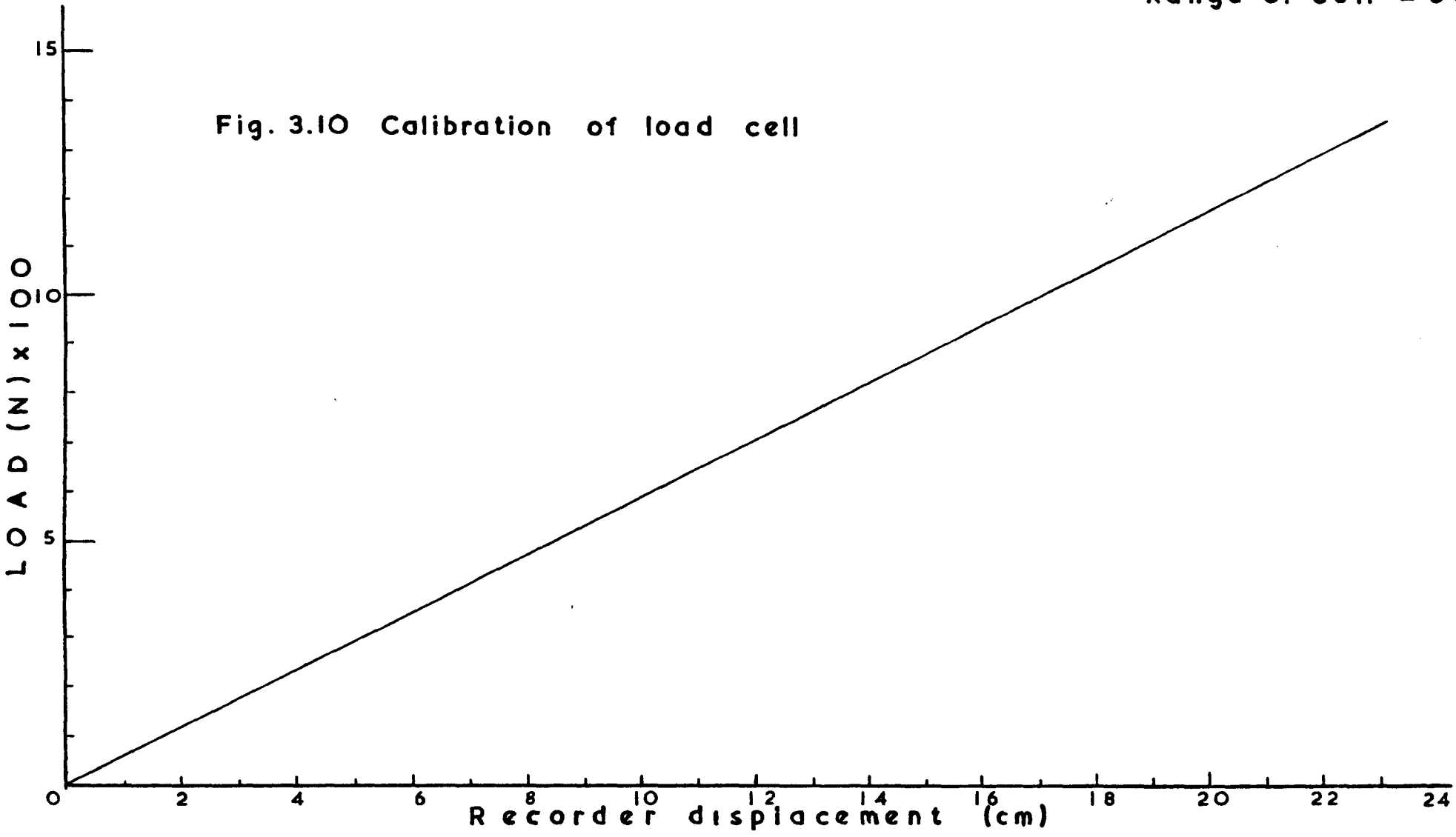

Supply voltage = 4.063V

Range of recorder = 0.5mV

Range of cell = 450 Kgf

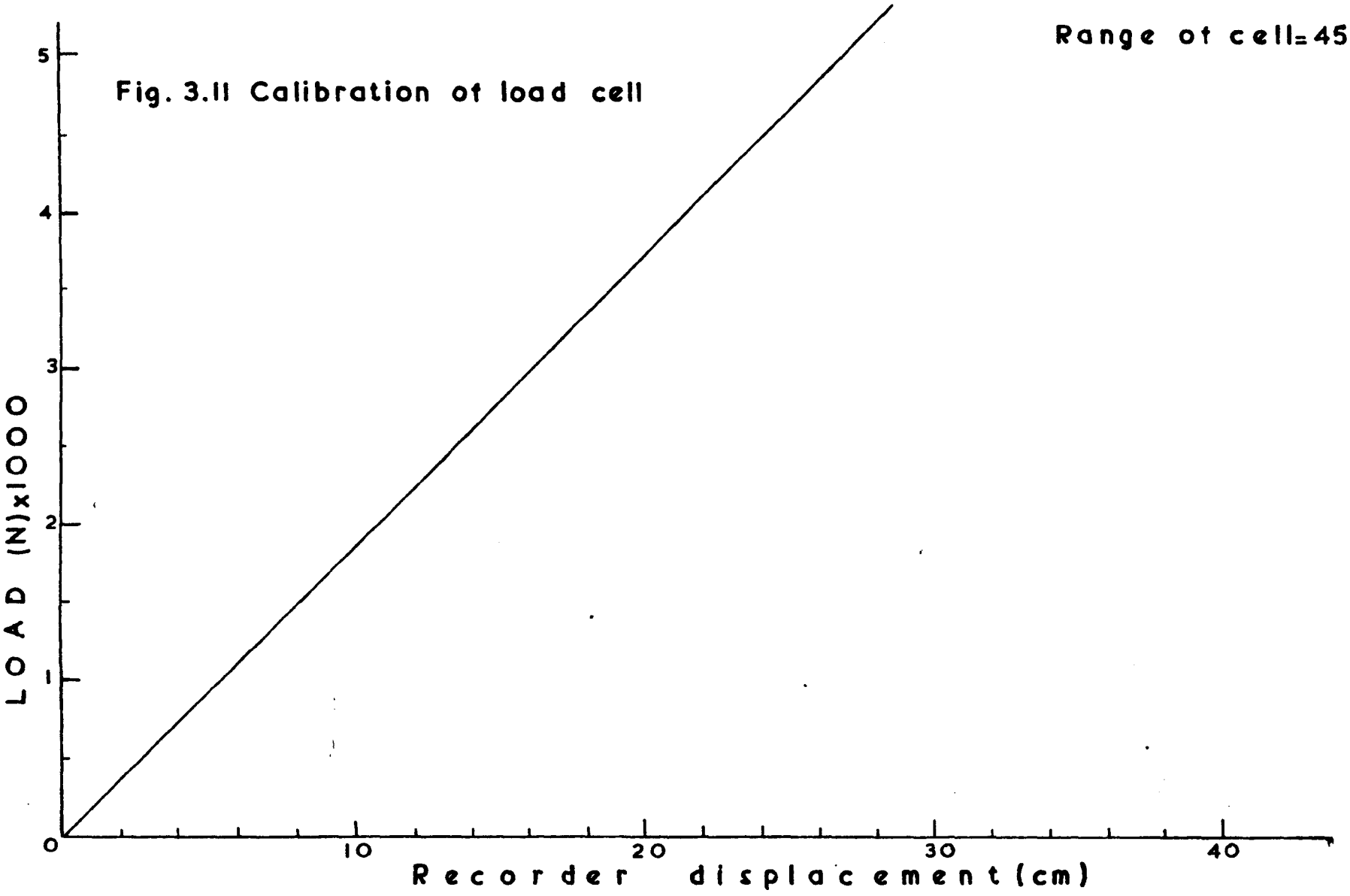

Fig. 3.11 Calibration of load cell

The pullout unit was calibrated to find the rate at which the anchor is being withdrawn out of the sand. With the thyristor set at a certain division, the distance travelled by the screw of the jack in a certain time was recorded. The procedure was repeated for all the 10 divisions marked on the thyristor. The rate in mm/min against the thyristor graduations is shown in Fig. 3.12.

3.10 Disadvantages encountered with the apparatus

A number of parts of the apparatus were modified during the preliminary tests. The improvements were made as to obtain a system which would enable the experiments to be performed accurately, faster and with the minimum of effort.

The main frame, the height of which was found insufficient although during the design it was thought otherwise, presented the following difficulties:-

(a) The insufficient space between the sand surface and the horizontal beam of the frame resulted in the use of different lengths of shaft.

(b) The use of shorter shafts resulted in the displacement transducer interfering with the vertical pullout of the anchor i.e. the transducer was touching the anchor head. The interference was avoided by designing the head of the anchor as shown in Fig. 3.7.

(c) The complete withdrawal of a deep anchor by the pullout unit was not possible.

(d) The use of the entire length of the screw of the jack was not possible, although it was not required.

The mounting of the pulleys above the frame rather than underneath, and the use of different lengths of steel

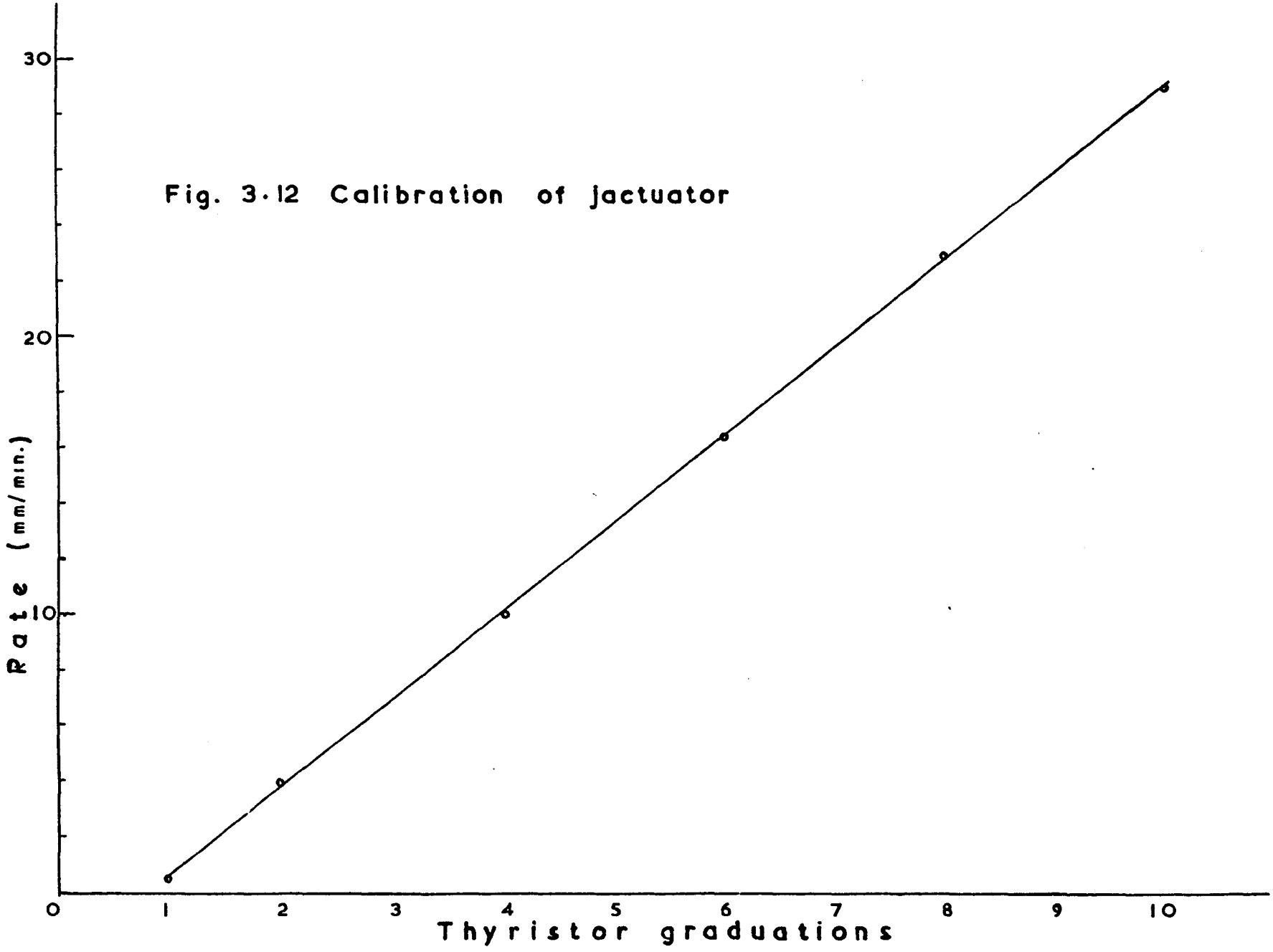

Fig. 3.12 Calibration of jactuator

rods between load cell and anchor head have eliminated some of the difficulties.

In each test, after the load-displacement curve was recorded, the motor was switched off. The vibrator was then switched on and the anchor was removed from the sand by hand in order to save time. The use of larger anchor plates than those used in the experimental programme would require another method for complete removal.

The extractor unit was found to be efficient. Although a 100mm diameter pvc tube would be inserted into the sand easily, a 125mm diameter tube would take more time and effort. Tubes with bigger diameters could not possibly be used due to the insufficient power of the fan. Therefore the maximum size of the anchor plate that can be installed is in fact governed by the power of the fan.

3.11 Observations

The following points should be observed when a test is performed:-

(a) Ensure that the anchor takes a vertical position under the pulley. Failure to do so would result in the anchor being pulled at an angle and the transducer rod sliding off the plate.

(b) Check the distances available to the steel cable and the screw of the jactuator during the experiment, i.e. to obtain the failure of the anchor.

(c) Ensure that the chosen ranges of the Y and X axes of the recorder would cover the ultimate load and the displacement of the anchor.

(d) Check that the thyristor is set at the correct rate; although variation of the rate would not affect the results in this experimental programme.

(e) Ensure that the motor is switched off. Failure to do so would result in the screw of the jactuator leaving the unit or reaching the shell cap of the jack. To avoid damaging the threads of the screw, two control switches could be fitted to the apparatus;i.e. to control the distance travelled by the lifting screw.

CHAPTER IV

METHOD OF PREPARING THE SAMPLE

4.1 General

Several workers, in order to obtain consistent results in their experimental work, used a number of methods to produce a sensible homogeneous and repeatable bed of sand. It is intended to discuss these methods and assess their relative advantages and disadvantages.

(a) Hopper method.

(b) Stirring method.

(c) Tamping method.

(d) Vibration method.

The method used in this research will also be described and its advantages and disadvantages will be pointed out.

4.2 Hopper method

In this method the compaction is controlled during the placing of the soil by the following factors.

(a) The height from which the soil is allowed to fall.

(b) The rate at which the grains are deposited.

The two factors have been dealt with in many published papers (Ref. 1,2,3,4,5,& 6), in which the authors presented methods of controlling them.

Kolbuszewskii and Jones (1961, Ref.2) designed an apparatus with which they were able to control the velocity and intensity of the falling grains. Although the apparatus was constructed to test the principles pointed out by Kolbuszewskii (1948,Ref. 1), the authors found that the

sand bed surface deviated from the level. Kolbuszewskii (1948, Ref. 1) stated that at low intensity the falling sand would give:-

(a) High porosity with low velocity

(b) Low porosity with high velocity.

He also said that the porosity increased as the intensity increased.

Researchers (Ref. 3,4,5 & 6) despite having used more sophisticated apparatus, found the following faults with the method:-

(a) Deviation of the sand bed from the level.

(b) Currents, set up by the displaced air due to the falling sand, disturb the uniformity of the bed.

(c) Reproducibility of the sample is prevented due to:-

(i) Loss of dust from the soil

(ii) Grain crushing.

(d) Sand in the tank is divided into layers, with each layer having a different porosity.

4.3 Stirring method

The method was used first by Carr (1970, Ref. 23) and later on by Yilmaz (1971, Ref. 32). The sand placed in the tank by bucket, was stirred using an 8mm diameter rod to obtain a loose state i.e. density of 1540 kg/m^3. The repeatability and uniformity of the sand sample was not

fully investigated by the above researchers, although penetrometer tests were performed after the ultimate load of the anchor was obtained.

4.4 Tamping method

The tamping method is used to produce a dense bed of sand. The sand is placed in layers by bucket and each layer of sand is vibrated by a Kango hammer. The method was used by Carr (1970, Ref. 23) to obtain a density of 1680 kg/m^3 for his dense sand.

An investigation into the state of the sample after tamping showed the following faults.

(a) The sample was separated into distinct homogeneous zones of porosity, (Ref. 8).

(b) The value of K_o was very high and has been reported to be greater than the coefficient of earth pressure in passive failure (Rankine state), (Ref. 7 & 24).

4.5 Vibration method

The sand could be directly placed in the tank in one filling and compaction is carried out by vibrating the tank horizontally or vertically, or in both directions.

A great deal of experimental work was carried out by different researchers in order to relate motion characteristics, i.e. acceleration and frequency, with soil parameters, i.e. porosity, density, shearing strength.

4.5.1 Vertical Vibration

The following findings were reported in papers dealing with the vertical vibration:-

(a) The density increases to a peak and then reduces as the acceleration increases. The position of the peak depends on the frequency for a certain amplitude, (Ref. 9 & 10).

(b) The shear strength of the sand decreases with the acceleration increasing, (Ref. 11).

(c) The density varies within the specimen, i.e. different densities at different depths, (Ref. 11).

(d) The density varies with the intensity of the vibration (Ref. 11).

(e) The density depends on the method of placing the sand i.e. during vibration, or before vibration (Ref.11).

(f) The acceleration required to produce the maximum density for given frequency depends on the particle size distribution and particle angularity, (Ref. 11).

(g) Repeatability of results depend on the particle shape. Sand with high mean sphericity, has poor repeatability (Ref. 12).

Therefore in order to obtain the maximum density of the sample the following should be taken into account:-

(i) Overburden should be kept as small as possible.

(ii) Vibration should not be intense.

(iii) Sand should be poured very slowly during vibration.

4.5.2 Horizontal Vibration

The following conclusions were reached by many researchers who subjected their sand to horizontal vibration:-

(a) Small vibratory motion produces a large volume change in the sand, (Ref. 13).

(b) For any frequency, amplitude and soil gradation, the density and settlement of the sample increases very quickly in the first few seconds. After a few seconds their maximum is reached, (Ref. 13).

(c) Density depends on the soil gradation, (Ref. 13).

  (i) Large change in density occurs with the smaller uniformity coefficient.

  (ii) Maximum density occurs with the largest uniformity coefficient.

  (iii) For the soil gradations with the same uniformity coefficient, the largest increase in density occurs in the soil with the largest grain size.

(d) The frequency effect on the soil is greater than the amplitude effect, (Ref. 13).

(e) Vibration reduces the angle of internal friction, (Ref. 14).

(f) Void ratio decreases exponentially with acceleration (Ref. 14).

(g) Shear strength is reduced as the intensity of vibration increases, (Ref. 14).

4.6 Disadvantages of the methods

The methods used by previous researchers, involve removal and placement of the sample. Considerable manual work and time, depending on the amount of soil to be used, is required to carry out a single experiment.

Some methods i.e. hopper and tamping, require the holding of the anchor during deposition of the sand. The structure holding the anchor and also the anchor itself interfere with the compaction. Even without the obstructions, it was pointed out by various papers as shown in the foregoing sections that perfect uniformity in the sand could not be obtained. The obstructions would also interfere with the repeatability of the soil sample.

McMullan (1975, Ref. 24) stated that the compacted sample obtained using vibration suffers from the following disadvantages:-

(a) Unaturally high horizontal stresses are induced.

(b) Relatively large variations in the porosity are produced.

4.7 Method used in this research

The suction unit consisting of : the pvc tube, flexible hose, cylindrical tank, fan and dust extractor, was described in Chapter III. The placing of the anchor and the preparation of the sand sample will be given in steps. The tank was filled with sand, which will be used throughout the entire experimental investigation.

The following steps are observed:-

(a) The cork is inserted in the outlet of the cylindrical tank, see Plate 1.

(b) The fan and dust extractor are switched on.

(c) The pvc tube is placed in the guide and on the surface of the sand.

(d) The flexible hose is inserted into the pvc tube touching the sand. While the sand is sucked out the tube is pushed into the soil.

(e) With the flange of the pvc tube reaching the top surface of the guide, the hose is taken out and both fan and extractor are switched off.

(f) The anchor is suitably suspended at the required depth of embedment.

(g) With the anchor placed in the pvc tube, the tube is pulled out of the sand.

(h) The anchor attachment is released and the tube is taken away leaving an embedded anchor in sand.

(i) The sand is emptied into the bin by removing the cork from the outlet of the cylindrical tank.

(j) The sand in the bin, mixed with the dust in the extractor, is emptied around the perimeter of the tank.

(k) The vibrator is switched on for a given duration, discussed in a following chapter.

4.8 Position of the cylindrical tank and size of pvc tube

During the preliminary investigation the position of the cylindrical tank was investigated. The tank was placed at

different heights above the surface of the sand and the time taken to sink the 101mm (4in.) diameter pvc tube was recorded. It was found that, with the top surface of the cylindrical tank being on the same level as the surface of the sand and the fan unit, little effort and time was needed to place the tube in the sand.

The pvc tubes mentioned in Chapter III, were used to find the biggest diameter of tube that can be inserted into the sand by the suction unit. Although the 127mm (5in.) diameter tube was sunk, twice the time and effort of that of the 101mm (4in.) diameter was needed. Bigger tubes were impossible to place in the sand.

4.9 Advantages and disadvantages of the method

The method has the following advantages:-

(a) The sand is placed in the tank once.

(b) The compaction requires no manual work.

(c) The process of embedding the anchor is easy and quick, taking between 5 minutes and 10 minutes depending on the size of the pvc tube.

(d) The amount of sand taken out of the tank is no more than a fraction of a cubic metre, i.e. depending on diameter and height of the pvc tube.

The only disadvantage of this method, is that the size of the anchor plate that can be used is limited by the suction unit. Disadvantages reported by other researchers such as K_o being too high and porosity varying, will be discussed in later chapters.

CHAPTER V

SAND AND ITS PROPERTIES, VIBRATION CHARACTERISTICS

5.1 General

The purpose of this research as mentioned previously, is to investigate the behaviour of ground anchors in sand. This chapter deals with the physical properties of the sand and the characteristics of the vibrating tank.

5.2 Sand

The type of sand used during this investigation was Halls No. 1. The sand was delivered wet and spread on the laboratory floor in 75mm thickness. In order to dry the sand, it was turned over twice a day for about two months. The dry sand was then passed through a No. 14 sieve to remove larger particles. It was thought that the dust should be removed by passing it through a sieve with small mesh i.e. No. 72, but the idea was abandoned due to the large quantity of sand in question.

5.3 Engineering properties

The sieve analysis test was performed and the grading curve in Fig. 5.1 was obtained. From the curve the following information is obtained:-

(a) Medium sand i.e. 85% of the grains have a size between 0.2mm and 0.6mm.

(b) Poorly-graded sand i.e. most of the grains are about the same size.

(c) Effective size is about 0.2.

(d) Uniformity coefficient is about 1.75.

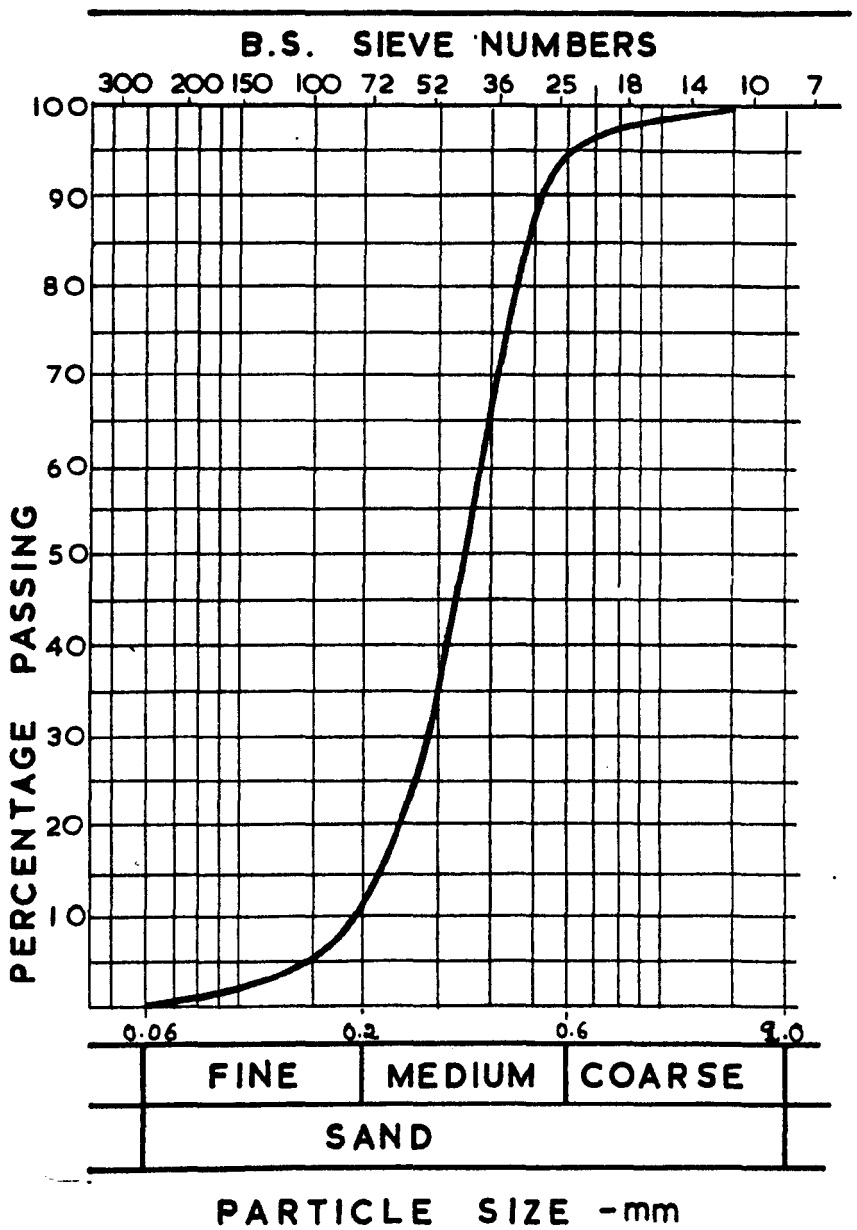

Fig. 5.1 PARTICLE SIZE DISTRIBUTION

5.4 Angle of internal friction

Standard constant rate of strain shear box tests were performed to obtain the angle of internal friction of the sample. From the tests, see Appendix B, the true angle of internal friction, i.e. taken into account the dilatancy effect, was found to be 43.2° for a density of 1.701 gr/cm^3. The angle of internal friction of sand with densities 1.566 gr/cm^3 and 1.674 gr/cm^3 was found to be 31.8° and 40.2° respectively.

5.5 Density

5.5.1 General

Because densities between loose and dense soil are difficult to reproduce using conventional methods, most of the experimental work on ground anchors was performed in loose or dense sand.

The maximum and minimum densities depend on the type of the soil. Bemben and Kupferman (1975, Ref. 48) found the maximum and minimum densities of their Sunderland sand to be 1.86 gr/cm^3 and 1.41 gr/cm^3 respectively. But they found those of their BBY sand to be 1.58 gr/cm^3 and 1.2 gr/cm^3.

Carr (1970, Ref. 23) used the Kolbuszewskii (1948, Ref. 1) method to calculate the maximum and minimum density of his sand. These were 1.799 gr/cm^3 and 1.402 gr/cm^3 respectively. He gave the bulk densities of his loose and dense sand states, used in his experimental work on ground anchors, to be about 1.532 gr/cm^3 and 1.685 gr/cm^3.

Larnach (1972, Ref. 46) who used a vibrating table to obtain a reproducible bed of sand, calculated the local densities of his dry sand by embedded tins in different places of the

sample. He obtained the overall density of his sand by considering the total weight of the soil and the volume occupied by it.

McMullan (1975 Ref. 24), who also used a vibrating table, divided the depth of the sand into three layers, i.e. 25cm each layer. In each of his layers, McMullan placed open tins of 80mm diameter and 25mm deep and determined the local densities of the sand for 25 seconds of vibration.

The top and bottom layers gave the same density, i.e. 1.650 gr/cm^3, while the middle layer gave a smaller value, i.e. 1.580 gr/cm^3. He explained the difference between the values, by saying that the sand in the middle layer had been through the minimum porosity at the optimum acceleration, whilst the top and bottom layers were still approaching it, i.e. part of the sand mass had been over-vibrated. McMullan then reduced the vibration time to 15 seconds and calculated the density over the tank to be 1.570 $\pm$ 0.020 gr/cm^3.

It was thought necessary as part of the investigation into the state of the sample, that the variation of the density with the depth of sand and the time of vibration should be determined. The method of using tins to find the local densities, involve the removal and replacement of the sand for each test. Larnach and McMullan in order to avoid wasting considerable time and manual work emptying their tank, designed one side of their tank to be formed by three removable sliding doors. Since a great number of tests were needed to determine the variation of density with different parameters, i.e. depth and time of vibration, an easy and quick method was required.

A density tube, designed and manufactured in the laboratory, gives the variation of the density of a column of sand of 60mm diameter.

5.5.2 Density tube

The density tube, Fig. 5.2, was made from a 1200mm long mild steel tube of internal and external diameter of 60mm and 76mm respectively. The tube consists of the base, the intermediate sections and the top section.

(a) Base, Fig. 5.3

A length of the mild steel tube, 150mm long, was welded to a circular plate of 88mm diameter and 5mm thickness. To the plate, two half pulleys of 28mm external diameter and a piece of mild steel of 9.5mm x 25mm x 28mm with two tapped holes were welded. In the plate, at each end of the half pulleys, a hole of 4.5mm diameter was drilled. The top end of the 150mm long tube was modified to accommodate the first of the intermediate sections. The external diameter was machined from 76mm down to 70mm. A V-shape groove 6mm wide and 1.6mm deep, was formed round the new perimeter of the tube.

In order to provide a flat surface to the bottom of the base and also keep the steel cables in place, i.e. in the grooves of the pulleys, a cup made from thin steel plate was screwed to the 9.5mm x 25mm x 28mm plate.

(b) Intermediate section, Fig. 5.4

The section was made from 175mm long tube. The length of 25mm from each end of the tube was modified. The internal diameter of one end was increased from 60mm to 70mm in order to fit the top of the base. Four tapped holes, 6mm diameter, were drilled round the modified perimeter to accommodate the 4mm long V-shape grub screws. The other end of the intermediate section was modified to the specifications of the base top. Although the section

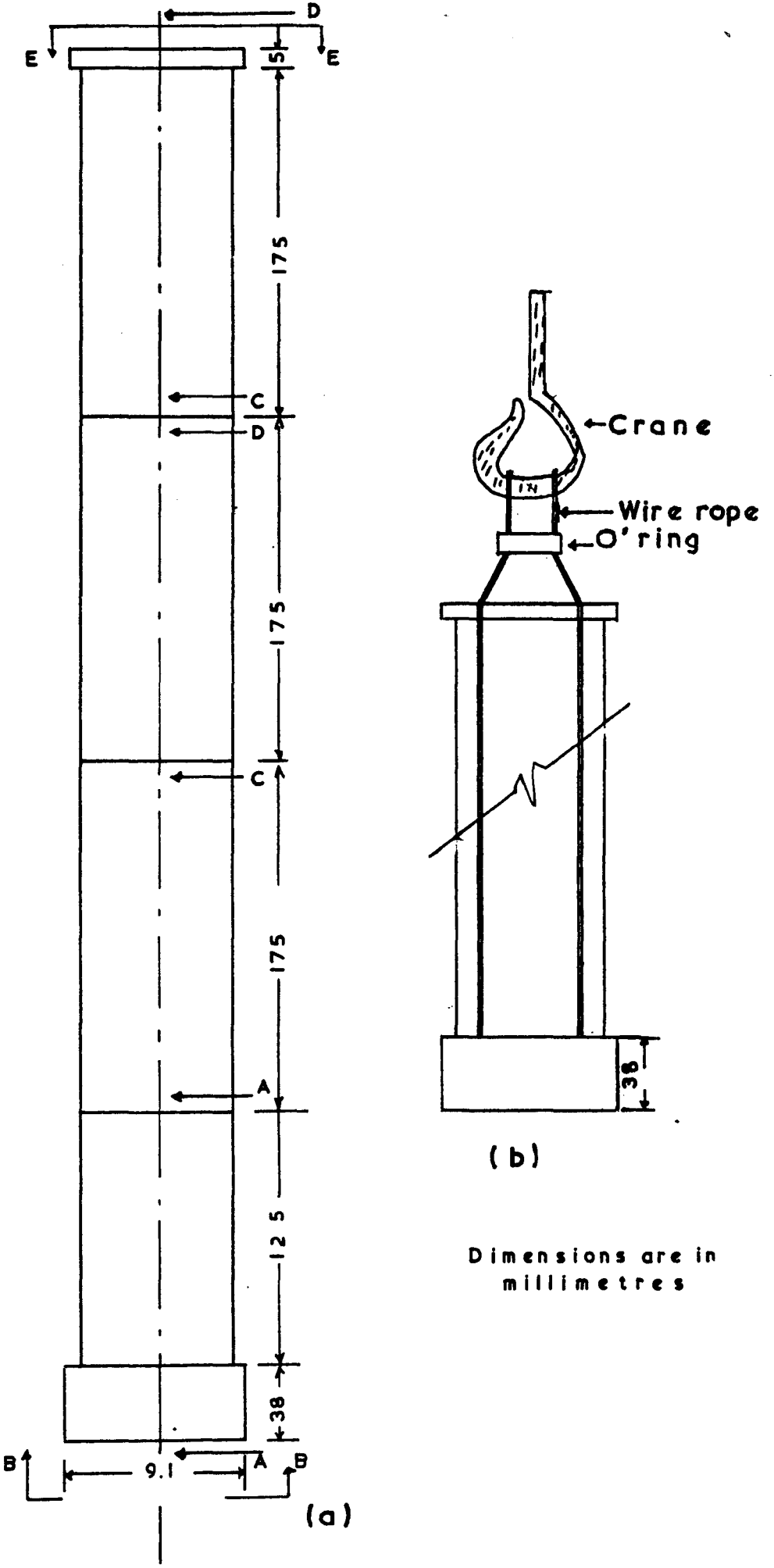

Fig. 5.2 Density tube

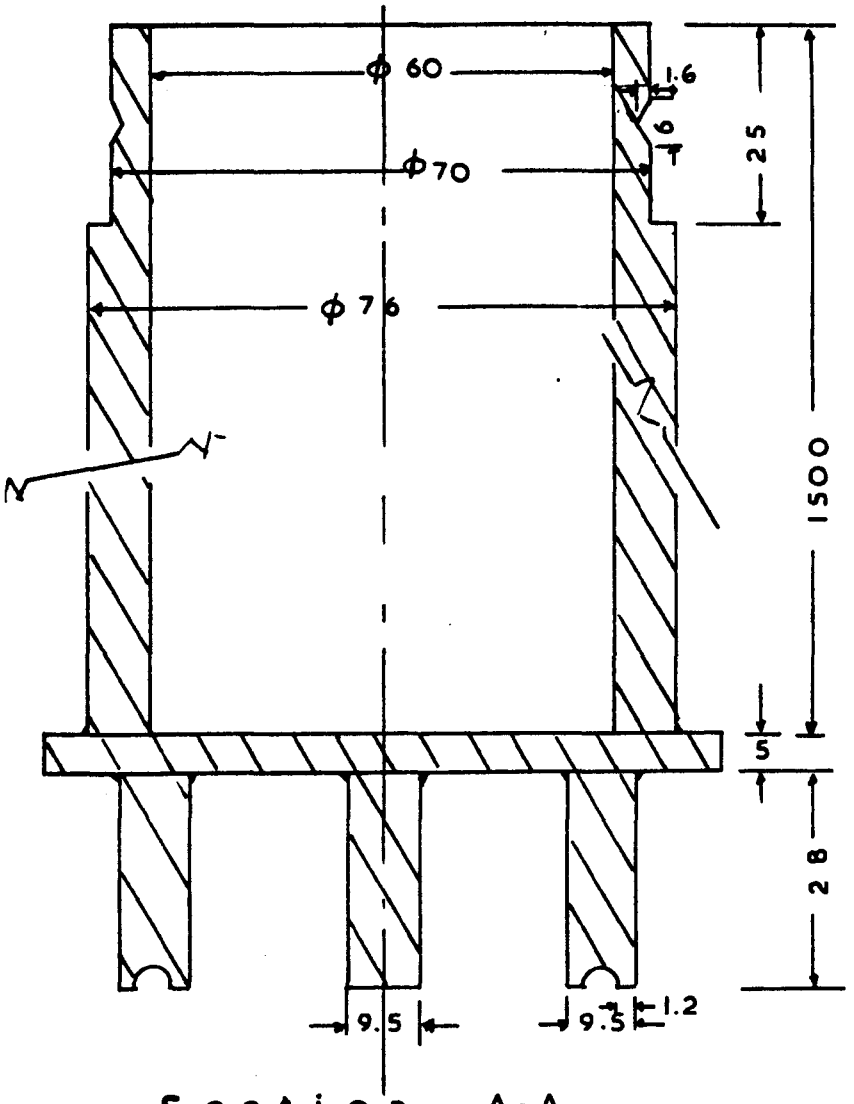

Dimensions are in millimetres

Section A-A

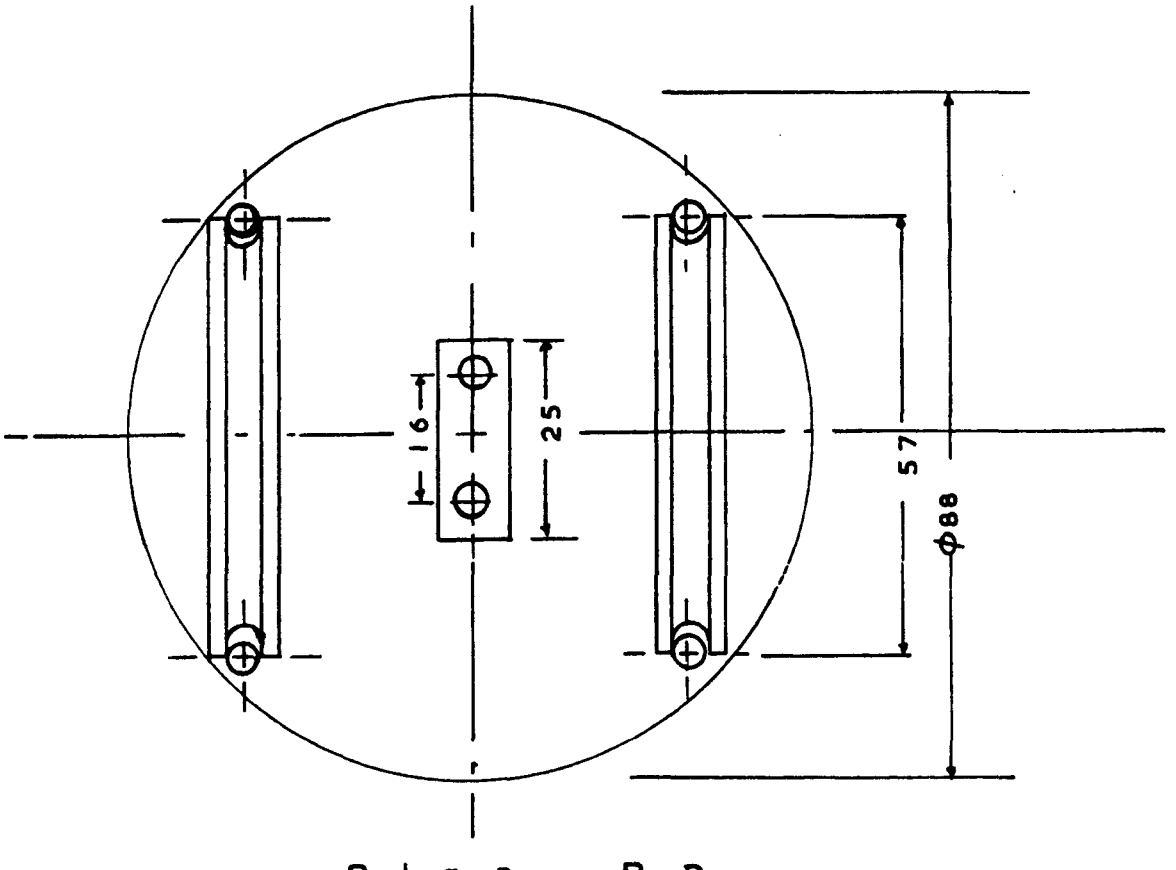

Plan B-B

Fig. 5.3

is 175mm long, only 150mm of its length comes into contact with the soil when the density tube is filled. The 25mm of the 175mm cover part of the section below.

(c) Cable guide, Fig. 5.5

It is a flat ring with internal and external diameter of 60mm and 86mm respectively and with 5mm thickness. Two 6mm diameter and two 4mm diameter holes were drilled at the positions shown in the figure. Four gaps were also formed in the ring directly above the four holes in the plate of the base. The guide, fitted to the top section and kept in place by two 6mm nuts, prevented the density tube from overturning when this was supported by the crane, Fig. 5.2.

5.5.3 Density measurement

The density tube is assembled as shown in Fig. 5.2, and the grub screws are tightened. The tube is then inserted into the cavity formed in the sand using the 101mm diameter pvc tube, and kept vertical while the pvc tube is withdrawn. The cable guide is removed and the cables are spread away from the tube to avoid interference with the movement of the sand particles. The sand is then vibrated for a certain duration. The layer of sand,i.e. 50mm covering the tube, is removed without disturbing the sand in the density tube. The cable guide is fitted to the top section and the cables are suitably connected. After the ends of the cables are connected to the crane, the tube is withdrawn from the tank without disturbing the contained sand and placed on a polythene sheet. The grub screws in the top section are loosened,and the section is removed allowing the sand to fall on the polythene sheet. The sand obtained from each section is collected and weighed,and hence the density is calculated.

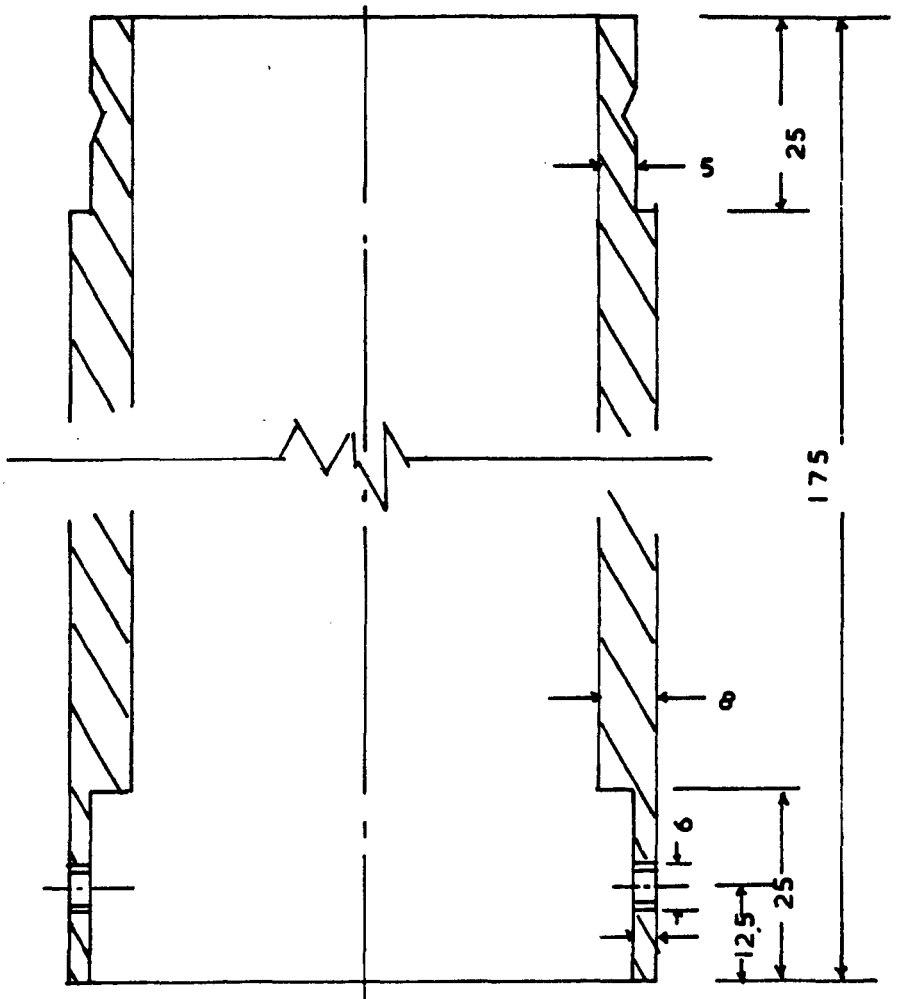

Section C-C

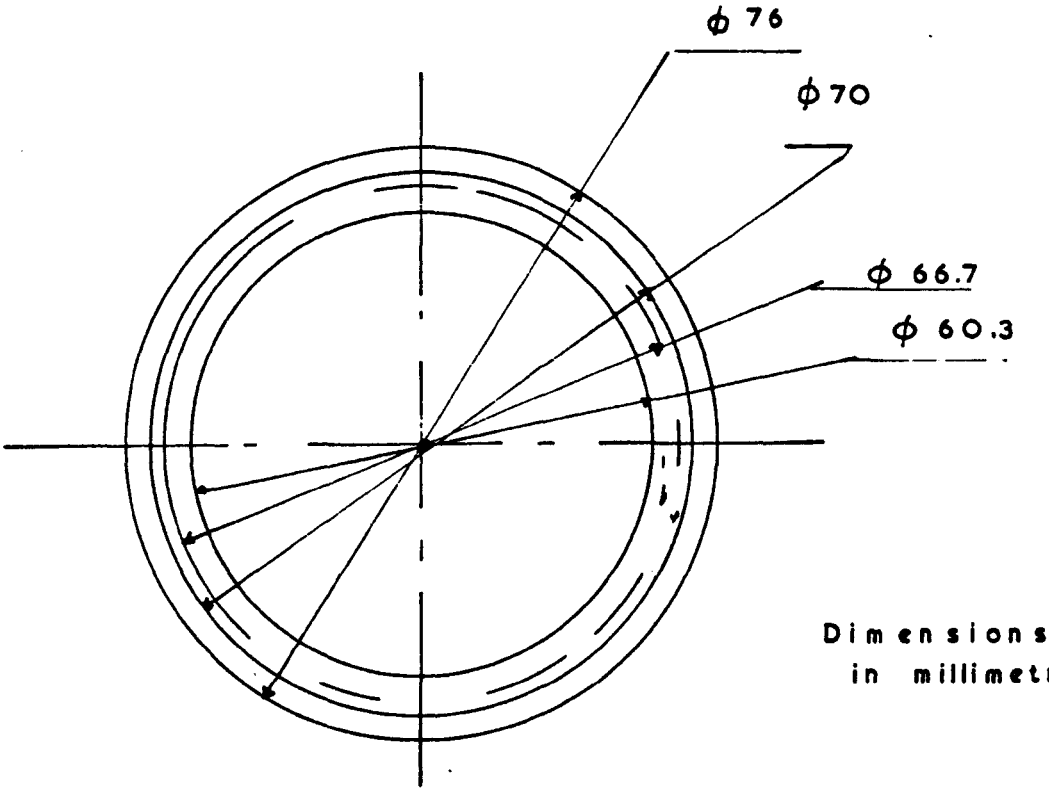

Dimensions are in millimetres

Fig. 5.4

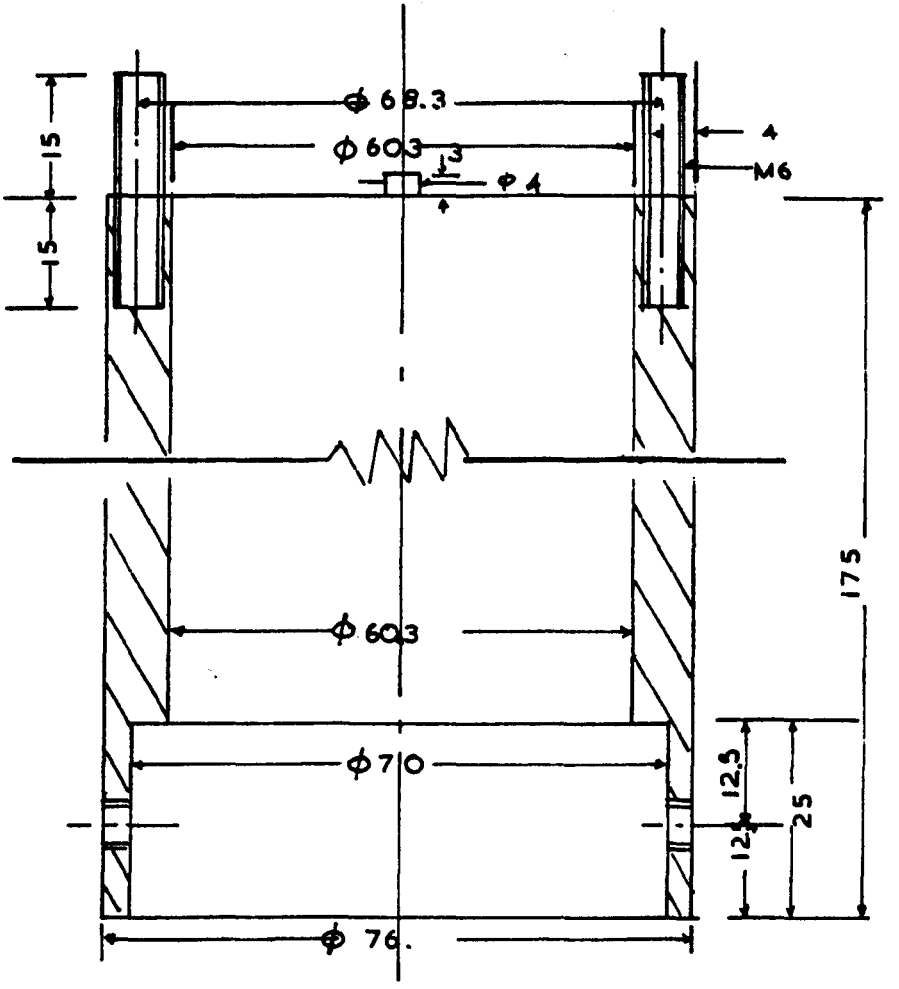

Section D-D

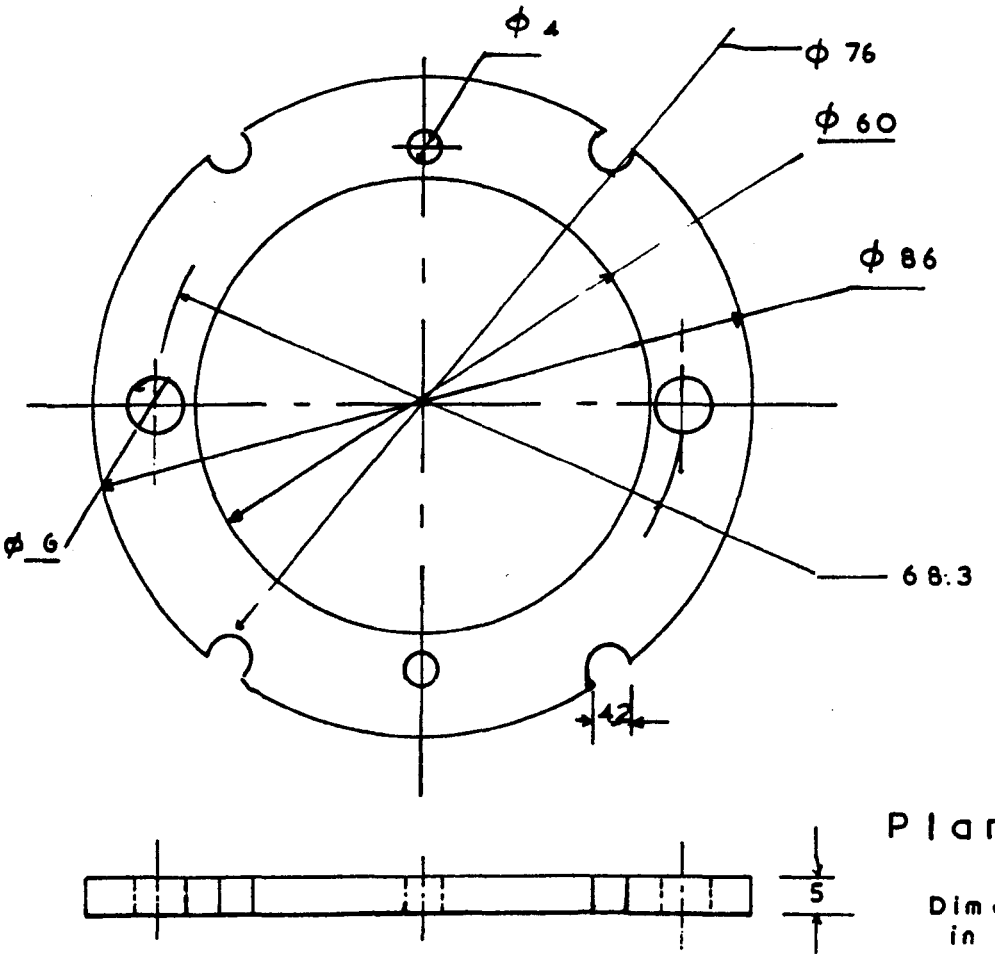

Plan E-E

Dimensions are in millimetres

Fig. 5.5

5.5.4 Results

The density distribution of four different times of vibration, i.e. 10, 20, 30, and 45 minutes was determined. For each time of vibration, four tests were performed and the average density of each layer of sand was calculated. The results are given in Table 5.1.

5.5.5 Discussion

Examination of Table 5.1, reveals that:-

(a) For a given time of vibration the density decreases with the depth of the sand.

(b) The density increases with the vibration time, and the increase varies with the depth of the sand. As the vibration time increases the middle layers are approaching the same density, while the densities of the top and bottom layers are still increasing.

The low value (i.e. 1.677 gr/cm^3)of the bottom layer can be explained by the fact that the sand particles near the bottom of the tank are affected firstly, by the overburden and secondly, by the continuous motion of the of the vibrator, which is attached underneath the tank. The high density value of the top layer could also be explained by the movement of the particles, i.e. they are free to move since there is no overburden to restrict their motion.

Although it may be debatable as to whether the obtained values are the actual values of the local densities, work carried out by Alyanak (Ref. 10) has suggested that the restriction of the particles by the tube may not cause a significant error.

TABLE 5.1

DENSITY DISTRIBUTION

DEPTH (cm)	DENSITY (gr/cm^3)			
	TIME OF VIBRATION (min)			
	10	20	30	45
5 - 20	1.692	1.705	1.709	1.738
20 - 35	1.657	1.685	1.686	1.700
35 - 50	1.655	1.678	1.685	1.700
50 - 65	1.653	1.673	1.679	1.700
65 - 80	1.645	1.657	1.661	1.677

5.6 Vibration Characteristics

5.6.1 General

The sand tank is vibrated in two directions i.e. vertical and horizontal. The motion in both directions is sinusoidal and therefore the characteristics of the vibration could be completely described by any two of the following parameters:-

(a) Frequency, f

(b) Maximum velocity, V_m

(c) Maximum acceleration, A_m

(d) Amplitude, a

The parameters are related, see Appendix C, by the following expressions:-

$$V_m = 2\pi a f \qquad (1)$$

$$A_m = 2\pi f V_m \qquad (2)$$

Where:-

T = period

ω = angular velocity

5.6.2 Experimental procedure

The following instruments, shown in Plate 7, were used to record the amplitude and frequency of the vibration.

(a) Cambridge Universal Vibrograph

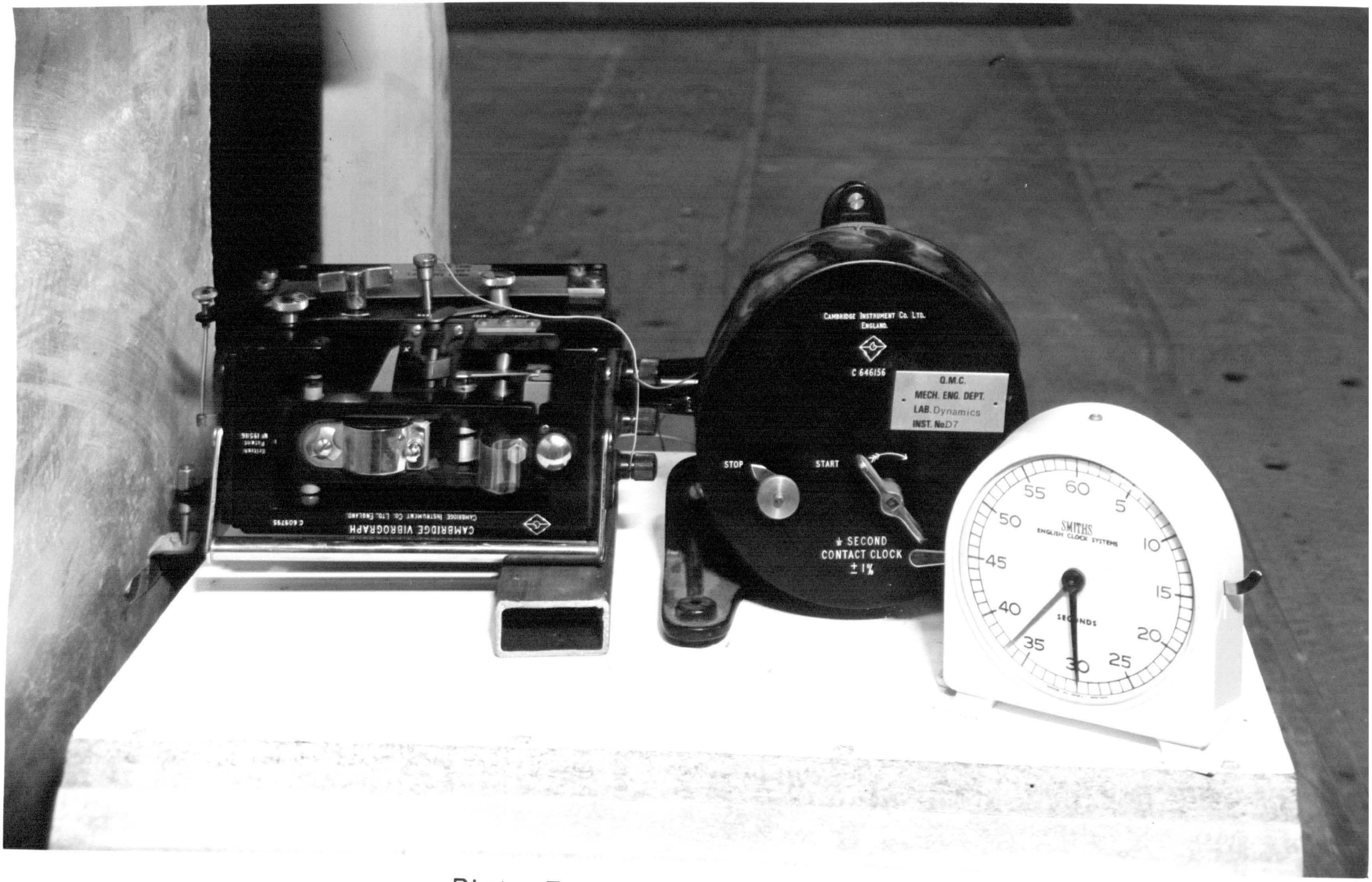
CAMBRIDGE VIBROGRAPH
CAMBRIDGE INSTRUMENT CO. LTD.
ENGLAND.
C 646156
Q.M.C.
MECH. ENG. DEPT.
LAB. Dynamics
INST. No. D7
STOP
START
SECOND
CONTACT CLOCK
± 1%
SMITHS
ENGLISH CLOCK SYSTEMS
SECONDS
60
5
10
15
20
25
30
35
40
45
50
55

Plate 7

(b) Cambridge Time Marker, 1/10 second time interval

(c) Stop watch

(d) 6 Volt battery

In order to investigate the distribution of the acceleration, eight points were marked on the outside surface of the tank i.e. four points on each of the two adjacent sides. At each point, the vibrograph was placed to act as a horizontal and vertical vibrograph. The vibrations recorded on the film were magnified and the amplitudes were measured.

5.6.3 Results

The recorded amplitudes and the calculated accelerations are given in Table 5.2. The frequency of the motion was 47.5 cycles/sec.

5.6.4 Discussion

Fig. 5.6 showing the distribution of acceleration in terms of the acceleration due to gravity, reveals that:-

(a) The horizontal acceleration increases with the height of the tank.

(b) Although the horizontal acceleration should be greater in the plane in which the vibrator operates, this is not so.

(c) The distribution of the vertical acceleration does not show any significant trend.

(d) The maximum accelerations in the vertical and horizontal directions, are well above the value of the acceleration due to gravity i.e. 5.87g and 2.16g respectively.

TABLE 5.2

ACCELERATION DISTRIBUTION

POINT	HORIZONTAL DIRECTION		VERTICAL DIRECTION	
	a (mm)	A_m $(\frac{mm}{sec^2})*10$	a (mm)	A_m $(\frac{mm}{sec^2})*10$
1	0.019	169.2	0.023	196.2
2	0.024	211.5	0.033	296.2
3	0.024	211.5	0.019	169.2
4	0.017	148.1	0.024	211.5
5	0.024	211.5	0.065	575.4
6	0.019	169.2	0.048	423.1
7	0.024	211.5	0.019	169.2
8	0.019	169.2	0.021	186.2

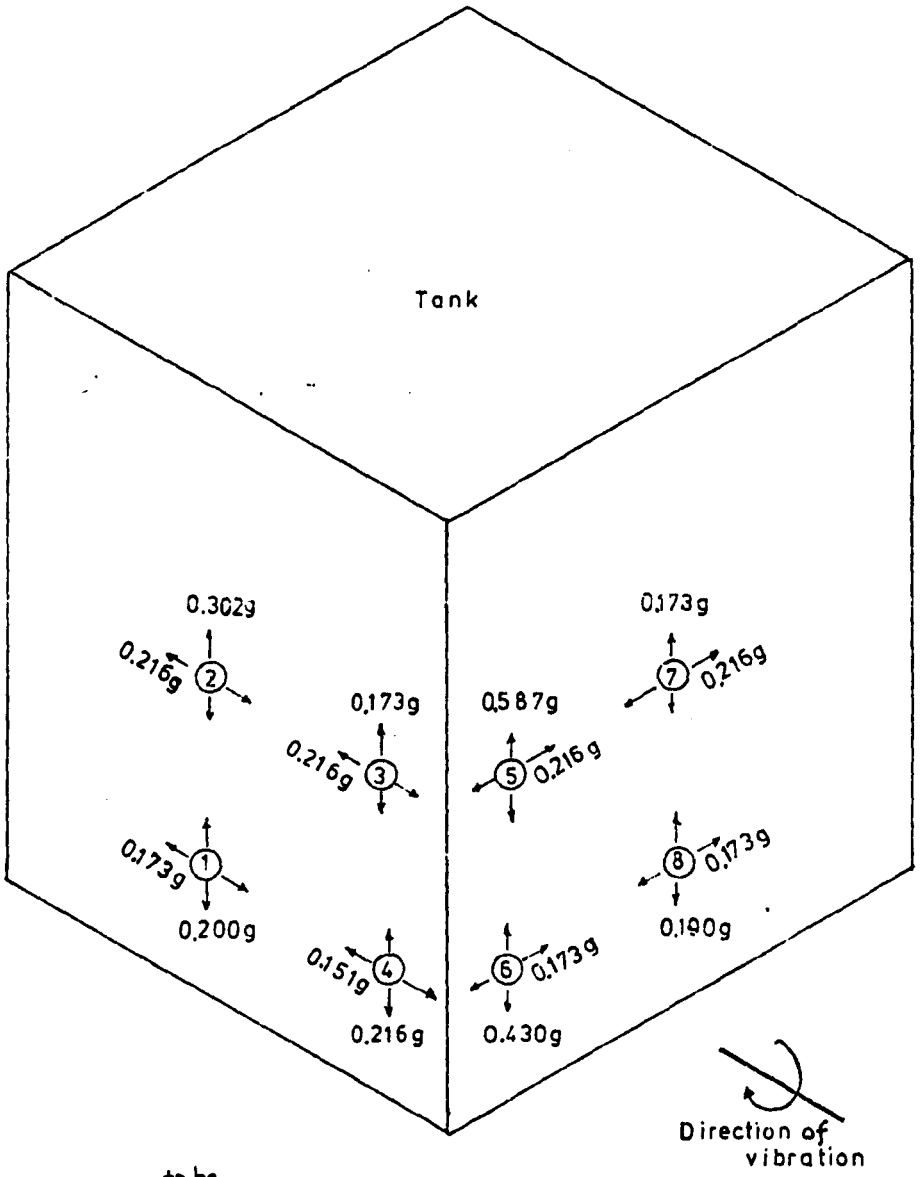

to be
ACCELERATION MULTIPLIED BY 10

AVERAGE VERTICAL ACCELERATION = 2.78g

" HORIZONTAL " = 1.85g

Fig. 5.6 Distribution of acceleration

McMullan (1975, Ref. 24) who carried out tests in order to determine the distribution of the vertical acceleration on one side of his vibrating tank, also found that the vertical acceleration varied from point to point without following any particular pattern. In order to obtain some information on the state of his sample, McMullan used Selig's (1963, Ref. 11) findings. He assumed that his sand, vibrated for 15 seconds, had not reached its maximum value, and therefore very little energy would have gone into increasing horizontal stresses. Using Selig's graph, maximum acceleration against frequency (Fig. 5.7) McMullan also stated that his frequency of 50Hz and maximum acceleration ratio of 0.33 placed the density in a set of parallel constant density values. He concluded that, since the density would decrease but it would be independent of frequency as the acceleration ratio decreased, the density would be constant and repeatable throughout his experimental programme, although this would vary through the tank.

The values obtained by the author, i.e. 47.5Hz and 2.78g, place the density of the sand in the innermost contour line, 1.75 gr/cm^3, on Selig's graph and therefore, according to Selig the density would be constant and repeatable throughout the experimental programme. The densities obtained using the denstity tube agree well with the above values. The small difference in the two values could be explained by the following facts:-

(a) Selig's investigation was performed using vertical vibration whilst the author's tank was vibrated in two directions.

(b) There is no evidence that the sand particles have the same acceleration as the vibrating tank itself.

Load - displacement curves, obtained with anchors embedded in sand, showed that the results are repeatable for any time of vibration.

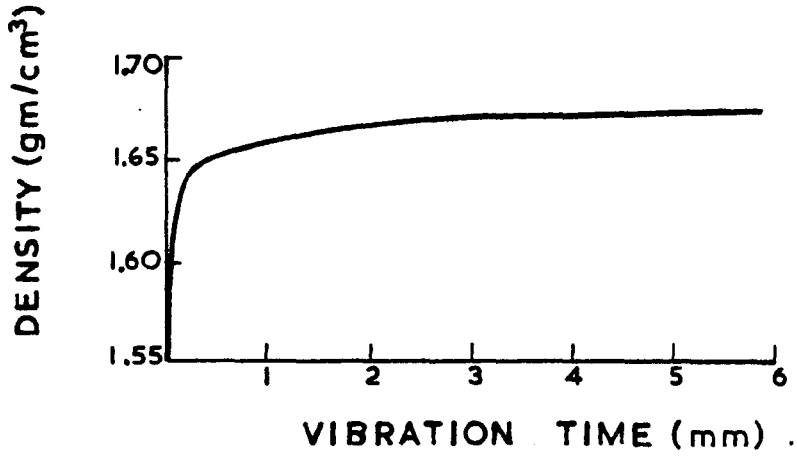

(a)

(Selig, 1963)

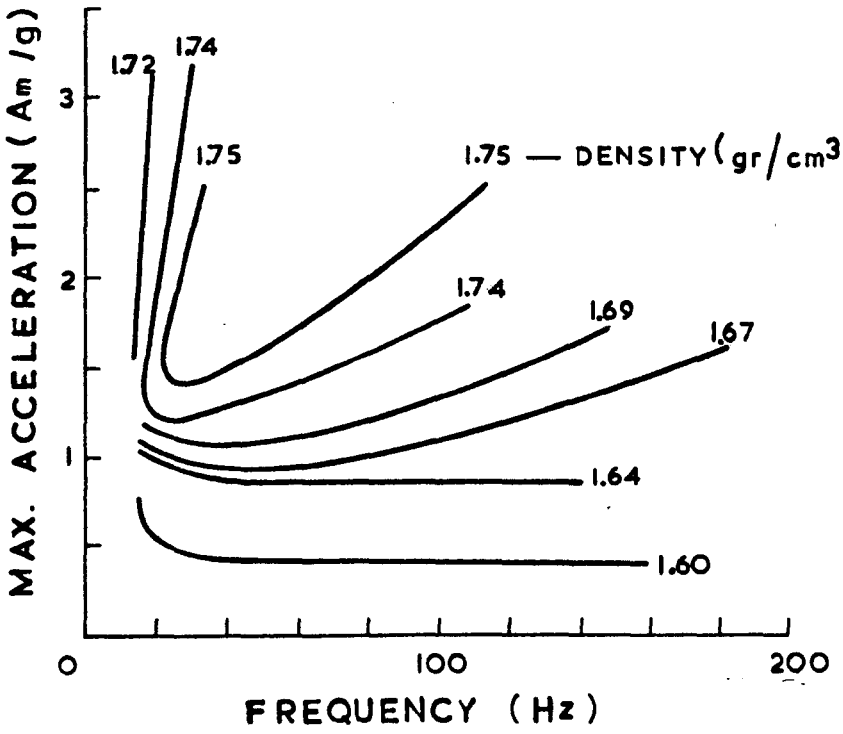

(b)

(Selig, 1963)

Fig. 5.7

Although the use of Selig's findings to prove the repeatability of the density could be argued, the use of the load - displacement curves cannot be disputed.

5.7 Other characteristics of sand

The following characteristics of sand were determined by performing the necessary tests:-

Specific gravity = 2.67

Maximum dry density = 1.73 gr/cm^3

Minimum dry denstity = 1.49 gr/cm^3

Relative density = 0.62% - 100%

Maximum void ratio = 0.79

Minimum void ratio = 0.54

CHAPTER VI

PRELIMINARY INVESTIGATION

6.1 Methods of placing the anchor during vibration

6.1.1 General

Previous researchers, in order to obtain a vertical anchor at a given depth for a number of tests, fixed their anchor unit in position during the placement and preparation of the sample.

Larnach (1972, Ref. 46) who performed tests on single and groups of anchors vertical and inclined, does not mention whether the anchor/anchors were held in place or were free to move when the sand bed was vibrated to obtain the required density. But considering that the individual positions of the anchors in his grouping were of importance, it is likely that each individual anchor was held securely in place.

McMullan (1975, Ref. 24), who also used the vibration method to compact the sand, had the anchor connected to the pullout unit during vibration. He stated that the pullout unit was designed to withstand the vibrational forces, and also sensitive enough to record the load on the anchor.

Yilmaz (1971, Ref. 32), using the method of stirring to obtain the necessary density, fixed the anchor unit during the process and obtained the required depth within an accuracy of ± 2mm. On releasing the anchor unit, after filling the tank, Yilmaz noticed that the anchor had settled a certain distance.

Howat (1969, Ref. 7) had the anchor fixed to a cross beam fitted over the tank, and partially filled the tank until the anchor was held firmly in position by the compacted sand. He completed the filling with the anchor free to move during the rest of the compaction.

Although researchers used a number of methods for anchor

placement, none of them produced any experimental results indicating that their installation procedure does not affect the load-displacement behaviour of the anchor. From Yilmaz's observation, i.e. the anchor moved when it was released from its fixed position, it can be concluded that there may be a difference in the final results due to the method of placing the anchor.

The author decided to investigate the methods of placing the anchor unit by carrying out tests with the anchor unit fixed and free during vibration time.

The vibration time of 45 minutes was used, as this time produced better repeatability of results for the two methods because the sample reached its maximum density. It was also thought that by using different anchor plates and depths of embedment a better understanding would be obtained. The anchor was pulled out at a constant rate of strain of 28mm/min in all the tests, as below this value there was no substantial difference in the load-displacement behaviour.

6.1.2 Experimental investigation

The investigation was separated into three parts, each part containing two sets of experiments. One set included load-displacement curves obtained with the anchor free and the second set with the anchor held in position during vibration.

The first part of the investigation was carried out with the anchor having a plate diameter of 19mm ($\frac{3}{4}$ in.) and a shaft diameter of 5mm ($\frac{3}{16}$ in.). The thickness of the plate was 102mm (4 in.). Ten experiments were performed, five with the anchor fixed and five with the anchor free. The best four from each set, were used to obtain the average load-displacement curves, shown in Fig. 6.1. The average depth of the embedded anchor was about 49cm.

The second part of the investigation was carried out using a 38mm (1.5 in.) diameter anchor plate. The shaft diameter was increased to 6mm ($\frac{1}{4}$ in.) since a bigger ultimate load was expected. The thickness of the plate was kept the same, i.e. 102mm (4 in.). Using the same vibration time, again the same numbers of experiments were carried out and the average load-displacement curves are shown in Fig. 6.2 (a). The average depth of the anchor was about 44cm.

An anchor plate, with diameter and thickness of 51mm (2 in.) and 102mm (4 in.) respectively, was used to carry out the third part of the investigation. A 6mm ($\frac{1}{4}$ in.) diameter shaft was connected to the anchor plate. Fig. 6.2 (b) shows the average load-displacement curves, with the anchor plates embedded at about 47cm in the sand.

6.1.3 Discussion

Considering the curves in Fig. 6.1, the curve obtained with the anchor free shows that the load increases smoothly and reaches its maximum value at about 55mm of displacement. The curve also shows that the anchor displaces for another 50mm before the load starts reducing. The second curve, i.e. anchor fixed, shows that the load increases sharply in the first 3mm of displacement and at about 4mm of displacement shows a marked "yield" point. The load then continues to increase with the ultimate load occurring at about 45mm displacement. Comparing the two curves, it is observed that the maximum difference between the loads occurs in the first few millimetres of displacement, and as the displacement increases the difference decreases. At 3mm displacement the load of the fixed anchor curve, about 66ON, is twice the load of the free anchor curve, about 33ON, and the ultimate loads are 714N and 544N respectively.

The graph in Fig. 6.2 (b) have a less well defined "yield" point. The fixed anchor curve shows that the load again

Fig. 6.1 Load V Displacement

Diameter of plate = 0.75 inch (19 mm)

Diameter of shaft = 0.2 inch (5 mm)

Depth = 49 cm

Vibration time = 45 min.

Pull out rate = 2.8 cm / min.

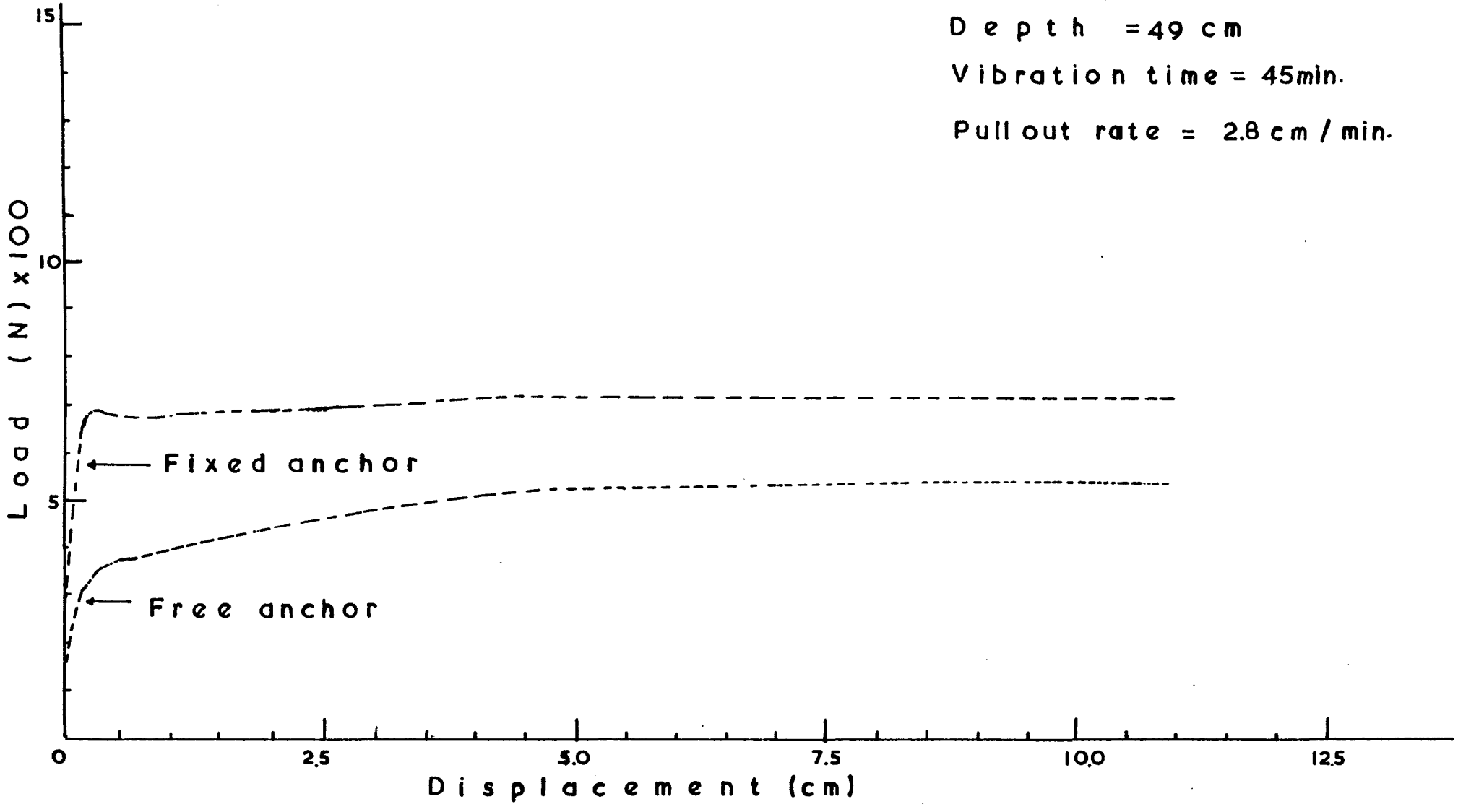

Fig. 6.2 Load V Displacement

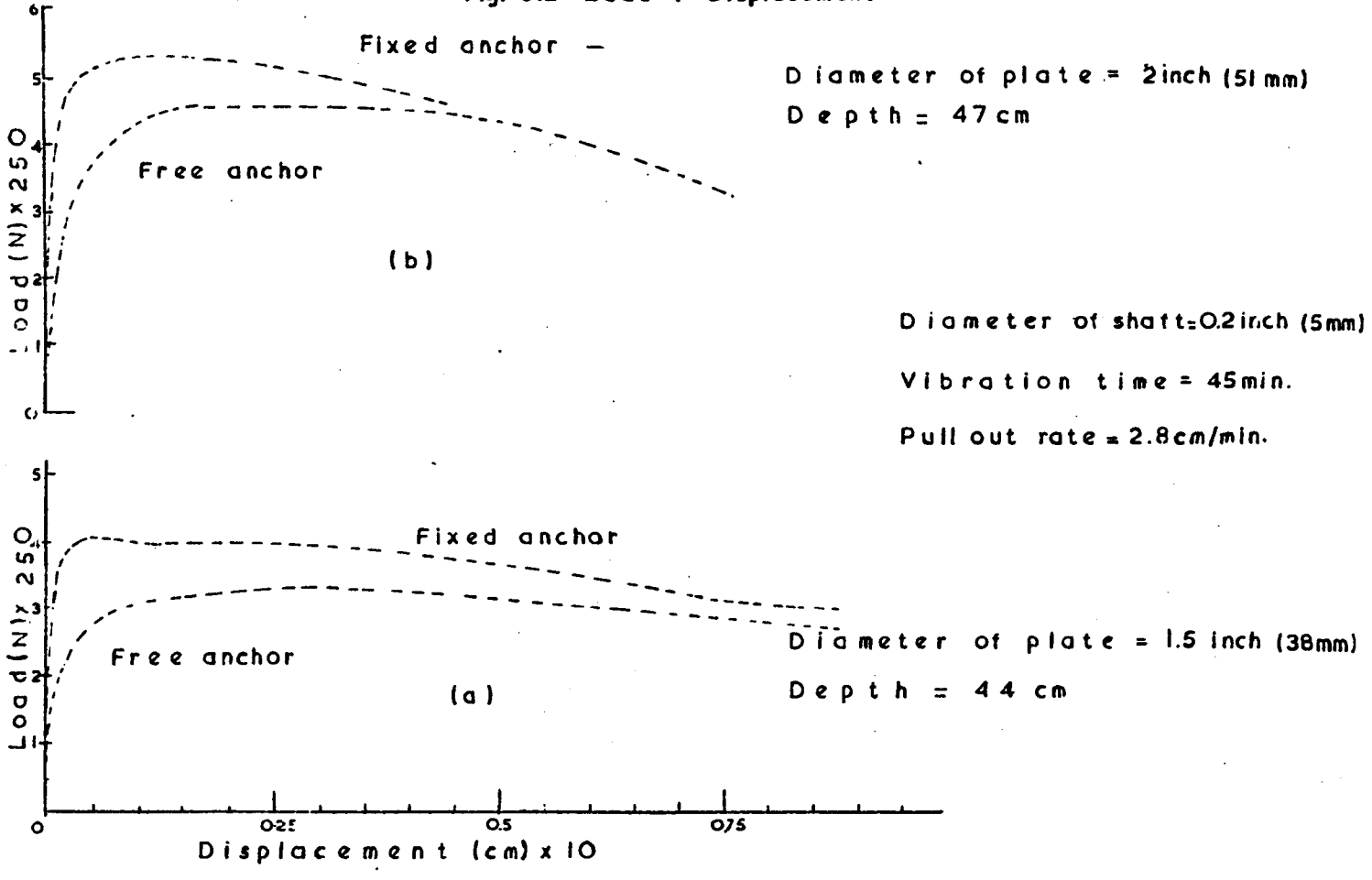

increases sharply, and the ultimate load is obtained at about 7mm of displacement which is constant for a further 10mm. The free anchor load rises at a lower rate and the ultimate load, remaining constant over a larger displacement, is also obtained at a greater absolute displacement. Again the range of maximum difference between loads occurs in the first few millimetres of displacement, with the fixed anchor having twice the load of the free anchor. The ultimate loads obtained from the fixed and free anchor load-displacement curves are about 1137N and 1314N respectively. The sudden decrease in the load after peaking, could be due to the anchors reaching shallow condition.

Considering Fig. 6.2 (a), the fixed anchor curve shows that the load again increases sharply as in Fig. 6.1, but after "yield" the load starts falling. The peak of the "yield" point gives the ultimate load of the fixed anchor. The free anchor curve is similar to the curves shown in Fig. 6.1 and Fig. 6.2 (b). In the first few millimetres of displacement, the two curves exhibit the same behaviour as the curves described previously. The ultimate loads obtained from the free and fixed anchor curves are about 830N and 1025N respectively.

6.1.4 Conclusion

From the investigation on the methods of placing the anchor, the following conclusions can be drawn.

(a) Although the load-displacement behaviour of both anchors, i.e. fixed and free, depends on the relative depth, that of the fixed anchor is affected to a greater degree. As the relative depth increases the "yield" point becomes more visible, but at low values of $\frac{H}{D}$ i.e. near the shallow condition, the "yield" point becomes invisible. For some relative depths, the ultimate load of the anchor is given by the peak of the "yield" point Fig. 6.2 (a).

(b) The ultimate load in both methods occurs at different displacements, with the fixed anchor reaching its ultimate load at a smaller displacement and holds it for a shorter further withdrawal distance than the free anchor.

(c) The post-peak part of the curves are similar in shape, although the fixed anchor load starts reducing at an earlier displacement than that of the free.

(d) The difference between the loads in the first few millimetres of displacement is very large. For the fixed anchor it is approximately twice that of the free anchor. This difference decreases as the displacement increases. The difference between ultimate loads is considerable.

For the rest of his experimental programme, the author decided that the anchor unit should be left free during vibration time, and each test should be repeated four times.

6.2 Constant rate of strain

6.2.1 General

Many researchers dealing with the anchorage problem were interested only in the ultimate load of an anchor. The anchor was withdrawn by applying gradually increasing dead load. It was then difficult to obtain the exact value of the ultimate load and also to understand the post peaking behaviour of the anchor. Recently, some researchers applied a constant rate of strain in order to obtain the load-displacement curve of the anchor.

Carr (1970, Ref. 23) obtained some of his load-displacement curves using a hydraulic ram to apply a load to the shaft. He found that the hydraulic ram, controlled by a double acting hand pump, was unsatisfactory for providing an uplift load to the anchor and replaced it with a loading

lever and weights. Although he was able to produce the post-peak part of the load-displacement curve using the former method, this was not possible using the latter method, and completed his curve by assuming that the peaks of the second and third cycles lay on the post-peak of the curve.

Larnach (1972, Ref. 46) used a motor to withdraw the anchor at a constant rate of strain of 4.66 mm/min. He obtained a complete load-displacement curve from which he recorded the ultimate load and the displacement at which this had occurred. He was also able to study the post-peak part of the curve.

Howat (1969, Ref. 7) and McMullan (1975, Ref. 24) also used constant rates of strain to withdraw their anchors, and these were 4.4 mm/min. and 3.46 mm/min. respectively.

Since the study of the load-displacement behaviour of the anchor was part of this research, the author, in order to investigate the effect of the constant rate of strain on the load-displacement curve, designed his pull-out unit so that constant rates of strains, between 0.5 mm/min. - 29.0 mm/min., could be obtained.

6.2.2 Experimental procedure

To examine the effect of the constant rate of strain on the load-displacement behaviour of the anchor, three sets of experiments were carried out. Two sets were performed using the same time of vibration but with the anchor embedded at two different depths. The third set was carried out at a different depth and time of vibration from the first two sets of experiments. Throughout this investigation the same anchor plate and shaft was used. The diameters of plate and shaft were 25mm (1 in.) and 5mm ($\frac{3}{16}$ in.) respectively. The thickness of the plate was 102mm (4 in.).

The first set of experiments was carried out using 10 minutes vibration and a depth of about 49cm. By adjusting the thyristor control unit, load-displacement curves for 0.5, 4, 10, 16.4, 23 and 29 mm/min. constant rate of strains were obtained. The curves obtained in this set, i.e. 30 curves - 5 for each strain, were plotted and shown in Fig. 6.3 (a). The area between the two extreme load-displacement curves is shaded.

The second set of experiments was performed using the same time of vibration as in the previous set, but with the anchor embedded at about 48cm depth. The same number of curves were again obtained and plotted in Fig. 6.3 (b).

The third set of tests was carried out using a 45 minutes vibration and with the anchor embedded at 59cm depth. Again the same number of experiments was performed for the same rates of strain, and the curves are shown in Fig. 6.4.

6.2.3 Conclusions

The shaded area of each graph indicates the load-displacement curves obtained from all the constant rates of strain. The maximum thicknesses of areas in Fig. 6.3 (a) & (b) and Fig. 6.4 are 26N, 26N and 35N respectively. Although a variation in the ultimate load of about 4% exists, there is no indication that this is due to the change in the constant rate of strain, since the ultimate load of each individual load-displacement curve was not increasing or decreasing with the rate. The only explanation that could be given to the 4% variation is that the anchor could not have been placed vertically and at the same depth throughout each set of experiments. The depth was varying between $\pm$ 0.5cm from the average value.

Therefore it can be said that the load-displacement behaviour of the anchor is not affected when the anchor is pulled out at any constant rate of strain between 0.5 mm/min. and

Fig. 6.3 Load V Displacement

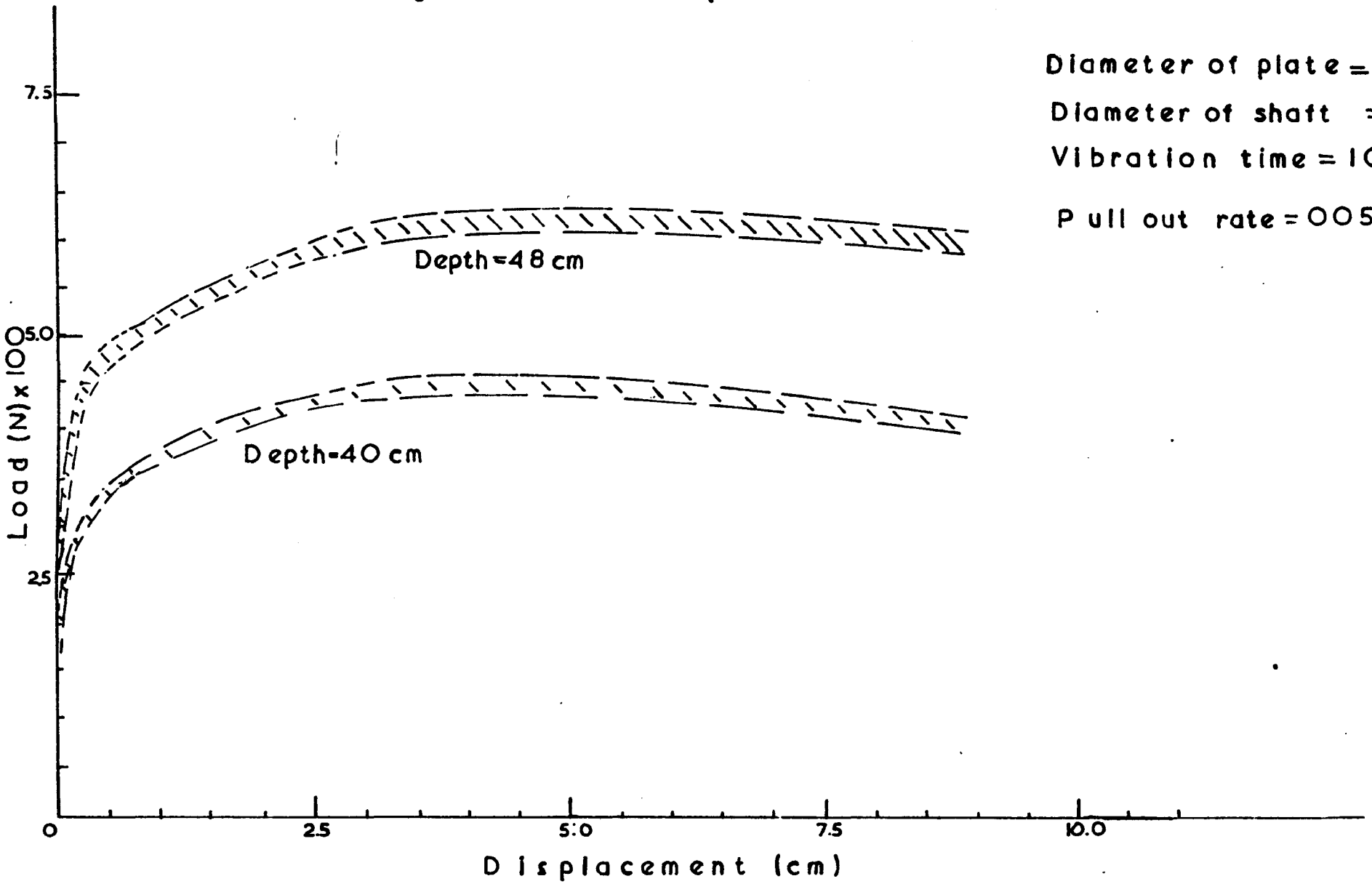

Fig. 6.4 Load V Displacement

Diameter of plate = 1 inch (25mm)
Diameter of shaft = 0.2 inch (5mm)

Depth = 58 cm

Vibration time = 45 min.
Pullout rate = 2.8 cm/min

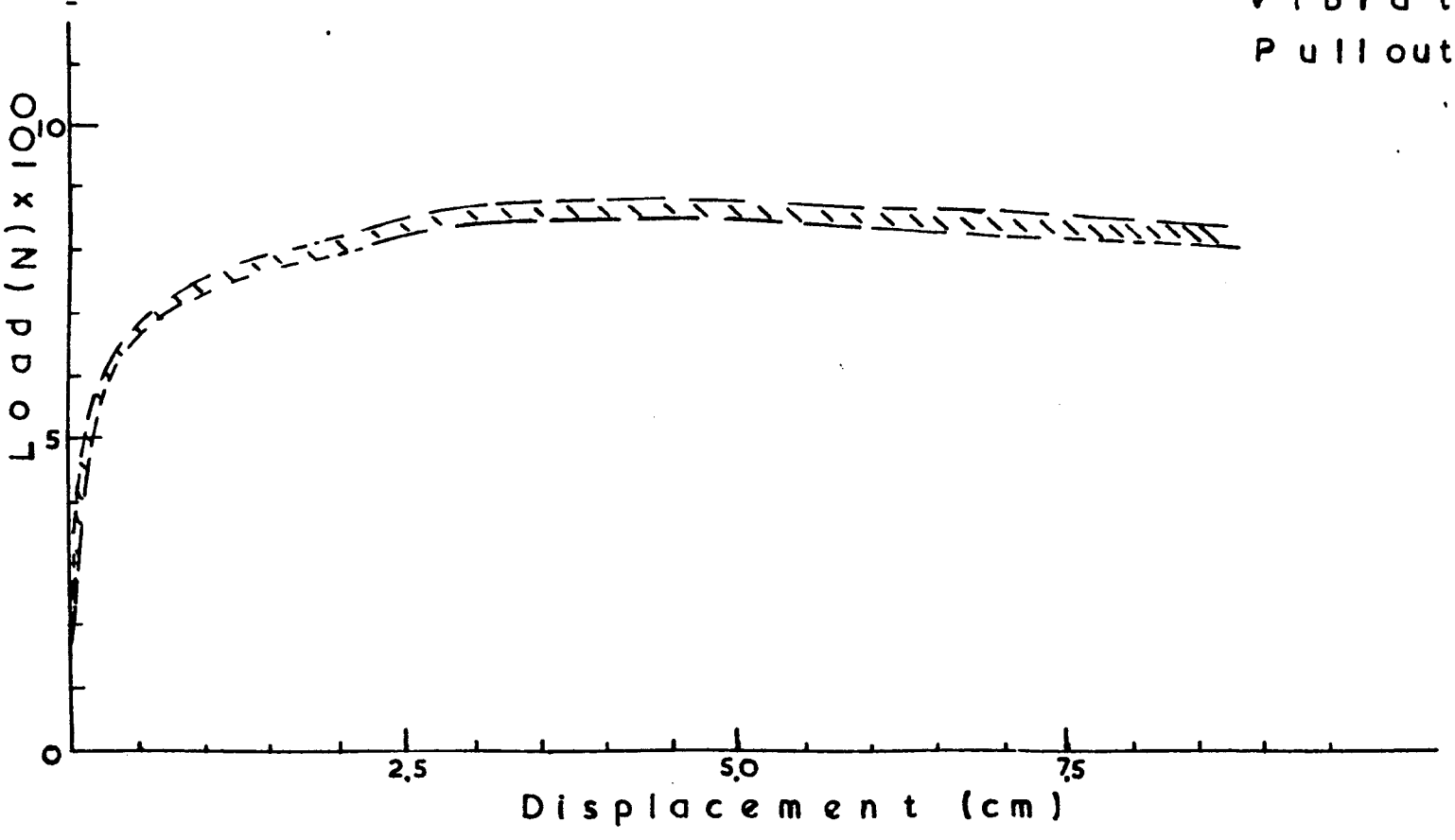

29 mm/min. in a loose or dense sand and in any depth.

For the rest of the experimental programme in this research, a constant rate of strain of 28 mm/min. will be used, and therefore performing each test more quickly. A typical load displacement curve would be obtained in 3 minutes whilst a 0.5 mm/min. rate would produce the same curve in about 3 hours.

6.3 Effect of Boundaries

6.3.1 General

In the past, the size of the tank was controlled by the method of preparing the sample. Researchers using methods involving filling and emptying the tank, in order to minimize the time spent on the manual part of their research, used reasonable sizes of tanks.

Carr (1970, Ref. 23) carried out his experimental investigation using a 46 in. x 46 in. x 36 in. deep (1.2m x 1.2m x 0.9m) tank. He stated that his box was big enough to take the failure surface of a 6 in. (152mm) diameter anchor plate embedded at 30 in. (76cm) in sand with an internal angle of friction of 45^{o}. Carr designed his box by taking into consideration Balla's assumption of a circular failure surface. Although he ruled out the idea of using a larger box due to the work involved in filling and emptying the sand, Carr admitted that a larger box would have been a better choice, but gave no further explanation.

Howat (1969, Ref. 7) adopted a method recommended by MEXE (now MVEE) that a scale not smaller than 1:8 should be used for model tests. From his preliminary investigation, he found that when a 4.5 in. (114mm) diameter plate was used at 36 in. (91cm) depth, the failure zone had a diameter of 36 in. (91cm) on the surface of the soil. Howat also

stated that the sides of his 4ft. x 4ft. x 4ft. (1.2m x 1.2m x 1.2m) tank were sufficiently large enough not to interfere with the failure surfaces of the anchor plates used during his experimental investigation.

Yilmaz (1971, Ref. 32) used a 1.06m x 1.06m x 0.53m deep box for his single anchor tests. In his experiments, he used strip anchors varying from 38mm x 190mm to 76mm x 343mm and therefore adopted a scale of 1:3.

Healy (1971, Ref. 29) tried to simulate field conditions in his experiments. He stated that by keeping the sides of his tank at least six anchor diameters away from the anchor, the field conditions as far as the boundaries were concerned, would be satisfied.
McMullan (1975, Ref. 24) chose his experimental tank by considering the results provided by Carr and Yilmaz. The height of the tank was chosen due to the fact that the anchor was to be placed in deep conditions.

The above review of literature shows that the effect of the boundaries on the behaviour of an anchor has not yet been fully investigated. Different researchers have used different scales, e.g. 1:8, 1:6, and 1:3. Therefore the only information that can be obtained is from the failure surfaces occurring when the anchor is placed at shallow depths. Also the investigation on group anchors could reveal some information, by comparing the ultimate load given by a single anchor with the ultimate load obtained using a group of anchors, i.e. two anchors.

6.3.2 Conditions

To investigate the effect of the boundaries on the behaviour of a single vertical anchor embedded in dry sand and at different depths, the following parameters were kept constant

throughout this investigation.

(a) The constant rate of strain, i.e. 28 mm/min.

(b) The time of vibration, i.e. 45 minutes.

(c) The material forming the sides of the boxes.

(d) The amount of sand vibrated.

6.3.3 Boxes

The 180cm x 180cm x 120cm deep tank, described in Chapter III, was used to hold the same amount of sand throughout this investigation. The boxes, made from 120cm x 90cm x 0.2cm steel plates bolted to four vertical steel angles, were embedded in the tank. To the top perimeter of the boxes, steel angles were bolted as additional reinforcement. The boxes had no bottoms.

The four plates, used to make the 120cm x 120cm x 90cm deep box shown in Fig. 6.5, were later rearranged to form the 90cm x 90cm x 90cm deep box. The 60cm x 60cm x 90cm and 30cm x 30cm x 90cm deep boxes were constructed using two and one of the steel plates respectively, Fig. 6.5.

6.3.4 Placement of boxes

The embedment of the boxes into the sand was the major problem in this investigation. In order to avoid emptying and filling the tank, it was decided to vibrate the boxes into the sand. Even with the application of a load of about 2 tons on the top of the box, the method proved unsuccessful.

The author, having examined other methods, i.e. sucking out the sand while the box was pushed in, decided that the soil had to be removed from the tank for each placing of a new box.

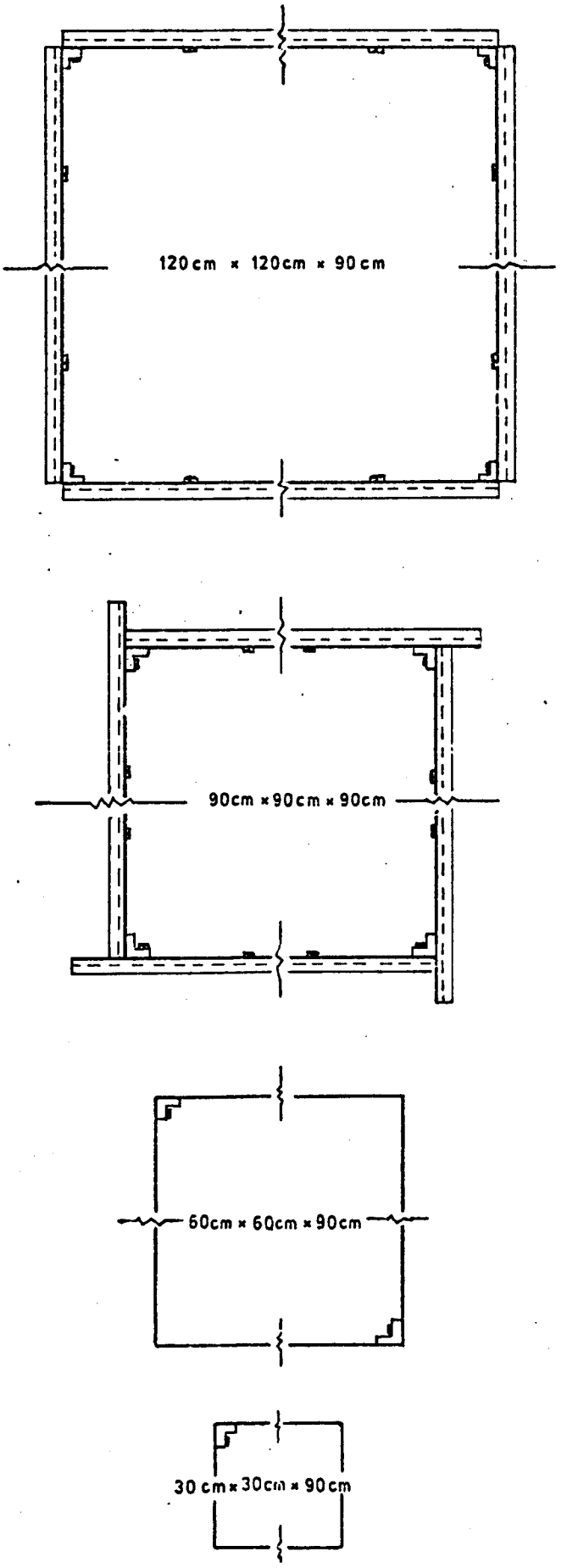

Fig. 6.5 Sketch plan view of tanks

6.3.5 Experimental procedure

The five different sizes of anchor plates, mentioned in Chapter III, were embedded at four or more different depths in the sand of each box, and the load-displacement curves were recorded.

Each test was performed at least four times and the average load-displacement curve was obtained using the best three, and generally these agreed to within 7% approximately.

6.3.6 Results

A number of selected load-displacement curves have been chosen to compare behaviour.

Fig. 6.6 shows the load-displacement curves of the 51mm (2in) diameter plate embedded at two different depths and in two different boxes. The curves obtained with the plate embedded at 56cm depth in the 30cm x 30cm x 90cm and 60cm x 60cm x 90cm deep boxes, are shown in Fig. 6.6 (a). Although the load-displacement curve a_1 of the anchor placed in the bigger tank is smooth, this is not so for the curve a_2 obtained with the plate buried in the smaller tank. Curve a_1 shows that the ultimate load is obtained at about 20mm, and curve a_2 shows that the anchor obtains its maximum load at about 60mm. The figure also shows that the anchor in the smaller box behaves as a shallow one, i.e. the load falls sharply after reaching its peak value. Fig. 6.6 (b) shows the two curves obtained at 32cm depth. Although both curves indicate shallow anchor failures, again the curve of the plate buried in the smaller box shows that the anchor fails at a small displacement. Both Fig. 6.6 (a) and Fig. 6.6 (b) indicate that the 51mm diameter plate embedded at any depth between 30cm and 56cm in the sand, gives a bigger ultimate load in the smaller than in the bigger box.

Fig. 6.6 Load V Displacement

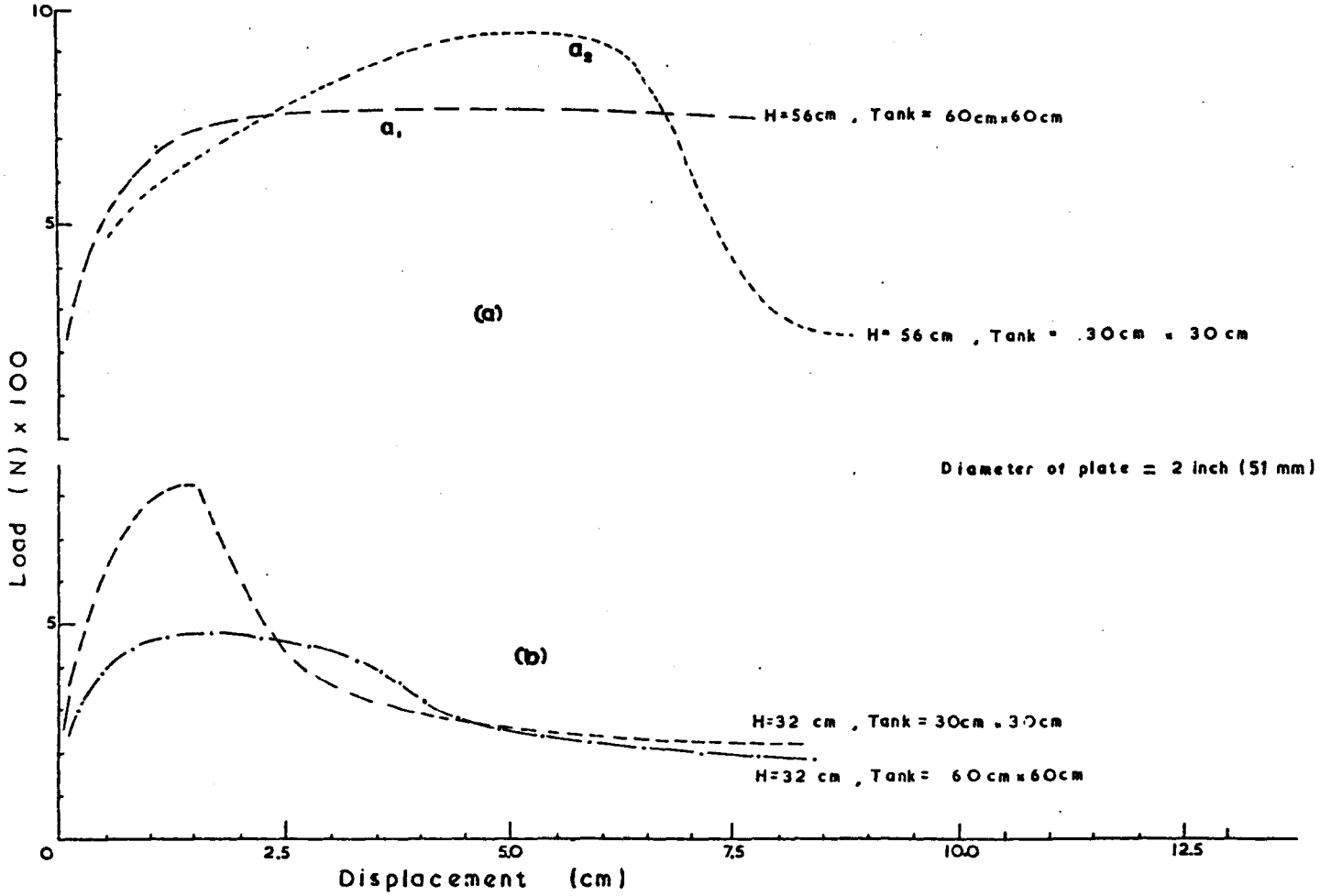

Fig. 6.7 Load V Displacement

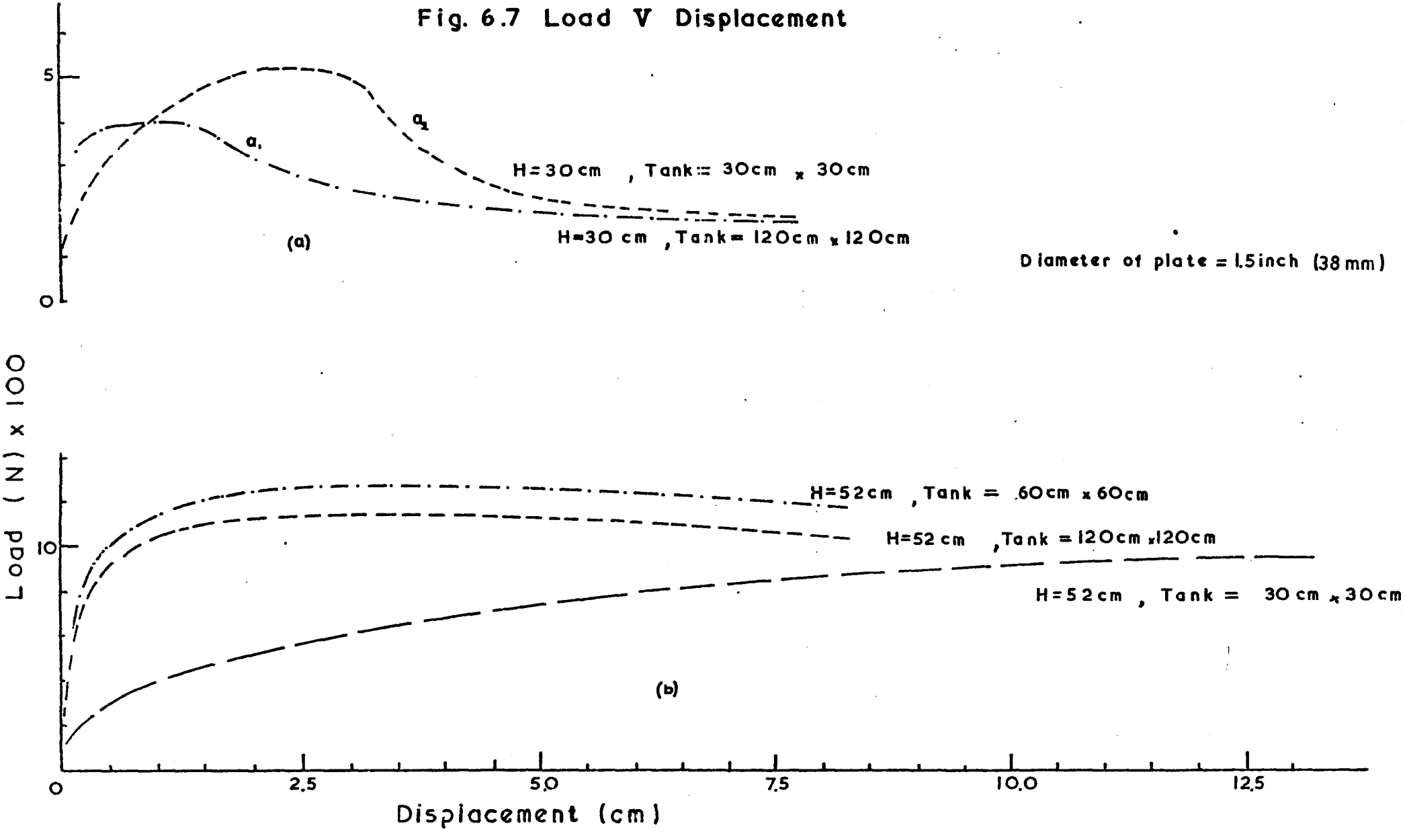

Fig. 6.7 shows the load-displacement curves of the 38 mm (1.5 in) diameter anchor plate embedded at different depths and in different boxes. The curve a_2 in Fig. 6.7 (a) obtained with the anchor embedded at 30cm and in the 30cm x 30cm x 90cm box, is similar to the load displacement curve, a_2, in Fig. 6.6 (a). This indicates that although a smaller diameter was used, the boundaries still affect the behaviour of the anchor. Comparing the two curves in Fig. 6.7 (a) it is now observed that the anchor, when embedded in the smaller box, fails at a greater displacement, although still obtains its ultimate load at a larger displacement than in the bigger box. At greater depths, the anchor plate exhibits a different behaviour, Fig. 6.7 (b). In the smallest tank, i.e. 30cm x 30cm x 90cm, the anchor obtains its ultimate load at a very large displacement, about 125 mm whilst in the bigger boxes the ultimate load is obtained at 35 mm. Although the shape of the load-displacement curves obtained with the anchor embedded in the 60cm x 60cm x 90cm and 120cm x 120cm x 90cm deep boxes is not affected by the boundaries, this cannot be said for the ultimate load.

Fig. 6.8 and Fig. 6.12 show the ultimate load plotted against the relative depths for all experiments carried out. The figures show that the three smaller sizes of anchor plates i.e. 12mm (0.5 in.), 19mm (0.75 in.) and 25mm (1 in.), develop their smallest ultimate loads when embedded in the 30cm x 30cm x 90cm box, and obtain their maximum ultimate loads when embedded in the 90cm x 90cm x 90cm box. The curve, ultimate load against relative depth, of the 51mm (2 in.) anchor plate in Fig. 6.12 shows that the ultimate load of the anchor remains approximately constant for relative depths greater than 11. This indicates that the same failure surface occurs for any $\frac{H}{D} > 11$ and the increase in the ultimate load as $\frac{H}{D}$ increases is due to the increase of the lifted mass of sand and its friction along the walls of the tank.

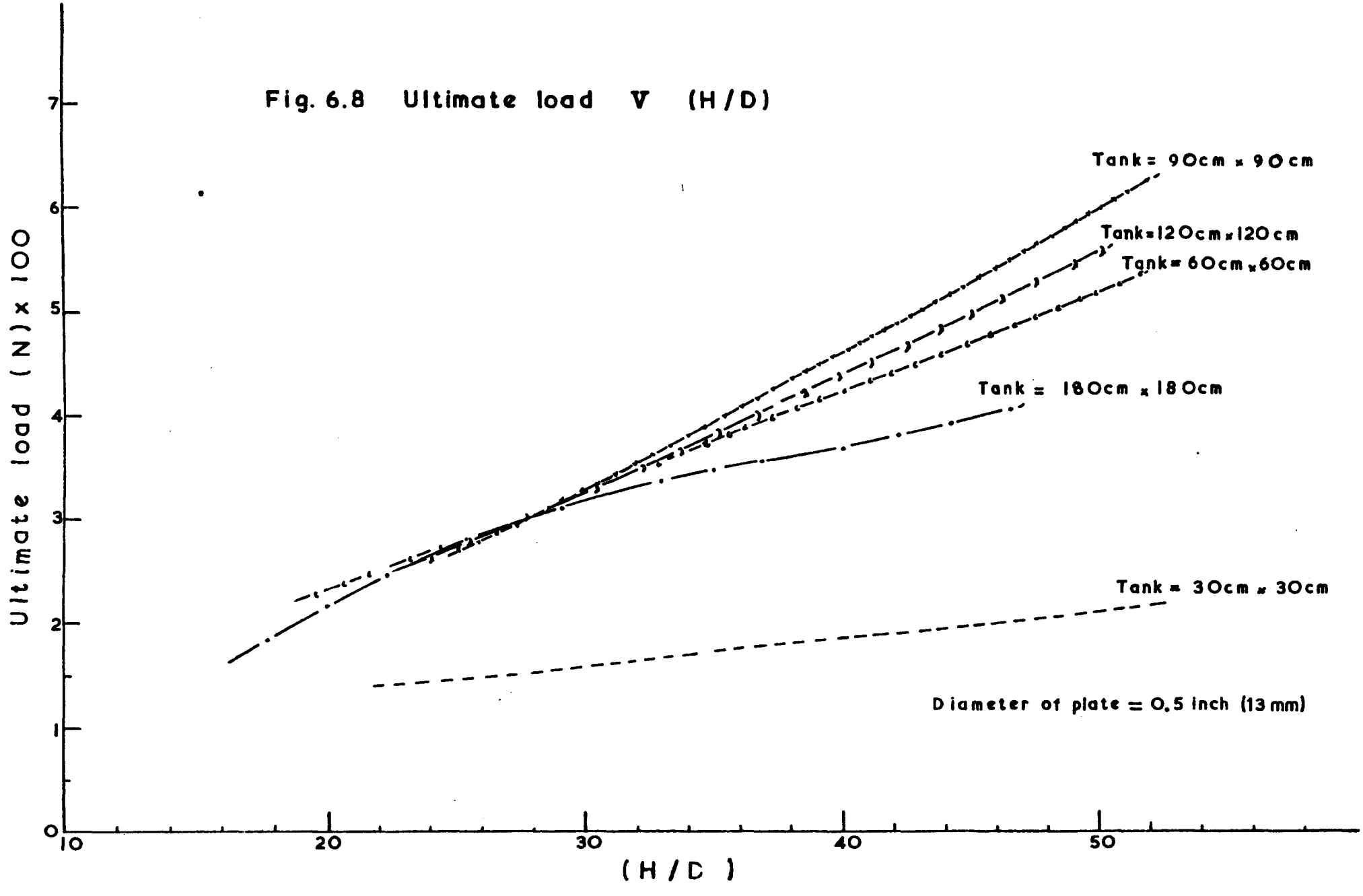
Fig. 6.8 Ultimate load V (H/D)
Tank = 90cm x 90cm
Tank = 120cm x 120cm
Tank = 60cm x 60cm
Tank = 180cm x 180cm
Tank = 30cm x 30cm
Diameter of plate = 0.5 inch (13 mm)
Ultimate load (N) x 100
(H/D)
0
1
2
3
4
5
6
7
10
20
30
40
50

Fig. 6.9 Ultimate load V (H/D)

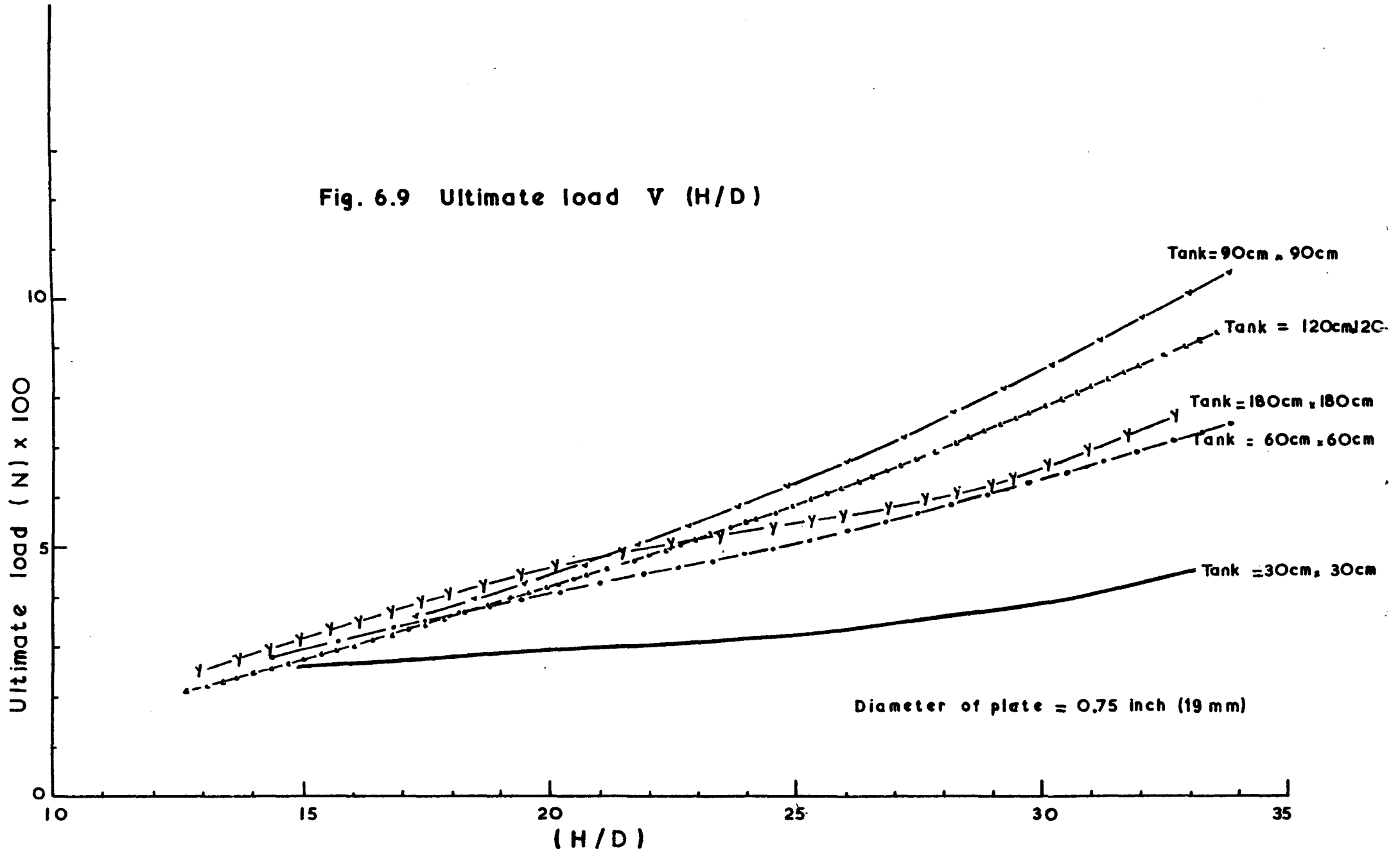

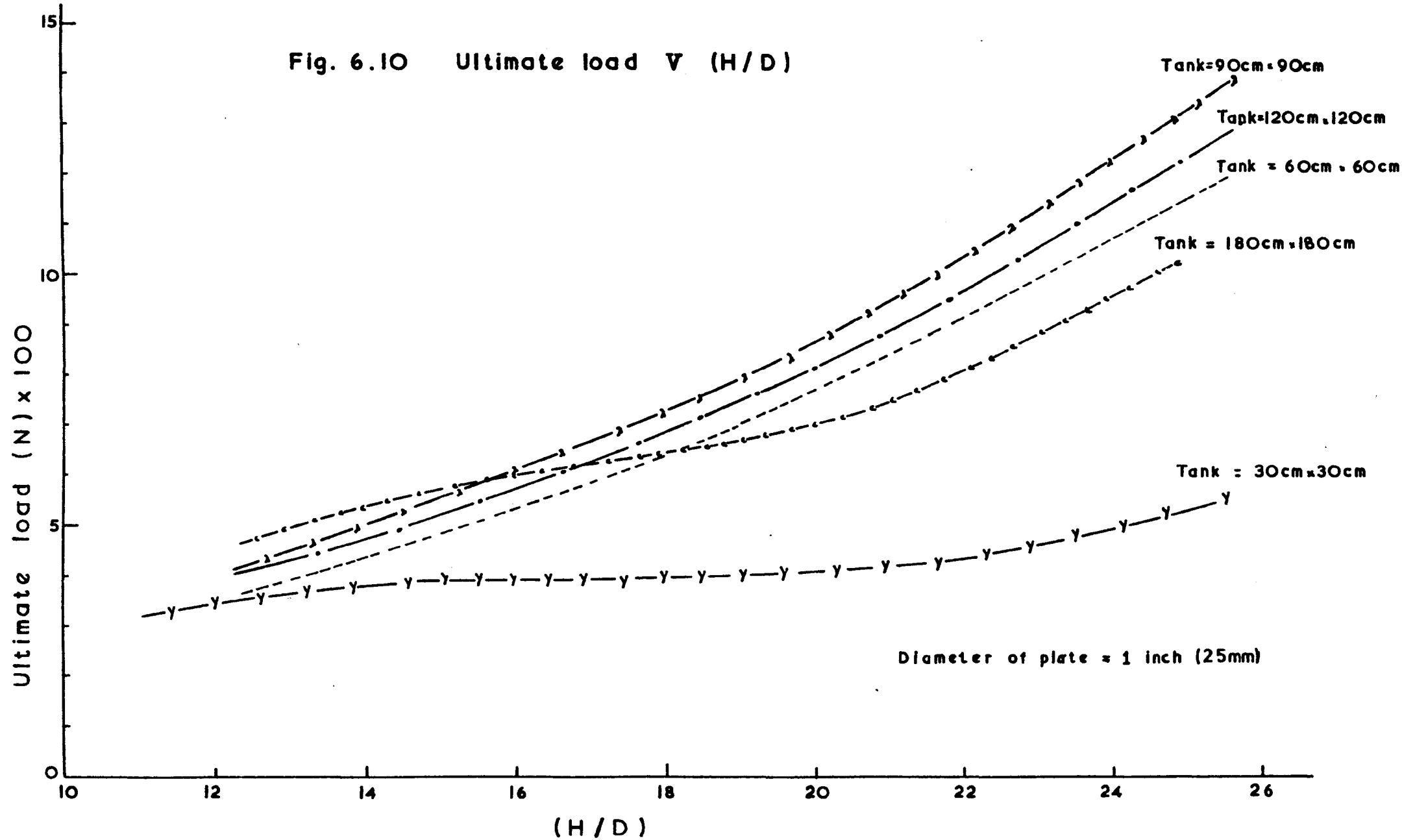
Fig. 6.10 Ultimate load V (H/D)
Tank=90cm×90cm
Tank=120cm×120cm
Tank = 60cm × 60cm
Tank = 180cm×180cm
Tank : 30cm×30cm
Diameter of plate = 1 inch (25mm)
Ultimate load (N) x 100
(H/D)
0
5
10
15
10
12
14
16
18
20
22
24
26

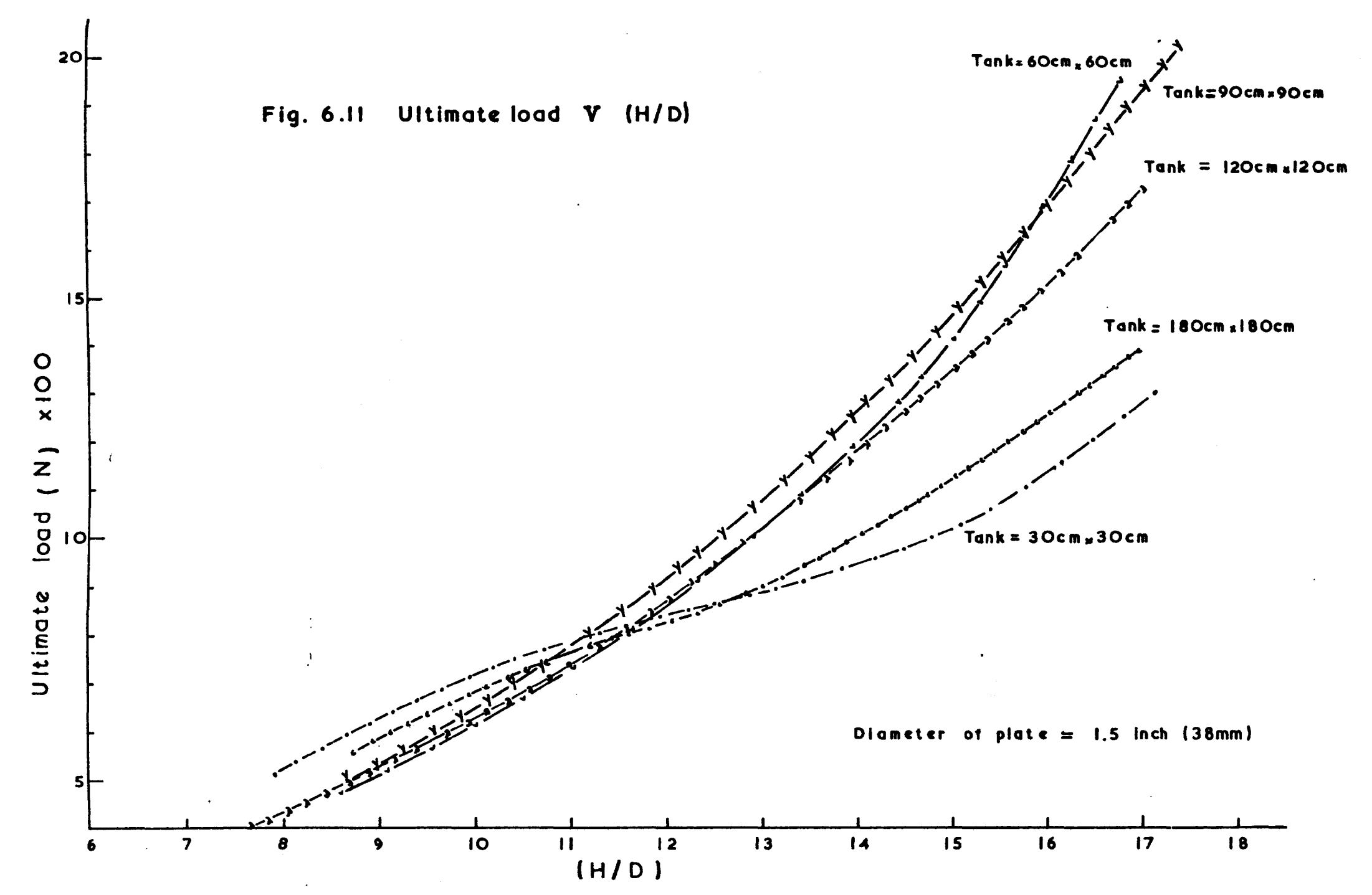
Fig. 6.11 Ultimate load V (H/D)
Tank = 60cm x 60cm
Tank = 90cm x 90cm
Tank = 120cm x 120cm
Tank = 180cm x 180cm
Tank = 30cm x 30cm
Diameter of plate = 1.5 inch (38mm)
Ultimate load (N) x100
(H/D)
20
15
10
5
6
7
8
9
10
11
12
13
14
15
16
17
18

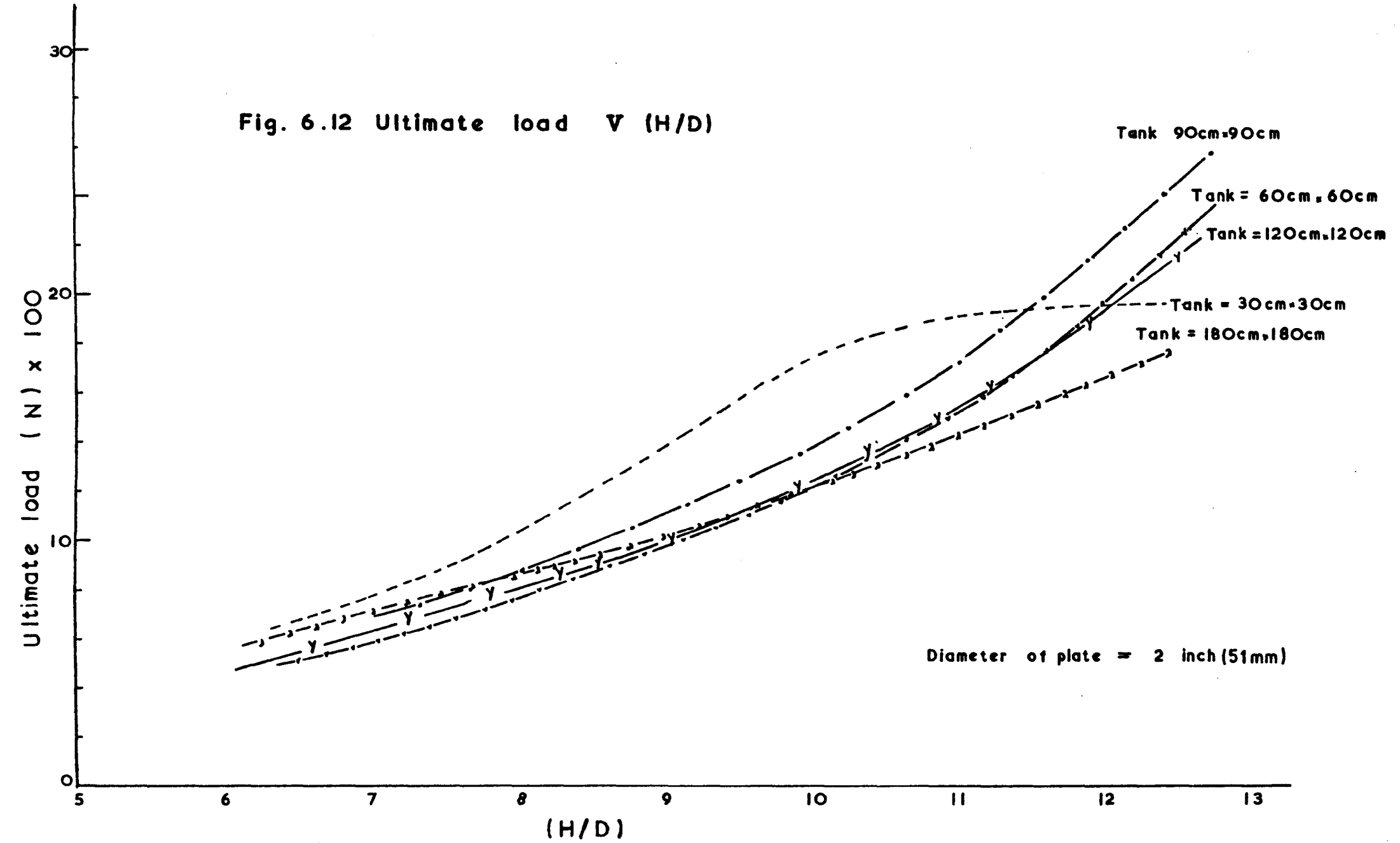
Fig. 6.12 Ultimate load V (H/D)
Tank 90cm×90cm
Tank = 60cm × 60cm
Tank = 120cm×120cm
Tank = 30cm×30cm
Tank = 180cm×180cm
Diameter of plate = 2 inch (51mm)
Ultimate load (N) x 100
(H/D)
0
10
20
30
5
6
7
8
9
10
11
12
13

6.3.7 Conclusions

Examination of the load-displacement curves and the graphs of ultimate load against relative depth revealed the following points:-

(a) The load-displacement of the anchor is affected by the boundary conditions and in some cases the anchor behaves as a shallow one although $\frac{H}{D} > 11$.

(b) The ultimate load varies with the distance of the boundaries from the shaft, but a general trend could not be obtained.

(c) The results show that the load-displacement behaviour of the anchor is definitely affected with scales, i.e. 1:8 and 1:6, used by other researchers. (plate diameter | boundary distance)

6.4 Effect of anchor shaft diameter

6.4.1 General

Although many researchers have investigated the influence of the anchor plate on the ultimate load of an anchor, very few have taken into consideration the effect of the shaft diameter in their analysis. In some papers the size of the shaft was considered small compared with the size of the anchor plate and in others, although the diameter of the shaft was initially introduced, it was later omitted from the final equation of the ultimate load.

Baker and Kondner (1965, Ref. 20) started their dimensional analysis by considering all the parameters of the anchor plate, but in the final stages of the analysis they replaced the cross-sectional area of the plate by its diameter. The use of

straight piano wire of 0.078 in.(2mm) diameter as a shaft in their experimental work, could explain the omission of the shaft parameter from the final equation. The maximum $\frac{D_s}{D}$ used was about 0.078.

Balla (1961, Ref. 40) has taken into account in his theoretical work, the volume occupied by the shaft in the soil. In his experimental work, although he specified the diameter of the anchor plates as being 6cm, 9cm, and 12cm he did not mention the diameters of the shafts.

Mariupol'skii(1965, Ref.19) in both of his analyses i.e. deep and shallow, considered the diameter of the anchor shaft. In his theoretical work on shallow anchors, he considered that the pressure on the soil is exerted by the net area of the anchor plate i.e. $\frac{\pi}{4} \cdot (D^2 - D_s^2)$, whilst in his work on deep anchors not only did he assume that the cylindrical cavity was expanded from $\frac{D_s}{2}$ to $\frac{D}{2}$ but also introduced a term taking into account the friction between soil and shaft. Mariupol'skii in his experimental work, used a maximum $\frac{D_s}{D}$ ratio of 0.06.

Hanna (1970, Ref. 47) suggested that the projection of the anchor plate $(D - D_s)$ is a more valid parameter than the diameter of the plate only. He plotted the average uplift pressure against $\frac{H}{D}$ and obtained a number of curves, one for each plate diameter. Hanna then plotted the same pressure against $\frac{H}{(D - D_s)}$ and found that one curve represented all the plates. A maximum and a minimum $\frac{D_s}{D}$ of 0.5 and 0.166 was used respectively.

The information obtained from other researchers, shows that the effect of the anchor shaft on the behaviour of the anchor should be examined and the critical ratio of $\frac{D}{D_s}$ must be found.

6.4.2 Experimental procedure

To investigate the effect of the diameter of the shaft on the behaviour of a vertical anchor subjected to an uplift force, eight different diameters of shafts were used. The investigation was based on the ultimate loads obtained with the shaft diameter being the only variable, and with the following parameters kept constant:-

(a) Time of vibration, i.e. 45 minutes.

(b) Constant rate of strain, 28 mm/min.

(c) Depth of embedded anchor plate, i.e. 60cm.

(d) Diameter of anchor plate, 25mm (1 in.).

(e) Thickness of anchor plate, 102mm (4 in.).

The different sizes of shafts used during this experimental investigation, had the diameters of: 3mm ($\frac{1}{8}$ in.), 5mm ($\frac{3}{16}$ in.), 6mm ($\frac{1}{4}$ in.), 8mm ($\frac{5}{16}$ in.), 10mm ($\frac{3}{8}$ in.), 13mm ($\frac{1}{2}$ in.), 19mm ($\frac{3}{4}$ in.) and 25mm (1 in.).

For each size of shaft, five experiments were performed and the best three were used to plot the average load displacement curve. The average ultimate load was then plotted against the ratio of the diameter of the plate to the diameter of the shaft, Fig. 6.13.

6.4.3 Conclusions

Fig. 6.13 shows that the ultimate load of the anchor increases as the $\frac{D}{D_s}$ ratio increases. This should be expected since the area of plate in contact with the sand is increased. The

Fig. 6.13 Ultimate load V (D/D_S)

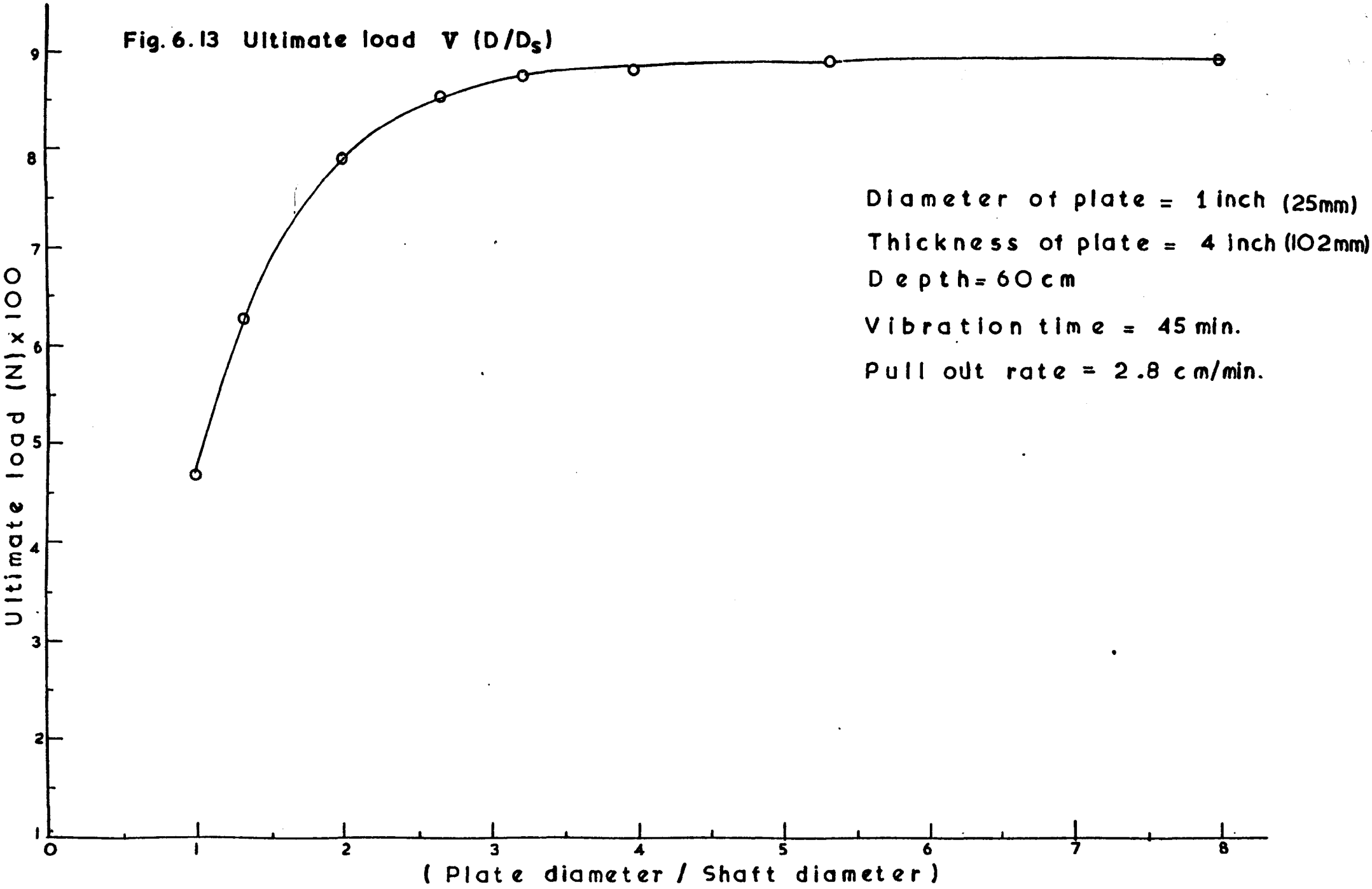

figure also, at $\frac{D}{D_s} = 1$, gives the frictional force of a 25mm (1 in.) diameter shaft embedded at 60cm in the sand. The Fig. 6.13 also shows that the increase in the ultimate load with $\frac{D}{D_s} > 4$ is negligible. Therefore the diameter of shaft could be ignored in any experimental or theoretical work if the scale 1:4 is used.

6.5 Effect of anchor plate thickness

6.5.1 General

Most of the experimental work on ground anchors was carried out in order to determine the ultimate load of different anchor plates embedded at different depths. Very little information exists on the importance of the anchor plate thickness, although this parameter is of significance.

Baker and Kondner (1965, Ref. 20) were the first researchers to emphasize the importance of the anchor plate thickness. Their ultimate load equation depends not only on the diameter and depth of the plate, but also on the thickness, (See Chapter III). Baker and Kondner's work, shows that an investigation into the effect of the plate thickness on the behaviour of the anchor should be made and the critical ratio of $\frac{t}{D}$ should be found.

6.5.2 Experimental procedure

The following parameters were kept constant throughout this experimental investigation;-

(a) Time of vibration, 10 minutes.

(b) Constant rate of strain, 28 mm/min.

(c) Anchor depth, 61cm.

(d) Plate diameter, 25mm (1 in.).

(e) Shaft diameter, 5mm ($\frac{3}{16}$ in.).

The thickness of the anchor plate, being the variable parameter, had the following sizes:- 6mm ($\frac{1}{4}$ in.), 13mm ($\frac{1}{2}$ in.), 19mm ($\frac{3}{4}$ in.), 51mm (2 in.), 76mm (3 in.), and 102mm (4 in.).

Each test was carried out four times and the best three were used to obtain the average load-displacement curves. The average ultimate load was obtained and plotted against $\frac{t}{D}$, shown in Fig. 6.15.

6.5.3 Conclusions

Fig. 6.14 shows typical load-displacement curves obtained using different thicknesses of plate. It is observed that with the thickness of the anchor plate increasing, the "modulated" curve becomes smoother and the displacement at which the ultimate load occurs increases. From the load-displacement curves obtained throughout this experimental programme, it was also observed that the accuracy of each test improved with the thickness of the plate increasing.

Fig. 6.15 shows that the ultimate load substantially increases with the $\frac{t}{D}$ ratio, but the rate of increase decreases. For $\frac{t}{D} > 3$ it is obvious that the increase in the ultimate load is negligible.

The increase in the ultimate load of the anchor, as the plate thickness increases, may be explained by the movement of the neighbouring soil in trying to fill the cavity left under the anchor plate. It seems that as the thickness of the plate increases, the movement of highly stressed soil on top of the anchor plate is more restrained, and the cavity is filled by sand particles further away from this stressed soil.

Fig. 6.14 Load V Displacement

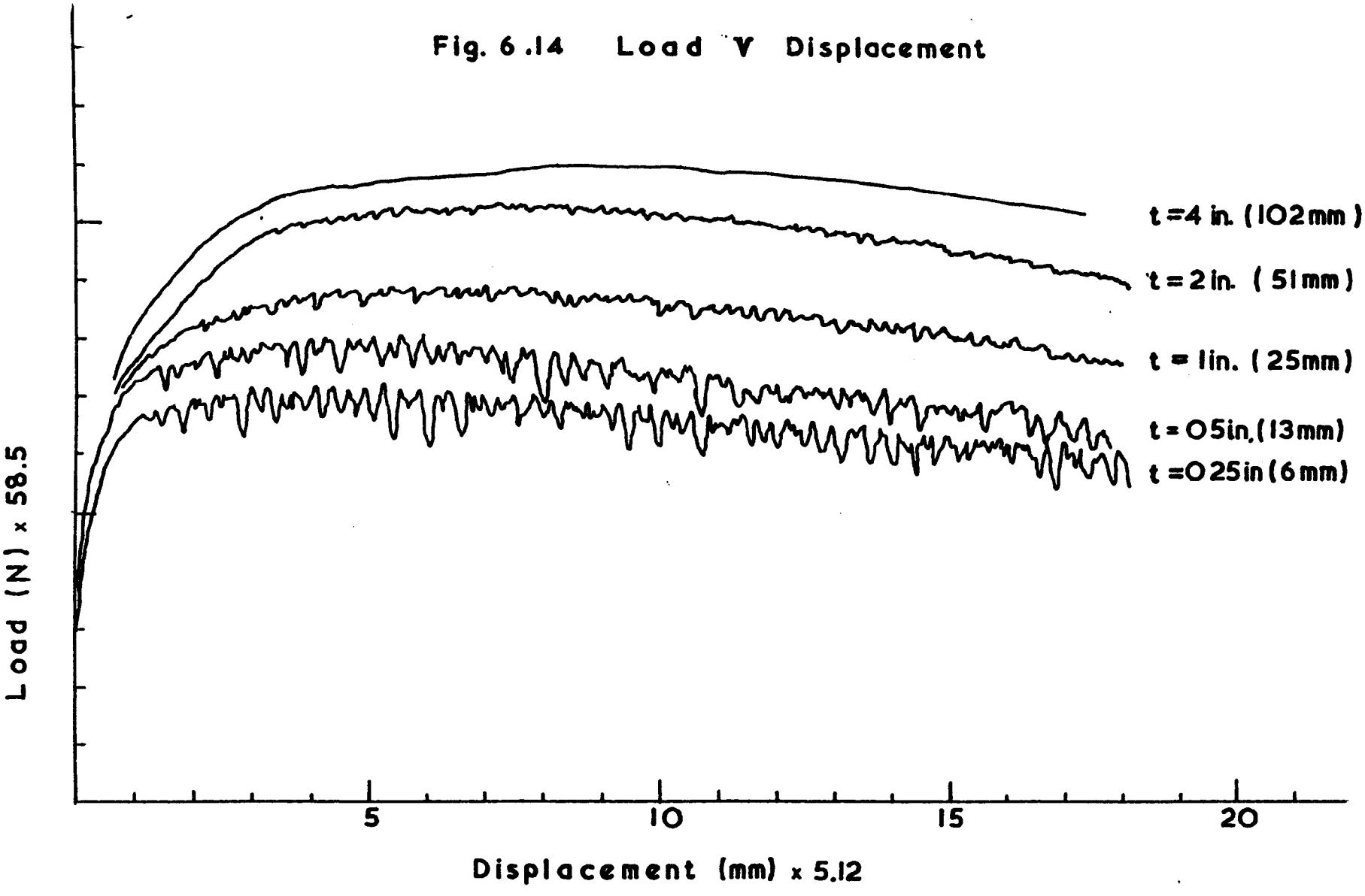

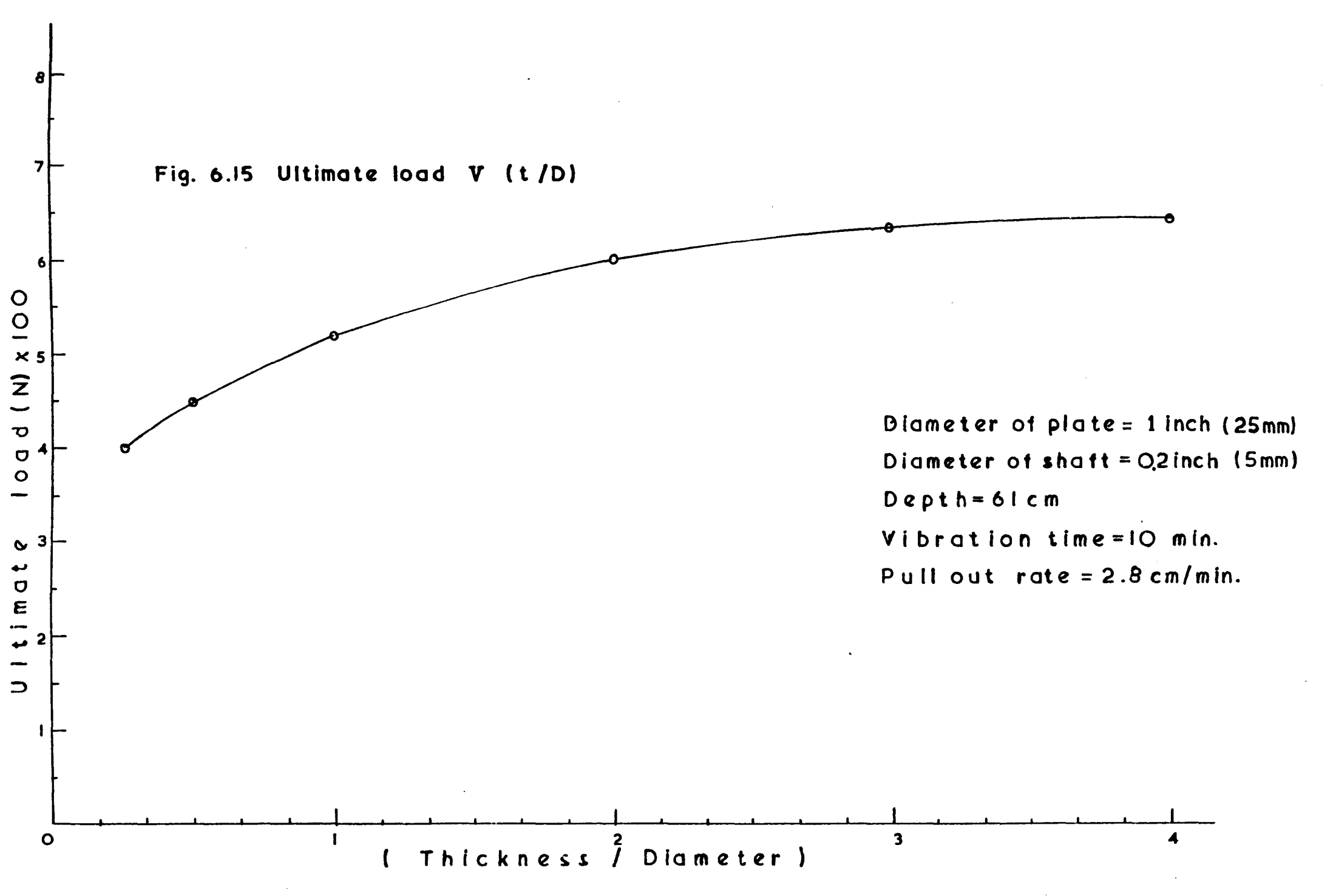
Fig. 6.15 Ultimate load V (t/D)
Ultimate load (N) x 100
8
7
6
5
4
3
2
1
0
1
2
3
4
(Thickness / Diameter)
Diameter of plate = 1 inch (25mm)
Diameter of shaft = 0.2 inch (5mm)
Depth = 61 cm
Vibration time = 10 min.
Pull out rate = 2.8 cm/min.

Frictional effects seem to have no important bearing on the results, since conventional theories predict that the increase in the ultimate load due to friction is only a fraction of the increase obtained in the experimental programme.

6.6 Variation of ultimate load with the time of vibration

6.6.1 General

McMullan (1975, Ref. 24) using the same sand throughout his investigation, filled and emptied the tank for each of his tests. He stated that with this method the load-displacement curve of the anchor was repeatable.

The author in order to investigate the repeatability of his results, since the sand was kept in the tank throughout the research, carried out tests by embedding a particular anchor at the same depth and vibrating the sand for different periods of time.

6.6.2 Experimental procedure

The following parameters were kept constant:-

(a) Depth of anchor, 60cm.

(b) Anchor plate diameter, 25mm (1 in.).

(c) Anchor shaft diameter, 6mm ($\frac{1}{4}$ in.).

(d) Constant rate of strain, $\dot{2}8$ mm/min.

Experiments were performed using different times of vibration between 5 minutes and 50 minutes. For each time of vibration,

Fig. 6.16 Ultimate load V Vibration time

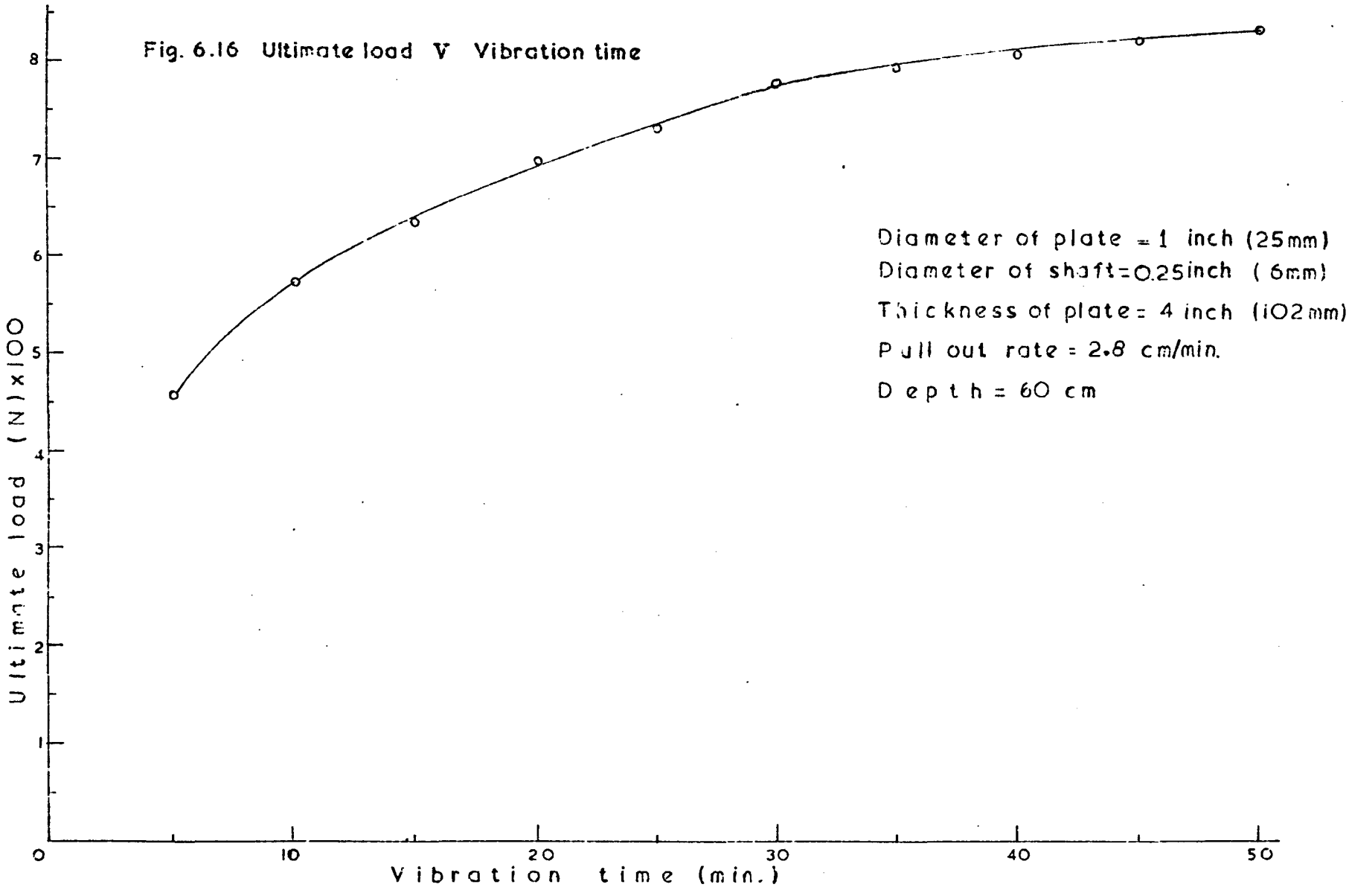

the test was repeated at least four times and the average ultimate load was calculated from the best three.

6.6.3 Conclusions

Fig. 6.16 shows that although the ultimate load increases with the time of vibration of the sand, the rate of change of the ultimate load decreases and at 45 minutes the rate becomes negligible.

From the load-displacement curves obtained throughout the investigation, it was found that these are repeatable for any time of vibration, within an experimental error of 7%. It was also observed that the overall experimental error decreased with the vibration time.

CHAPTER VII

DETERMINATION OF COEFFICIENT OF EARTH PRESSURE AT REST

7.1 General

In recent years, numerous methods have been developed to determine the vertical and horizontal pressures in soils using different types of sensing instruments. Pressure gauges were developed to measure the pressures in soil under a vehicle wheel, in earth dams, embankments and cofferdams.

In an attempt to define the initial state of the sand bed for this investigation, two pressure gauges had to be designed and manufactured in the laboratory, since a great deal of effort was put in the search for a marketed gauge and proved to be unsuccessful. The vertical and horizontal stresses at different depths for various vibration times were measured. A soil pressure cell obtained at a later stage, was also used to verify the results (see Appendix D).

7.2 Description of Gauges

The diaphragm pressure gauges, shown in plate 8 and fig. 7.1, are of hydraulic type. These, made of brass, are modifications of the gauge developed by Briggs (1960, Ref 49).

(a) Horizontal gauge. A cylindrical piece of brass, 46 mm in diameter and 14 mm in length, was machined to the dimensions shown in Fig. 7.2. The active chamber of the gauge, 44 mm diameter and 1.9 mm deep, was enclosed by the main body and a 0.6 mm thick brass diaphragm. A nylon dowel (see Fig. 7.4), made from nylon rod, was screwed to the tapped hole (¼ in. B.S.F.) in the main body. Through the

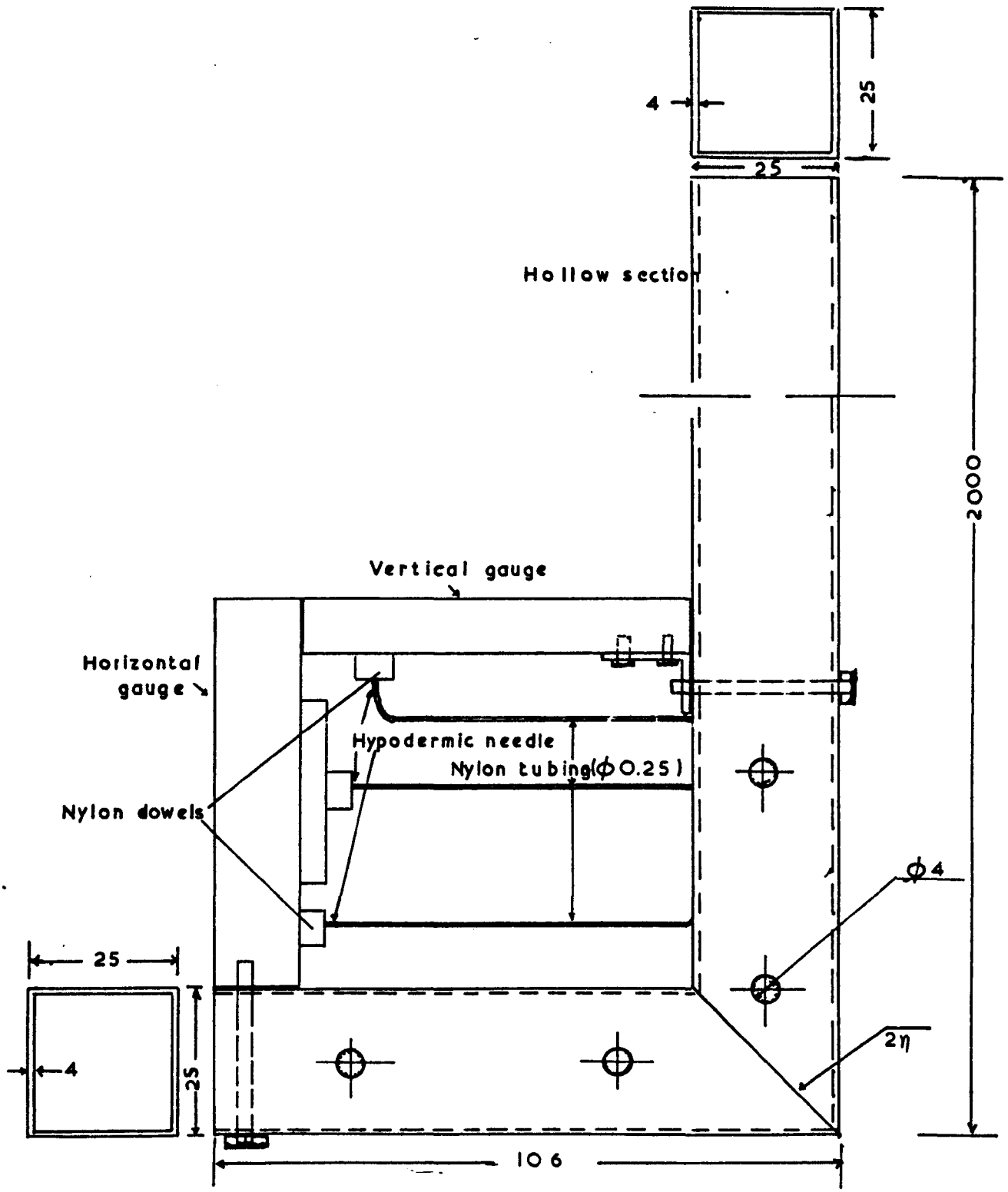

Dimensions are in millimetres

Fig. 7.1 Pressure cell

centre of the dowel, a 1 mm diameter hole was drilled and a nylon tube was fitted and glued. The dummy chamber was sealed off by a brass blank (see Fig. 7.4) of 31 mm diameter and 8 mm thick. A second nylon dowel was fitted to the brass blank.

(b) Vertical Gauge . This gauge, similar to that previously described, contains only an active chamber, Fig. 7.3. The dummy chamber was omitted due to the fact that both gauges were to be used at the same time and in the same location, thus one dummy chamber would be enough to provide a temperature correction.

7.3 Assembling of Gauges

Before assembling the gauges, all surfaces were cleaned with fine emery paper. Both gauges were submerged in water with the diaphragms facing downwards, and filled by means of several cycles of boiling and cooling under water. The process was stopped when further boiling did not result in appearance of more bubbles from the three chambers. The fine nylon tube, with paraffin syphoning through it, was inserted into the dowel hole with the connection completed under water.

Before calibration, both gauges were left to stand for a week and the levels of paraffin in the nylon tubes were marked every several hours. It was found that the paraffin levels dropped, and close examination showed some leakage through the nylon dowel threads. It was then decided to glue the dowels to the main body, and again the gauges were left to stand for a few days. Although there was no

Plate 8

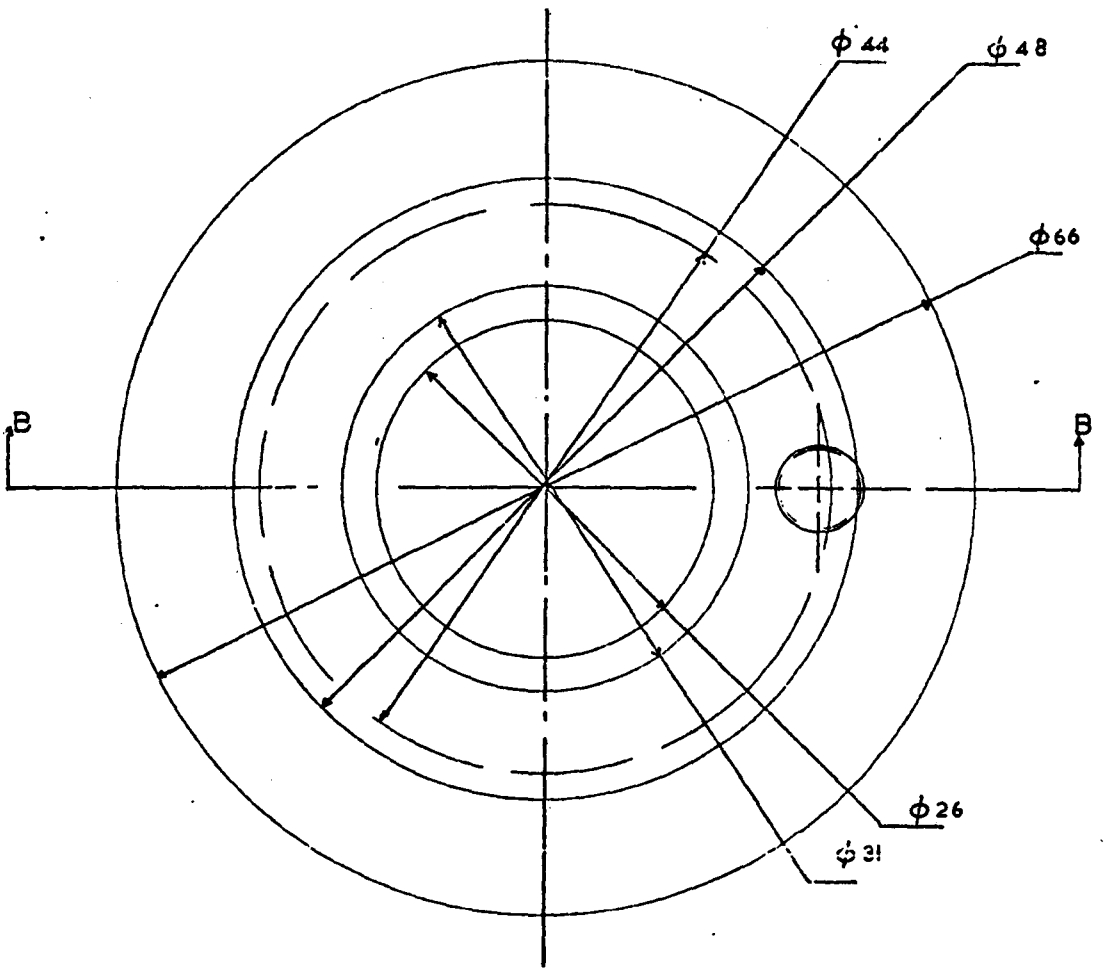

Diamensions are in millimetres

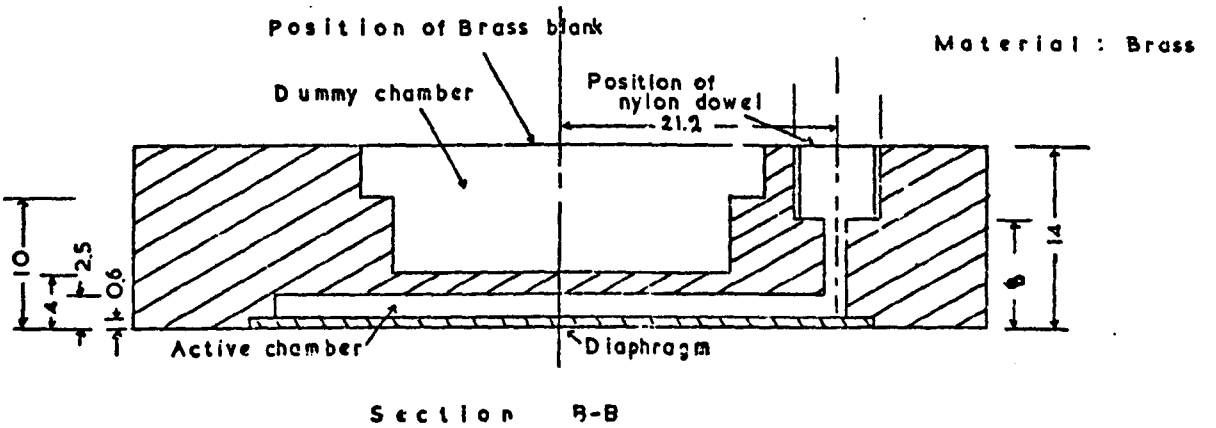

Section B-B

Fig. 7.2 Horizontal gauge

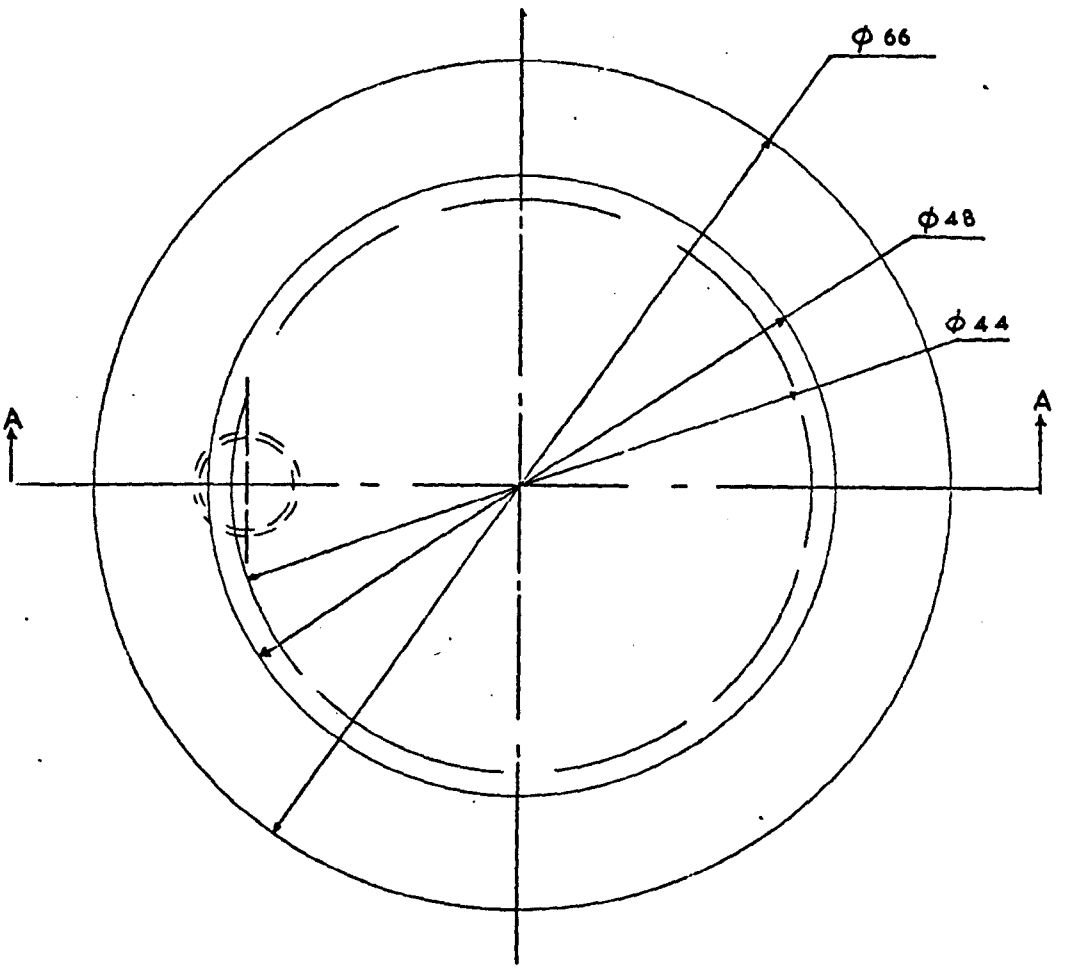

Material: Brass

Dimensions are in millimetres

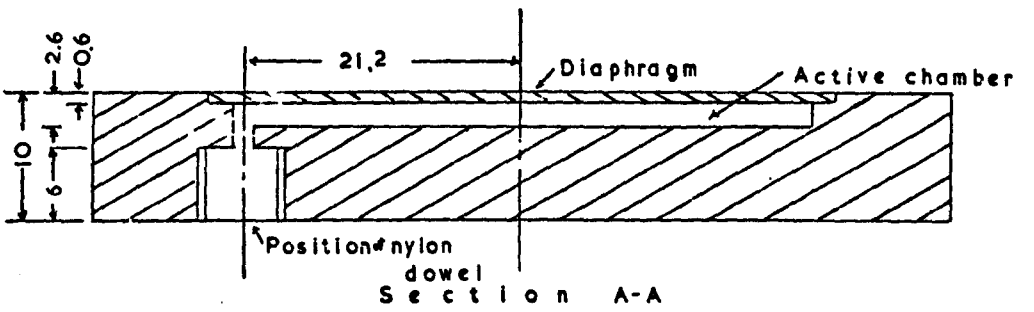

Fig. 7.3 Vertical gauge

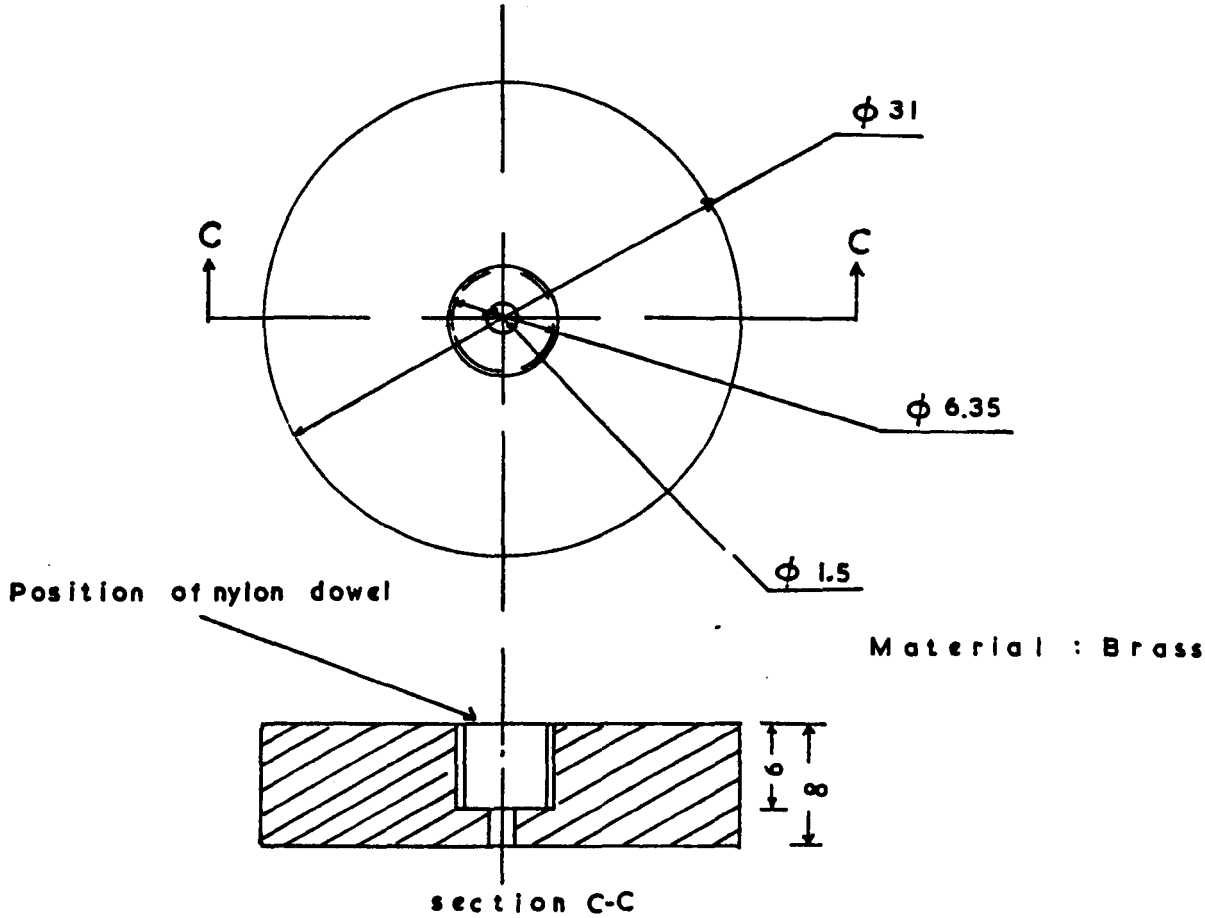

brass blank

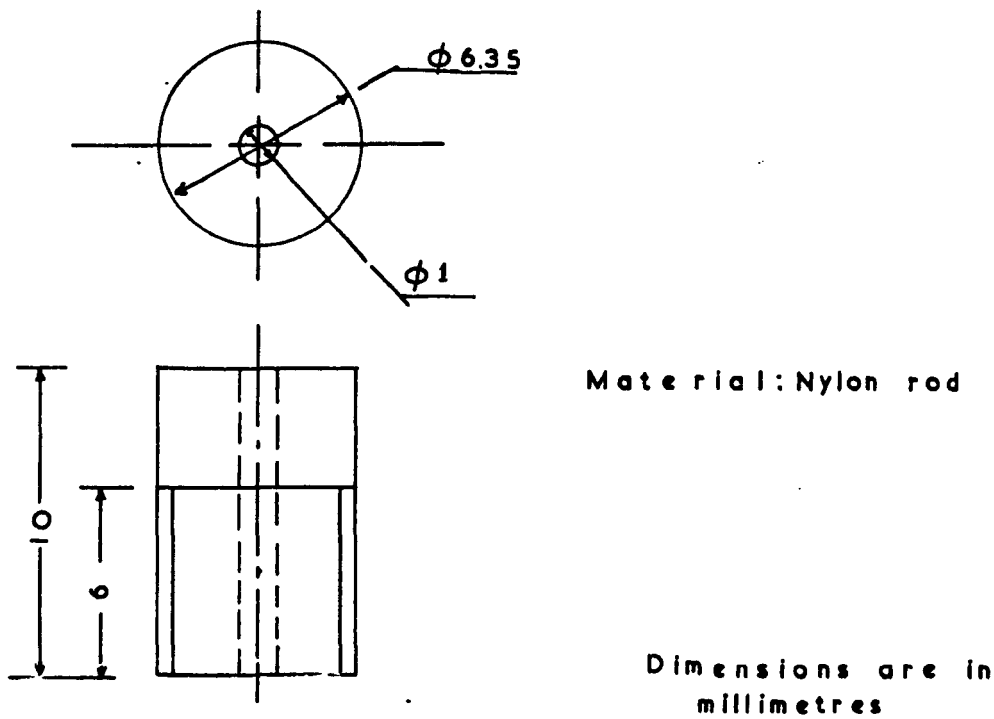

nylon dowel

Fig. 7.4

leakage, it was found that when pressing the membrane of the active chamber of the horizontal gauge, the paraffin level in the nylon tube of the dummy chamber rose by a very small amount. A further modification of the gauge was made by removing the dowel and enclosing the dummy chamber permanently, after filling with water.

The decision to leave out the temperature correction by ignoring the dummy chamber, was taken due to the fact that the time taken to carrying out a single test would be very short, and both calibrations and experiments would be conducted at laboratory temperatures.

The gauges were connected to a light hollow section, 25 mm x 25 mm x 4 mm, and the nylon tubes were attached along the length of the section, Fig. 7.1 and Plate 8. The cell unit was placed in the sand and vibrated for a short period of time. On removal of the gauges from the sand, examination showed that the glue connecting the nylon tubes to the dowels, was removed due to the vibration of the particles. Surgical needles were then used to replace the glue; and two thin plates were screwed to the hollow section in order to protect the connections. A further vibration of the cell unit in the sand showed that the levels of paraffin in both tubes remained constant.

7.4 Calibration

The calibration of the gauges was carried out using 25cm diameter glass tube. The tube, 3 m long, was filled with water and left to stand for some time, until the water

obtained the laboratory temperature. The cell unit was inserted at different depths into the glass tube and the level of the paraffin in each tube was marked. The procedure was repeated several times and the mean value of the increase in the level of the paraffin was plotted against the height of the water above the gauge, see Fig. 7.5.

7.5 Measurements of Stresses in Sand

The unit cell was placed in the sand using the 127 mm (5 in.) diameter pvc tube. The hollow section was clamped to a rigid bar placed across the tank. The sand was vibrated for a given period of time and the increase in the paraffin levels were recorded. Repeating the test, it was found that both gauges gave inconsistent readings. Repetition of the test with the unit cell free to move during vibration, showed that although the horizontal gauge gave consistent readings, the vertical gauge gave very low or high values. In the case of the high readings, the level of the paraffin dropped after the hollow section was gently tapped. Since the horizontal gauge was found to function consistently, it was decided to ignore the vertical gauge and only record the horizontal gauge readings.

In order to find the distribution of the coefficient of earth pressure at rest for various states of the sand sample, the unit cell was placed at different depths and the soil was vibrated for different times. Six different vibration times, between 10 minutes and 50 minutes, were used and the horizontal stresses were calculated, Table 7.1. Using the densities obtained from the density tube, the vertical pressure and K_o were also calculated.

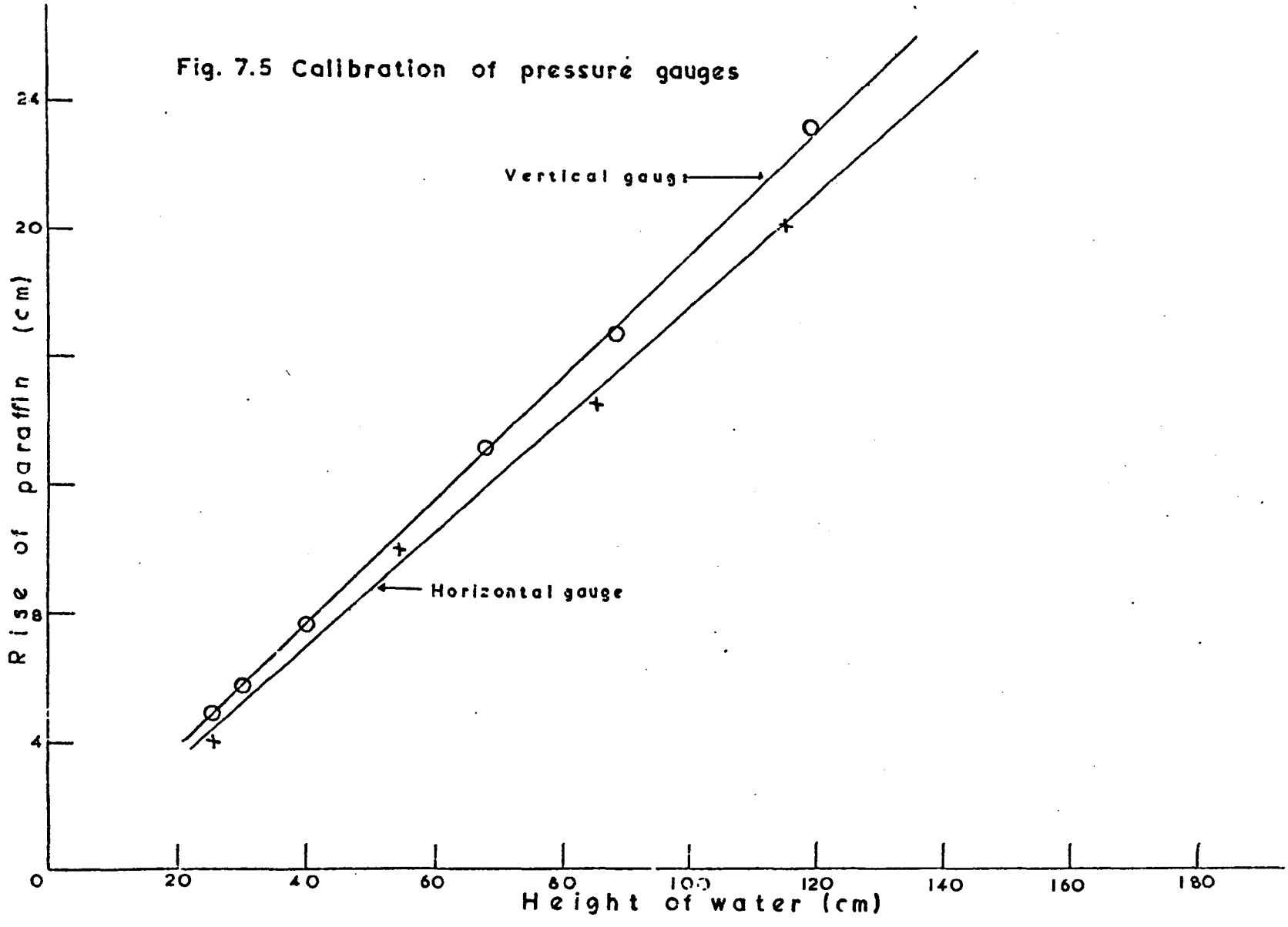
Fig. 7.5 Calibration of pressure gauges
Vertical gauge
Horizontal gauge
Rise of paraffin (cm)
Height of water (cm)
0
4
8
20
24
20
40
60
80
100
120
140
160
180

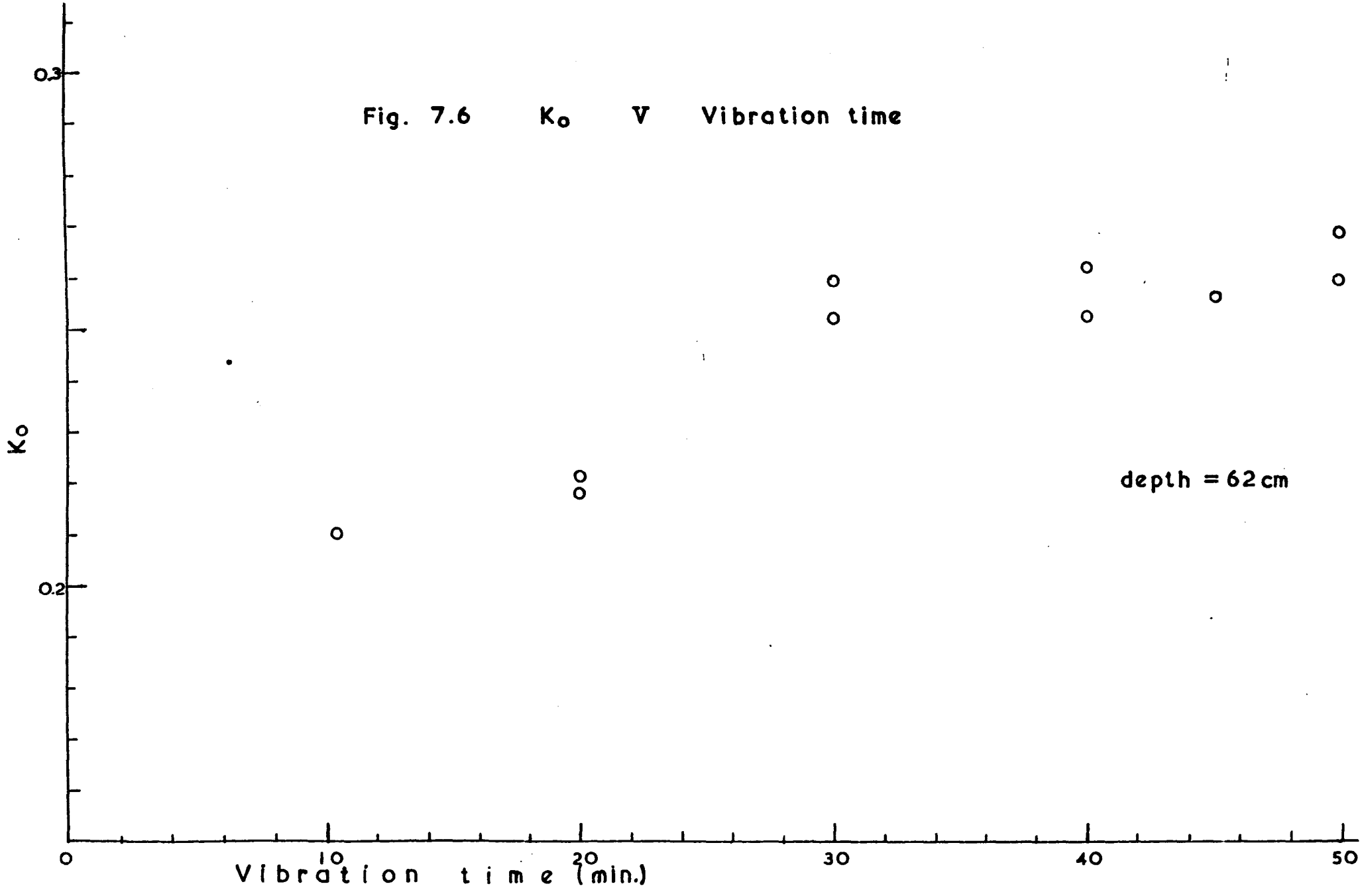
Fig. 7.6 Ko V Vibration time
0.3
0.2
Ko
depth = 62 cm
0
10
20
30
40
50
Vibration time (min.)

7.6 Discussion

The values of K_o obtained at 62cm depth, were plotted against vibration time, Fig. 7.6. The figure shows K_o increasing with the vibration time and at about 40 minutes obtaining a value of about 0.27. The variation of density and ultimate load with vibration time also showed the same trend, i.e. the state of sand remains nearly constant after 40 minutes of vibration. The figure also shows that K_o varies from 0.21 to 0.27 between 10 minutes and 50 minutes of vibration.

The values of K_o for 45 minutes vibration time, were also plotted against depth, Fig. 7.7. K_o decreases with depth and obtains a constant value of about 0.25 - 0.26 at a depth of 52cm. The high value obtained near the surface of the soil, could be explained by the fact that the particles are freer to move than in deeper depths. The figure shows that K_o varies between 0.46 and 0.25 for depths between 30cm and 70cm.

In Appendix D K_o, calculated using the soil pressure cell and the density tube, was found to vary between 0.15 and 0.7 for a 45 min. vibration. The high value was obtained at about 31cm depth and the low value between 50 and 70cm depth. At 42cm depth K_o was calculated to be about 0.34.

Both types of gauges were found to function reasonably well for measuring the horizontal stresses. The vertical stresses were found to be low, and when calculating the densities these were found to vary between 0.21 gr/cm^3 and 0.79 gr/cm^3 although it is known to have a value greater than 1. The inconsistencies inherent in the vertical gauge could be due to the following reasons.

(a) Arching occurred above the gauge due to the hollow section forming an obstruction to the movement of the sand particles

TABLE 7.1

TIME OF VIBRAT. (min.)	DEPTH (cm)	HOR. STRESS (gr/cm^2) x 10^2	VERT. STRESS (gr/cm^2) x 10^2	K_o x 10^{-2}
10	61.5	0.20	1.00	19.6
	62.0	0.22	1.02	21.0
	63.0	0.23	1.04	22.2
20	36.0	0.22	0.60	37.4
	62.0	0.23	1.04	21.9
	62.0	0.23	1.04	21.9
	62.0	0.24	1.04	23.2
	63.0	0.23	1.05	21.9
30	59.0	0.25	0.99	25.4
	62.0	0.27	1.04	25.9
	62.0	0.27	1.04	25.9
	64.3	0.28	1.08	26.0
40	33.0	0.23	0.56	41.2
	34.0	0.27	0.57	47.0
	36.6	0.29	0.61	46.9
	62.0	0.25	1.05	23.8
	62.0	0.26	1.05	24.8
	62.0	0.27	1.05	25.7
	63.0	0.25	1.06	23.5
45	34.0	0.26	0.58	45.0
	35.0	0.27	0.59	44.5
	37.0	0.28	0.63	45.3
	41.0	0.22	0.68	31.6
	49.0	0.25	0.83	30.6
	52.0	0.23	0.88	25.5
	63.0	0.27	1.07	25.2
	65.0	0.28	1.10	25.3
50	61.5	0.27	1.05	25.8
	62.0	0.27	1.05	25.6
	62.0	0.28	1.05	27.0

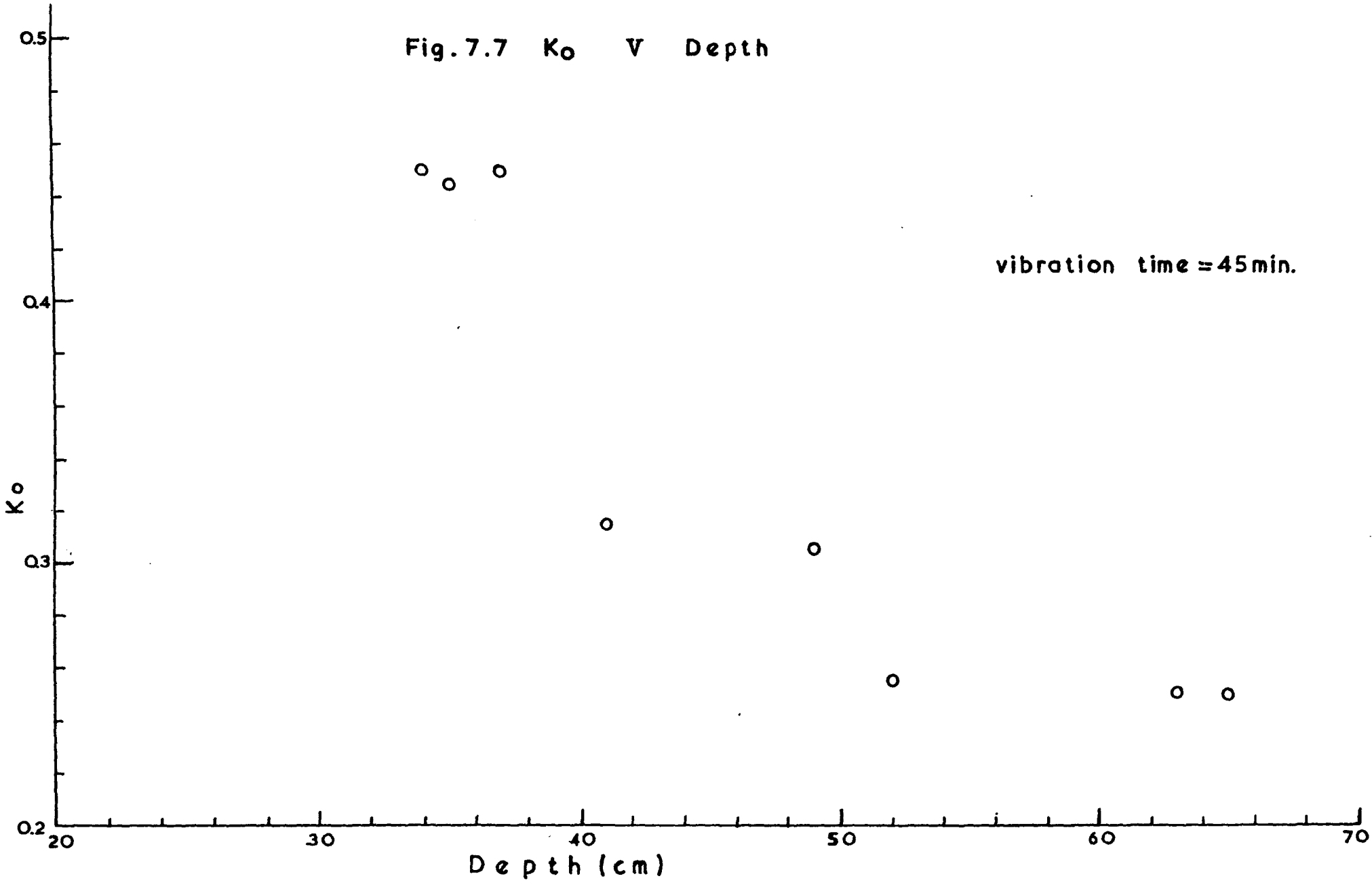
Fig. 7.7 Ko V Depth
vibration time = 45 min.
0.5
0.4
0.3
0.2
Ko
20
30
40
50
60
70
Depth (cm)

during vibration. Durelli and Rilley (1961, Ref. 50) stated that a phenomenon similar to arching in static soil mechanics also seems to exist under dynamic conditions but it is not well understood.

(b) Although a small rotation of the gauge from its horizontal position would introduce a very small error in the reading of the hydraulic type gauge, the error in the soil pressure cell would be considerable since the initial voltage readings of the gauge in the vertical and horizontal positions are 2.40 mV and 1.75 mV respectively. Durelli and Rilley (1961, Ref. 50) also found that their gauge was sensitive only to the vertical component of stress normal to its surface.

CHAPTER VIII

EXPERIMENTAL RESULTS

8.1 General

In Chapter III it was mentioned that the pullout unit was designed and constructed in such a way that the entire load-displacement curve of an anchor can be obtained. In this Chapter some of the curves obtained using the following data, will be presented and their features will be discussed.

(a) Constant rate of strain = 28 mm/min.

(b) Thickness of plate = 102 mm (4 in.).

(c) Diameter of shaft for 38 mm (1.5 in.) and 51 mm (2 in.) diameter plate = 6 mm (0.25 in.).

(d) Diameter of shaft for 13 mm (0.5 in.), 19 mm (0.75 in.) and 25 mm (1 in.) diameter plate = 5 mm (0.2 in.).

The following variables were used during this investigation:-

(a) Depth of the anchor.

(b) Diameter of the anchor.

(c) Vibration time.

Although it was shown in Chapter VI that a 45 min. period of vibration of the sample would be an ideal time, due to the fact that the density and the coefficient of earth pressure at rest would increase no further with longer vibration, tests with different times of vibration were also performed and used for comparison.

8.2 Load-displacement curve

Fig. 8.1 shows typical load-displacement curves obtained with the anchor plate embedded at about the same depth in each

Fig. 8.1 Load V Displacement

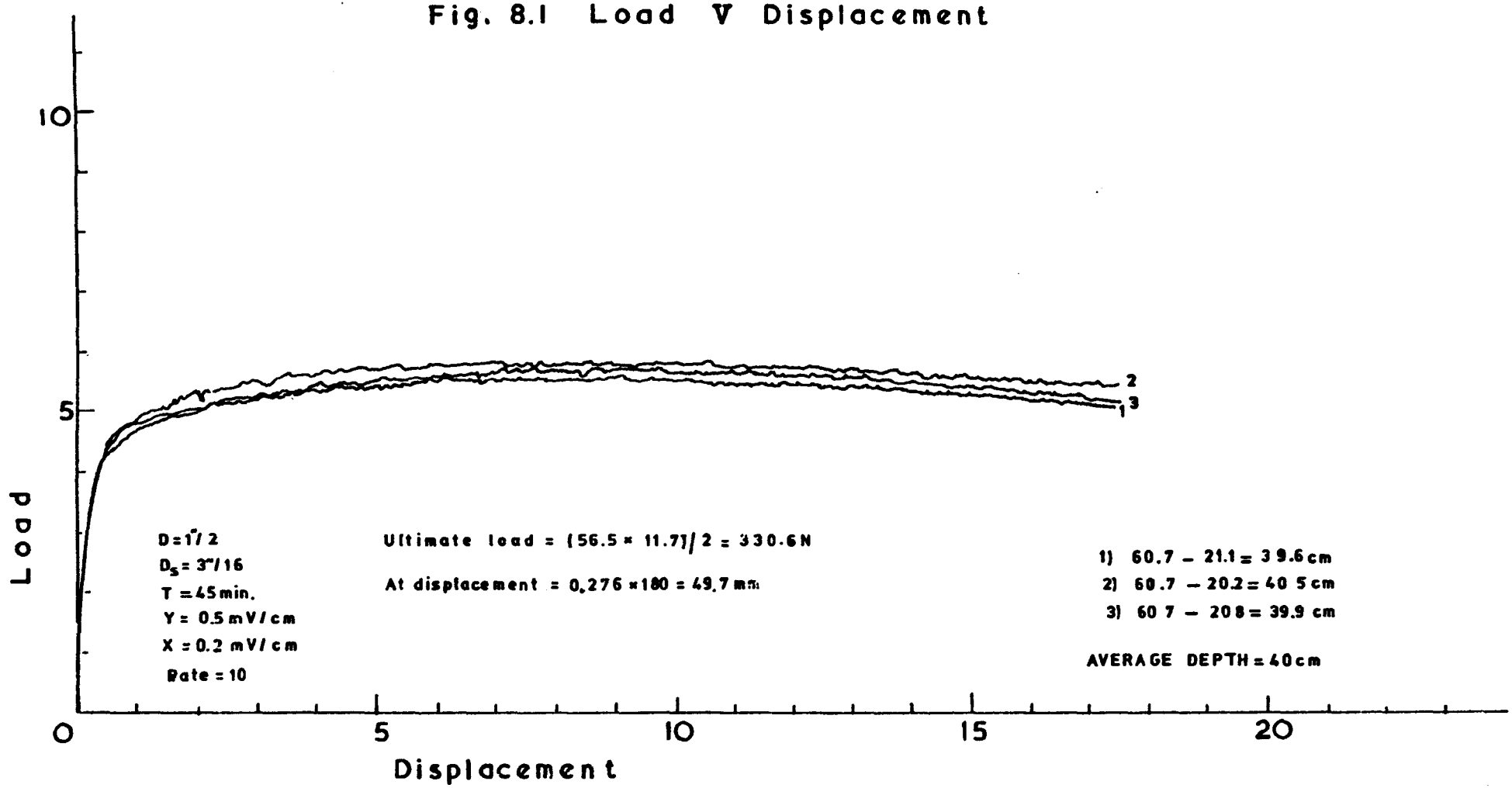

test. Each curve consists of three sections. The initial section, a straight line, is followed by the second section, a smooth curve, which reaches a peak at a substantially greater displacement than the initial portion. The third section, the post peak part, in this case is a smooth curve although its shape depends on various factors such as depth, density, diameter of plate and boundary conditions.

For each anchor plate, embedded at a given depth and vibrated for a required time, an average load-displacement curve was obtained from which the information needed was extracted. The average curve was obtained by repeating the test four times,and taking the mean load at every centimetre of displacement on the graph paper of the best three load-displacement curves. The depth of the anchor was calculated by averaging the depths of the tests.

Fig. 8.2 shows the load-displacement curves of a 51mm (2 in.) diameter anchor plate embedded at different depths in a 45 minutes vibrated sand bed. At a small relative depth of about 6, i.e. H = 30cm, the figure shows a substantial reduction of load during post peak testing. Carr (1970, Ref.23) stated that this reduction in load can be attributed to dilatancy of the shearing sand,causing a reduction in shearing strength along the failure surface. As the depth and $\frac{H}{D}$ increase due to D remaining constant, the load decreases less rapidly after reaching its maximum load. This could be explained by the fact that the failure surface adjacent to the anchor plate becomes more and more localised. Carr stated that the reduction in strength due to the loosening effects of dilatancy is less pronounced. From the curves obtained with the anchor plate embedded at 30cm and 40cm depth it could be concluded that the transition point from "shallow" to deep occurs between $\frac{H}{D} = 6$ and $\frac{H}{D} = 8$.

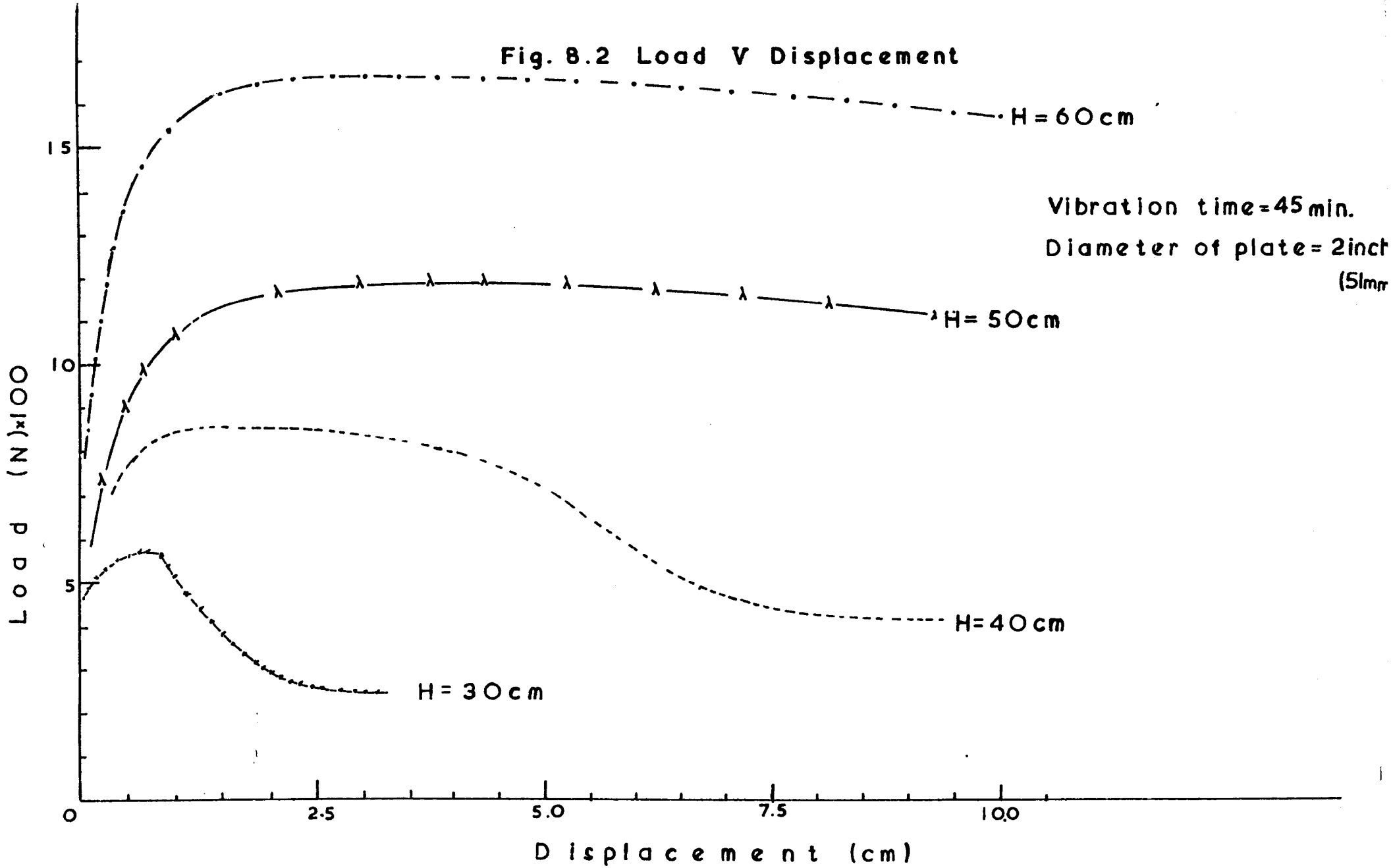
Fig. 8.2 Load V Displacement
H = 60 cm
Vibration time = 45 min.
Diameter of plate = 2inch
(51mm
H = 50 cm
H = 40 cm
H = 30 cm
Load (N) x 100
15
10
5
0
2.5
5.0
7.5
10.0
Displacement (cm)

Fig. 8.3 was obtained using a 51mm (2 in.) diameter anchor plate embedded at a number of depths. Two times of vibration were used, i.e. 10 min. and 45 min., in order to obtain different initial states of sand samples; sample A and B respectively. Comparing the curves at each depth, it can be observed that anchor restraint in dense sand, i.e. 45 min., is greater than that in the less dense sand, i.e. 10 min. At smaller relative depth, although the initial restraint of the anchor embedded in sample B is greater than that in sample A, this is not so for the post-peak portion of the curve. The figure also shows that the anchor, when embedded in sample B, obtains its maximum load at a smaller absolute displacement, and its load decreases at a greater rate after peak. From the load-displacement curves, H = 30cm for T = 10 min. and T = 45 min, it could be said that the transition point from "shallow" to "deep" varies with the initial state of the sample.

8.3 Influence of anchor depth

From the load-displacement curves, obtained by performing tests using different sizes of anchor plates and embedding them at various depths, the ultimate load was recorded and plotted against depth see Fig. 8.4. Although the ultimate load increases, the rate of increase varies with the depth. Considering the curves, obtained with D = 19mm (0.75 in.) and D = 25mm (1 in.), it can be observed that these are of similar shape, indicating that the depth has the same effect on both plates. Each curve is made up of three sections. The first section, a straight line, shows that the ultimate load is directly proportional to the depth. The second section a smooth curve with its slope initially decreasing and then increasing, is followed by the third section, which is a straight line with a slope greater than that of the first line. As the diameter of the plate decreases, i.e. D = 13mm (0.5 in.), the curvature of the curve is less marked due to

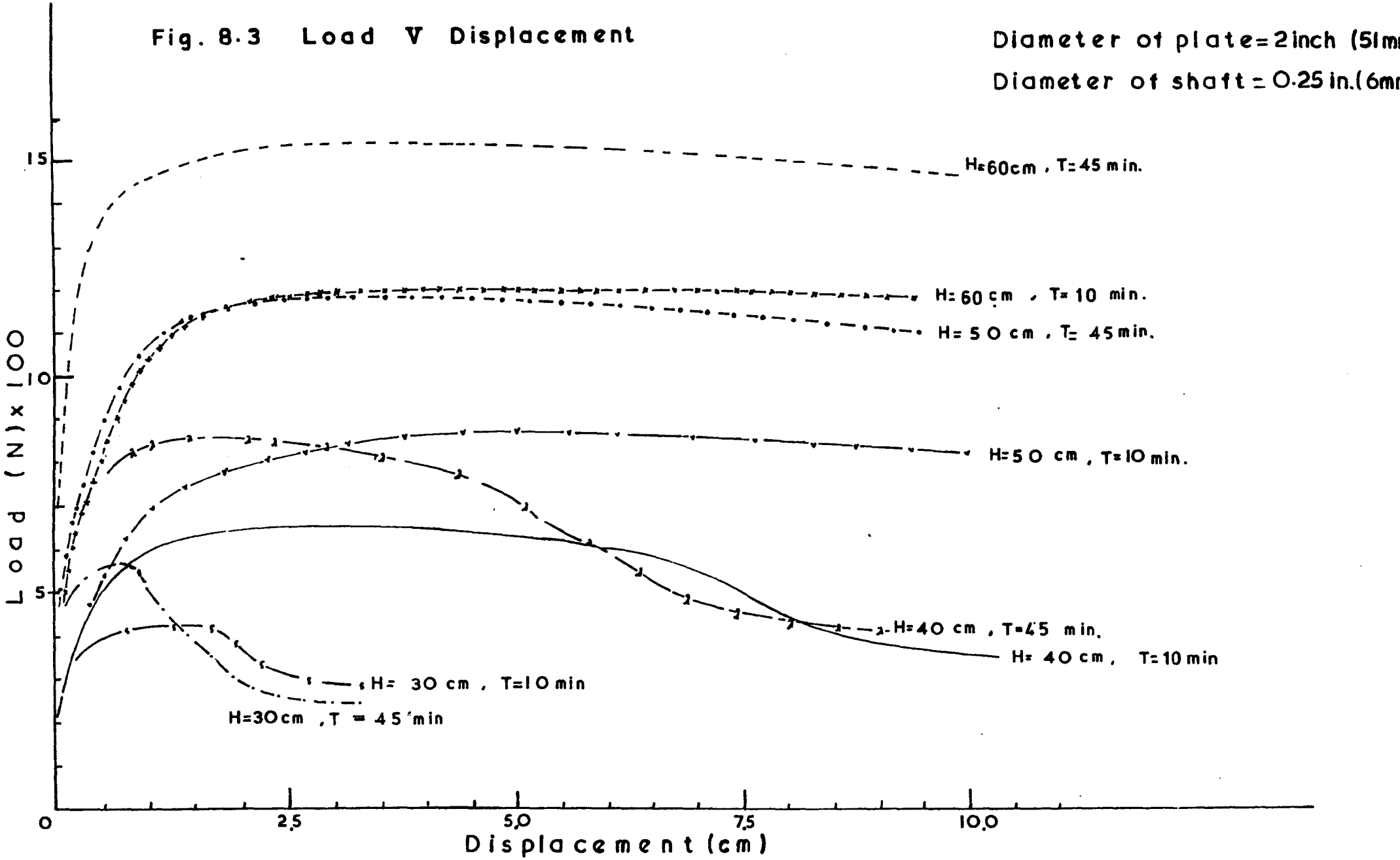
Fig. 8.3 Load V Displacement
Diameter of plate=2inch (51mm)
Diameter of shaft = 0.25 in.(6mm)
H=60cm , T=45 min.
H= 60 cm , T= 10 min.
H= 50 cm , T= 45 min.
H= 50 cm , T=10 min.
H=40 cm , T=45 min.
H= 40 cm , T=10 min
H= 30 cm , T=10 min
H=30cm , T = 45 min
Load (N) x 100
15
10
5
0
2.5
5.0
7.5
10.0
Displacement (cm)

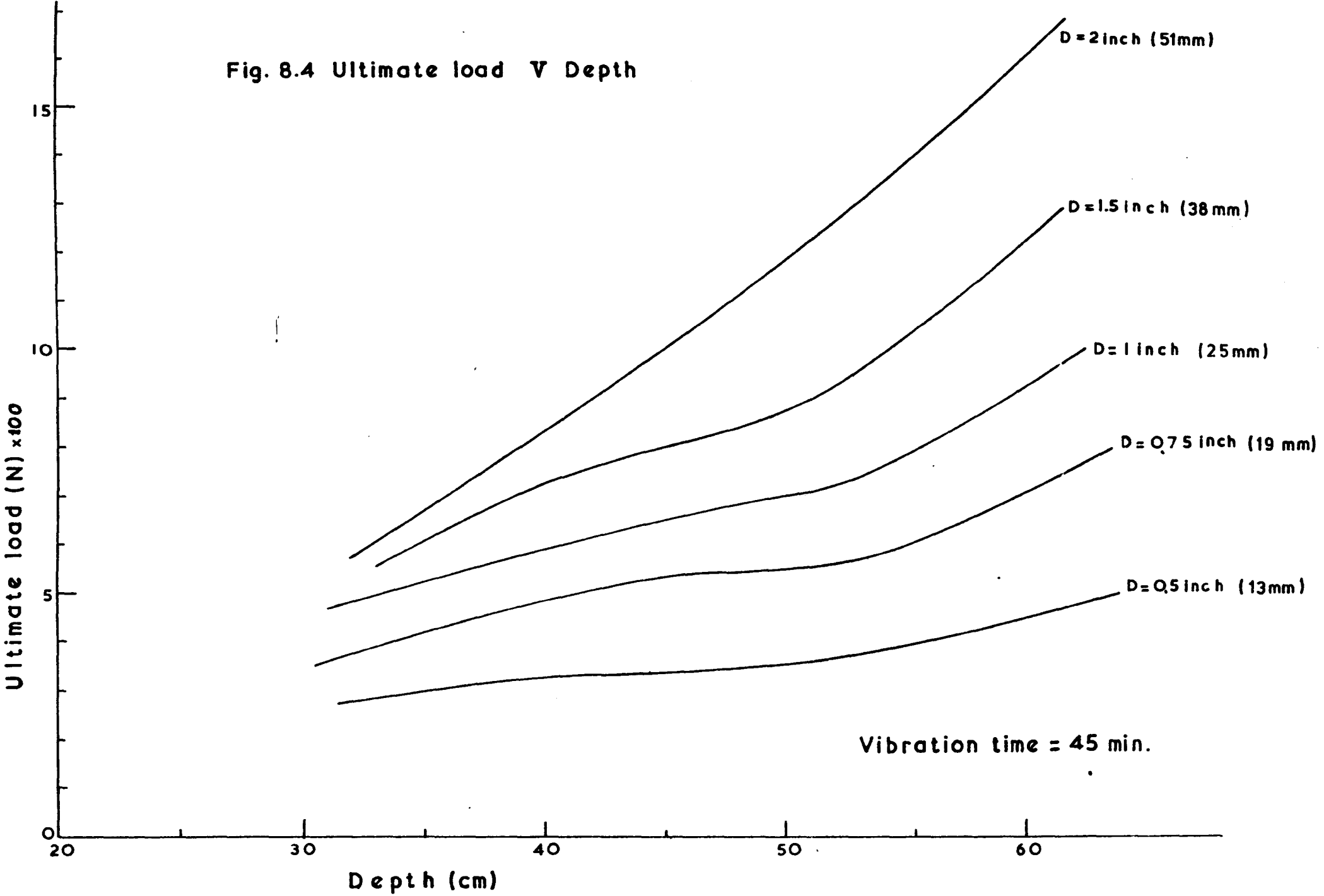
Fig. 8.4 Ultimate load V Depth
D = 2 inch (51mm)
D = 1.5 inch (38 mm)
D = 1 inch (25mm)
D = 0.75 inch (19 mm)
D = 0.5 inch (13mm)
Vibration time = 45 min.
Ultimate load (N) x100
Depth (cm)
0
5
10
15
20
30
40
50
60

the small increase of the ultimate load with the depth. Although part of the D = 38 m (1.5 in.) curve is similar to the curves described previously, its initial section has a greater slope. As the diameter of the plate increases, i.e. D = 51mm (2 in.), the relationship is a smooth curve and the rate of change of the ultimate load increases as the depth increases from H = 30cm to H = 60cm.

8.4 Influence of the anchor plate diameter

Fig. 8.5 to Fig. 8.8 show the load-displacement curves obtained with different sizes of anchor plates embedded at various depths between H = 30cm and H = 60cm. In the first few millimetres of displacement, the load increases more rapidly as the diameter of the plate increases from D = 25mm (1 in.) to D = 51mm (2 in.). The absolute displacement at which the ultimate load occurs, decreases with the diameter of the plate increasing.

Fig. 8.9 shows the ultimate load plotted against the diameter of the anchor plate with the depth of embedment varying from H = 30cm to H = 60cm. At small depths, i.e. from H = 30cm to H = 40cm, the ultimate load is directly proportional to the plate diameter, and as the depth increases the rate of change of each relationship increases. At greater depths, i.e. H = 50cm and H = 60cm, although the ultimate load increases with the diameter of the plate, the rate of change also increases with the depth and the diameter of the anchor plate.

The maximum average pressure on the anchor plates at different depths was calculated and plotted against the diameter of the plates, see Fig. 8.10. It is observed that for a given depth, the pressure decreases with the diameter of the plate increasing, and also for D > 38mm the maximum

Fig. 8.5 Load V Displacement

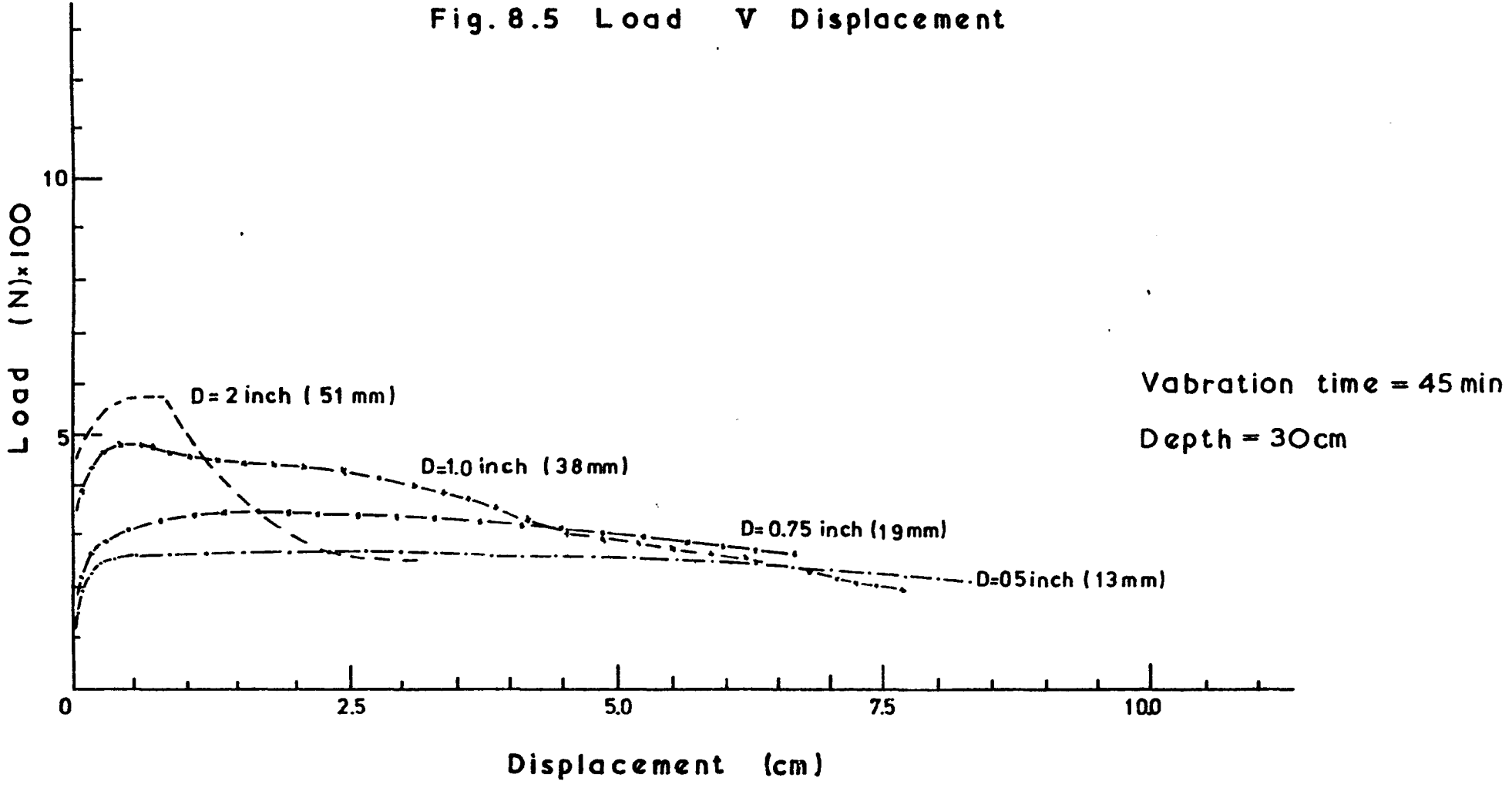

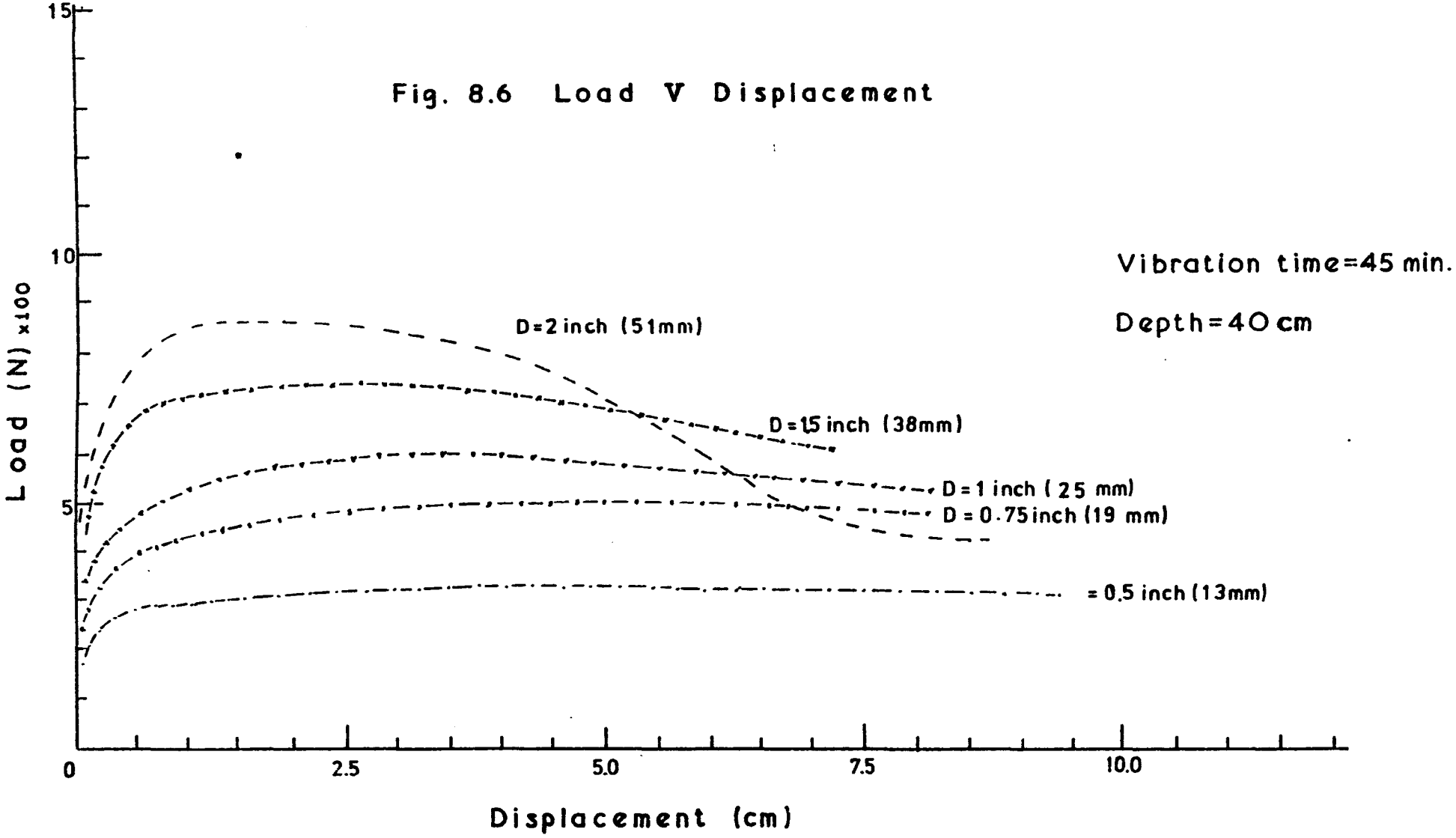
Fig. 8.6 Load V Displacement
Load (N) x100
15
10
5
0
2.5
5.0
7.5
10.0
Displacement (cm)
Vibration time=45 min.
Depth=40 cm
D=2 inch (51mm)
D=1.5 inch (38mm)
D=1 inch (25 mm)
D=0.75 inch (19 mm)
=0.5 inch (13mm)

Fig. 8.7 Load V Displacement

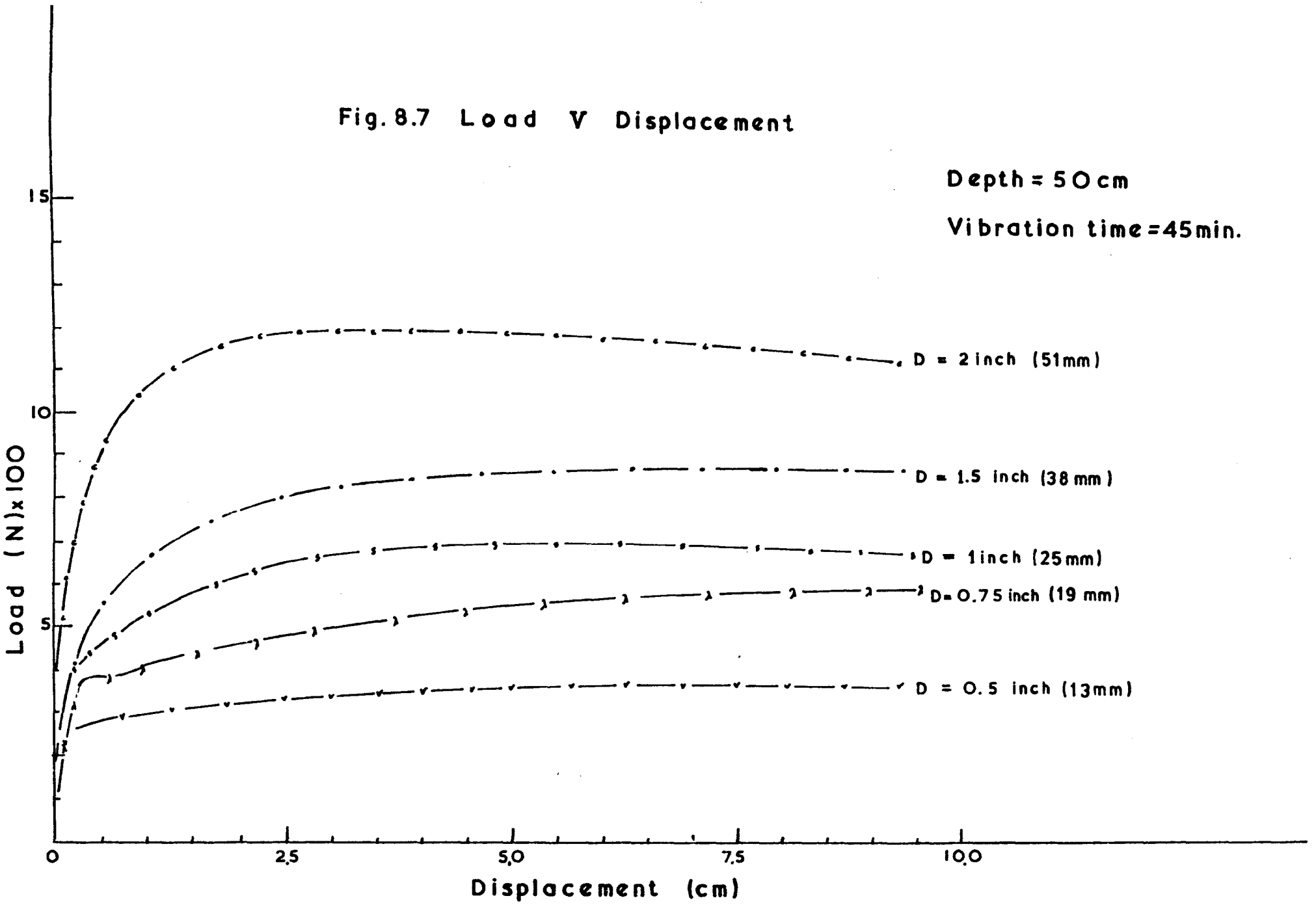

Fig. 8.8 Load V Displacement

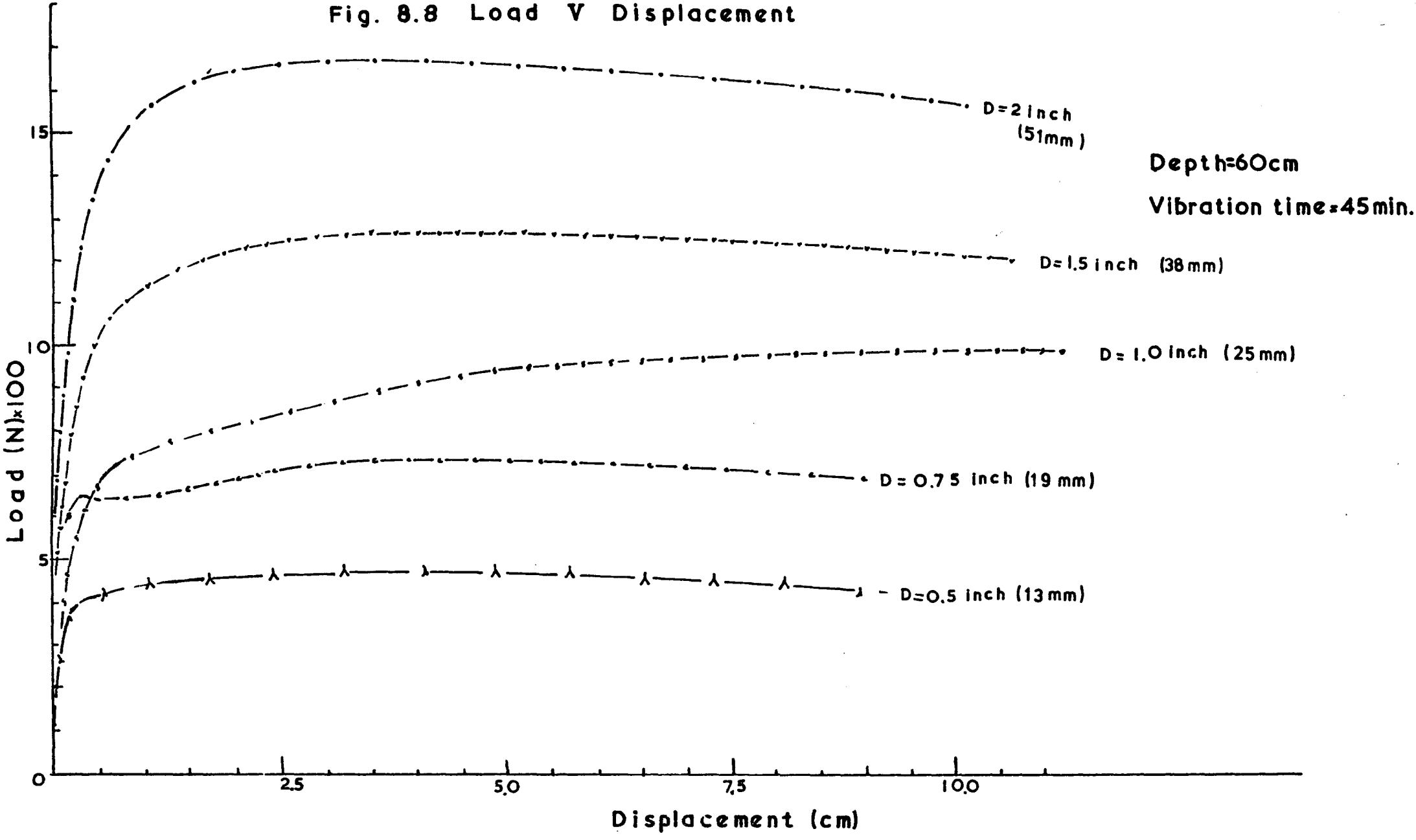

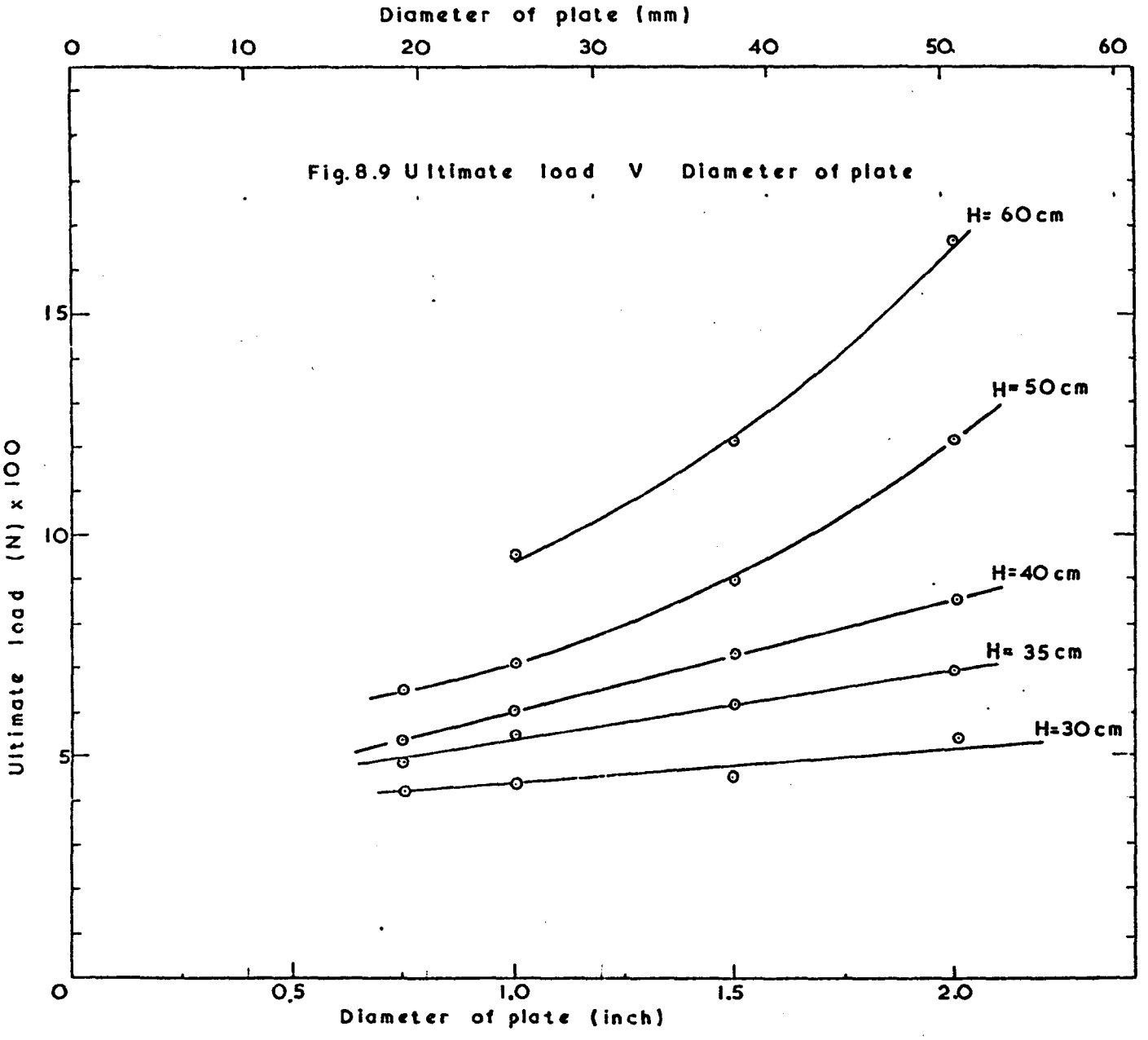
Diameter of plate (mm)
0
10
20
30
40
50
60
Fig. 8.9 Ultimate load V Diameter of plate
H= 60 cm
H= 50 cm
H=40 cm
H= 35 cm
H=30 cm
Ultimate load (N) x 100
15
10
5
0
0.5
1.0
1.5
2.0
Diameter of plate (inch)

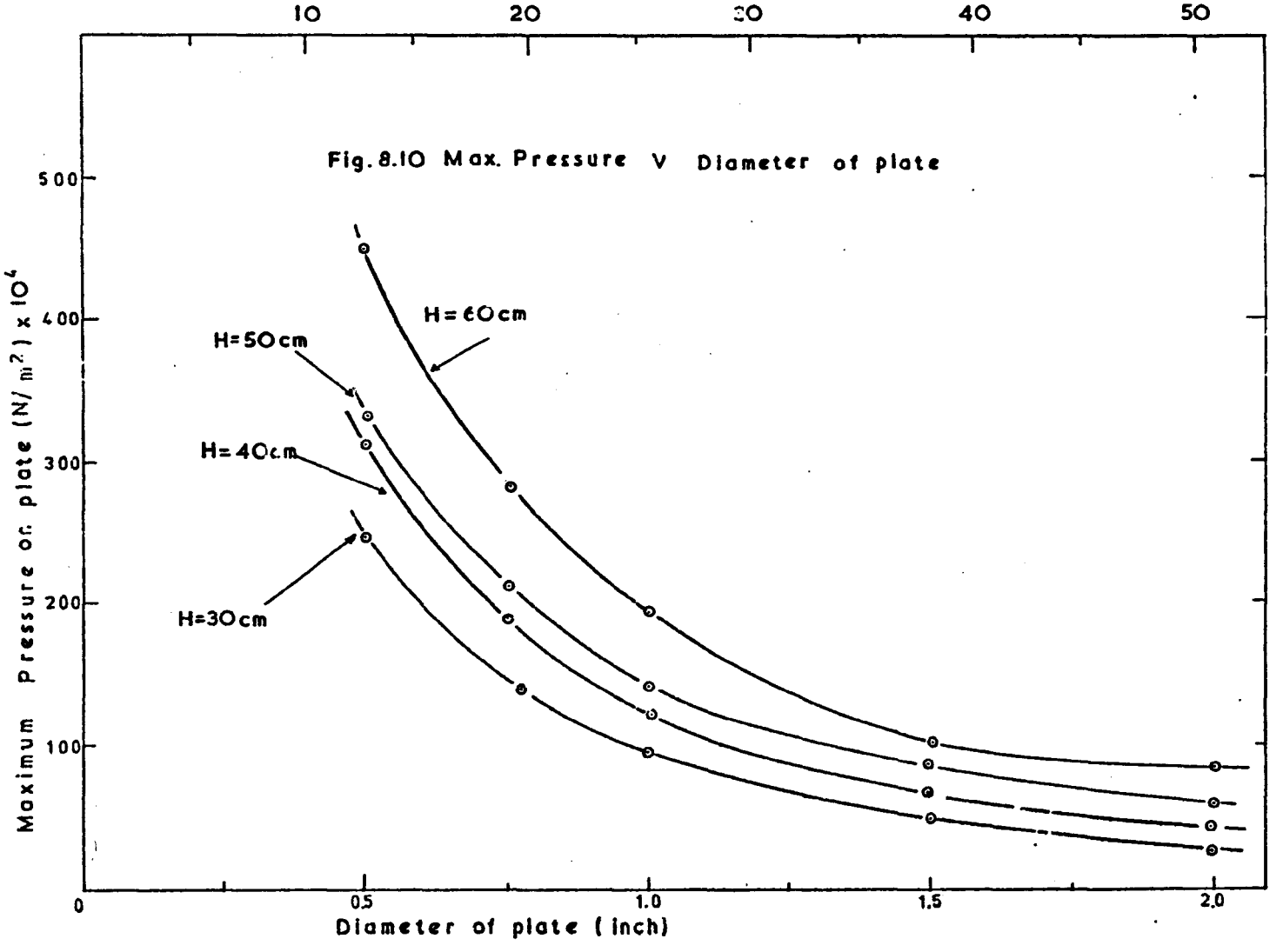

Fig. 8.10 Max. Pressure V Diameter of plate

average pressure on the plate remains approximately constant. The figure also shows that for a given diameter, the pressure increases with the depth of the anchor. Carr (1970, Ref. 23) also plotted the same parameters, and his curves showed a similar trend to the curves in Fig. 8.10. He concluded that the smaller the relative depth of the anchor, the less the anchor plate pressure would be permitted to develop.

8.5 Variation of ultimate load with $\frac{H}{D}$

In previous sections it was shown that neither of the two parameters, i.e. H and D, can produce on its own a general trend as far as the ultimate load is concerned. Therefore the two parameters are combined to produce a relationship with the ultimate load, see Fig. 8.11. The curve, obtained using a 13mm (0.5 in.) diameter anchor plate, shows that the ultimate load increases linearly between $\frac{H}{D} = 16$ and $\frac{H}{D} = 27$. From $\frac{H}{D} = 27$ to $\frac{H}{D} = 43$ the increase of the rate of change of the load with the relative depth decreases, and for $\frac{H}{D} > 43$ this increases reaching a maximum slope at about $\frac{H}{D} = 49$. Curves D = 19mm to D = 38mm, show a similar trend to the curve described; the rate of change of the ultimate load with $\frac{H}{D}$ increases with the diameter of the anchor plate increasing. The variation of the ultimate load of a 51mm (2 in.) diameter anchor plate with the relative depth is approximately linear.

Fig. 8.12 shows the ultimate load plotted against $\frac{H}{D}$, for different sizes of anchor plates and different times of vibration. The curves show that the effect of the vibration time is comparatively small with the effects of the anchor plate diameter and its depth of embedment on the ultimate load.

Fig. 8.11. ULTIMATE LOAD V (H/D)

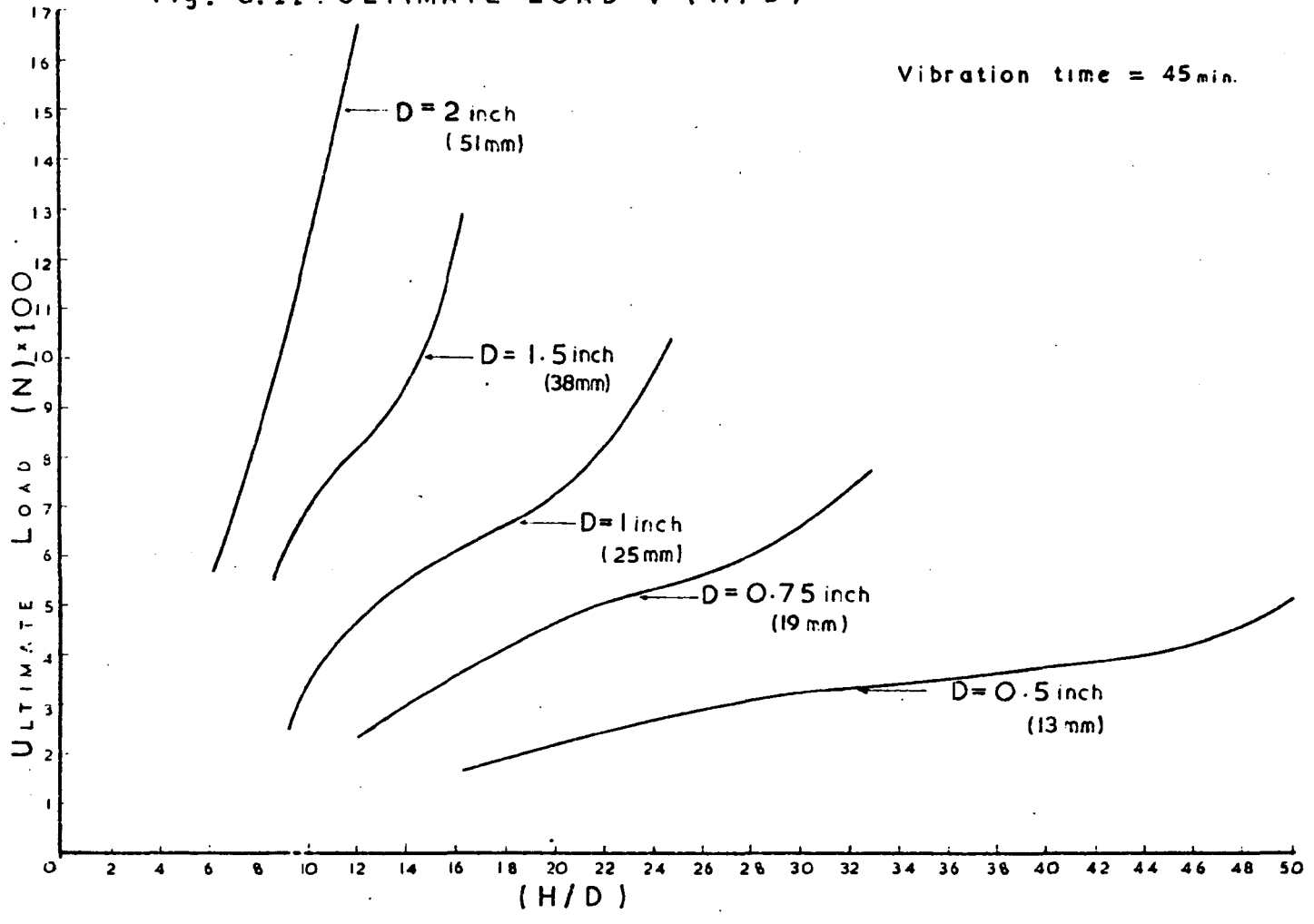

Fig. 8.12 Ultimate load v H/D

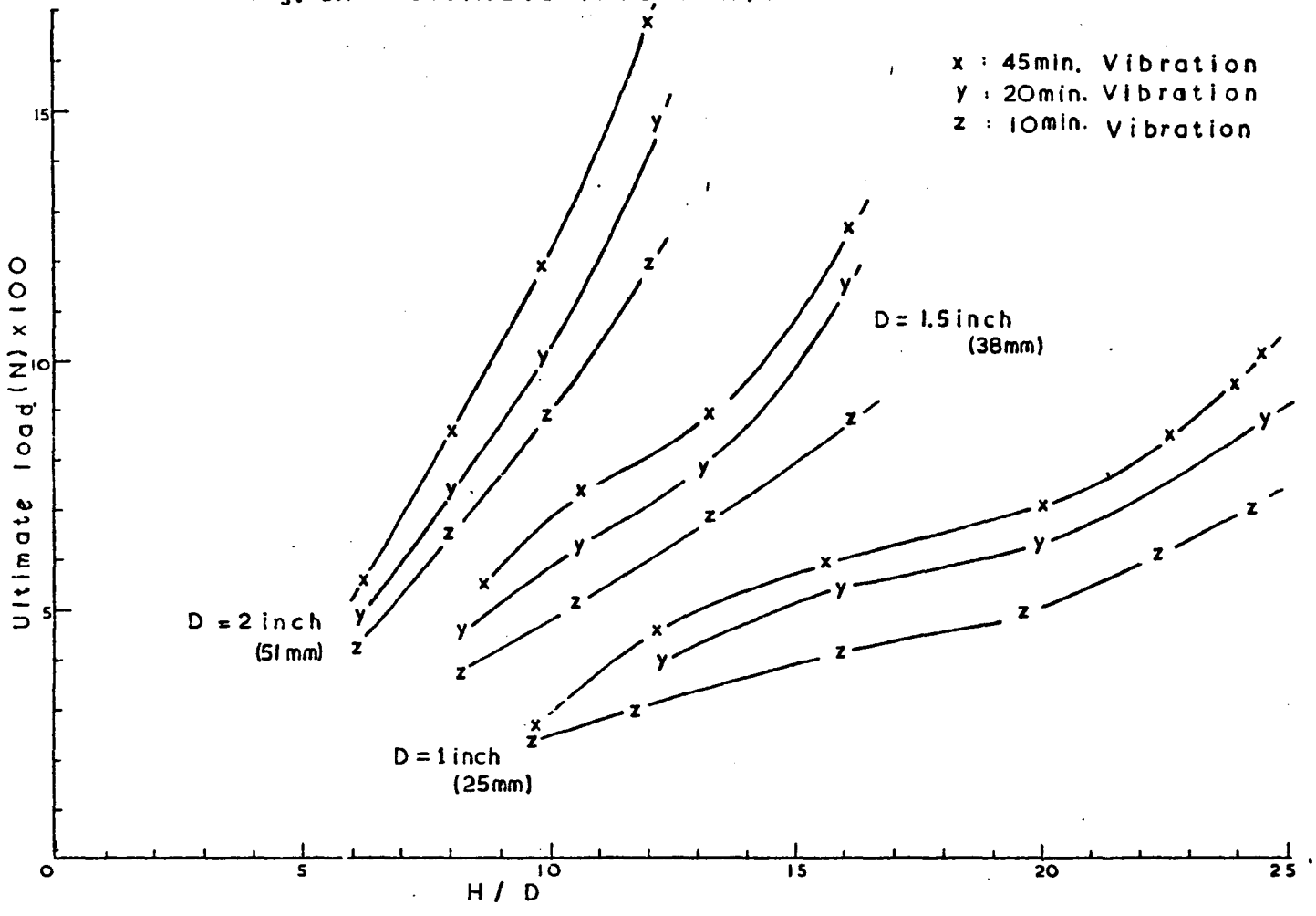

8.6 Variation of breakout factor

The breakout factor, defined as $\frac{4 P_m}{\pi D^2 H \gamma}$, was used by previous researchers in order to obtain some relationship between laboratory and field tests. This dimensionless parameter is usually plotted against another dimensionless parameter, $\frac{H}{D}$.

Baker and Kondner (1965, Ref. 20) plotted $\frac{P_m}{D^2 H \gamma}$ against $\frac{H^2}{D^2}$ and found that there was a good correlation, for low values of $\frac{H}{D}$, between the different anchor plate diameters used during the experimental work, Fig. 8.13 (b). But as the value of $\frac{H}{D}$ increased, each curve, i.e. for each diameter plate, followed a different path, indicating that a relationship between $\frac{P_m}{D^2 H \gamma}$ and $\frac{H^2}{D^2}$ did not exist for large relative depths. Fig. 8.13 (a).

Carr (1970, Ref. 23) also plotted breakout factor against $\frac{H}{D}$, and stated that he found a perfect correlation between the different diameters of anchor plates for $\frac{H}{D}$ varying from zero to 15, Fig. 8.14 (a). Carr also found that the breakout factor of the 51mm (2 in.) diameter plate was larger than that of the 152mm (6 in.) diameter plate at every $\frac{H}{D}$, and explained it by saying that the shaft diameter, not taken into consideration, reduces the effective area of the anchor plate. He then plotted $\frac{4 P_m}{(D^2 - D_s^2) H \gamma \pi}$ against $\frac{H}{(D - D_s)}$, and found that although the breakout factor of the 152mm (6 in.) diameter plate was larger than that of the 51mm (2 in.) diameter plate at every $\frac{H}{(D - D_s)}$; he also found that two curves were generated, Fig. 8.14 (b).

Fig. 8.15 shows the author's breakout factors for each anchor plate plotted against $\frac{H}{D}$. The area of the anchor shaft was taken into consideration. From the figure, it is observed

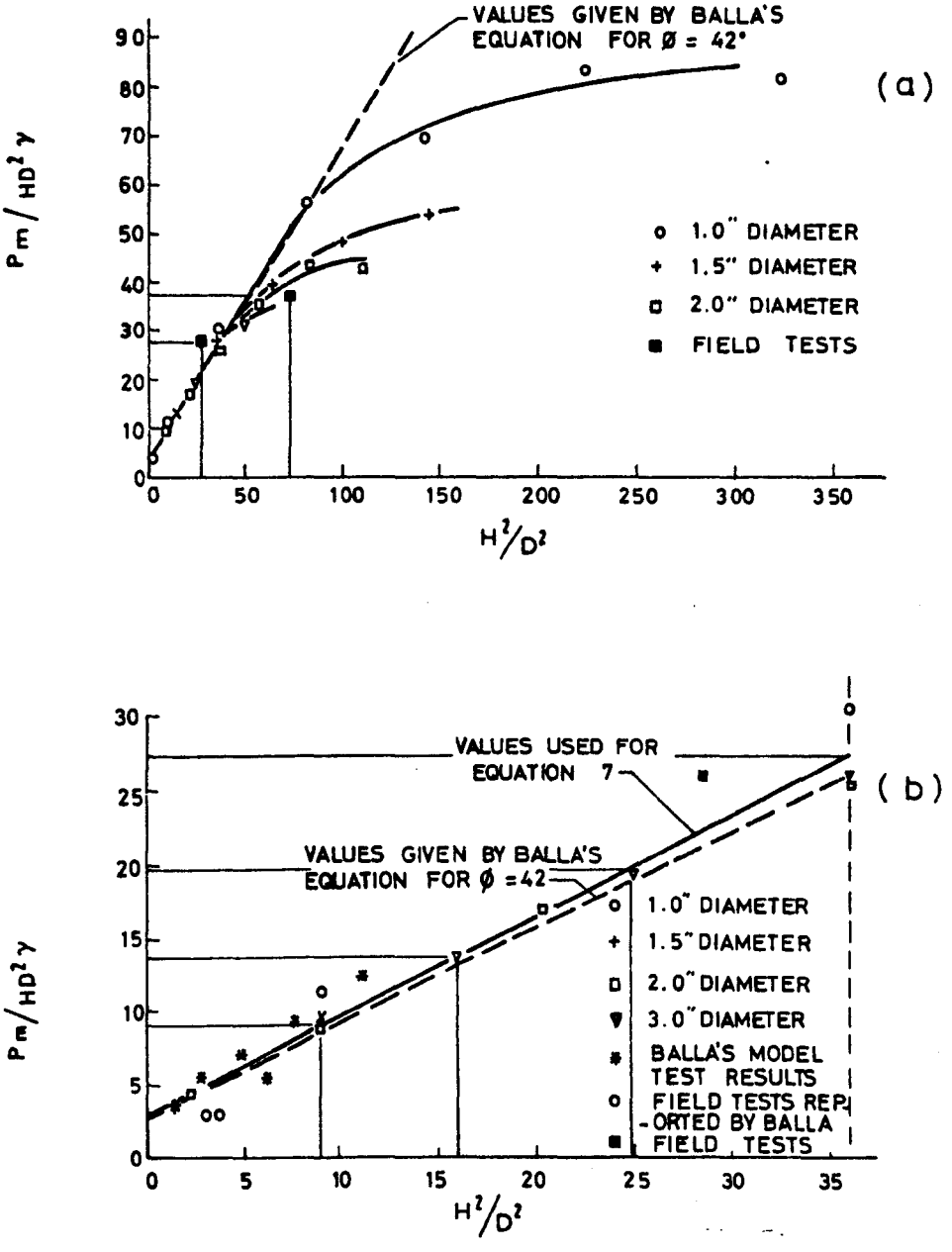

Fig. 8.13

(Baker & Kondner)

Fig . 8.14
(Carr)

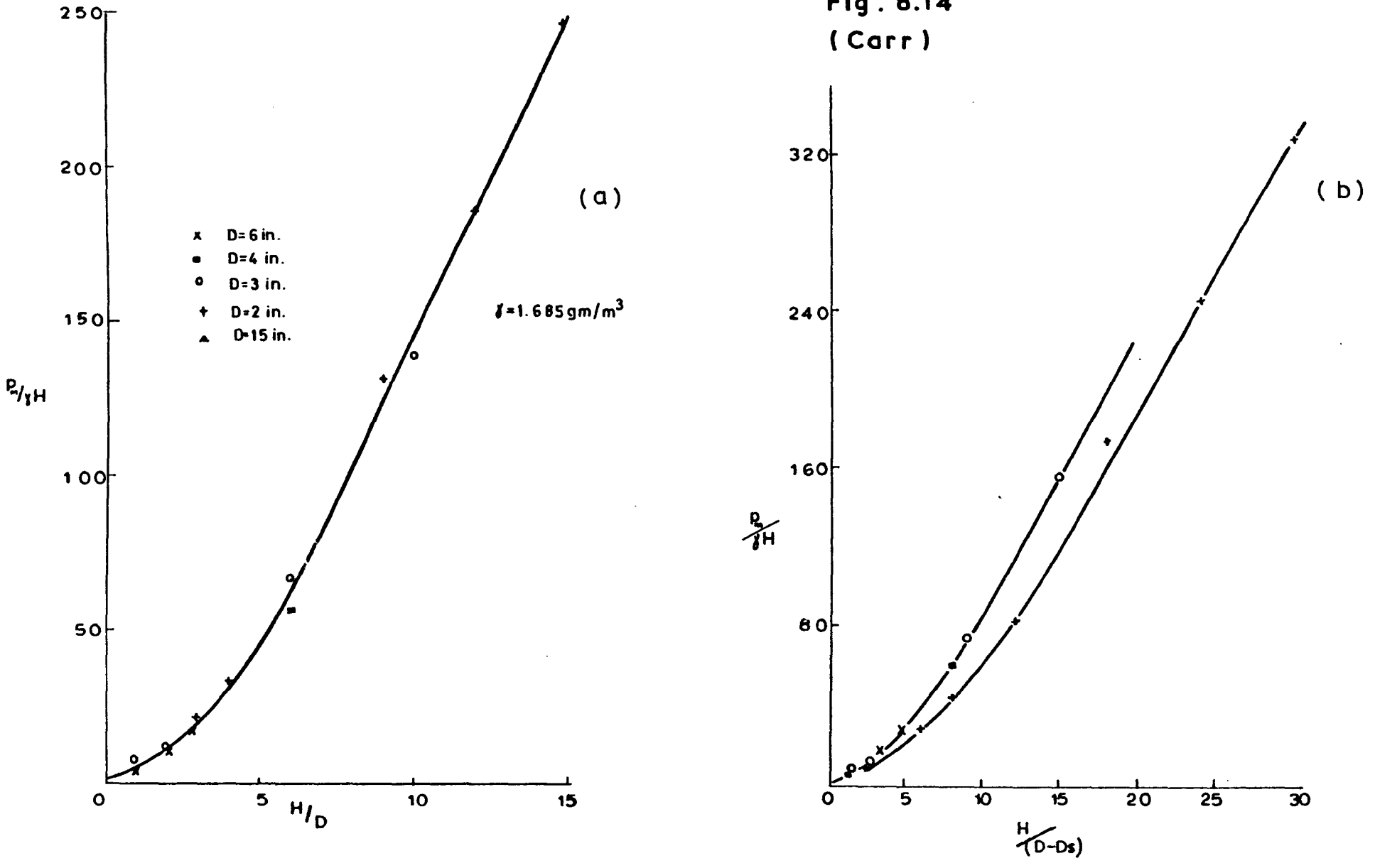
250
200
150
100
50
0
5
10
15
H/D
Pm/γH
(a)
x D=6 in.
■ D=4 in.
o D=3 in.
+ D=2 in.
▲ D=1.5 in.
γ=1.685 gm/m³
320
240
160
80
0
5
10
15
20
25
30
H/(D-Ds)
Pm/γH
(b)

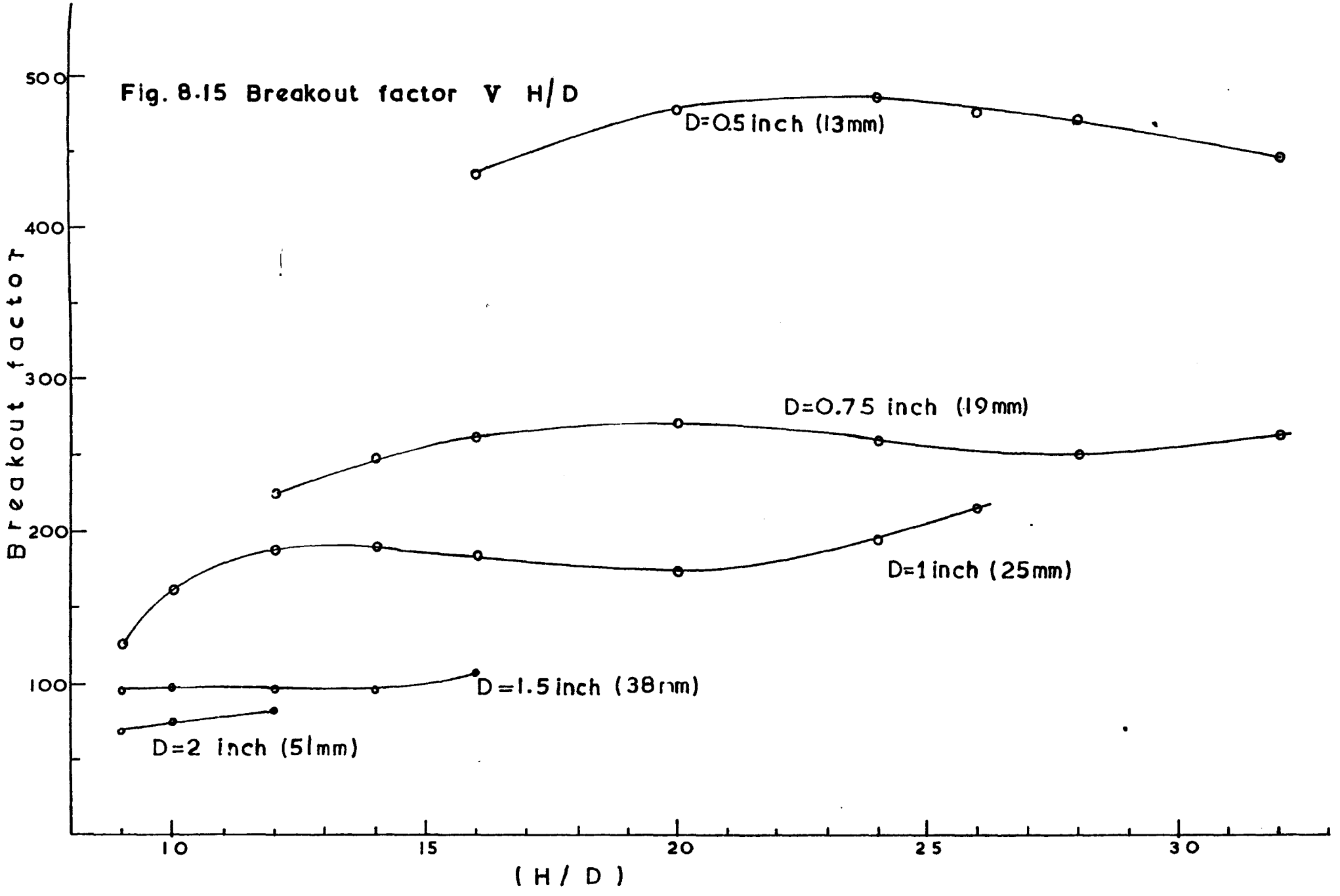
Fig. 8.15 Breakout factor V H/D
D=0.5 inch (13mm)
D=0.75 inch (19mm)
D=1 inch (25mm)
D=1.5 inch (38mm)
D=2 inch (51mm)
Breakout factor
500
400
300
200
100
10
15
20
25
30
(H/D)

that each anchor plate follows a different curve. The curve for D = 13mm (0.5 in.) shows that the breakdown factor increases from 450 to 500,and then decreases again to 450 as the relative depth increases. The breakout factors of the 19mm (0.75 in.) and 25mm (1 in.) diameter plates oscillate between the values 220 and 270, 120 and 220 respectively. Although the breakout factors of the two bigger anchor plate diameters, i.e. D = 38mm (1.5 in.) and D = 51mm (2 in.), remain approximately constant with $\frac{H}{D}$ varying, the relationships are not pronounced due to insufficient results. From Fig. 8.15 the following points, are clear for $\frac{H}{D} > 6$.

(a) A relationship between breakout factor and relative depth exists for each diameter anchor plate.

(b) The breakout factor increases with the diameter of the plate decreasing, and as the diameter increases the breakout factor tends to obtain a constant value for $\frac{H}{D}$ increasing.

A full comparison between the two Figures, Fig. 8.13 and 8.15, cannot be made due to difference in the ranges of $\frac{H}{D}$. Although Baker and Kondner have drawn smooth curves through their results of 25mm (1 in.) and 51mm (2 in.) plate diameters for $\frac{H^2}{D^2} > 144$ and $\frac{H^2}{D^2} > 50$ respectively, the breakout factors increase and then decrease for the relative depths greater than those specified above. The breakout factor of the D = 25mm (1 in.) at $\frac{H^2}{D^2} = 225$ ($\frac{H}{D} = 15$) is greater than the one at $\frac{H^2}{D^2} = 325$ ($\frac{H}{D} = 18$). Similarly the breakout factor of the D = 51mm (2 in.) at $\frac{H^2}{D^2} = 81$ ($\frac{H}{D} = 9$) is greater than the one at $\frac{H^2}{D^2} = 110$ ($\frac{H}{D} = 10.5$).

A comparison between Carr's curves and those of the author cannot be made due to the difference in the ranges of $\frac{H}{D}$ and anchor plate diameters. Carr's first statement that there was no separation of the individual curves, (i.e. for

different anchor plate diameters) must be true only for small relative depths, a fact also found by Baker and Kondner. His second assumption that the breakout factor was affected by the diameter of the shaft, although true in his case, this cannot be employed as a general rule. It was found and described in a previous chapter, that the ultimate load is not affected if the ratio of the anchor plate diameter to the anchor shaft diameter is kept greater than 4. The results, in Fig. 8.15, still show that the breakout factor decreases with the diameter of the plate although a ratio of $\frac{D}{D_s} = 4$ was used.

Fig. 8.16 shows the variation of the breakout factor with the anchor plate diameter for different relative depths. The figure shows that for a given relative depth, the breakout factor decreases with the diameter of the plate and tends to obtain a constant value. The curves, $\frac{H}{D} = 10$ and $\frac{H}{D} = 16$, also indicate that the breakout factor is not affected considerably by the relative depth for any plate diameter greater than 25mm (1 in.). It can also be said that the breakout factor is independent of anchor plate diameter for D > 38mm (1.5in) and obtains a value of about 90.

8.7 Variation of the displacement at ultimate load with $\frac{H}{D}$

From the load displacement curves, the displacement at which the ultimate load of each anchor plate occurred was recorded and plotted against the relative depth, Fig. 8.17. Carr (1970, Ref. 23) who also plotted the same parameters, drew a straight line to represent the variation, although his results were also scattered. Fig. 8.17 shows that each plate diameter follows its own straight line, and the

Fig. 8.16 Breakout factor V Diameter of plate

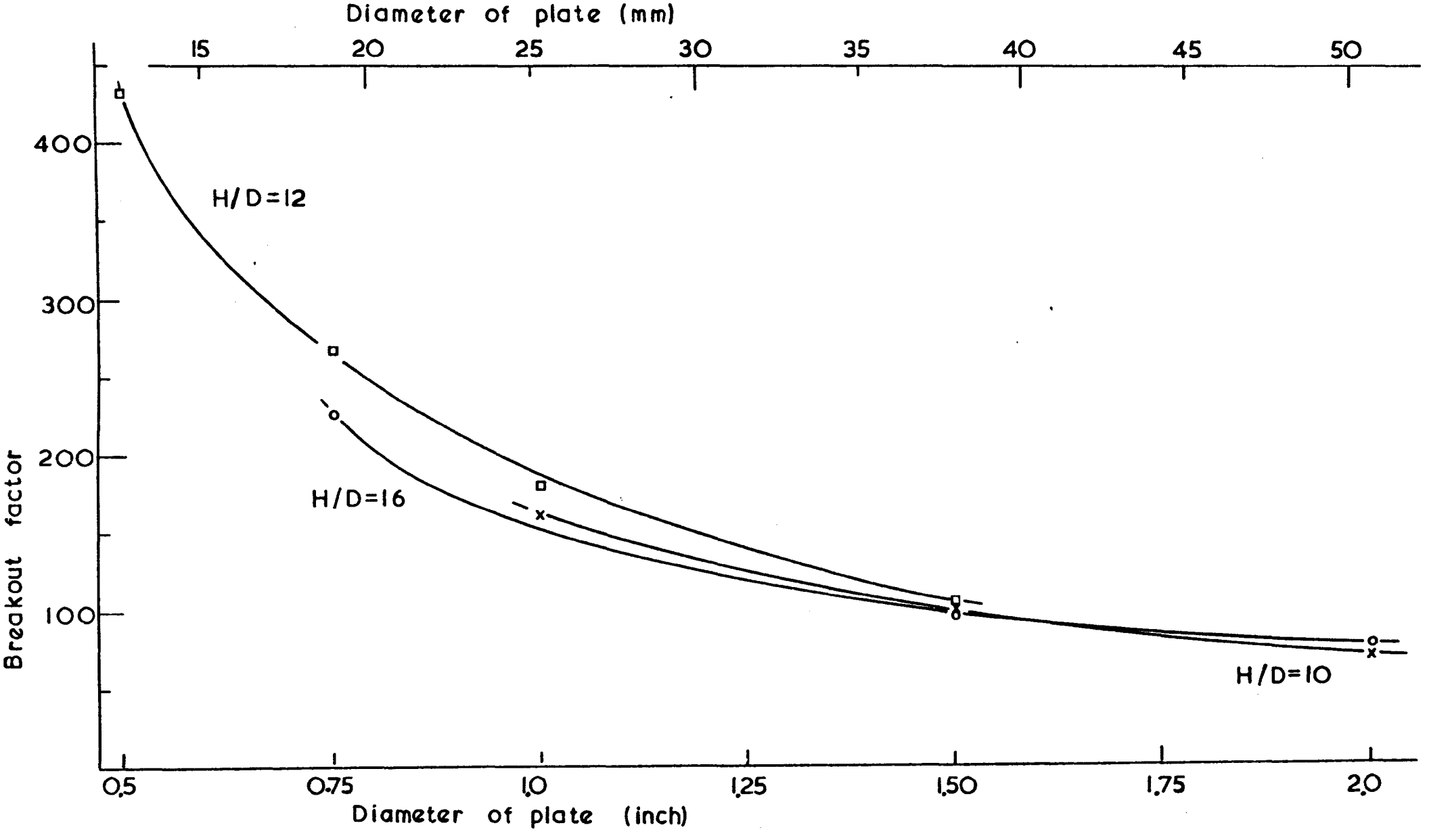

Fig. 8.17 Displacement V (H/D)

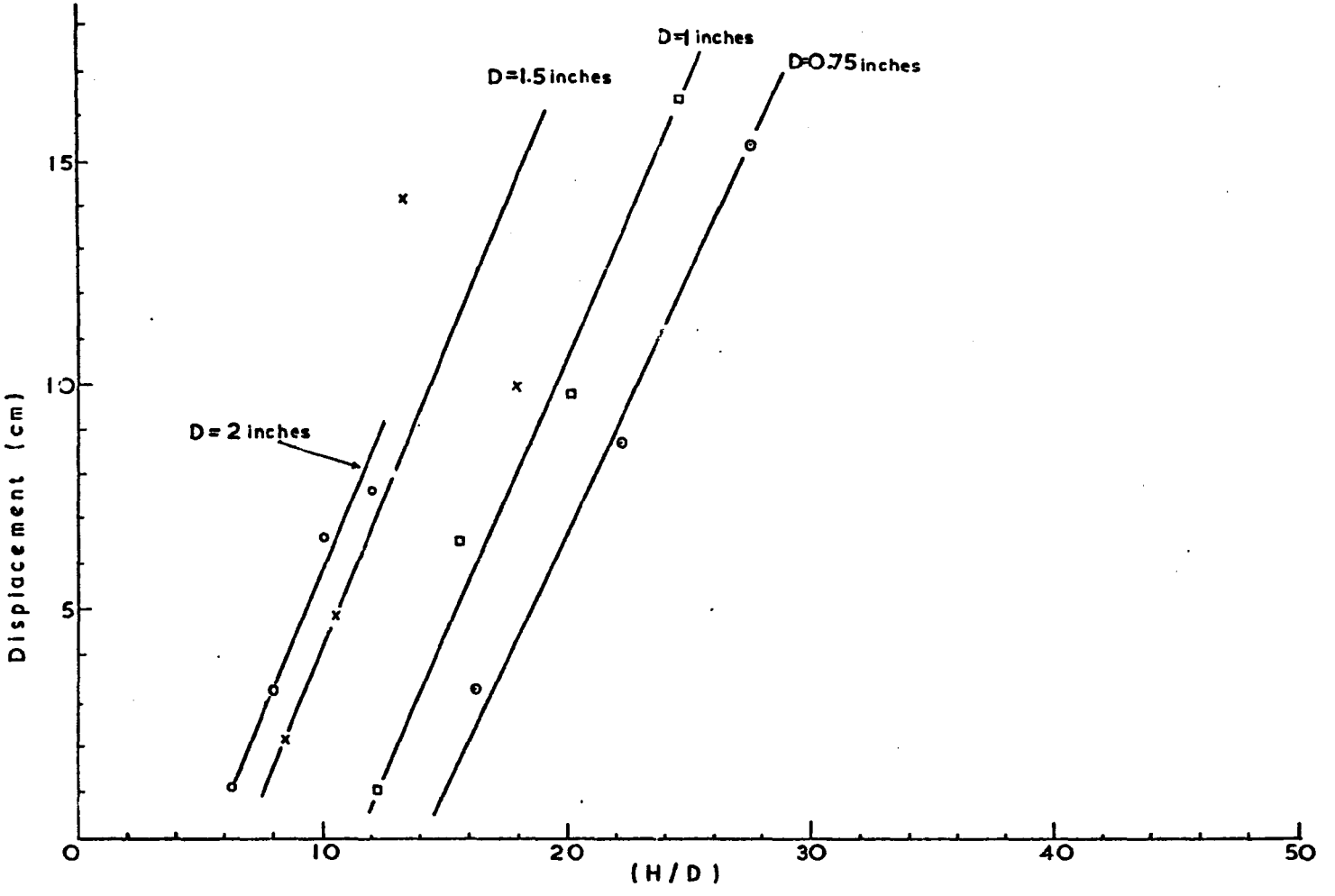

displacement increases with the relative depth increasing. Comparing the lines, it is observed that these are parallel to each other and therefore the displacement increases with $\frac{H}{D}$ at the same rate for all the anchor plates. It can be concluded that as the depth of the embedded anchor increases, a larger displacement is needed in order for the anchor to obtain its ultimate load, and also this displacement increases with the diameter of the plate.

CHAPTER IX

THEORY

9.1 The axially symmetric case

A number of problems in soil mechanics can be considered as axisymmetrical cases. A point Q in the soil is defined in Cartesian coordinates by X_q, Y_q and Z_q Fig. 9.2 (a), but polar coordinates are more conveniently used when the axially symmetrical case arises and Q is represented by r_q and z_q where $r_q = (x_q^2 + y_q^2)^{1/2}$ Fig. 9.2 (b). The stresses, see also Fig. 9.3, acting on an element in the soil are:-

σ_z = Vertical stress.

σ_θ = Tangential or circumferential stress.

σ_r = Radial stress.

τ_{rz} = Shear stress in the (r,z) plane.

The anchor problem can be solved using rectangular elements in the (r,z) plane, Fig. 9.4.

A force applied to the anchor shaft would displace the anchor plate by a vertical displacement, shown in Fig. 9.1. All elements would be subjected to vertical and horizontal displacements, i.e. no circumferential displacement.

The following displacement functions for a rectangular element in the (r,z) plane are assumed:-

$$u(r,z) = a_1 + a_2 r + a_3 z + a_4 rz$$

$$\omega(r,z) = a_5 + a_6 r + a_7 z + a_8 rz$$

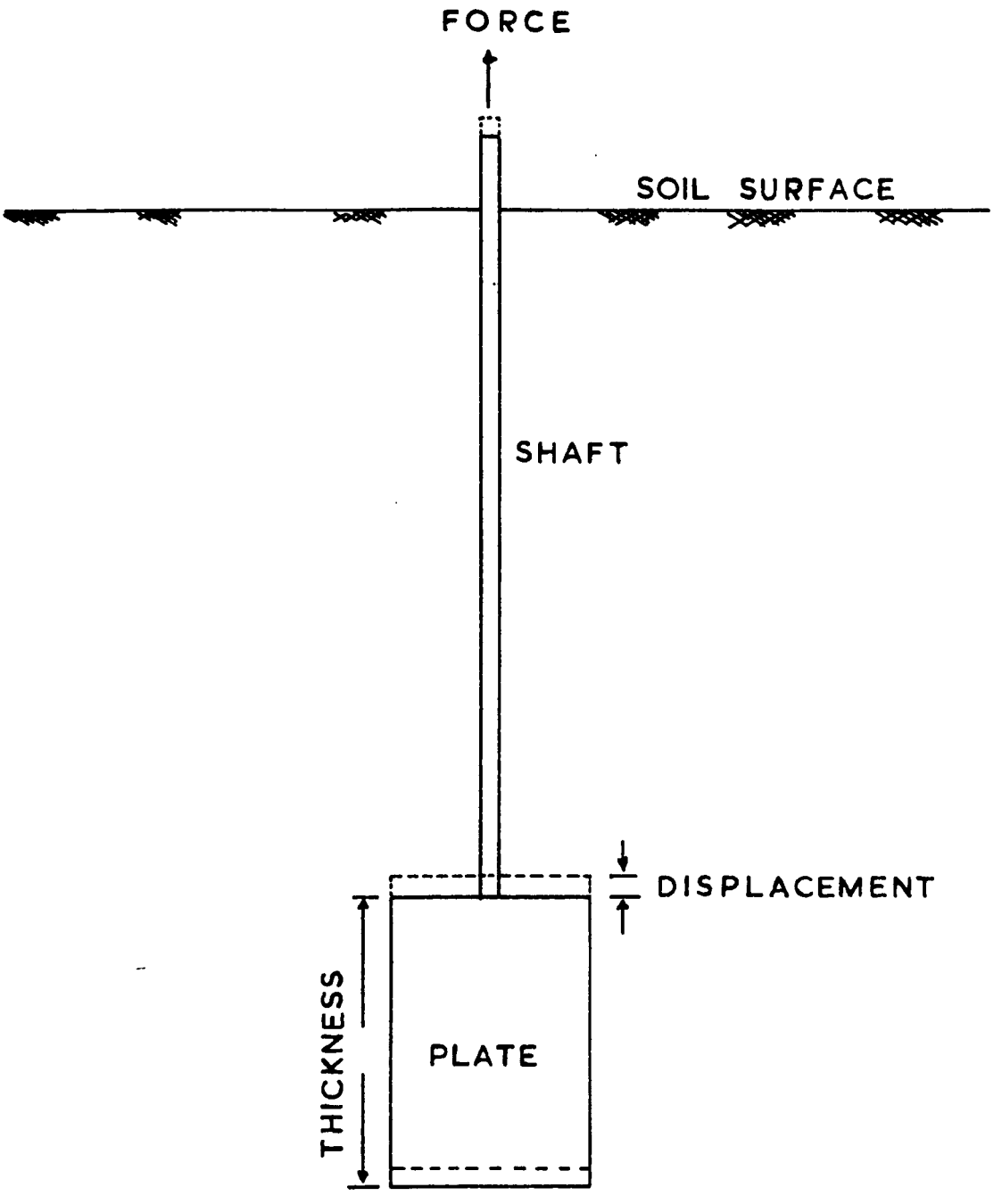

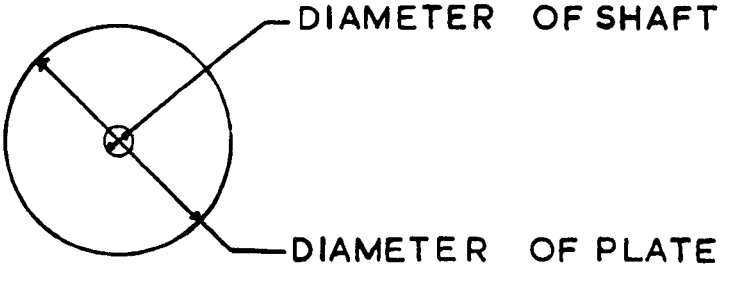

Fig.9.1 Anchor

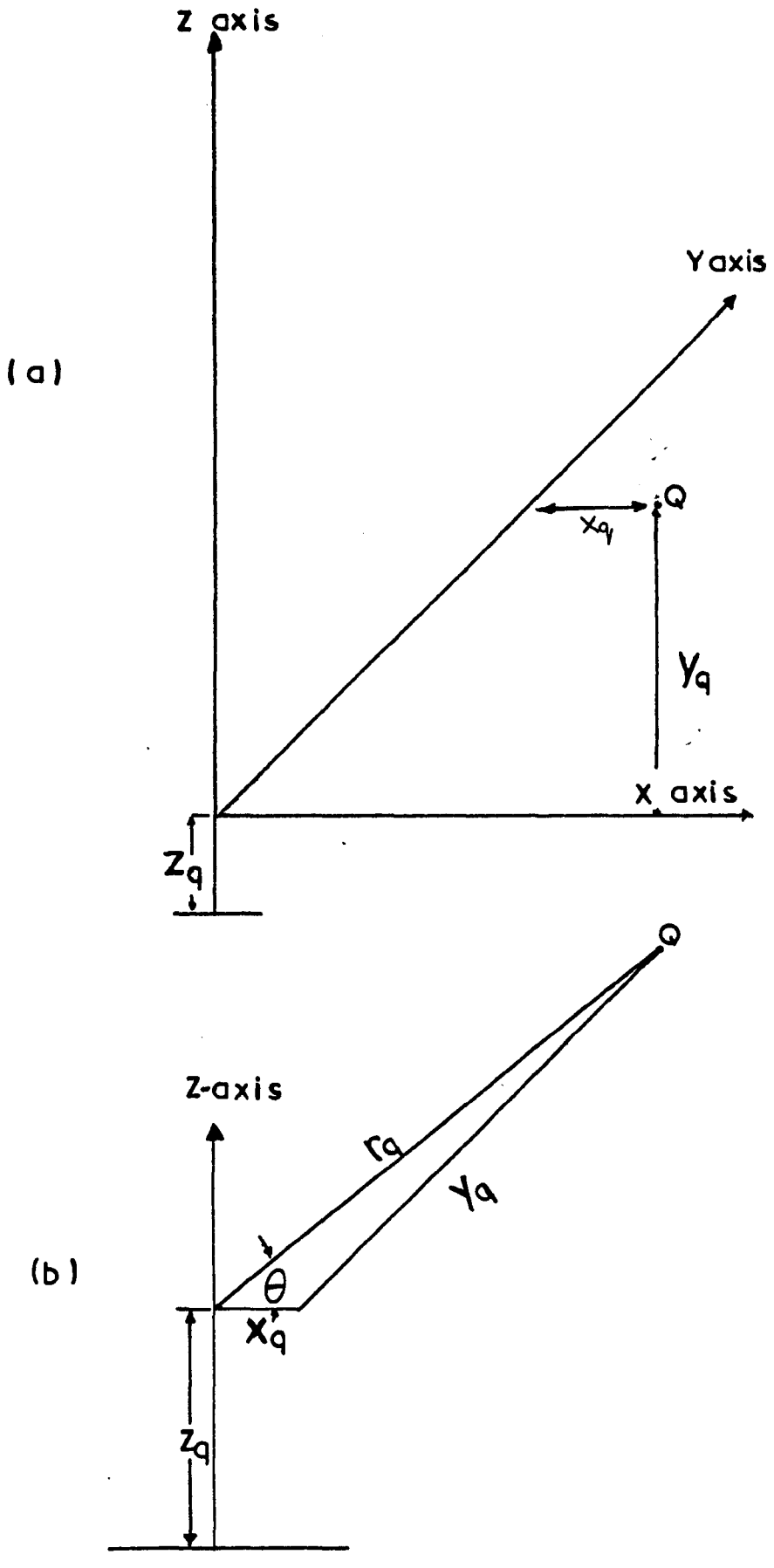

Fig. 9.2 Polar coordinates

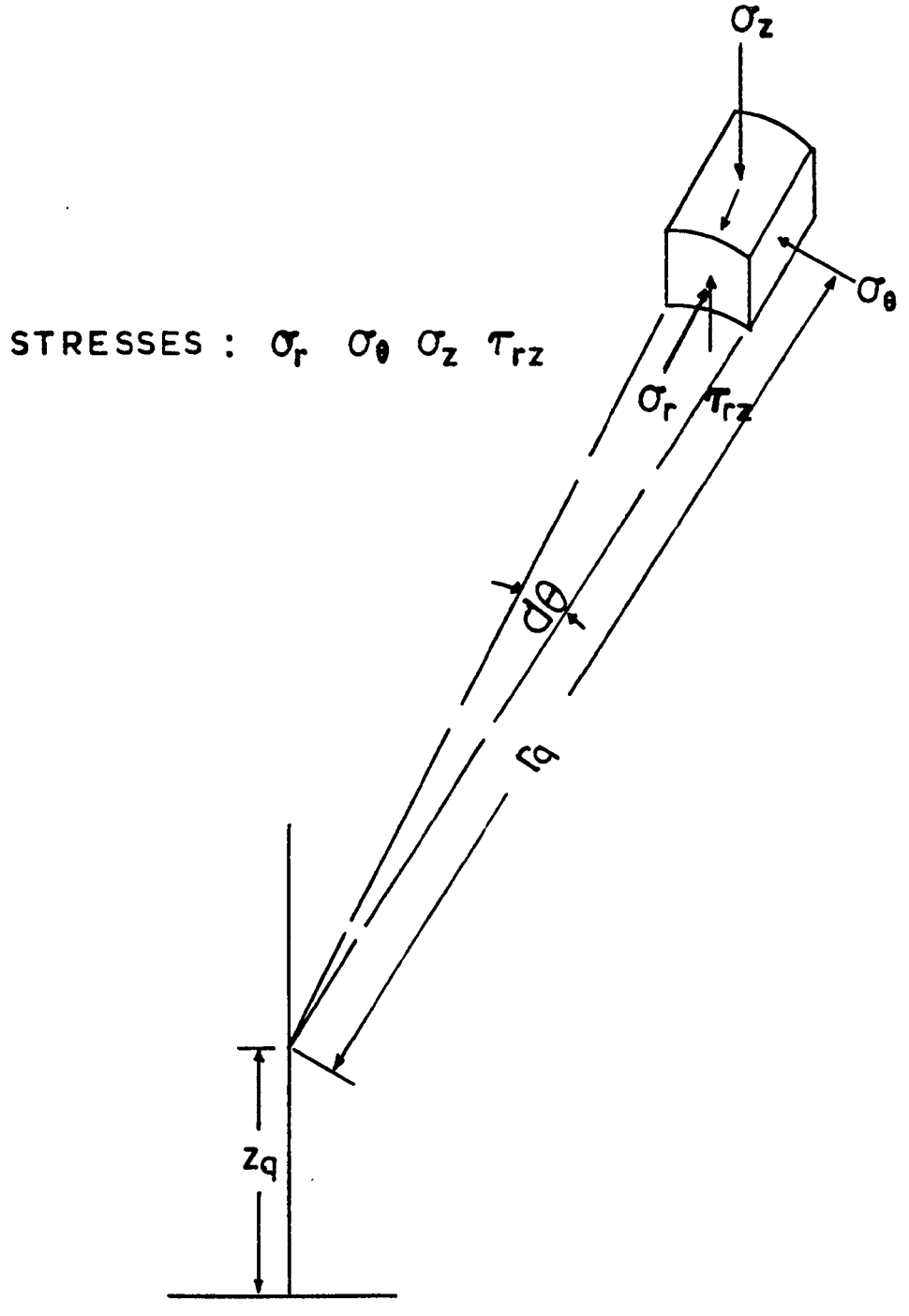

Fig. 9.3 Stresses on element

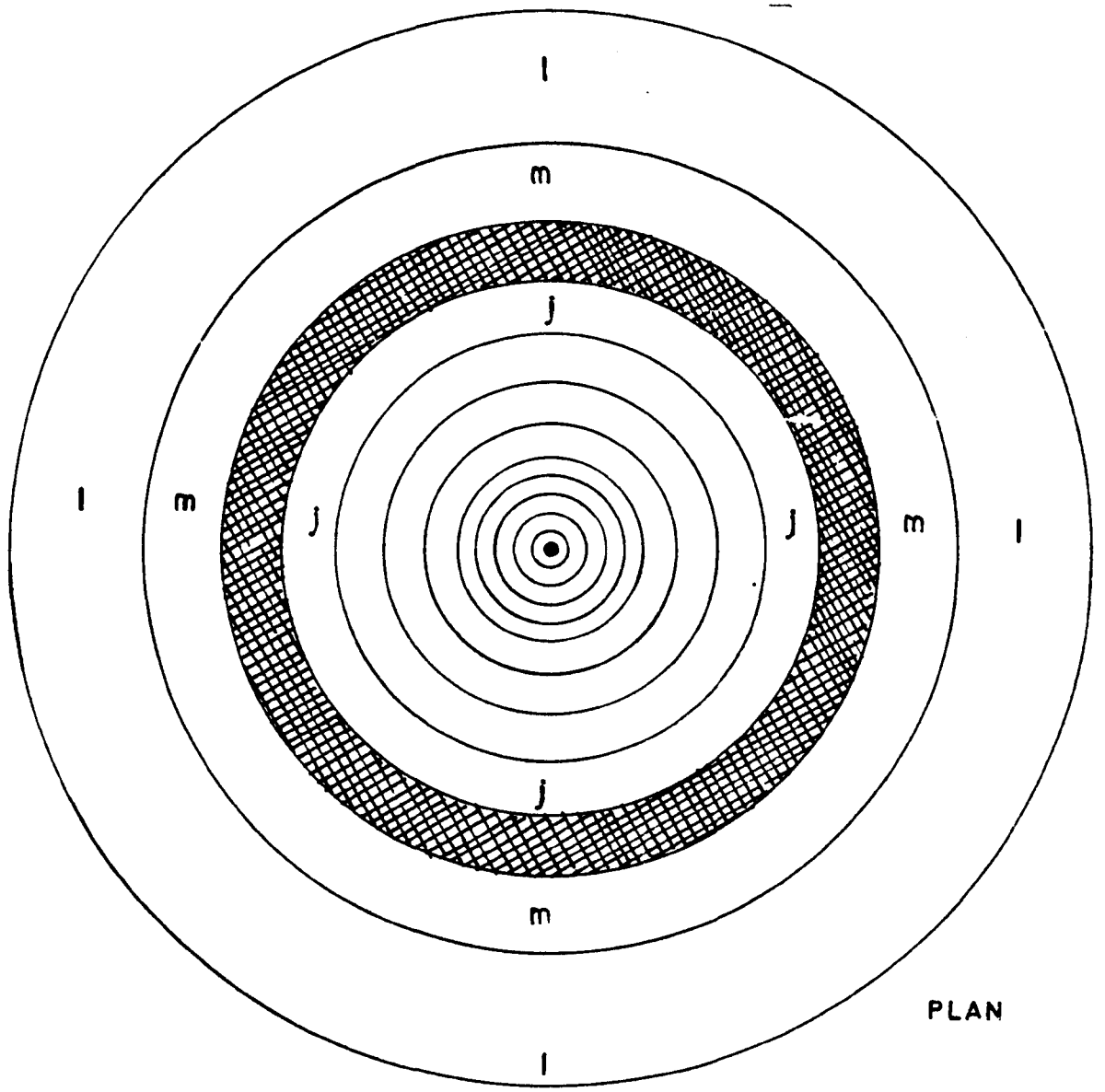

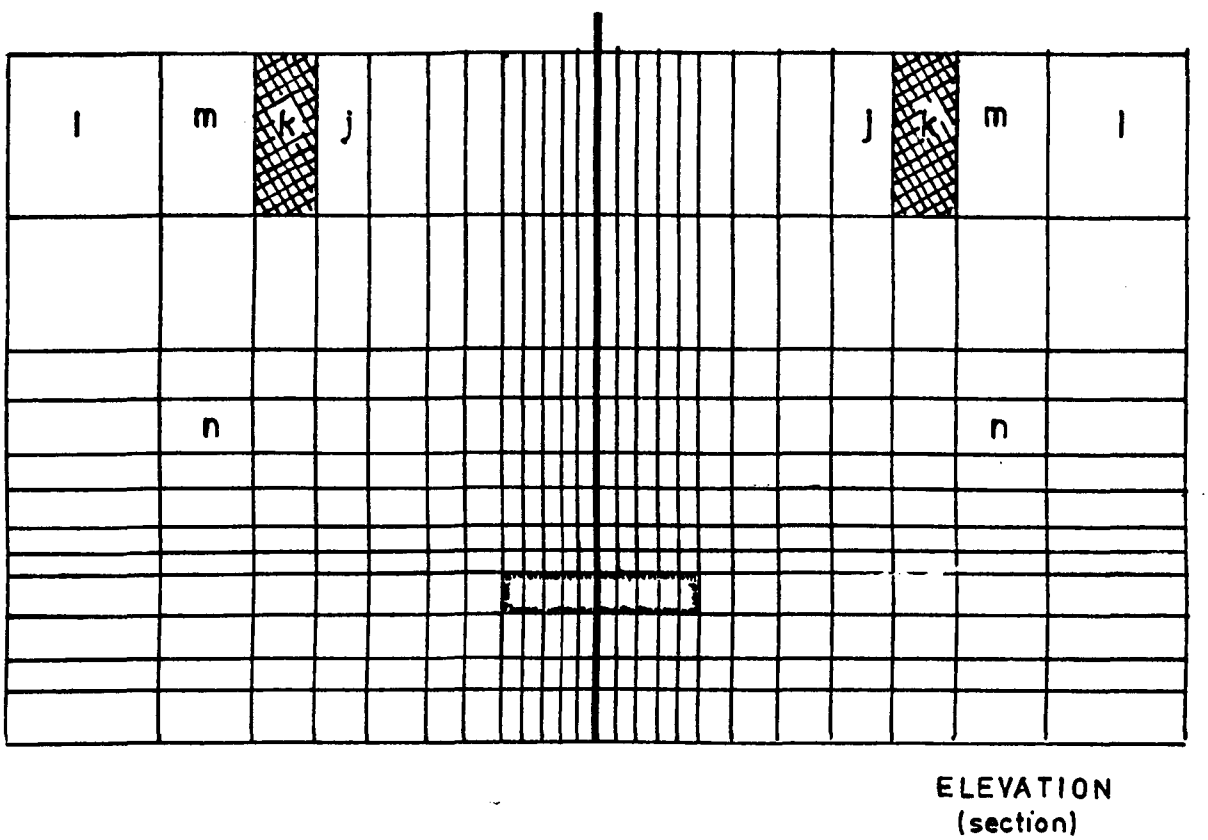

Fig. 9.4 Finite element model

Where,

u = Displacement component in the r direction

ω = Displacement component in the z direction

in matrix form the functions are expressed as:-

$$\{U\} = [M]\{A\} \qquad (1)$$

Where,

$$\{U\} = \begin{Bmatrix} u \\ \omega \end{Bmatrix} \qquad [M] = \begin{bmatrix} 1 & r & z & rz & 0 & 0 & 0 & 0 \\ 0 & 0 & 0 & 0 & 1 & r & z & rz \end{bmatrix} \qquad \{A\} = \begin{Bmatrix} a_1 \\ a_2 \\ \vdots \\ a_8 \end{Bmatrix}$$

At each node, i.e. 1, 2, 3, and 4, two components of displacement exist and these are evaluated by substituting the actual coordinates of the nodes into the matrix $[M]$

$$\begin{Bmatrix} u_1 \\ \omega_1 \\ u_2 \\ \omega_2 \\ u_3 \\ \omega_3 \\ u_4 \\ \omega_4 \end{Bmatrix} = \begin{bmatrix} 1 & r_1 & z_1 & r_1z_1 & 0 & 0 & 0 & 0 \\ 0 & 0 & 0 & 0 & 1 & r_1 & z_1 & r_1z_1 \\ 1 & r_2 & z_2 & r_2z_2 & 0 & 0 & 0 & 0 \\ 0 & 0 & 0 & 0 & 1 & r_2 & z_2 & r_2z_2 \\ 1 & r_3 & z_3 & r_3z_3 & 0 & 0 & 0 & 0 \\ 0 & 0 & 0 & 0 & 1 & r_3 & z_3 & r_3z_3 \\ 1 & r_4 & z_4 & r_4z_4 & 0 & 0 & 0 & 0 \\ 0 & 0 & 0 & 0 & 1 & r_4 & z_4 & r_4z_4 \end{bmatrix} \begin{Bmatrix} a_1 \\ a_2 \\ a_3 \\ a_4 \\ a_5 \\ a_6 \\ a_7 \\ a_8 \end{Bmatrix}$$

The above can be expressed as:-

$$\{\delta_e\} = [N]\{A\} \qquad (2)$$

By letting $[C]$ be the inverse of $[N]$ then;

$$\{A\} = [C]\{\delta_e\} \qquad (3)$$

Each element is subjected to the following strains:-

$$\varepsilon_r = \frac{\partial u}{\partial r} \quad , \quad \varepsilon_z = \frac{\partial w}{\partial z} \quad , \quad \varepsilon_\theta = \frac{u}{r} \quad \text{and} \quad \gamma_{rz} = \frac{\partial u}{\partial z} + \frac{\partial w}{\partial r}$$

From relationship (1) the strains can be obtained and are as follows:-

$$\varepsilon_r = \frac{\partial u}{\partial r} = a_2 + a_4 z \qquad \frac{\partial u}{\partial z} = a_3 + a_4 r$$

$$\frac{\partial w}{\partial r} = a_6 + a_8 z \qquad \varepsilon_z = \frac{\partial w}{\partial z} = a_7 + a_8 r$$

$$\varepsilon_\theta = \frac{u}{r} = \frac{a_1}{r} + a_2 + a_3 \frac{z}{r} + a_4 z$$

$$\gamma_{rz} = a_3 + a_4 r + a_6 + a_8 z$$

In matrix form:-

$$\begin{Bmatrix} \varepsilon_r \\ \varepsilon_\theta \\ \varepsilon_z \\ \gamma_{rz} \end{Bmatrix} = \begin{bmatrix} 0 & 1 & 0 & z & 0 & 0 & 0 & 0 \\ 1/r & 1 & z/r & z & 0 & 0 & 0 & 0 \\ 0 & 0 & 0 & 0 & 0 & 0 & 1 & r \\ 0 & 0 & 1 & r & 0 & 1 & 0 & z \end{bmatrix} \left\langle \begin{matrix} a_1 \\ a_2 \\ a_3 \\ a_4 \\ a_5 \\ a_6 \\ a_7 \\ a_8 \end{matrix} \right\rangle$$

By letting the above 4 x 8 matrix be represented by $[L]$ then:-

$$\{\varepsilon_e\} = [L]\{A\} \qquad (4)$$

The stress-strain relationship is given by

$$\{\varepsilon_e\} = [B]\{\sigma_e\} \qquad (5)$$

and by letting $[D]$ be the inverse of $[B]$, then the stress-strain relationship is given by:-

$$\{\sigma_e\} = [D]\{\varepsilon_e\} \qquad (6)$$

The stiffness matrix of an element is given in Appendix F as:-

$$[K_e] = \int_{vol} [H]^T [D] [H] \, dv \qquad (7)$$

and $[H]$ is found from the following relationship:-

$$\{\varepsilon_e\} = [H] \{\delta e\} \qquad (8)$$

substituting $\{\varepsilon_e\}$ with relationship (4) then:-

$$[L] \{A\} = [H] \{\delta e\}$$

Replacing $\{A\}$ by relationship (3), then:-

$$[H] = [L] [C] \qquad (9)$$

Therefore the element stiffness matrix becomes:-

$$[K] = [C]^T [S] [C]$$

Where,

$$[S] = \int_{vol} [L]^T [D] [L] \, dv$$

The matrix $[S]$ is evaluated in Appendix G, where the product of $[L]^T [D] [L]$ is found, multiplied by $2\pi r \, dr \, dz$ and integrated over the limits $r_1 \rightarrow r_2$ and $z_1 \rightarrow z_2$.

The matrix $[C]$, i.e. the inverse of $[N]$, is found in order to save computer time and to avoid rearrangement of $[N]$ so its inversion becomes possible, see Appendix H.

9.2 Stress-strain relationship

A typical compressive stress-strain relationship for a soil is shown in Fig. 9.5 (a). The solution of a given problem could be obtained by assuming the relationship to behave as shown in Fig. 9.5 (b). The elastic part of the curve is used when the stresses induced by the load are comparatively small, i.e. elastic behaviour, and the plastic part of the curve when the stresses are larger, i.e. plastic behaviour.

In this theoretical work two stress-strain relationships will be used;

(a) The elastic part of the curve shown in Fig. 9.5 (b).

(b) A non-linear stress-strain relationship obtained from a "true" tri-axial test.

(a) Elastic behaviour

The two matrices $[B]$ and $[D]$ are given as follows:-

$$[B] = \frac{1}{E}\begin{bmatrix} 1 & -\nu & -\nu & 0 & 0 \\ -\nu & 1 & -\nu & 0 & 0 \\ -\nu & -\nu & 1 & 0 & 0 \\ 0 & 0 & 0 & 0 & 2(1+\nu) \end{bmatrix}$$

(a)

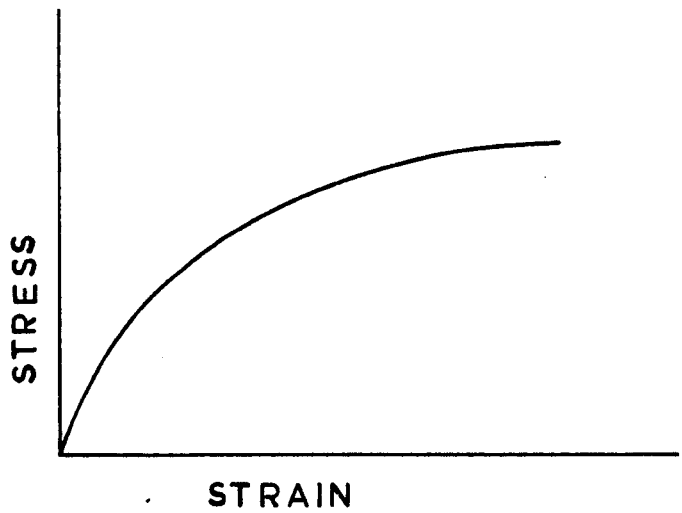

(b)

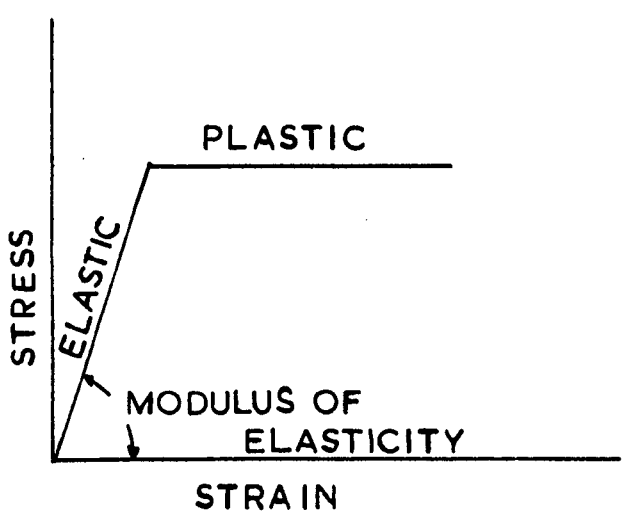

Fig. 9.5 Stress – strain behaviour

$$[D] = \frac{E}{(1+\nu)(1-2\nu)} \begin{bmatrix} 1-\nu & \nu & \nu & 0 \\ \nu & 1-\nu & \nu & 0 \\ \nu & \nu & 1-\nu & 0 \\ 0 & 0 & 0 & \frac{1-2\nu}{2} \end{bmatrix}$$

Where,

E = Modulus of elasticity.

ν = Poisson's ratio.

(b) Non-linear case

The non-linear stress-strain behaviour of soils is governed by various factors such as type and duration of loading, stress history and soil structure. Daniel (1957, Ref. 51) in order to investigate the behaviour of sand, performed "true" tri-axial tests and obtained the following generalised stress-strain relationships.

$$\delta\varepsilon_x = \frac{\delta\sigma_x}{K\left[\sigma_x - \frac{\sqrt{\sigma_z\sigma_y}}{K_r}\right]} - \left(2 - \frac{\sigma_x}{\sigma_z}\right)\left[\frac{m}{\left(\frac{\sigma_x}{K_r} - \sigma_y\right)} - \frac{n}{\frac{\sigma_x}{K_r}}\right]\delta\sigma_y -$$

$$\left(2 - \frac{\sigma_x}{\sigma_y}\right)\left[\frac{m}{\left(\frac{\sigma_x}{K_r} - \sigma_z\right)} - \frac{n}{\frac{\sigma_x}{K_r}}\right]\delta\sigma_z$$

$$\delta\varepsilon_y = -\frac{\sigma_z}{\sigma_y}\left[\frac{m}{\left(\frac{\sigma_z}{K_r} - \sigma_x\right)} - \frac{n}{\frac{\sigma_z}{K_r}}\right]\delta\sigma_x + \frac{\delta\sigma_y}{K\left(\sigma_y - \frac{\sqrt{\sigma_x\sigma_z}}{K_r}\right)} -$$

$$\frac{\sigma_y}{\sigma_y}\left[\frac{m}{\left(\frac{\sigma_y}{K_r} - \sigma_z\right)} - \frac{n}{\frac{\sigma_x}{K_r}}\right]\delta\sigma_z$$

$$\delta\varepsilon_z = -\left(2 - \frac{\sigma_z}{\sigma_y}\right)\left[\frac{m}{\left(\frac{\sigma_z}{K_r} - \sigma_x\right)} - \frac{n}{\frac{\sigma_z}{K_r}}\right]\delta\sigma_x \quad \frac{\sigma_z}{\sigma_z}\left[\frac{m}{\left(\frac{\sigma_z}{K_r} - \sigma_y\right)} -\right.$$

$$\left.\frac{n}{\frac{\sigma_z}{K_r}}\right]\delta\sigma_y + \frac{\delta\sigma_z}{K\left[\sigma_z - \frac{\sqrt{\sigma_x\sigma_y}}{K_r}\right]}$$

Where,

$\delta\varepsilon_x$, $\delta\varepsilon_y$, $\delta\varepsilon_z$ = increments of strain in x, y and z direction respectively.

$\delta\sigma_x$, $\delta\sigma_y$, $\delta\sigma_z$ = increments of stress in x, y and z direction respectively.

σ_x, σ_y, σ_z = initial stresses in x, y and z direction respectively.

K, m, n = experimental constants.

K_r = Rankine ratio(active).

The relationships show that the incremental strains depend on the stresses in the soil and also on the type of sand defined by K, m, n.

Daniel, Harvey, Burley (1975) carried out experiments in order to investigate the behaviour of dry sand under loading, unloading and reloading conditions. True tri-axial tests were performed; with the three principal stresses being independently varied, two of them held constant and the third being varied during each increment. The following incremental stress-strain relationships were derived to represent the behaviour of dry sand when it is first loaded.

$$\{\delta\epsilon\} = \begin{bmatrix} \frac{1}{K_1\left[\frac{\sqrt{\sigma_y\sigma_z}}{K_T} - \sigma_x\right]} & \frac{-1}{K_2\frac{\sigma_x}{\sigma_z}\left[\frac{\sqrt{\sigma_x\sigma_z}}{K_T} - \sigma_y\right]} & \frac{-1}{K_2\frac{\sigma_x}{\sigma_y}\left[\frac{\sqrt{\sigma_x\sigma_y}}{K_T} - \sigma_z\right]} \\ \frac{-1}{K_2\frac{\sigma_y}{\sigma_z}\left[\frac{\sqrt{\sigma_y\sigma_z}}{K_T} - \sigma_x\right]} & \frac{1}{K_1\left[\frac{\sqrt{\sigma_x\sigma_z}}{K_T} - \sigma_y\right]} & \frac{-1}{K_2\frac{\sigma_y}{\sigma_x}\left[\frac{\sqrt{\sigma_y\sigma_y}}{K_T} - \sigma_z\right]} \\ \frac{-1}{K_2\frac{\sigma_z}{\sigma_y}\left[\frac{\sqrt{\sigma_y\sigma_z}}{K_T} - \sigma_x\right]} & \frac{-1}{K_2\frac{\sigma_z}{\sigma_x}\left[\frac{\sqrt{\sigma_x\sigma_z}}{K_T} - \sigma_y\right]} & \frac{1}{K_1\left[\frac{\sqrt{\sigma_x\sigma_y}}{K_T} - \sigma_z\right]} \end{bmatrix} \{\delta\sigma\}$$

Where K_1 and K_2 are experimental constants, and

$$\sigma_x \leq \sigma_y \leq \sigma_z$$

From their experiments they also found, when plotting stress against strain, that a hysteresis loop exists due to unloading/reloading which becomes larger at higher strain relief. The unloading portion of the hysteresis loop is given in matrix form by the following incremental equations:-

$$\{\delta\varepsilon\} = \begin{bmatrix} \dfrac{e^{-\frac{\gamma_1\sigma_x}{\sqrt{\sigma_y\sigma_z}}}}{f_1\sqrt{\sigma_y\sigma_z}} & \dfrac{-e^{-\frac{\gamma_2\sigma_y}{\sqrt{\sigma_x\sigma_z}}}}{f_2\left(\frac{\sigma_z}{\sigma_x}\right)^{g'}\sqrt{\sigma_x\sigma_z}} & \dfrac{-e^{-\frac{\gamma_3\sigma_z}{\sqrt{\sigma_x\sigma_y}}}}{f_2\left(\frac{\sigma_y}{\sigma_x}\right)^{g'}\sqrt{\sigma_x\sigma_y}} \\ \dfrac{-e^{-\frac{\gamma_1\sigma_x}{\sqrt{\sigma_y\sigma_z}}}}{f_2\left(\frac{\sigma_z}{\sigma_y}\right)^{g'}\sqrt{\sigma_y\sigma_z}} & \dfrac{e^{-\frac{\gamma_2\sigma_y}{\sqrt{\sigma_x\sigma_z}}}}{f_1\sqrt{\sigma_x\sigma_z}} & \dfrac{-e^{-\frac{\gamma_3\sigma_z}{\sqrt{\sigma_x\sigma_y}}}}{f_2\left(\frac{\sigma_x}{\sigma_y}\right)^{g'}\sqrt{\sigma_x\sigma_y}} \\ \dfrac{-e^{-\frac{\gamma_1\sigma_x}{\sqrt{\sigma_y\sigma_z}}}}{f_2\left(\frac{\sigma_y}{\sigma_z}\right)^{g'}\sqrt{\sigma_y\sigma_z}} & \dfrac{-e^{-\frac{\gamma_2\sigma_y}{\sqrt{\sigma_x\sigma_z}}}}{f_2\left(\frac{\sigma_x}{\sigma_z}\right)^{g'}\sqrt{\sigma_x\sigma_y}} & \dfrac{e^{-\frac{\gamma_3\sigma_z}{\sqrt{\sigma_x\sigma_y}}}}{f_1\sqrt{\sigma_x\sigma_y}} \end{bmatrix} \{\delta\sigma\}$$

Where,

$$\gamma_1 = \frac{\sigma_x\,(\text{ultimate})}{\sigma_{xi}}, \qquad \gamma_2 = \frac{\sigma_y\,(\text{ultimate})}{\sigma_{yi}}, \qquad \gamma_3 = \frac{\sigma_z\,(\text{ultimate})}{\sigma_{zi}},$$

σ_{xi}, σ_{yi} and σ_{zi} are the stresses just before the unloading starts and f_1, f_2, g' are experimental constants.

The above sets of equations predict the behaviour of dry sand under loading, unloading and reloading (see Appendix I); the intermediate principal stress has been included in the elasto-plastic behaviour and in the rupture theory. The

constants used in the elastic theory, E and ν have been replaced by coefficients which depend on the stresses.

In this anchorage problem, only the loading and unloading sets will be used, since a constant rate of displacement causes the anchor to fail, i.e. there is no cyclic loading.

9.3 Solution of the anchor problem

Fig. 9.6 shows the sample in the tank divided into elements. A number was given to each node and each element. In order to make the enumeration easier the anchor plate was also included.

The bottom and sides of the tank were considered rigid and the nodes, i.e. 1 to 13 in steps of 1 and 26 to 169 in steps of 13, were given a zero displacement in both directions, i.e. r and z. The surface of the sand was considered free. The nodes along the anchor shaft and plate were taken to have one degree of freedom, i.e. in the vertical direction, since there was no movement of the sand in the horizontal direction.

The following procedure was used to develop the computer program :-

(a) A table containing the degrees of freedom at each node was generated; i.e. Node vs Degrees of freedom.

(b) A table giving the nodes of each element was formed; i.e. Element vs Nodes.

(c) The nodes in (b) were replaced by the degrees of freedom (a); i.e. Element vs Degrees of freedom.

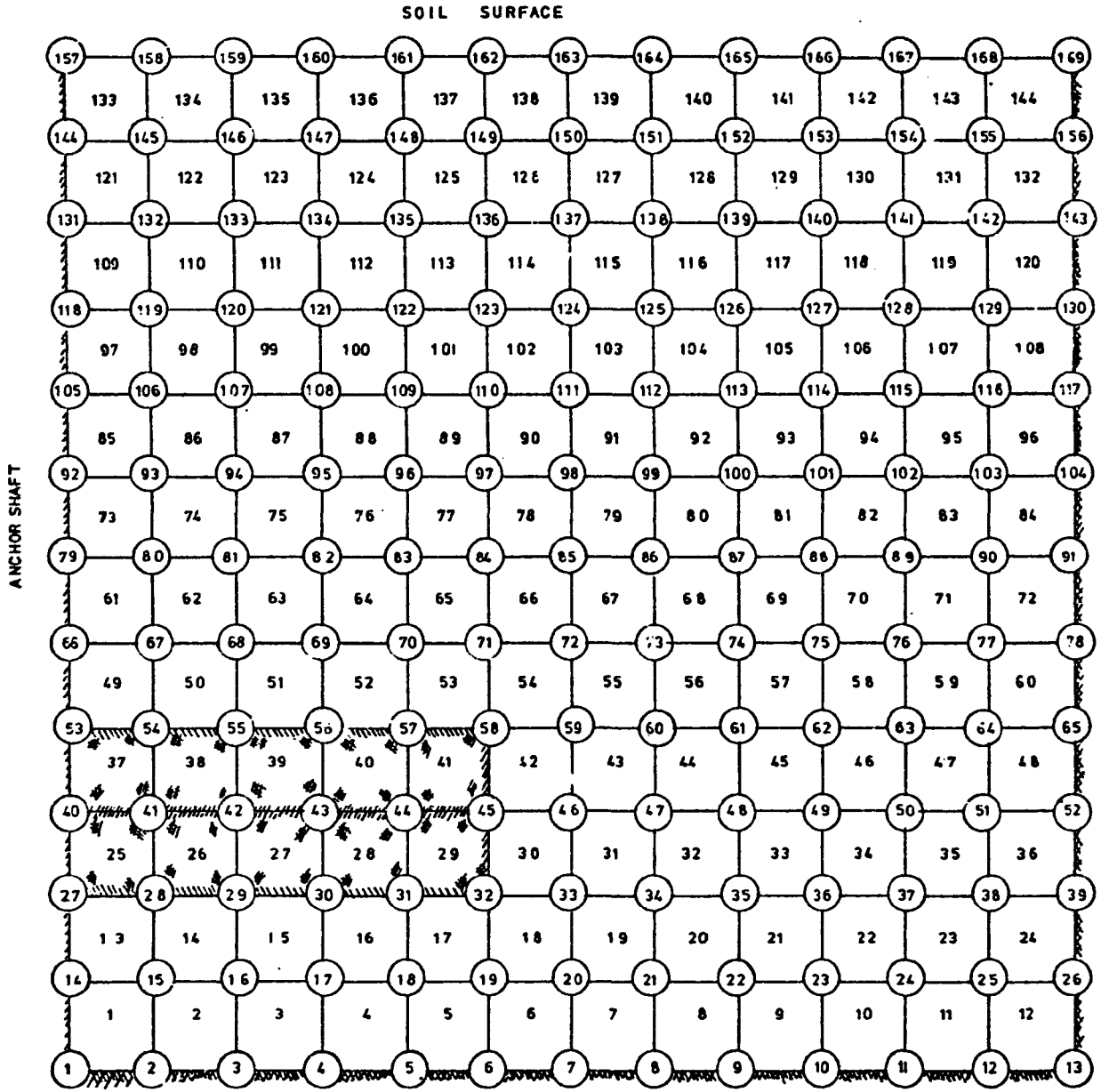

Fig.9.6 Finite Element mesh used for Anchor model

(d) A table giving the coordinates of each node was also formed; i.e. Nodes vs Coordinates.

(e) Using (d) and the appropriate [D] matrix, the matrices [S] and [C] were calculated. The equation $[SS] = [C]\,[S]\,[C]$ was used to evaluate the stiffness matrix [SS] of each element.

(f) The overall stiffness matrix, [K], was assembled using (e) and (c). A banded matrix was obtained.

(g) To each node on the anchor plate, i.e. 53, 54, 55, 56, 57 and 58, was given a known value of displacement and the matrix $\{\delta\}$ was obtained.

(h) The nodes on the anchor plate were the only nodes in the continuum that had any external load. The rest of the nodes had zero external load. The total load was the sum of the loads acting at the six nodes in the vertical direction, since the nodes had zero load in the horizontal direction. The matrix $\{F\}$ was obtained using the above information.

(i) The overall stiffness matrix was modified to make the solution of $[K]\ \{\delta\} = \{F\}$ possible, since the matrices [F] and $[\delta]$ were partially known. The elements of the rows of [K] matrix corresponding to the degrees of freedom with external load, i.e. 62, 64, 66, 68, 70 and 72, were given a zero value, but the elements on the leading diagonal of these rows were given the value of 1. The matrix $\{F\}$ was also modified. The elements of 62, 64, 66, 68, 70 and 72 were given the known value of the displacement.

(j) A standard computer subroutine was used to solve

$[K]\{\delta\} = \{F\}$, and the displacements at each node were calculated.

(k) The original rows 62, 64, 66, 68, 70, 72 of $[K]$ matrix, i.e. before modification, were multiplied by the matrix $\{\delta\}$ to obtain the external load at each node, and these were added to give the load applied to the shaft.

(l) The strains at the centre of each element were evaluated using the equation $\{\varepsilon_e\} = [H]\{\delta_e\}$. Also the stresses in each element were calculated using the equation $\{\sigma_e\} = [D]\{\varepsilon_e\}$.

9.4 Step by step method

In the non-linear case, the solution of the problem depends on the following factors:-

(a) The stress-strain relationship.

(b) The stress field throughout the continuum bearing in mind the failure criteria (see later work).

The initial stresses in each element of sand were calculated using the equations:-

$$\sigma_z = \gamma h \quad , \quad \sigma_v = K_o \sigma_z \quad , \quad \sigma_\theta = K_o \sigma_z$$

Where,

K_o = the values in Table 7.1

γ = the values in Table 5.1

h = depth of the centroid of the element from the soil surface.

The stress-strain relationship was formed using the two sets of equations in section 9.2 (b). The elements were assumed to be loaded in the r and z direction but unloaded in the third direction, since the initial behaviour of each element was not known in the first iteration of the first increment. A second iteration was carried out if the obtained incremental stresses did not agree with the assumed directions. At the end of the second iteration the directions were checked again, and a third iteration was carried out if again the incremental stresses did not correlate with the incremental stresses obtained from the second iteration.

At the end of each increment, the total stresses in each element were calculated and the two failure criteria were checked, i.e.

$$\sigma_r < \frac{\sqrt{\sigma_\theta \sigma_z}}{K_r} \quad , \quad \sigma_\theta < \frac{\sqrt{\sigma_z \sigma_r}}{K_r} \quad , \quad \sigma_z < \frac{\sqrt{\sigma_r \sigma_\theta}}{K_r} \quad \text{and}$$

$$\sigma_\theta > 0 \quad , \quad \sigma_r > 0 \quad , \quad \sigma_z > 0 .$$

CHAPTER X

THEORETICAL RESULTS

10.1 Linear case

The program developed to investigate the elastic part of the load-displacement curve, i.e. the first few millimetres of displacement, is given in Appendix J. The investigation was based on an anchor plate of 51mm diameter embedded at 60cm depth. The anchor was given a 0.4mm displacement, and the load at each node was calculated and added together to obtain the total load applied to the anchor shaft.

10.1.1 Variation of modulus of elasticity

Values of modulus of elasticity, E, varying between 10^6 N/m^2 and 2.5 x 10^6 N/m^2 were used in the computation, and the load on the anchor was calculated. The Poisson's ratio, ν , was kept constant.

Fig. 10.1 shows the load varying with the anchor displacement for different values of E. Fig. 10.1 (a), where ν = 0.2, indicates that the rate of increase of the load increases with E increasing. Fig. 10.1 (b) and Fig. 10.1 (c) show a similar trend, where ν = 0.4 and ν = 0.3 respectively. McMullan (1975, Ref. 24) applied a load to the anchor plate to calculate the displacement, and found that with the modulus of elasticity increasing, the displacement decreased.

Fig. 10.2 shows the variation of the load with the modulus of elasticity. The relationship is a straight line, with the slope of the line depending on the Poisson's ratio, i.e. the rate of increase of the load increases with ν increasing. McMullan also found that the displacement increased by a factor of two when the modulus of elasticity was halved.

Fig. 10.1 Load V Displacement

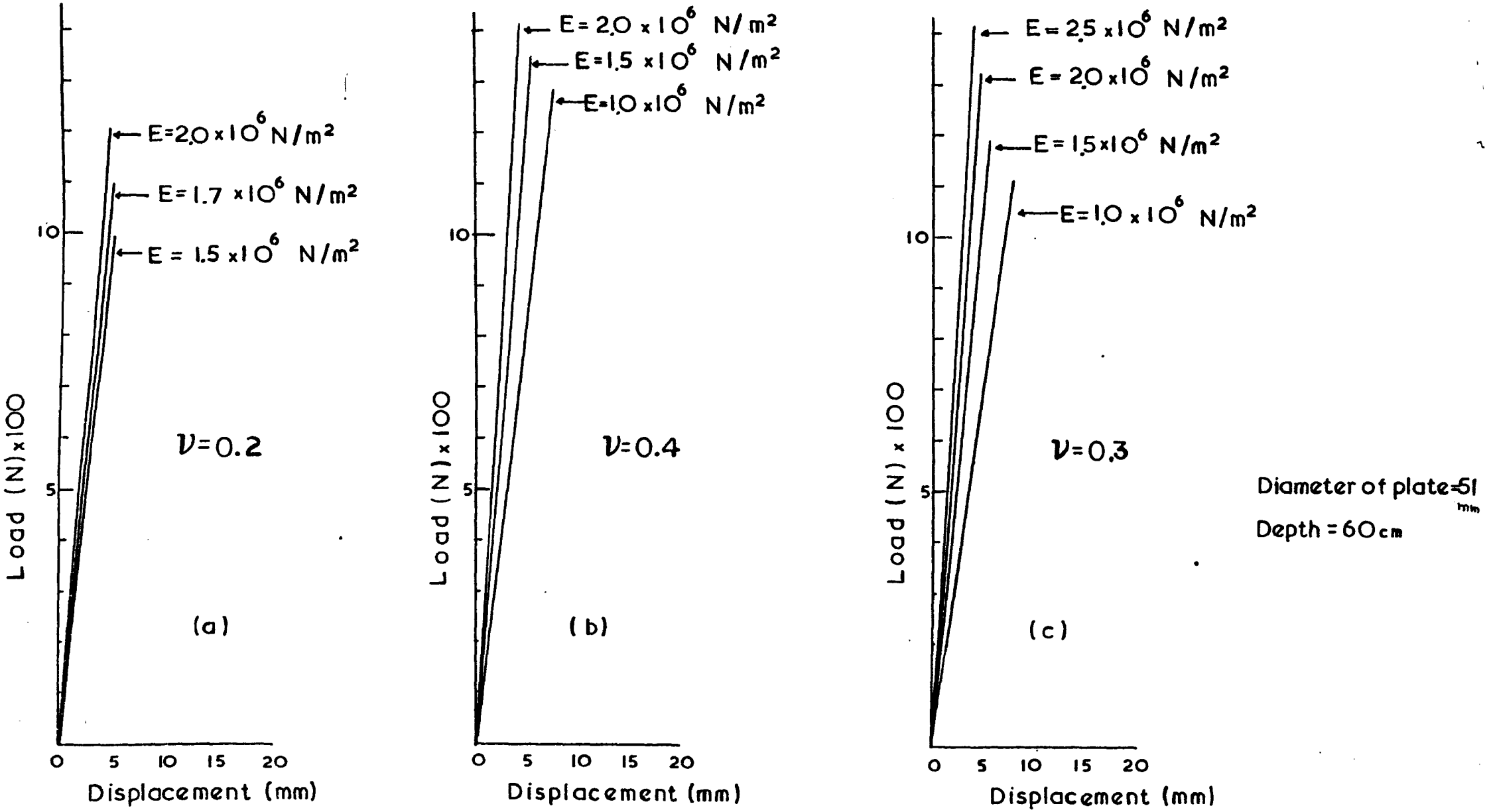

Fig. 10.2 Load V Modulus of elasticity

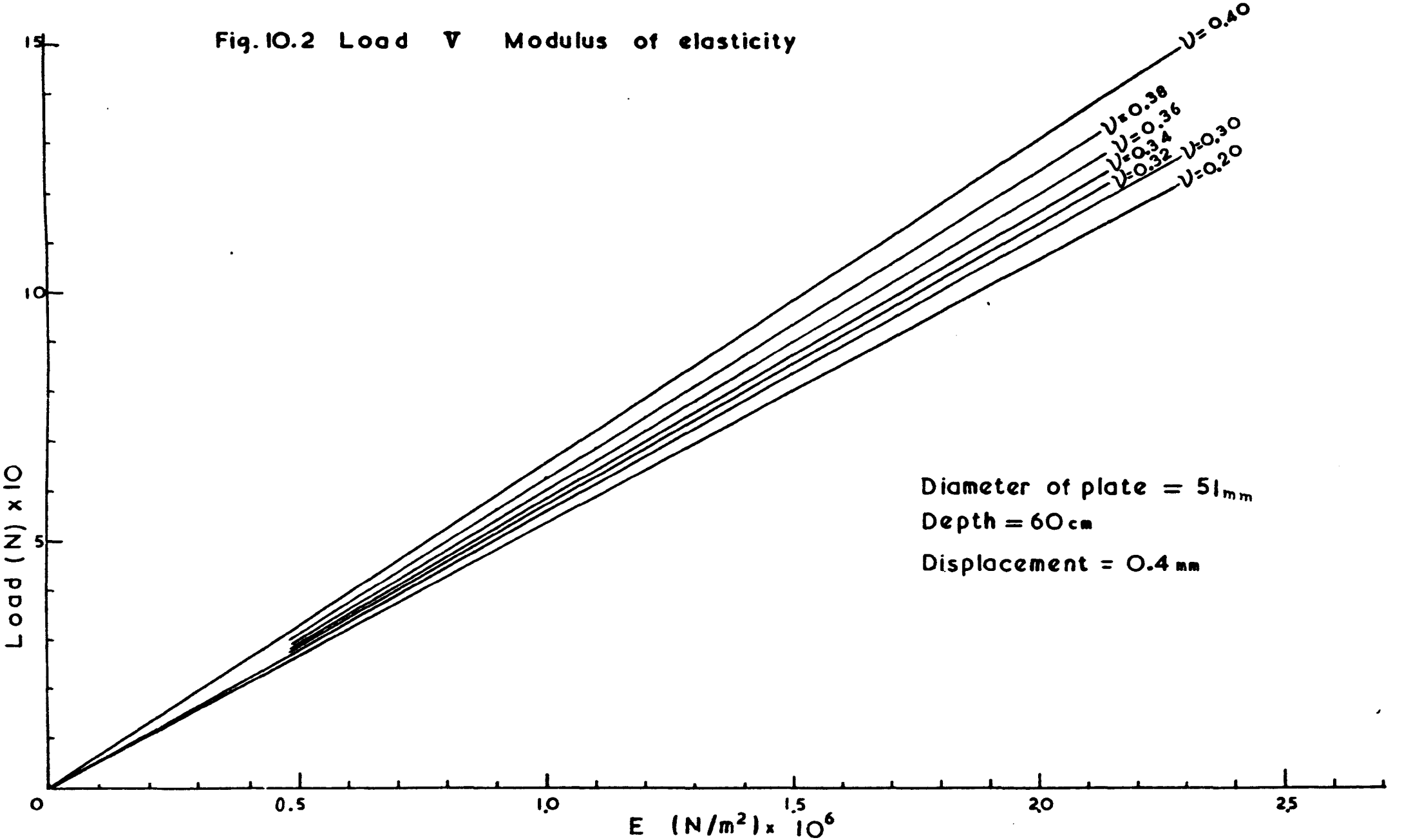

10.1.2 Variation of Poisson's ratio

With the modulus of elasticity constant, values of Poisson's ratio between 0.2 and 0.4 were used for the computations, and the loads were determined.

Fig. 10.3 shows that for any value of E between 10^6 N/m^2 and 2.5×10^6 N/m^2, the rate of change of the load with the displacement increases with ν increasing. McMullan also found that the displacement decreased with the Poisson's ratio increasing, for a given load and modulus of elasticity.

Fig. 10.4 shows the variation of the load with the Poisson's ratio for different values of E. From the figure it is observed that:-

(a) The load increases with ν for a given value of E.

(b) The curves, load against ν, are asymptotic to $\nu = 0.5$.

(c) The rate of change of the load with ν increases with E increasing.

Observation (c) is also supported by McMullan, who found that the increase in the slope of the load-displacement lines with ν varying from 0.2 to 0.4 is very small. This could be explained by the high value of E, i.e. 1.8×10^8 N/m^2, used in the computation.

10.1.3 Examination of the displacement field

Carr (1970, Ref. 23) measured the sand movement for 16 positions in his sand mass, and found that the direction and magnitude of the movements depended on the following:-

Fig. 10.3 Load V Displacement

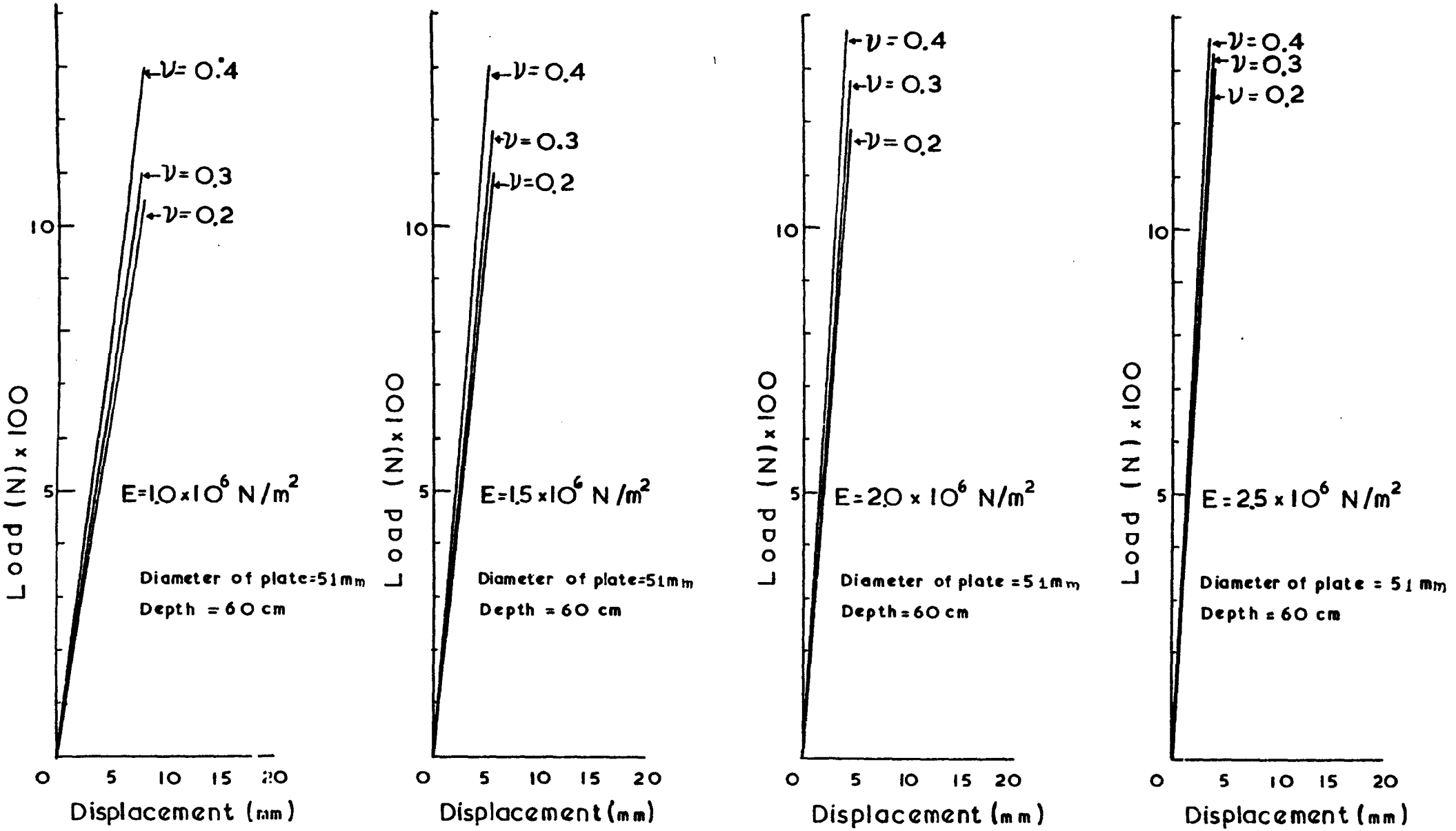

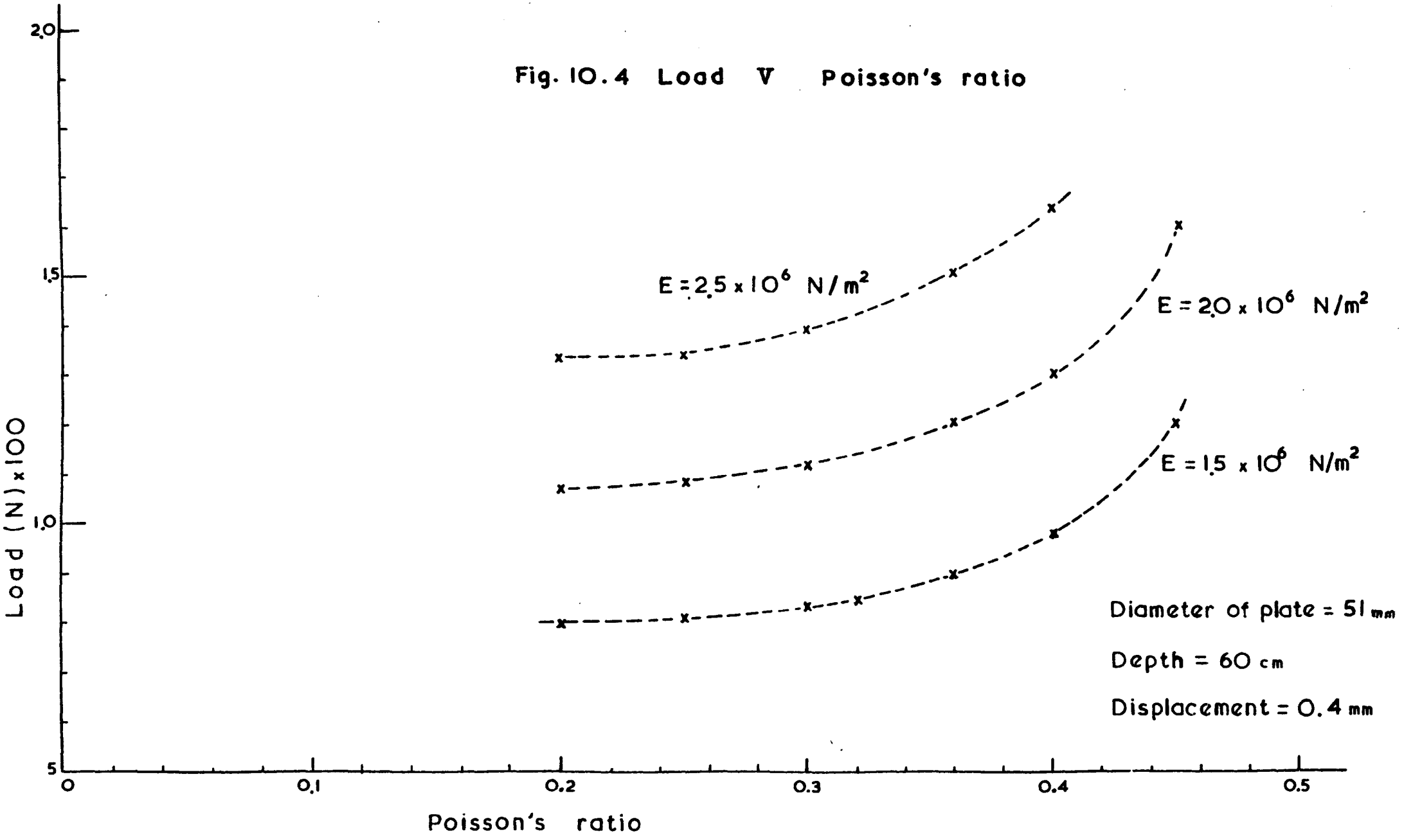
Fig. 10.4 Load V Poisson's ratio
E = 2.5 x 10^6 N/m^2
E = 2.0 x 10^6 N/m^2
E = 1.5 x 10^6 N/m^2
Diameter of plate = 51 mm
Depth = 60 cm
Displacement = 0.4 mm
Load (N) x 100
Poisson's ratio
2.0
1.5
1.0
5
0
0.1
0.2
0.3
0.4
0.5

(a) The state of sample, i.e. consolidated or overconsolidated.

(b) The density of sample.

(c) The relative depth of the anchor.

The displacements at each node, predicted by the computer program , are plotted in Fig. 10.5. The shaded area represents the shaft and plate of the anchor. From the distribution of the displacements the following observations are made:-

(a) The sand above and around the top surface of the anchor plate moves upwards and outwards away from the plate. Carr's distribution shows a similar trend, but near the vertical boundaries an inward movement of sand occurs which he explained by stating that his sand was overconsolidated.

(b) The sand under and around the bottom of the anchor plate moves upwards and towards the plate. Although the anchor was displaced by 0.4mm, only about 0.04mm of the gap left by the anchor plate is filled by the sand. Although Carr did not measure the displacement of the sand around and under the anchor plate, from the trajectory of sand movement at a position near the anchor plate he concluded that a flow of sand into the cavity below the plate exists.

(c) The vertical and horizontal displacements, above the plane passing through the top surface of the anchor plate, decrease with the radius increasing and the depth decreasing.

(d) At any position in the sand, the vertical displacement is greater than the horizontal one. The direction of the displacement at a distance of about 320mm from the shaft is nearly vertical. Carr also found that for $\frac{H}{D} = 10$ the

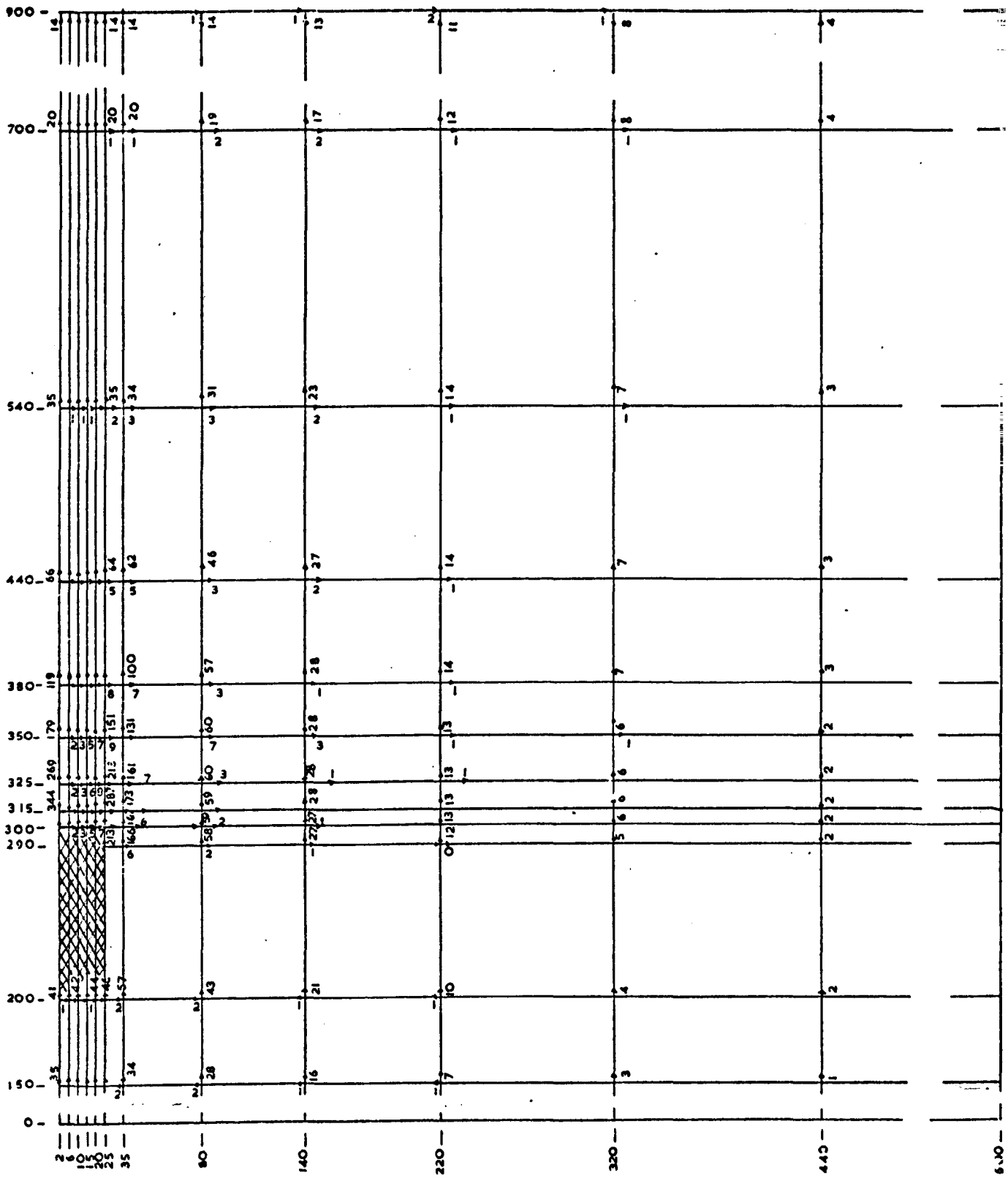

Units :

length = mm

displacement = 10^{-3} mm

Applied displacement = 0.4 mm

Scale 1:2

Fig. 10.5 Displacement distribution

(linear case)

movements in dense sand are predominantly vertical.

(e) The sand on the surface moves upwards and towards the vertical boundaries, and the movement is predominantly vertical. Carr also stated that for $\frac{H}{D}$ = 10 and dense sand, soil movements are still recorded even at and near to the sand surface.

10.1.4 Distribution of vertical stress

Fig. 10.6 shows the distribution of the incremental stress in the sample, due to the 0.4mm of displacement applied to the anchor plate. The sand, enclosed by the dotted line and the shaft of the anchor, is subjected to an additional compressive stress, while the rest of the soil loses some of its original compression. The compression of the sand in the vicinity of the anchor plate reduces due to the sand displacing into the cavity left by the movement of the anchor plate.

The distribution of the stress on the anchor plate, due to the increment of displacement, takes the form of a parabola, see Fig. 10.7. The stress increases with the distance from the shaft, and at the edge of the anchor plate the value of the stress is about twice the stress value near the shaft.

10.1.5 Distribution of load on the anchor plate

Fig. 10.8 shows that the distribution of the load on the anchor plate also has the form of a parabola, with the edge of the anchor plate obtaining most of the load. Therefore it may be concluded that the method of applying a uniform distributed load on the anchor plate, in order to calculate the displacement of the anchor, may prove to be a less accurate approach.

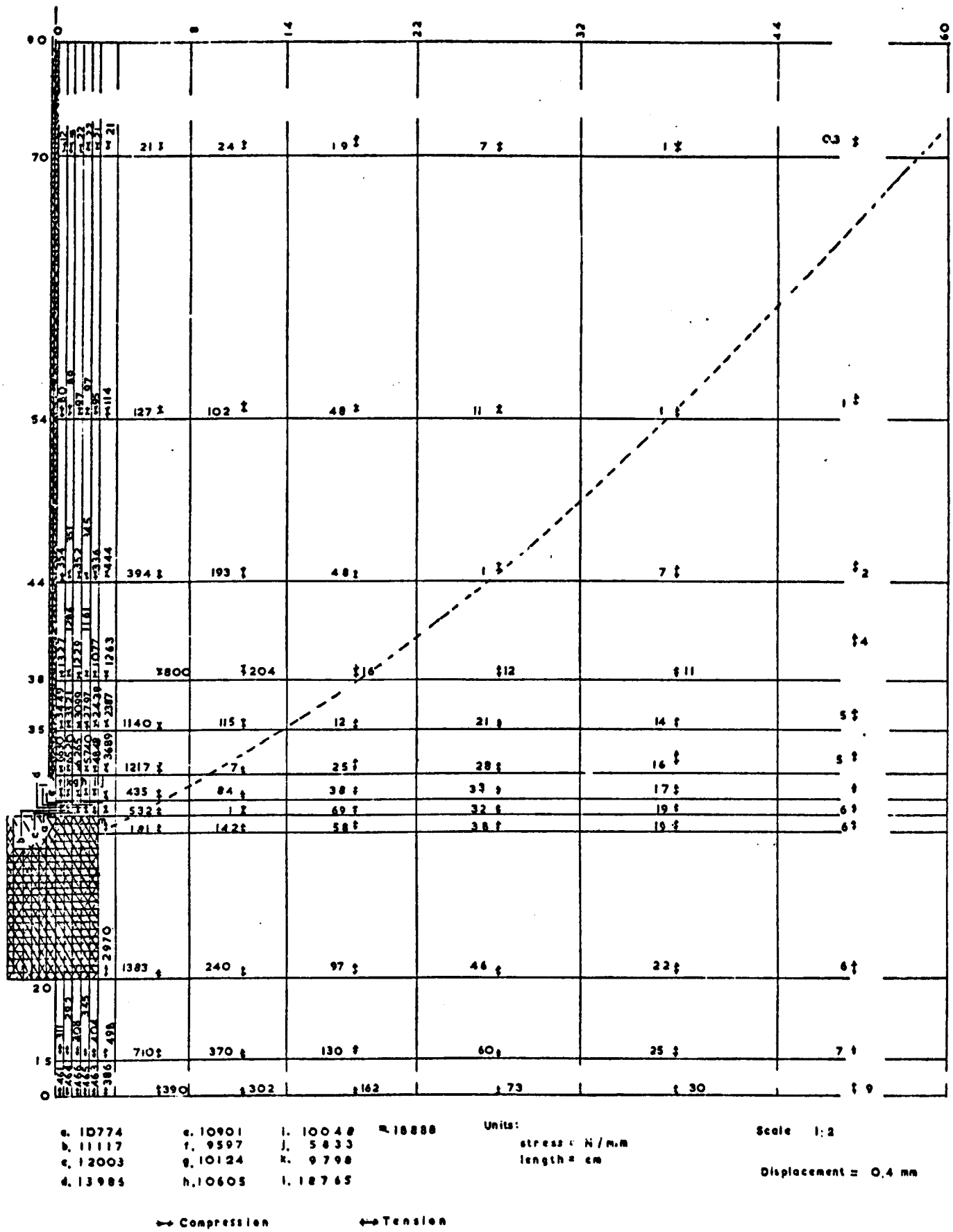

Fig. 10.6 Distribution of vertical stress
(linear case)

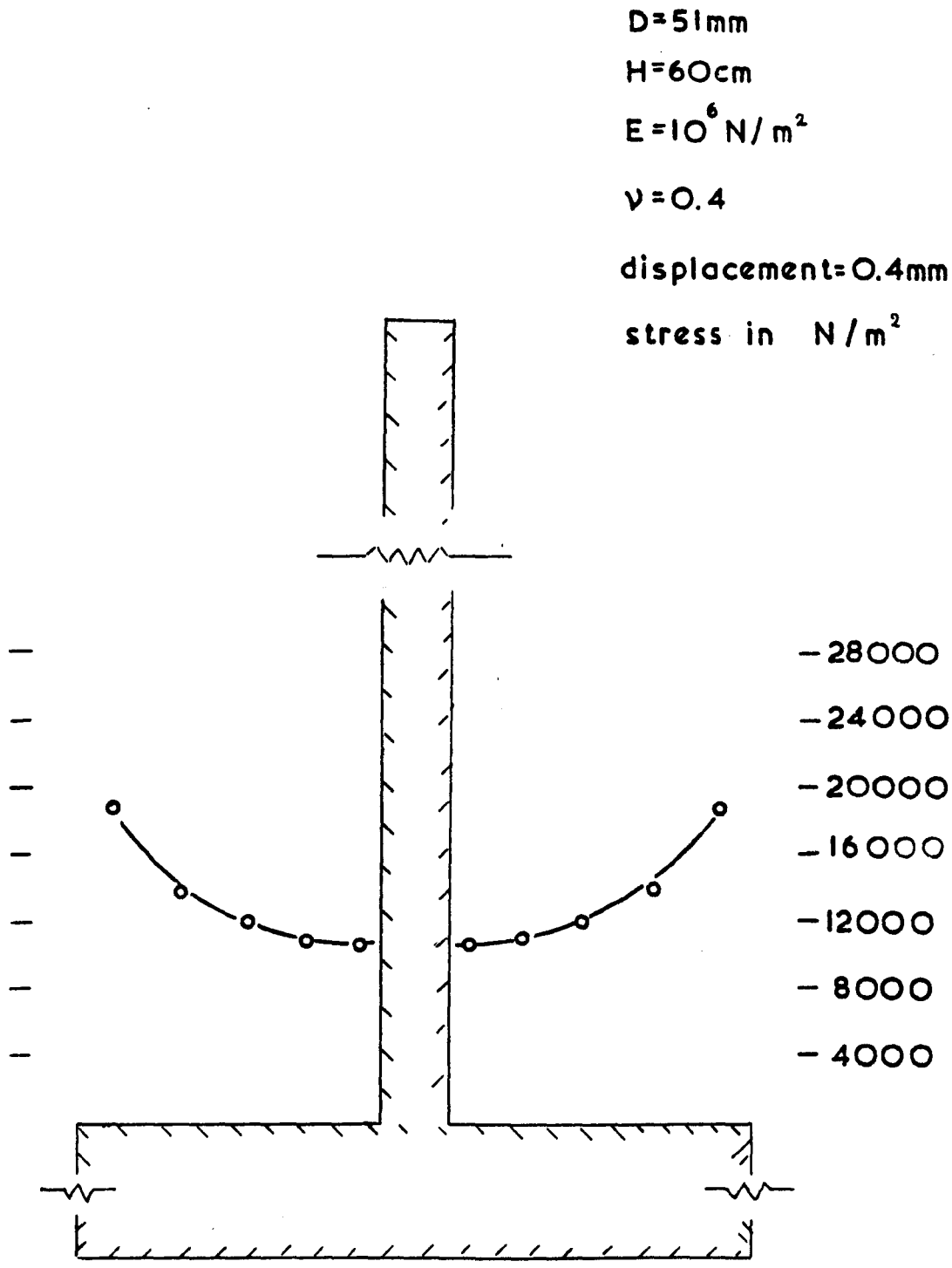

Fig. 10.7 Distribution of vertical stress

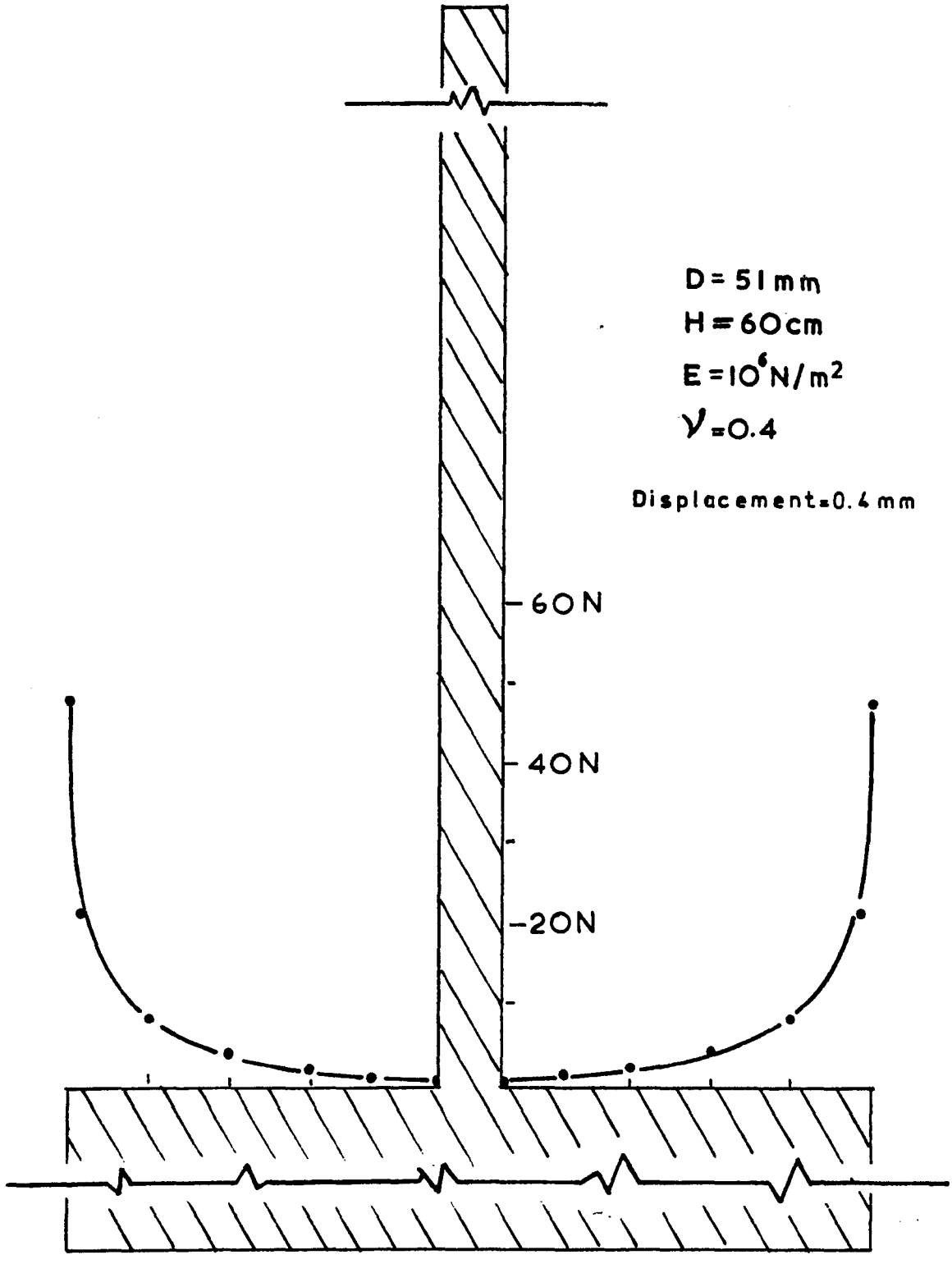

Fig. 10.8 Distribution of load on plate

10.2 Non-linear case

The program developed to investigate the load-displacement behaviour of the anchor is given in Appendix K. The following parameters were used in the computer program :-

(a) An average value of K_o was given to each layer of elements in the sample; obtained from Table 7.1.

(b) An average value of γ obtained from Table 5.1, was given to each layer of elements in the soil.

(c) The value of the Rankine ratio, $K_r = \frac{1 - \sin\phi}{1 + \sin\phi}$, was calculated using the angle of friction, ϕ, given by the shear box tests, i.e. $\phi = 43.2^{o}$.

(d) The constants in the stress-strain relationship were obtained from tests performed by other researchers working in the same field;

$K_1 = 45.0$

$K_2 = 1650.0$

$f_1 = 70.0$

$f_2 = 1470.0$

$g' = 0.0$

(e) The value of $E = 10^6$ N/m^2 and $\nu = 0.4$ were used to obtain the shear modulus, $G = \frac{E}{2(1+\nu)}$.

10.2.1 Development of computer program

The computer program was initially developed using a small number of elements, iterations and steps. During development it was found that the solution depended on the following factors:-

(a) The number of elements on the anchor plate.

(b) The number of elements in the vicinity of the anchor plate.

(c) The initial assumption of the direction of the incremental stresses, i.e. loading or unloading.

(d) The size of the applied incremental displacement.

Due to the limited computer time, the following choices were available:-

(a) To use the available computer time for obtaining a few load-displacement curves, which would have been the final results of the theoretical investigation, i.e. introducing a large number of elements, iterations and increments,
or
(b) To use the computer time in obtaining information on various parameters affecting the anchor problem.

The author decided that the anchor problem would be better understood by obtaining as much information as possible. Therefore the time taken by running the computer program was minimised by undertaking the following investigation:-

(a) The soil and the anchor plate were divided into 144 elements.

(b) One iteration could be used for each increment of displacement.

(c) The maximum number of steps used in any run would be no more than thirty.

Preliminary runs of the computer program, revealed the following information:-

(a) For any increment of displacement, the incremental load converges in about six or seven iterations, although the incremental stresses in some elements never converge.

(b) The smaller the incremental displacement, the quicker the incremental load converges.

(c) By dividing the soil on the anchor plate into five or six elements, the ultimate load remains the same.

(d) The ultimate load is affected more by the size of the elements around the anchor plate, than by those further away.

10.2.2 Load-displacement curve

The program predicts only part of the load-displacement curve, as an incremental procedure is used to obtain the load for a given increment of displacement, i.e. the post-peak section of the curve cannot be predicted.

Fig. 10.9 shows the load-displacement curves of an anchor with different diameters of plates embedded at two different depths. The curves were obtained by plotting the predicted

Fig. 10.9 Load V Displacement

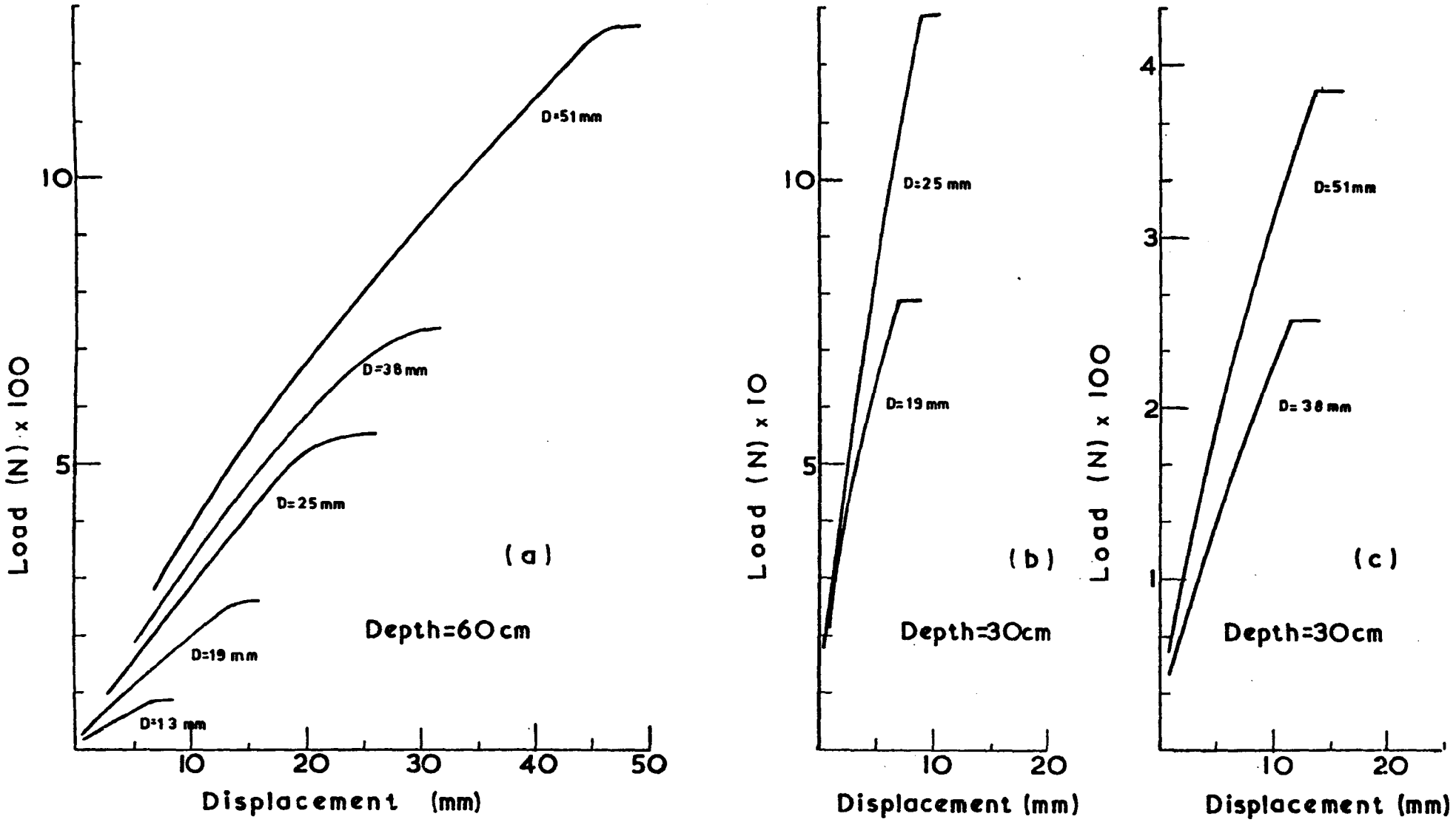

incremental load against the applied increment of displacement.

Fig. 10.9 (a) shows the predicted load-displacement curves of the five anchor plates used during the experimental programme embedded at 60cm depth. The predicted curves of the same plates embedded at 30cm depth are shown in Fig. 10.9 (b) and Fig. 10.9 (c). It is observed that for any load-displacement curve, the load increases with the displacement but the rate of change decreases and finally the relationship breaks down, indicating the ultimate load of the anchor. The figures also show that the rate of change of the load with the displacement increases, as the anchor plate diameter and the depth of embedment increase. The displacement at which the ultimate load is predicted, also increases with the depth and the diameter of the plate.

The load-displacement curves of the 51mm diameter anchor plate embedded at 60cm, obtained experimentally and theoretically, are plotted in Fig. 10.10. In the linear case, the rate of change of the load with the displacement tends to coincide with that of the experimental curve, as the values of E and ν increase. The rate of change of the load with the displacement in the predicted load-displacement curve, also tends to coincide with the experimental curve as the value of E increases for the first few millimetres of displacement. The figure also shows that the ultimate load of the experimental curve falls between the predicted curves, with $E = 10^6$ N/m^2 and $E = 10^7$ N/m^2. Although for the first 7mm of displacement the experimental curve correlates better with the predicted curve of $E = 10^7$ N/m^2 than with the curve of $E = 10^6$ N/m^2, the ultimate load of the experimental curve correlates better with the second one.

Fig.10.10 Load V Displacement

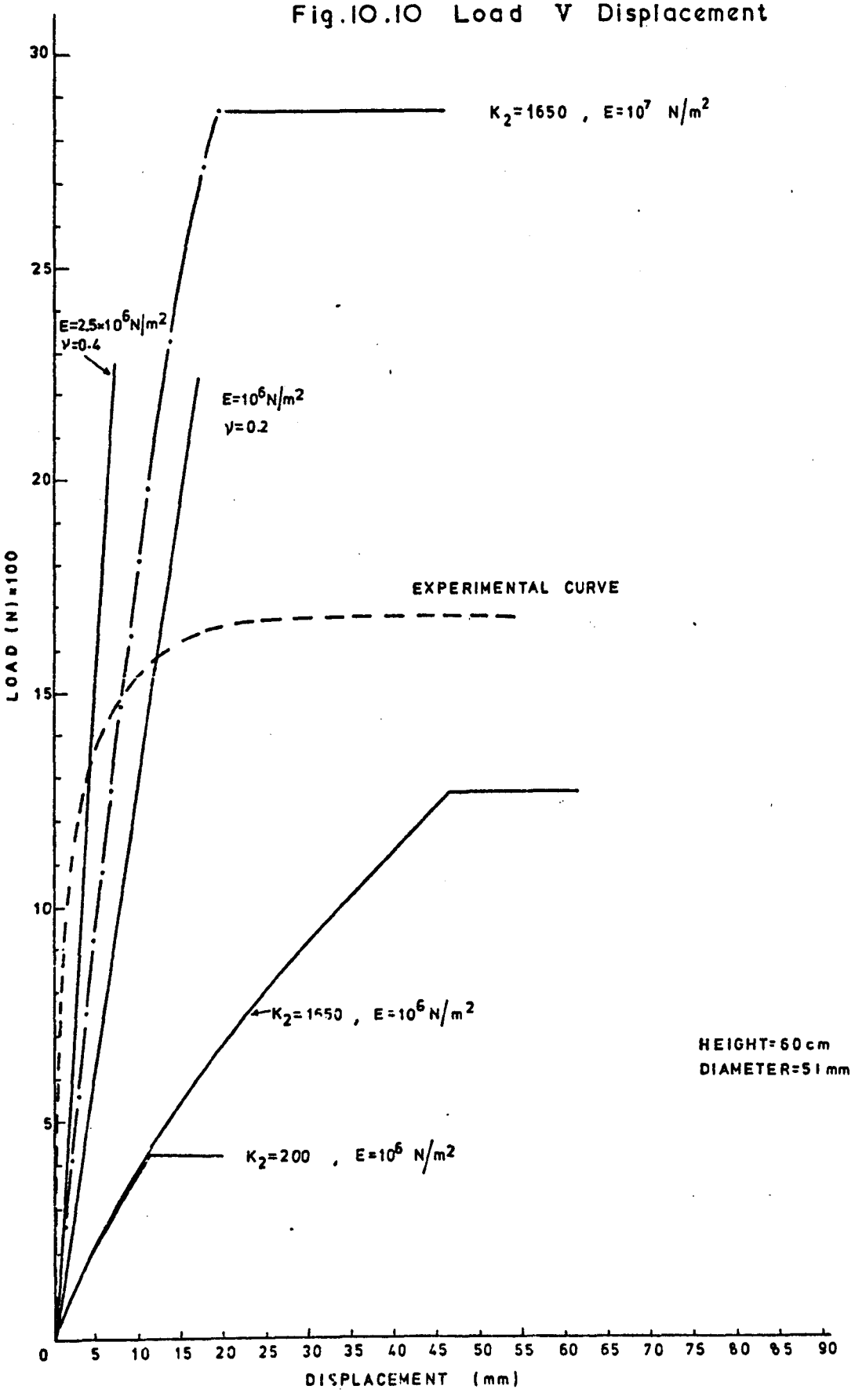

The ultimate load of the experimental curve is about 1.3 times that of the predicted load-displacement curve with $E = 10^6$ N/m^2 and a little over half of the curve with $E = 10^7$ N/m^2.

Fig. 10.9 showed that for each anchor plate the ultimate load occurred at a different displacement. The ultimate loads of the anchor plates embedded at 60cm depth are plotted against their corresponding displacement in Fig. 10.11. The figure shows that the absolute displacement at which the ultimate load occurs, is directly proportional to the anchor plate diameter. The experimental results also showed a similar relationship, see Fig. 8.17.

10.2.3. Distribution of incremental load on the anchor plate

Fig. 10.12 shows the distribution of two predicted increments of load on the 51mm diameter anchor plate embedded at 60cm depth. The plate, originally displaced by 0.01mm, was given an additional displacement of 0.01mm, and the predicted load at each node was plotted, curve A. The predicted load of the 21st increment of displacement, with the anchor plate originally displaced by 19mm and given an additional displacement of 1mm, was plotted and curve B was obtained. From the figure it can be concluded that the distribution of the predicted increment of load depends:

(a) On the size of the increment of displacement, and

(b) On the state of the sample; i.e. elements of soil fail during each increment of displacement and the overall stiffness matrix is modified.

Fig. 10.11 Displacement V Diameter of plate

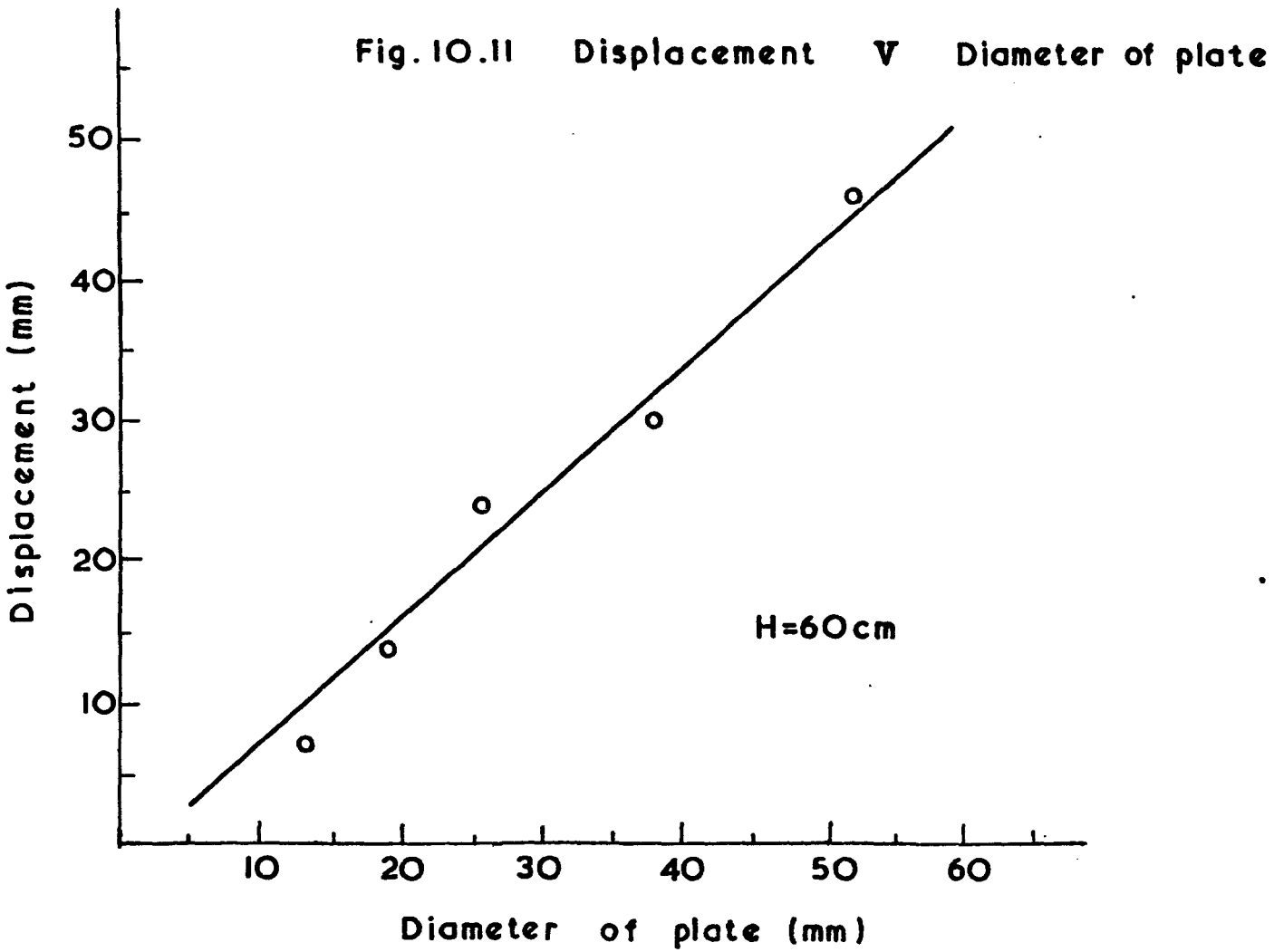

Fig. 10.12 Distribution of load

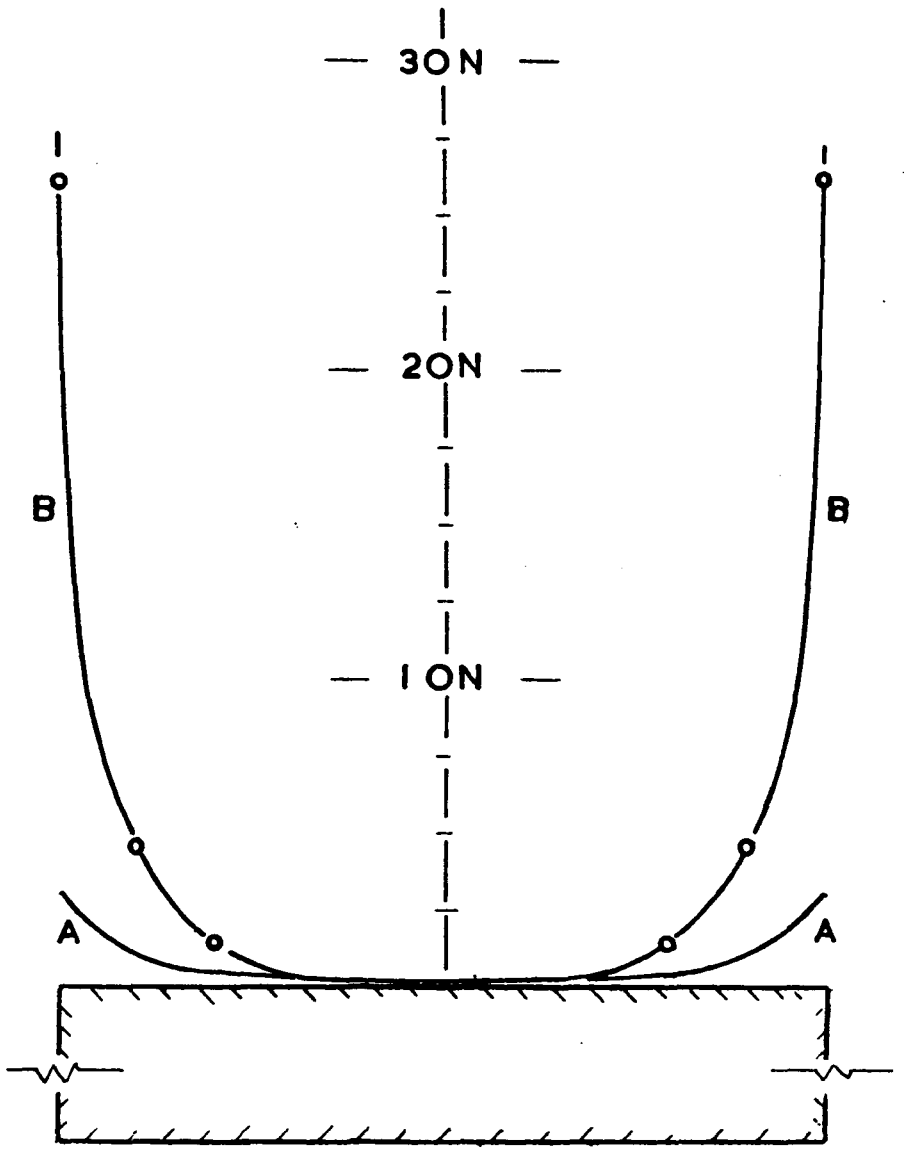

diameter = 51 mm

depth = 60 cm

10.2.4 Stress distribution on the anchor plate

The distribution of the stress on the anchor plate at various percentages of the ultimate load is shown in Fig. 10.13. At a very low load, i.e. 3% of P_m, the stress is uniformly distributed on the plate but as the load increases the distribution takes the form of a parabola. At about 25% of the ultimate load, the stresses on the anchor plate between $\frac{D}{2} = 0$ and $\frac{D}{2} = 12.5$mm, tend towards substantially constant values, whilst on the outer part of the plate the stresses increase until 50% of the ultimate load is reached. As the load increases from 50% to 100% of the ultimate load, the stresses between $\frac{D}{2} = 17$mm and $\frac{D}{2} = 25$mm increase while on the rest of the anchor plate the stresses remain constant. Therefore it can be concluded that the distribution of the stress on the anchor plate varies as the anchor is displaced; and it is only uniform in the first 3% of the ultimate load.

10.2.5 Influence of shaft diameter on the ultimate load

The effect of the shaft diameter on the ultimate load of the anchor was investigated using the 25mm diameter plate embedded at 60cm depth. Two different diameters of shaft, i.e. 5mm and 12mm, were used for the purpose of computations and the two predicted loads of 550 N and 387 N were obtained respectively. To compare these values with those obtained experimentally, the ratios of the diameter of the plate to the diameter of the shaft are used. For $\frac{D}{D_s} = 5$ and $\frac{D}{D_s} = 2$ the experiments gave the values of the ultimate loads to be about 890 N and 790 N respectively. Comparing the increase in the ultimate load due to the decrease in the diameter of the shaft, in both cases, the predicted ultimate load increased by 42% whilst the experimental by 13%. From this investigation it can be concluded that the diameter of the shaft does affect the ultimate load.

Fig. 10.13 Distribution of stress

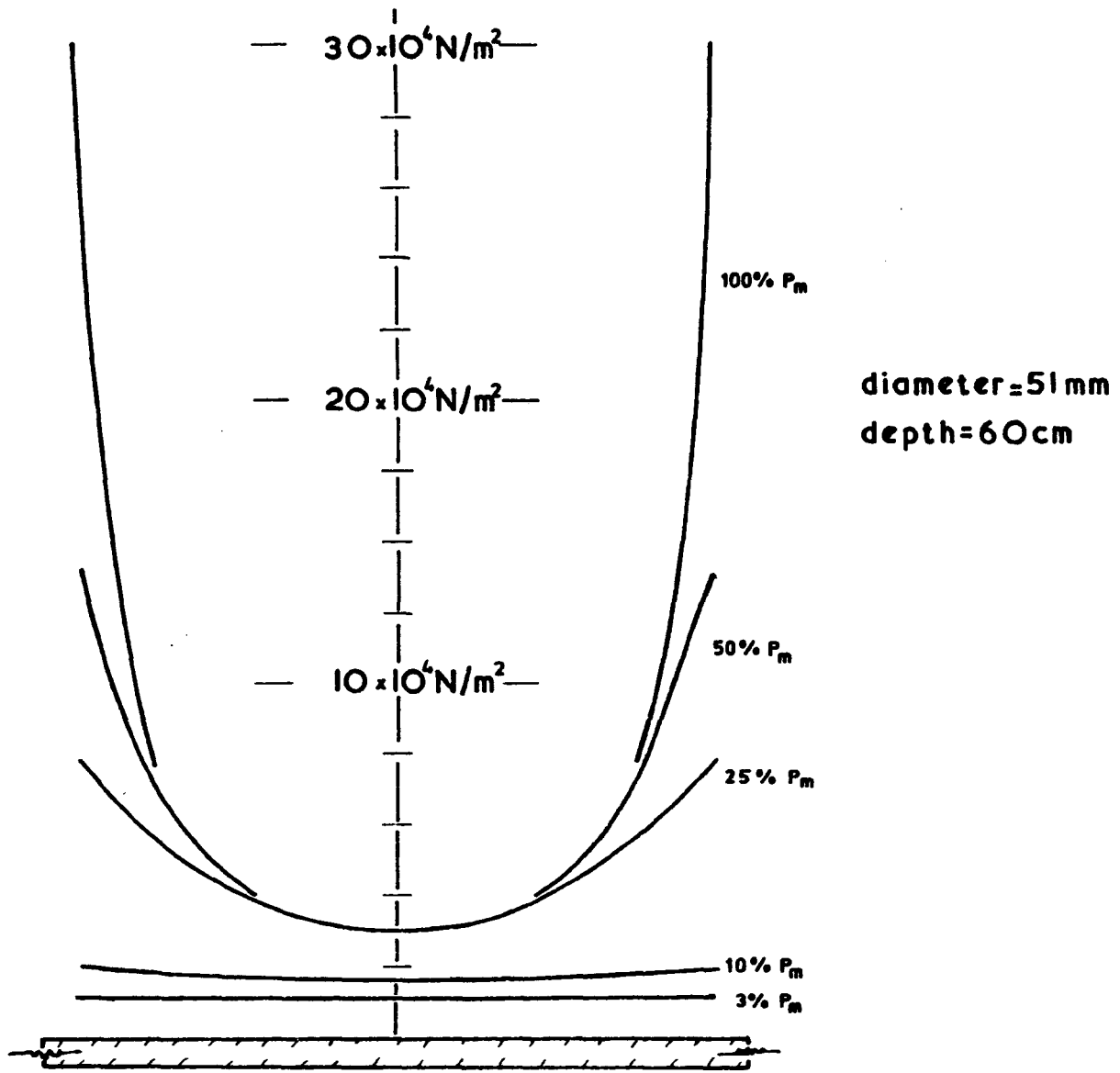

10.2.6 Influence of plate thickness on the ultimate load

The effect of the thickness of the anchor plate on the ultimate load was investigated using the 51mm diameter plate embedded at 60cm depth. Two thicknesses of plate, i.e. 25mm and 100mm, were used during the computation. The anchor plate with 25mm thickness, i.e. $\frac{t}{D} = 0.5$, gave an ultimate load of about 815 N whilst the 100mm thick plate, i.e. $\frac{t}{D} = 2$, gave a load of 1265 N. In the experimental programme, the 25mm diameter plate gave the ultimate load of 450 N and 605 N for $\frac{t}{D} = 0.5$ and $\frac{t}{D} = 2$ respectively. Calculations show that the experimental and theoretical ultimate loads for $\frac{t}{D} = 0.5$, are 64% and 74% of the ultimate loads for $\frac{t}{D} = 2$, respectively. Therefore, both experiments and theory show that the ultimate load decreases with $\frac{t}{D}$ decreasing from $\frac{t}{D} = 2$ to $\frac{t}{D} = 0.5$. The predicted results suggest that the change in the ultimate load is solely due to the change in the thickness of the plate, since the friction was ignored in the computation.

10.2.7 Variation of ultimate load with the plate diameter

The predicted ultimate loads together with the experimental ones, were plotted against the anchor plate for two different depths, i.e. 30cm and 60cm, see Fig. 10.14. For the smaller depth, both the experimental and theoretical results produce straight line graphs, with the ultimate loads increasing with the diameter of the plate. The two graphs obtained at 60cm depth, are smooth curves with the rate of change of the ultimate load increasing with the anchor plate diameter.

10.3 Zones of disturbance in the sand

The anchor plate of 51mm in diameter embedded at 60cm depth

Fig. 10.14 Ultimate load V Diameter of plate

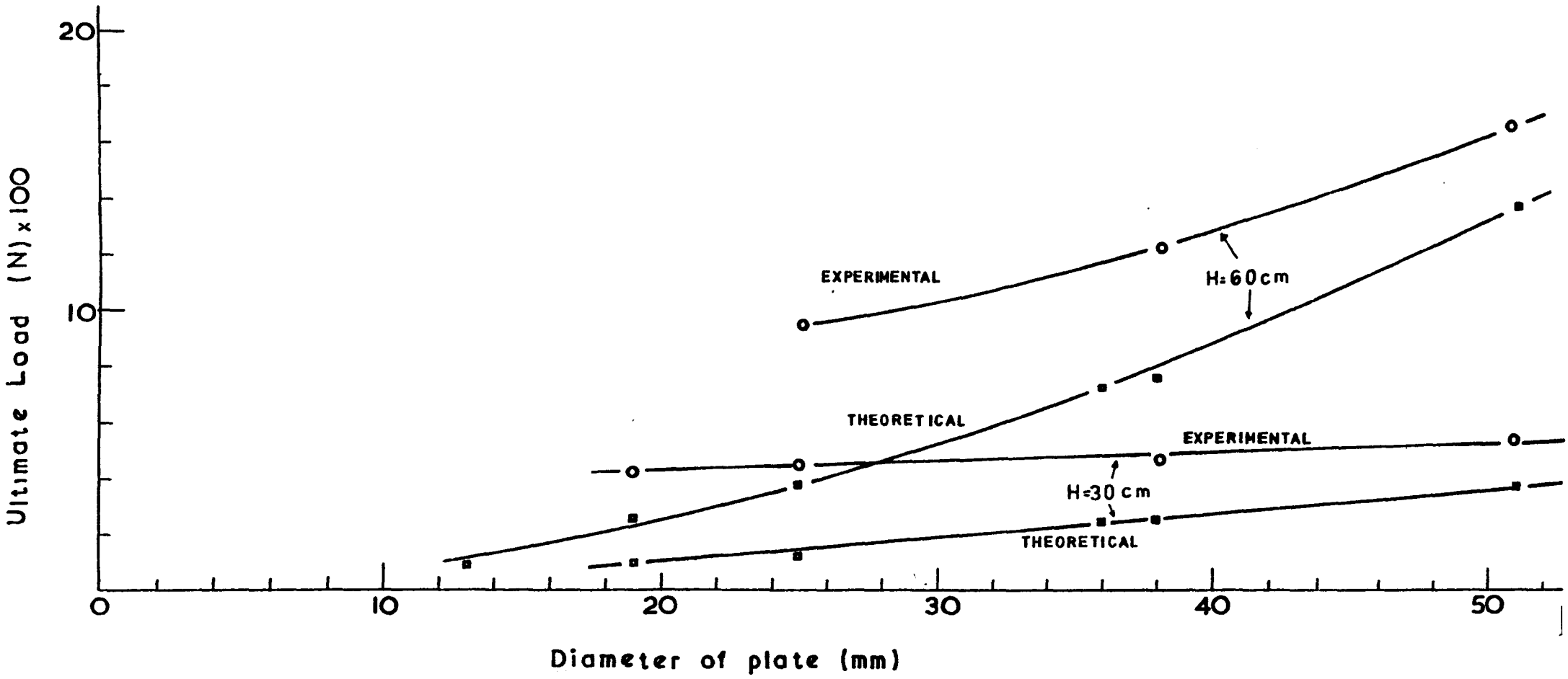

was displaced by 4.6mm in the computation, and the displacement contours for the vertical direction are plotted in Fig. 10.15. The program predicted that there is little horizontal displacement in the sample, and therefore this negligible amount is insufficient to materially affect the total displacement. On the same figure, the contours obtained experimentally by Edwards (1974, Ref. 52) for the same relative depth but D = 25.4mm, are also plotted.

The contour lines obtained using the linear program, show that the vertical displacement is well spread over the area. The shape of the zone is elliptical but as the displacement increases, the shape tends to be circular. The contours also show that the displacement is spread under the anchor plate, which is due to the method used; i.e. an elastic stress-strain relationship was employed for the calculations of the displacements.

The vertical displacements predicted by the non-linear program were also plotted, and the contours are shown in Fig. 10.15. The shape of the contour line of 0.5mm displacement appears to be elliptical with the major axis vertical, whilst that of the 2mm displacement tends to be circular.

Comparison of the contour lines of the non-linear case with the contours obtained by Edwards in a narrow tank shows the following interesting points.

(a) They originate near the top surface of the anchor plate.

(b) They become larger in the vertical direction as the displacement field decreases.

Fig. 10.15 Displacement zones

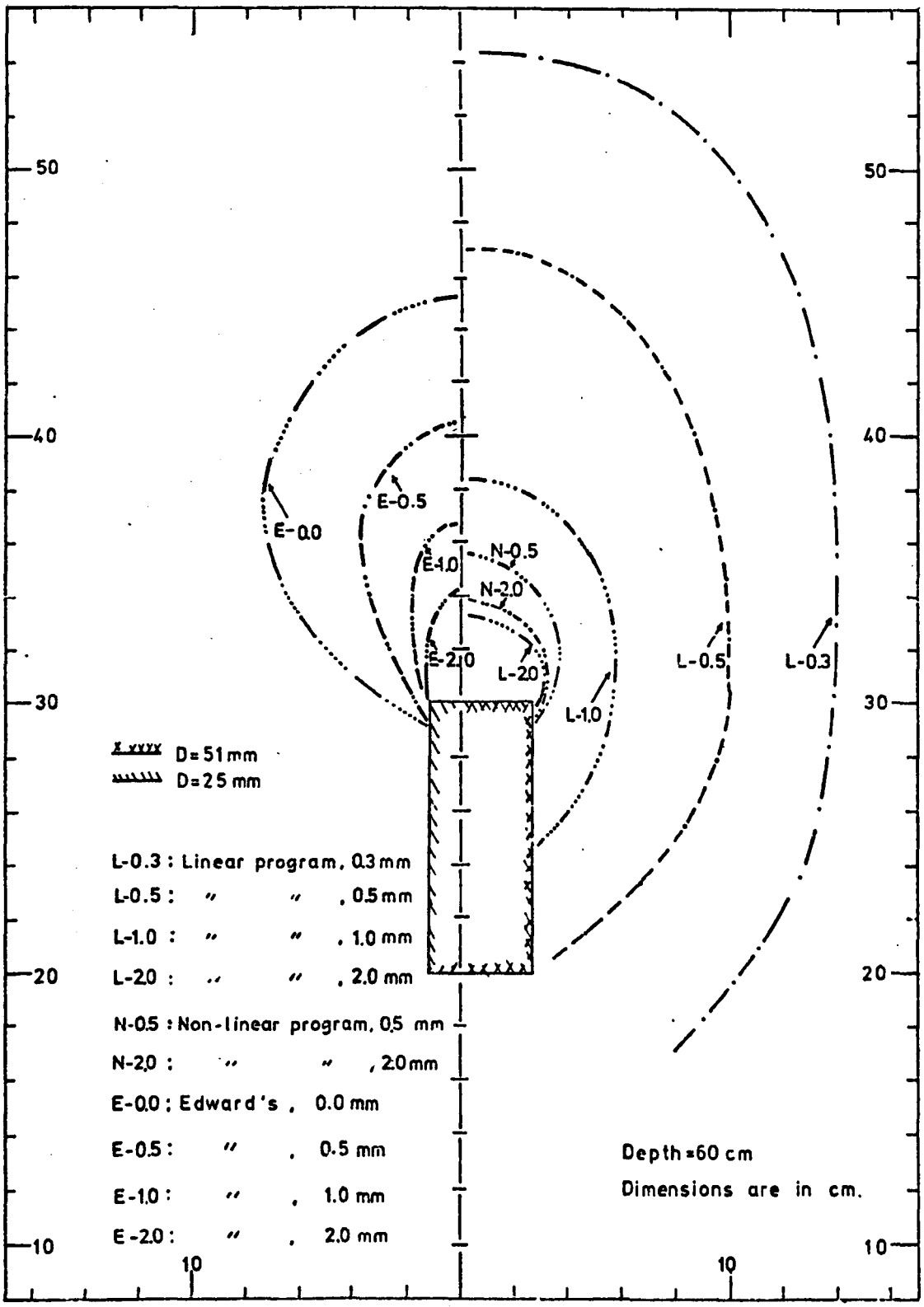

(c) The overall shape is nearly similar.

Direct comparison of the actual values of displacements could not be made, due to the different sizes of anchor plates and properties of the samples ($\phi = 35.4°$ and $\gamma = 104.2$ lbs/ft^3 for Edwards' sample) used by the two researchers.

The contour lines of 0.006mm vertical displacement for two different stages in the load-displacement behaviour of the anchor are plotted in Fig. 10.16. It is observed that as the anchor plate is displaced from the absolute displacement of 0.415mm to the absolute displacement of 3.715mm, the zone increases approximately by the same distance in all directions except under the anchor plate. McMullan (1975, Ref. 24) mapped the zone of influence for an elastic displacement of 1.924mm, and his contour line also indicates that the zone extends under the anchor plate, see Fig. 10.16.

In the same figure, the increments of displacements prior to and during ultimate load are also plotted. Contour A, i.e. prior to ultimate load, shows that the soil in the zone has displaced the same distance as the anchor plate. During ultimate load the amount of soil travelling with the anchor plate decreases, see contour B. The existence of an elastic wedge on top of the anchor plate was also observed by Carr (1970, Ref. 23) and Kalajan (1971, Ref. 70).

10.4 Extent of failure zone

The failure zones in this section were obtained by considering the blocks of elements failing due to the failure criteria mentioned in Chapter IX. Fig. 10.17 shows the failure zones

Fig. 10.16 Displacement zones

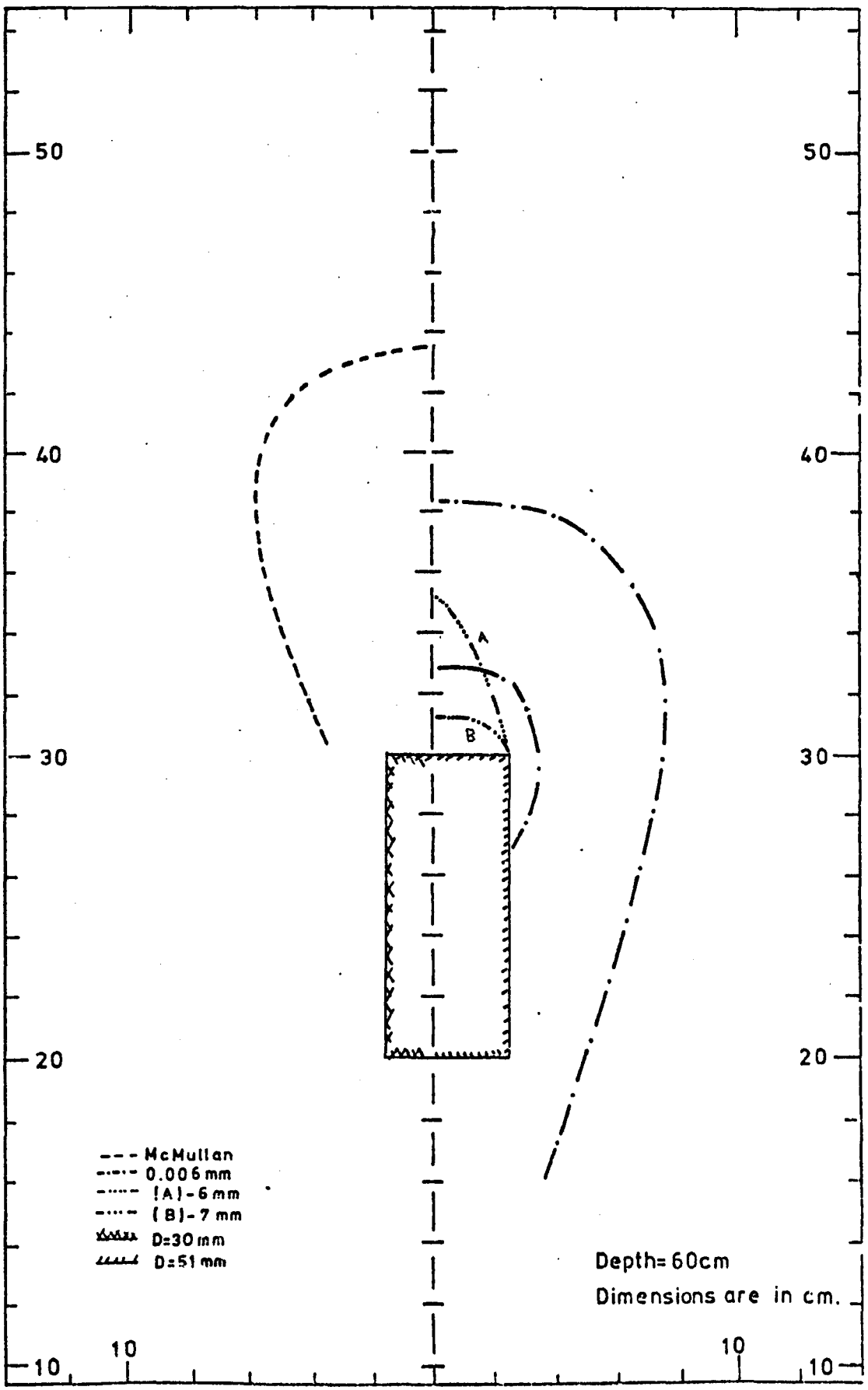

Fig. 10.17 Failure zones

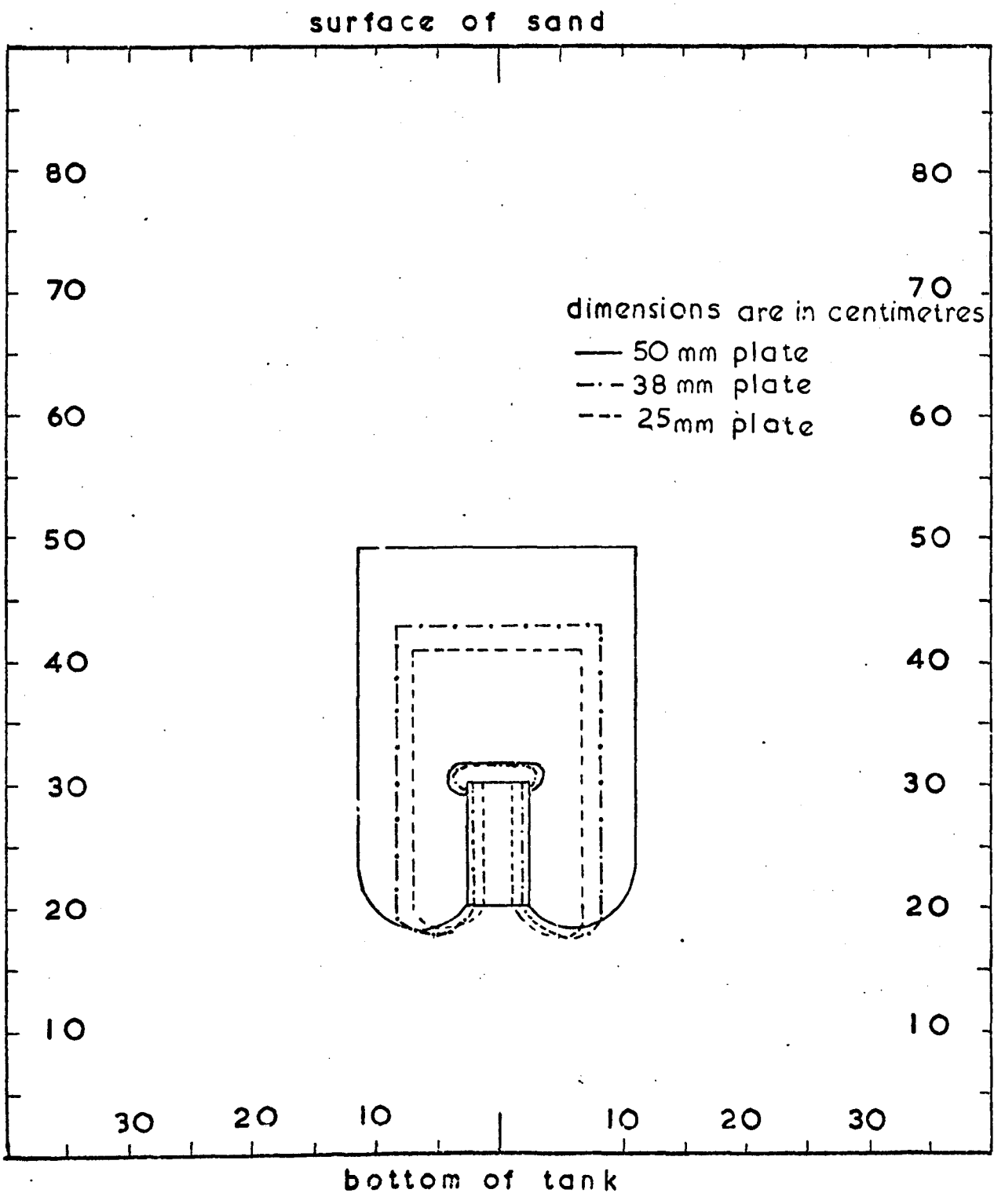

of the anchor plates of 25mm, 38mm and 51mm diameter embedded at 60cm depth. The following interesting points are observed:-

(a) The extent of the failure zone increases with the diameter of the anchor plate.

(b) The soil outside the failure zone is also affected; the stresses decrease or increase.

(c) The soil in the vicinity of the top end of the anchor plate does not fail.

(d) The failure zone of the 51mm diameter plate suggests that the anchor behaves as "deep". This suggests that the critical relative depth is less than 12.

(e) The failure zone emanates from the bottom end of the anchor plate and extends downwards for about 25mm.

Fig. 10.18 shows the failure zones of the 38m and 51mm diameter plates embedded at 30cm. Although the failure zone of the smaller plate is well within the surface of the sample, that of the bigger plate extends to the soil surface, indicating that at $\frac{H}{D} \leq 6$ the anchor behaves as "shallow".

The failure zones of the 13mm and 19mm diameter anchor plates, H = 30cm, are shown in Fig. 10.19. It is observed that the failure zones are elliptical with the major axis vertical, and the zones again emanate from the bottom end of the anchor plate but without extending downwards.

Fig. 10.18 Failure zones

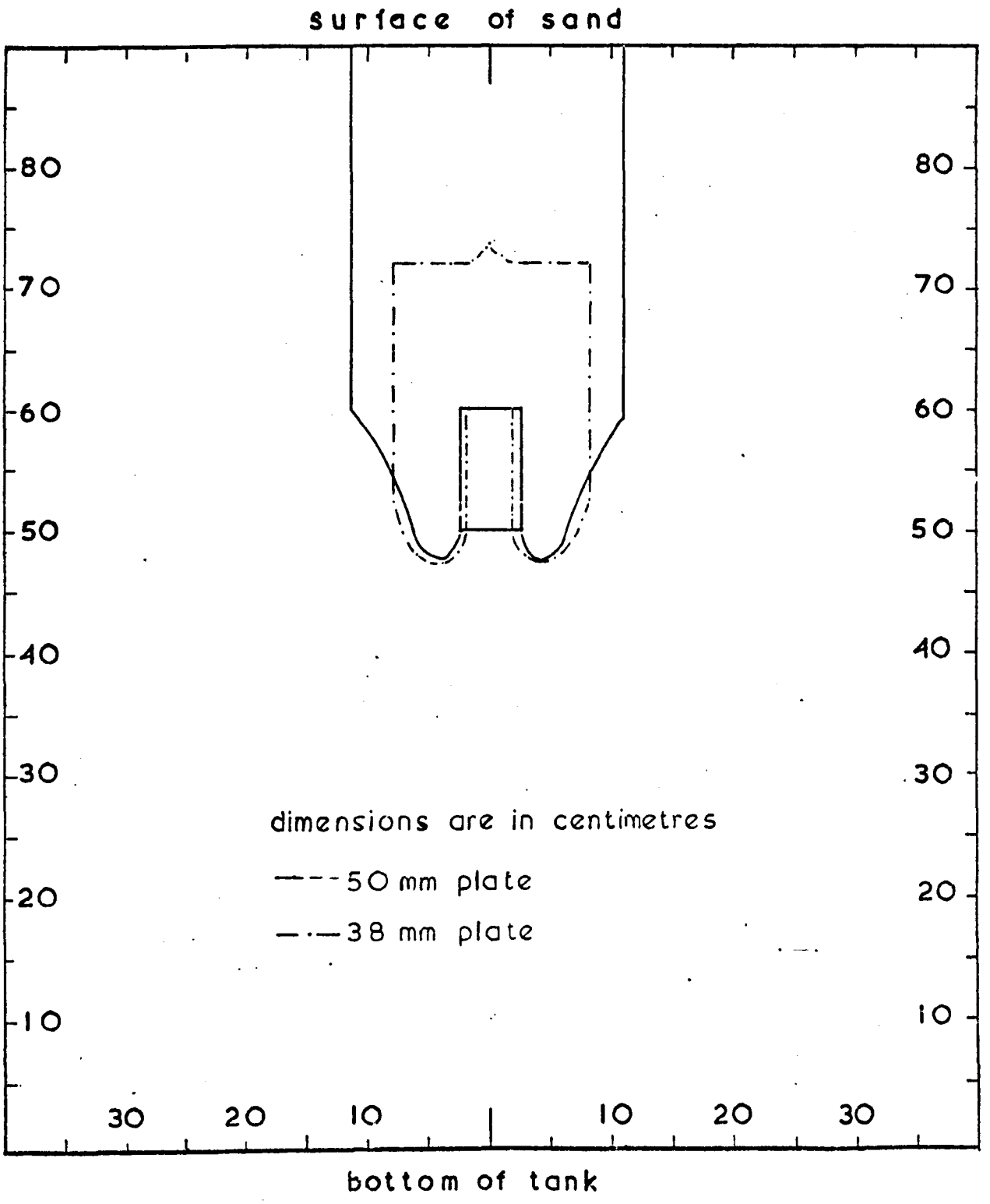

Fig. 10.19 Failure zones

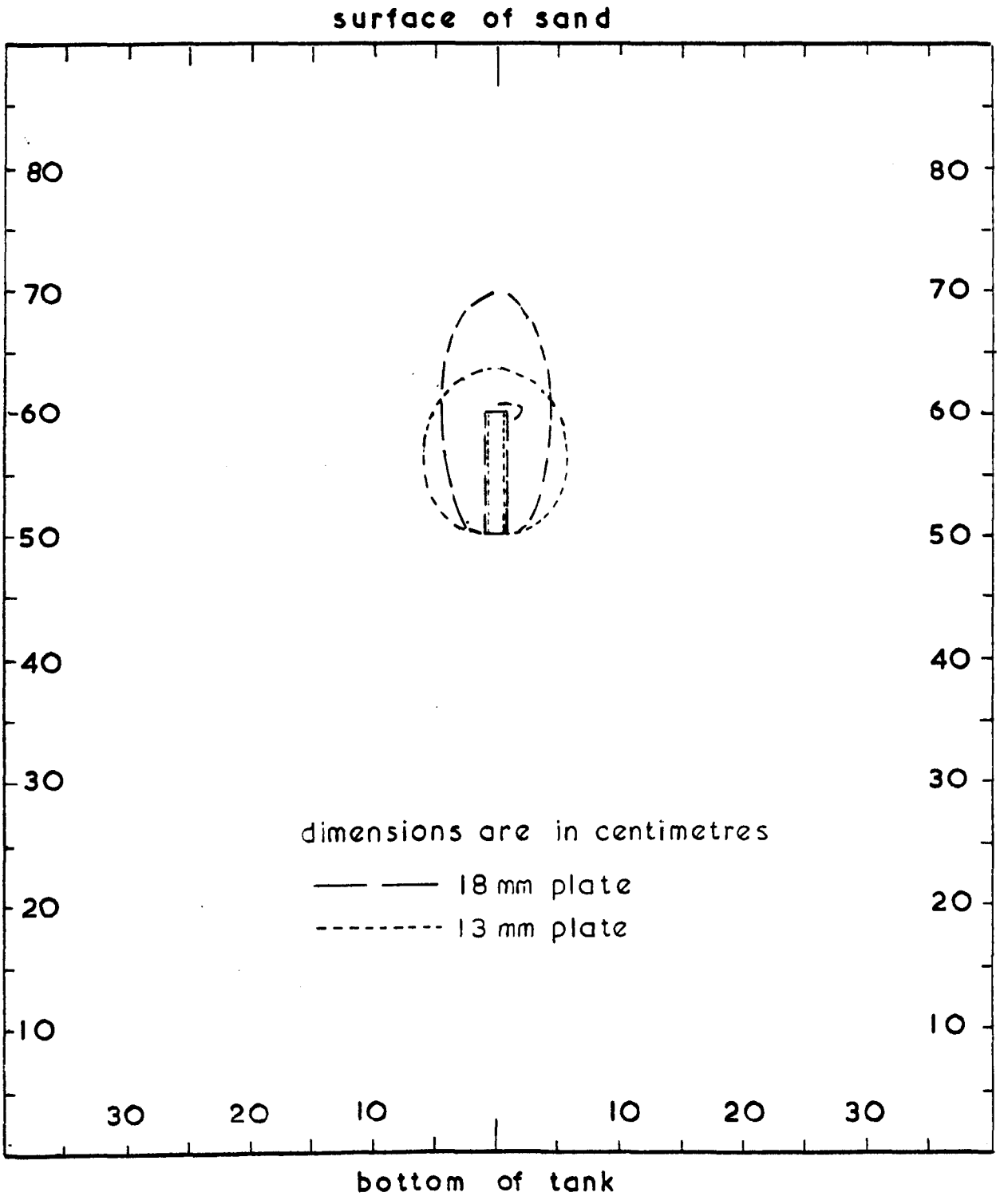

10.5 Discussion

In the previous sections, the load-displacement curves of the different anchor systems were predicted by considering the following factors:-

(i) $\sigma_r < \frac{\sqrt{\sigma_\theta \sigma_z}}{K_T}$, $\sigma_\theta < \frac{\sqrt{\sigma_r \sigma_z}}{K_T}$, $\sigma_z < \frac{\sqrt{\sigma_\theta \sigma_r}}{K_T}$

(ii) $\sigma_r > 0$, $\sigma_\theta > 0$, $\sigma_z > 0$

(iii) Elements not satisfying conditions (i) or (ii) have zero stiffness.

The load-displacement behaviour of the anchor was also predicted using the following conditions:-

(i) $\sigma_r < \frac{\sqrt{\sigma_\theta \sigma_z}}{K_T}$, $\sigma_\theta < \frac{\sqrt{\sigma_r \sigma_z}}{K_T}$, $\sigma_z < \frac{\sqrt{\sigma_r \sigma_\theta}}{K_T}$

(ii) $\sigma_{pc} > 0$, $\sigma_{pt} > 0$, $\sigma_\theta > 0$

Where σ_{pc} , σ_{pt} and σ_θ are the principal stresses.

(iii) Elements not satisfying conditions (i) or (ii) have zero stiffness.

The anchor plate of 51mm diameter embedded at 60cm depth was used in the computation. The load-displacement curves, obtained using different modulus of elasticity and $\nu = 0.4$, are shown in Fig. 10.20. The following observations are made:-

(a) The rate of the load with the displacement increases, with E increasing.

(b) The ultimate load increases with E decreasing, and at about $E = 10^5$ N/m^2 the ultimate load obtains a constant value of about 160 N.

(c) The displacement at which the ultimate load occurs, decreases with the value of E increasing.

An attempt was also made to obtain the load-displacement curve of the above anchor by considering the following criteria:-

(i) $\sigma_r < \frac{\sqrt{\sigma_\theta \sigma_z}}{K_r}$, $\sigma_\theta < \frac{\sqrt{\sigma_r \sigma_z}}{K_r}$, $\sigma_z < \frac{\sqrt{\sigma_\theta \sigma_r}}{K_r}$

(ii) $\sigma_{pc} > 0$; $\sigma_{pt} > 0$

(iii) Elements not satisfying condition (ii) obtain constant stresses; i.e. the total stresses at failure are used until condition (i) or (iv) is obtained.

Fig. 10.20 Load V Displacement

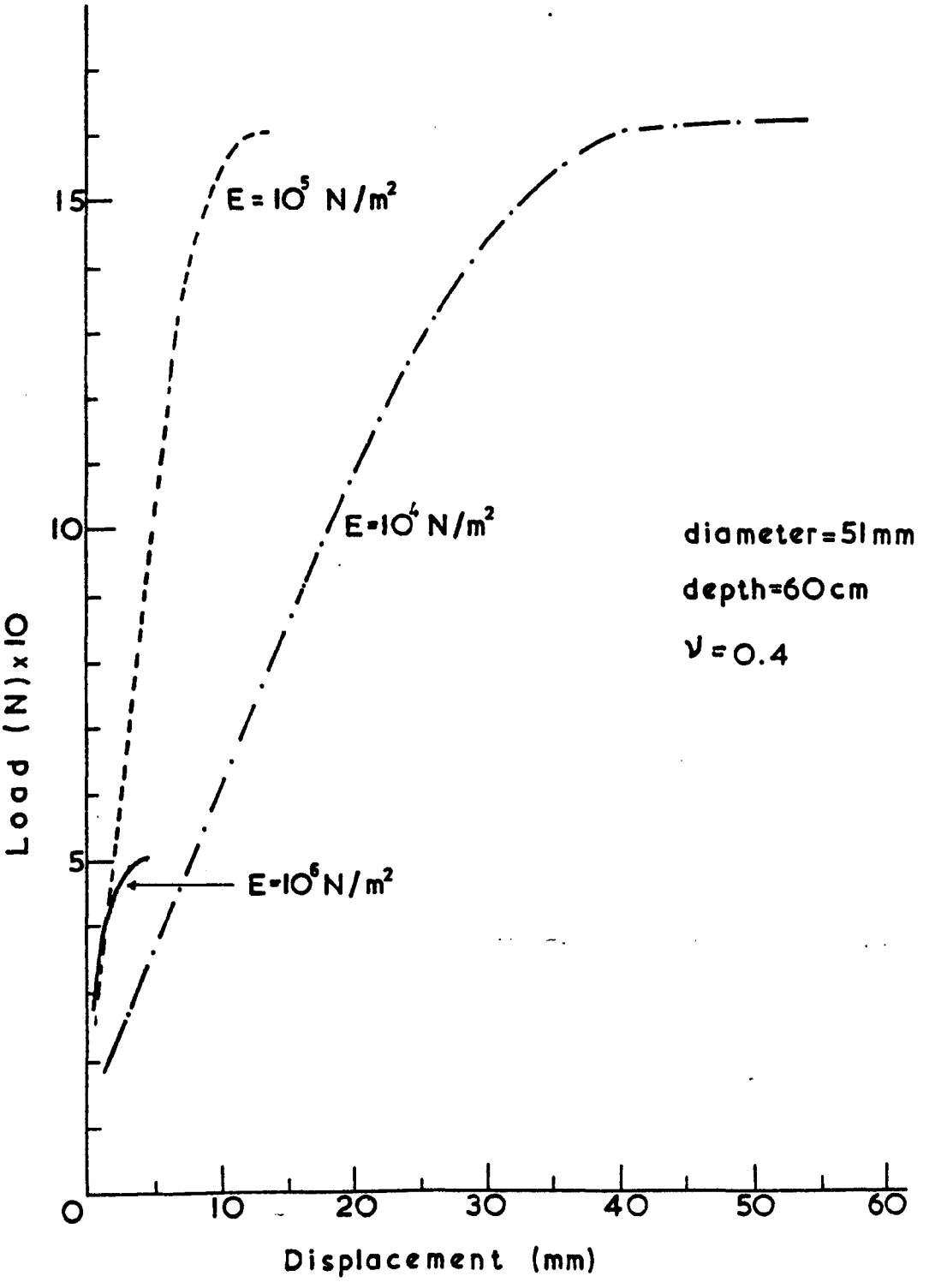

(iv) $\sigma_r > 0$, $\sigma_\theta > 0$, $\sigma_z > 0$

(v) Elements not satisfying conditions (i) or (iv) have zero stiffness.

Fig. 10.21 shows the predicted part of the load-displacement curve. It is clear that the ultimate load would be greater than 2200 N, and this value would be larger than the previous predicted and experimental ultimate loads of the same anchor system.

The investigation into the failure criteria of the soil elements on the load-displacement behaviour of the anchor , suggests that the immediate removal of elements by considering them to obtain a zero stiffness after failure, is debatable . New criteria of "freezing" the stresses of the elements after failure for some part of the loading should be found. If the principal stresses are considered as one of the failure criteria, the stresses of the already failed elements along the axes, should be calculated from the principal stresses for part of the loading.

Although the present procedure has its drawbacks, as far as the failure criteria and procedural formulation are concerned, it is considered that it has gone part of the way towards a solution. However, a good deal of research is still necessary particularly into the stress-strain relationship for the soil.

Fig. 10.21 Load V Displacement

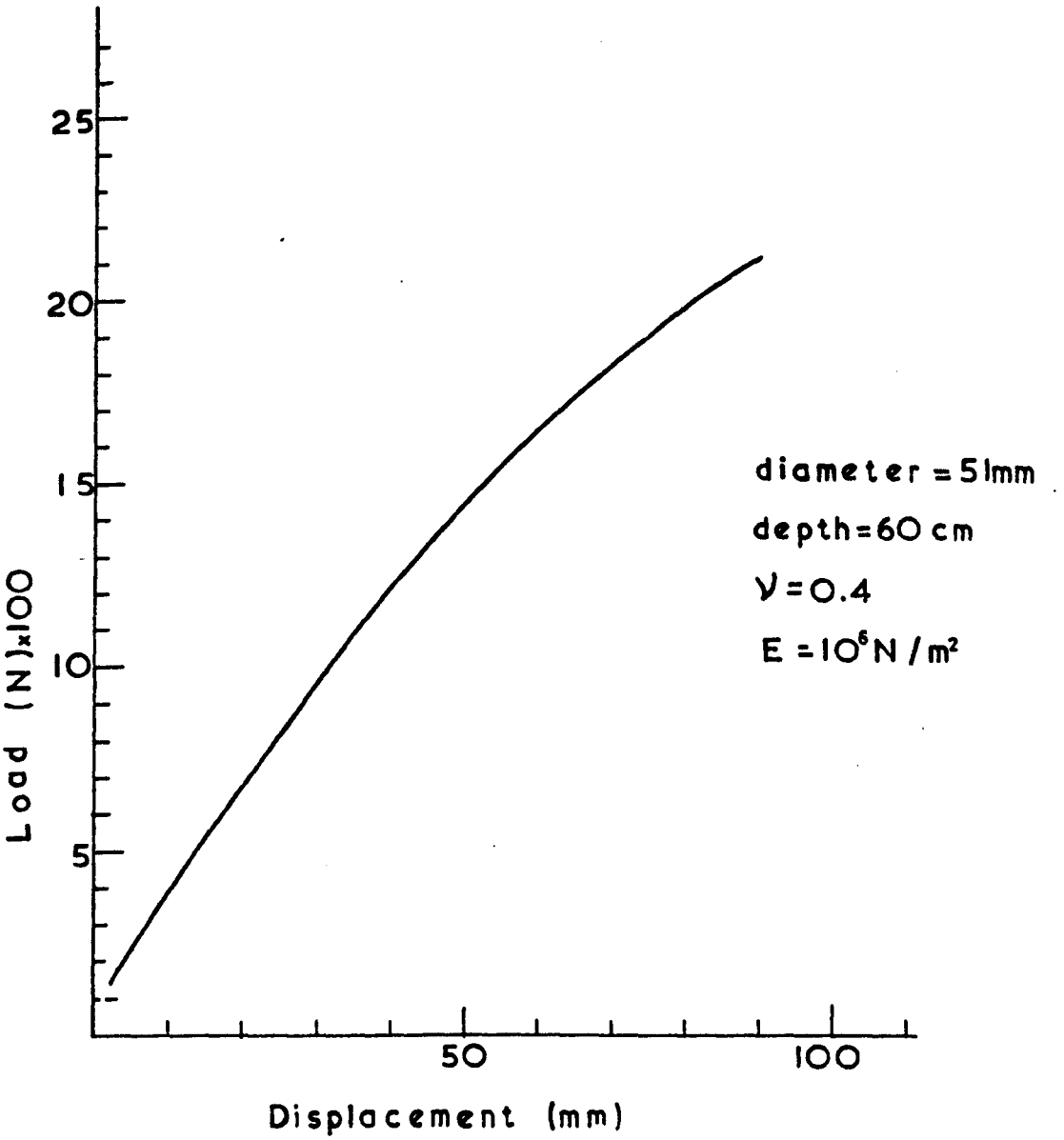

CHAPTER XI

COMPARISON OF RESULTS WITH VARIOUS THEORIES

11.1 General

In this chapter, theories produced by previous workers will be used to calculate the ultimate load of the anchor configurations used in this research programme in order to, as far as is possible, compare the results. The following theories will be employed:-

(a) Meyerhof and Adam's

(b) Vesic's

(c) Baker and Kondner's

The sand will be considered to have the following characteristics:-

$\gamma = 1.7 \text{ gr/cm}^3$

$\phi = 43.2^{\circ}$

The finite element, developed by the author, will also be used to predict the load-displacement curves of the anchors used by Baker and Kondner in their field tests.

11.2 Meyerhof and Adam's theory

For calculating the ultimate load of a deep anchor with a circular plate, the following equation was used:-

$$P_m = \frac{\pi}{2} \gamma D (2H - H_1) H_1 (s K_u) \tan\phi + W_1$$

Where

$sK_u = 5.63$

$H_1 = 9D$

$W_1 = V \gamma q$

$V = \frac{\pi H_1}{3}(R_2^2 + R_1R_2 + R_1^2)$

$R_1 = D/2$

$R_2 = R_1 + H_1 \tan\frac{\phi}{3}$

A computer program was written (see Appendix L), and the ultimate loads of the five different anchor plates were calculated at different relative depths.

11.3 Vesic's theory

The ultimate pressure of an expanded cylindrical cavity was given by:-

$P_u = q F_q$

Where

$F_q = (1 + \sin\phi)\ (I_{rr}\ \sec\phi)^{\left(\frac{\sin\phi}{1+\sin\phi}\right)}$

I_{rr} = the rigidity index

q = the initial ground stress = γH

Vesic stated that for sand I_{rr} varies between 70 and 100, and for $\phi = 44^{\circ}$ F_q varies from 13.27 to 15.70.

A computer program , based on the equation:- $P_m = \frac{\pi}{4}(D^2 - D_i^2)\left(q F_q + F_\gamma \frac{D}{6H}\right)$, was written (see Appendix L) to determine the ultimate load of the different anchor configurations. For each anchor plate and relative depth, two ultimate loads were determined i.e. with $F_q = 13.27$ and $F_q = 15.70$.

11.4 Baker and Kondner's theory

Following the procedure used by Baker and Kondner, the author plotted his experimental results and obtained Fig. 11.1 ie. $\frac{P_m}{D^3\gamma}$ against $\frac{H}{D}$. Due to the lack of experimental results at shallow depths i.e. $\frac{H}{D} < 8$, the value of $\frac{P_m}{D^3\gamma}$ where the curves converge, could not be obtained. Baker and Kondner found that the parameter $\frac{P_m}{D^3\gamma}$ converges to $\frac{P_m}{D^3\gamma} = 170$ and modified their equation to take the form $\left(\frac{P_m}{D^3\gamma} - 170\right)\frac{D}{t} = C_3 + C_4 \frac{H}{D}$

The $170\frac{D}{t}$ term was ignored by the author since its value is very small compared with the values of $\frac{P_m D}{D^3\gamma t}$, and the parameter $\frac{P_m}{D^2 t\gamma}$ was plotted against $\frac{H}{D}$, see Fig. 11.2. The graph shows that the parameter $\frac{P_m}{D^2 t\gamma}$ varies linearly with $\frac{H}{D}$. Calculations also show that the line intercepts the $\frac{P_m}{D^2 t\gamma}$ axis at - 150. The slope of the line is $\frac{400}{9}$. Therefore the equation of the ultimate load becomes:-

$$\frac{P_m}{D^2 t \gamma} = -150 + \frac{400}{9}\frac{H}{D}$$

$$P_m = D t \gamma \left(\frac{400}{9} H - 150 D\right)$$

Fig. 11.1 $(P_m / D^3\gamma)$ V (H / D)

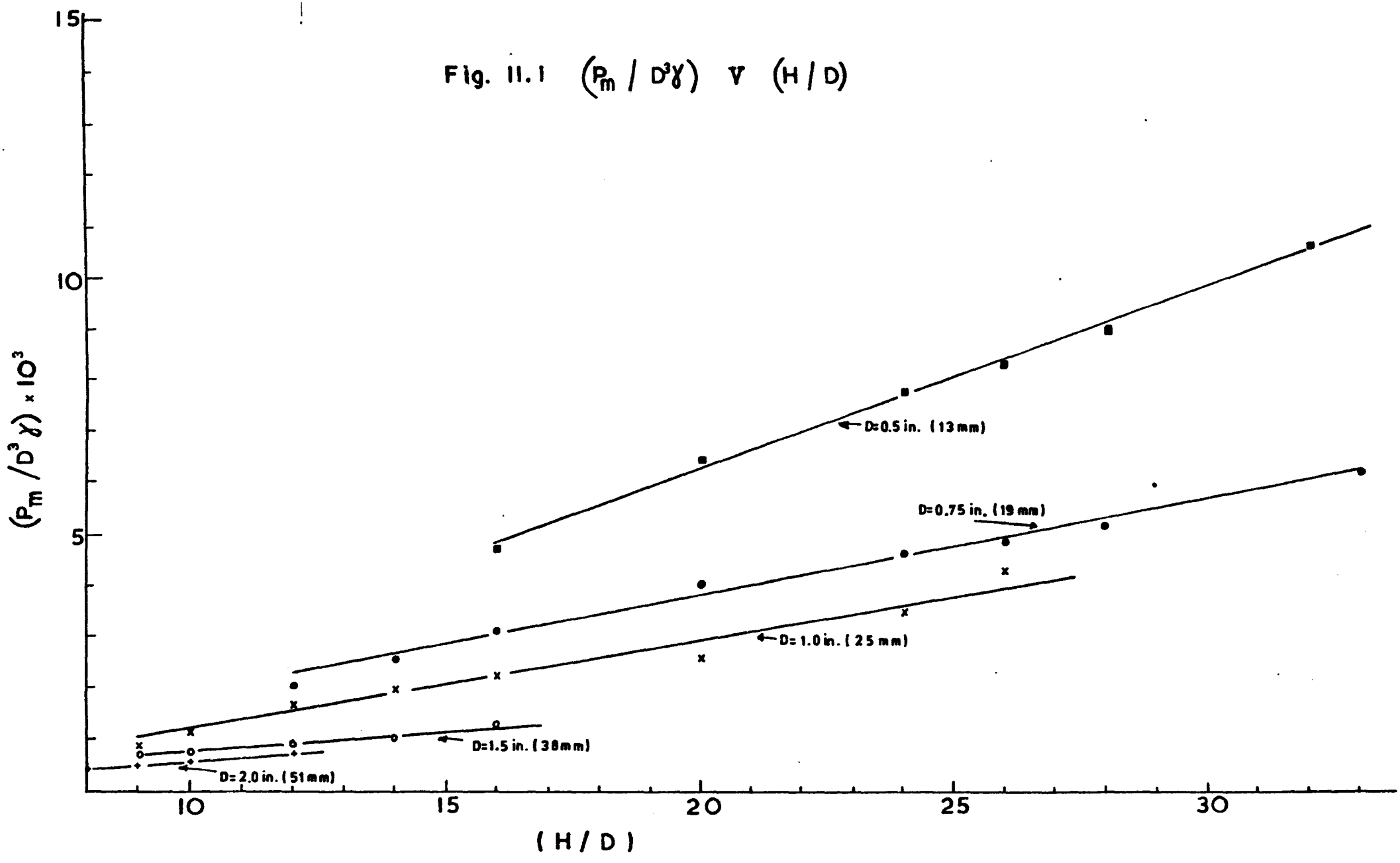

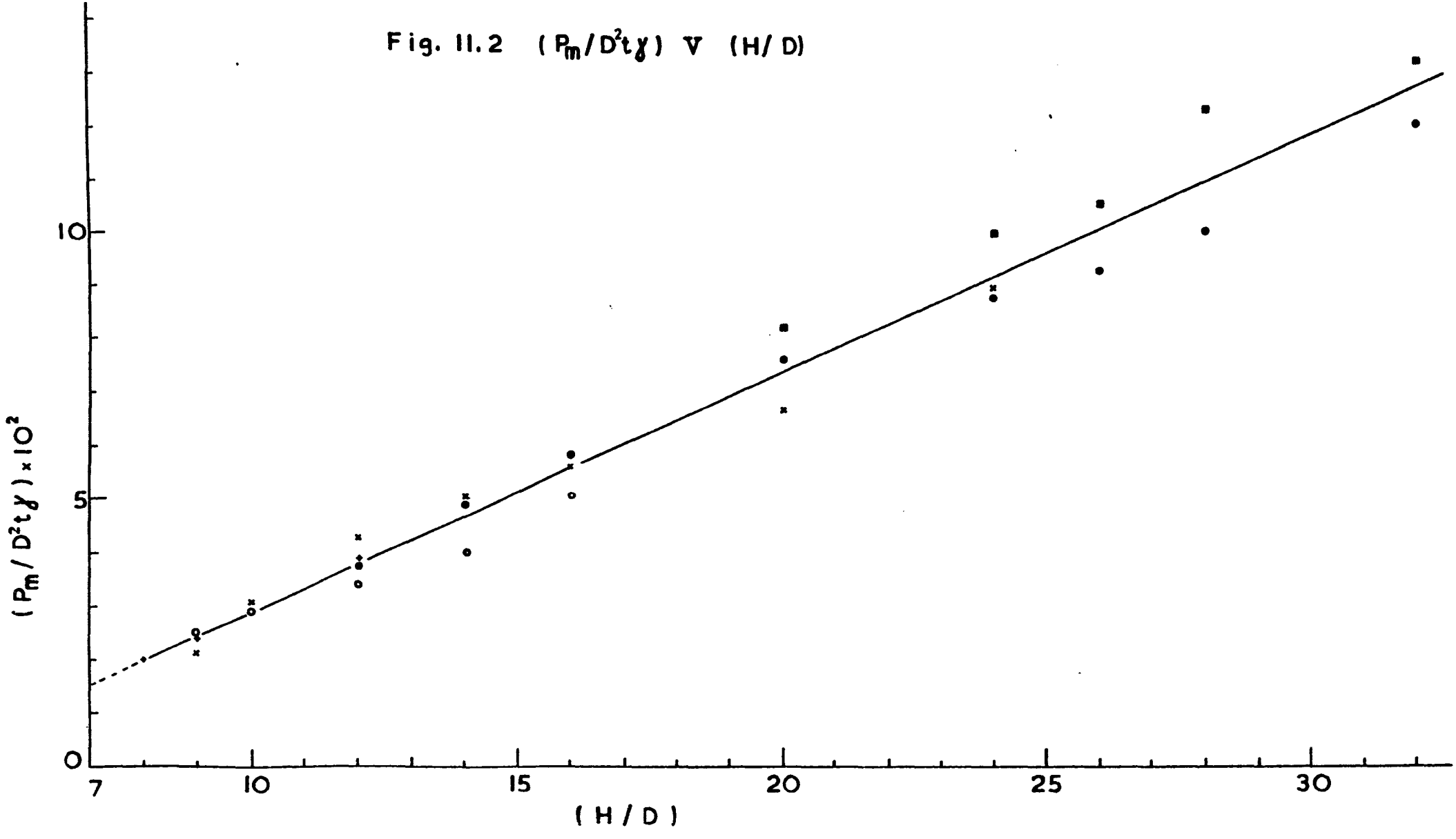
Fig. 11.2 ($P_m/D^2t\gamma$) V (H/D)
$(P_m/D^2t\gamma)\times10^2$
0
5
10
7
10
15
20
25
30
(H/D)

A computer program was written (see Appendix L), and the ultimate loads of the different anchor plates at various $\frac{H}{D}$ ratios were calculated.

11.5 Results

The predicted ultimate loads together with the experimental ultimate loads of this thesis are plotted against $\frac{H}{D}$, see Fig. 11.3. From the figure the following points are observed:-

(a) For the 51mm and 38mm diameters of the anchor plates, the Meyerhof - Adam theory gives a higher ultimate load, for any $\frac{H}{D}$, than the other theories.

(b) For the 25mm,19mm and 13mm diameters of the anchor plates, the Baker - Kondner theory gives the largest ultimate load for any $\frac{H}{D}$, with Vesic's theory giving the smallest ultimate load.

(c) Vesic's theory gives the ultimate loads of the 51mm and 31mm diameters of the anchor plates, to be approximately equal to the ultimate loads of the 19mm and 13mm plate diameters obtained by using the Baker - Kondner theory, respectively.

(d) The modified method of Baker and Kondner gives a good correlation with the experimental results. This should be expected since the constants of the ultimate load equation were found from the experimental results themselves.

11.6 Finite element method

The computer program was used to predict the load-displace-

Fig. II.3 ULTIMATE LOAD V (H/D)

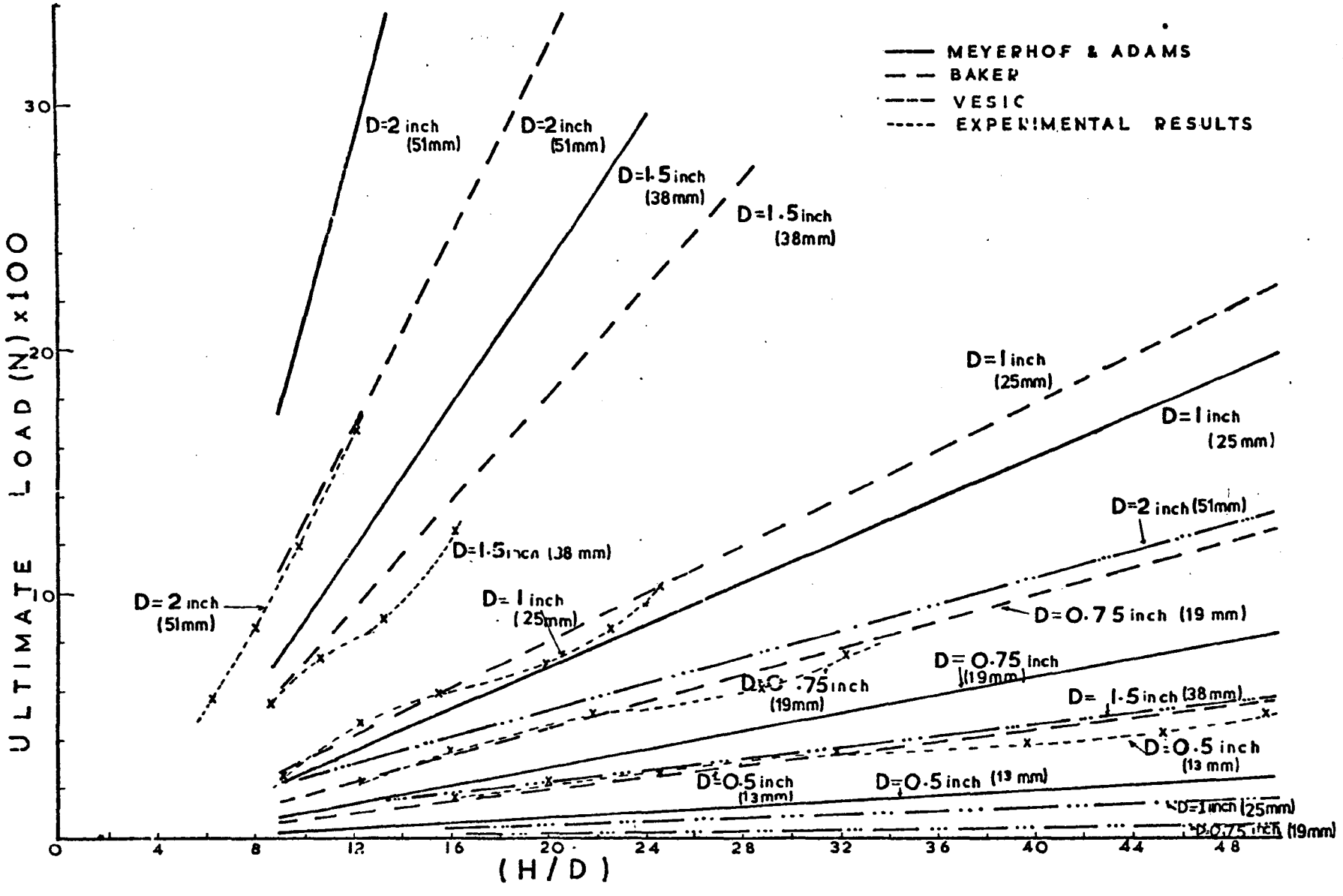

ment curves obained by Baker and Kondner in their field tests. The following soil properties were used in the computations:-

(a) $\phi = 37^{o}$

(b) $\gamma = 112\ lb/ft^3 = 1.79\ gr/cm^3$

Two anchors were tested by Baker and Kondner, and had the following parameters:-

(a) Diameter of shaft = 5 in. = 127mm

(b) Diameters of plates and depths.

(i) D = 12 in. = 305mm H = 64 in. = 1626mm

(ii) D = 16 in. = 406mm H = 137 in. = 3480mm

(c) Assumed plate thickness

(i) t = 270mm

(ii) t = 570mm

The predicted load-displacement curves, together with those obtained by Baker and Kondner during their field tests, are shown in Fig. 11.4.

Fig. 11.4 (a) shows the predicted and experimental load-displacement curves of the 305mm (12 in.) diameter anchor plate, embedded at 163cm in the sand described above. The figure shows that both predicted loads, i.e. with $E = 10^6\ N/m^2$ and $E = 10^7\ N/m^2$, are obtained at greater

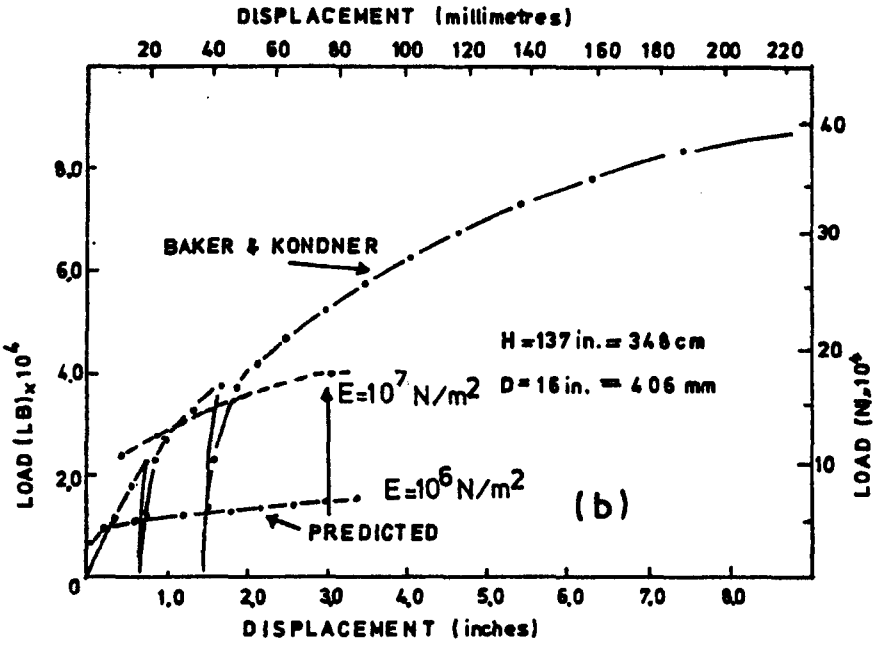
DISPLACEMENT (millimetres)
20 40 60 80 100 120 140 160 180 200 220
BAKER & KONDNER
H=137 in. = 348 cm
D=16 in. = 406 mm
E=10^7 N/m^2
E=10^6 N/m^2
PREDICTED
(b)
LOAD (LB)x10^4
LOAD (N)x10^4
DISPLACEMENT (inches)
1.0 2.0 3.0 4.0 5.0 6.0 7.0 8.0

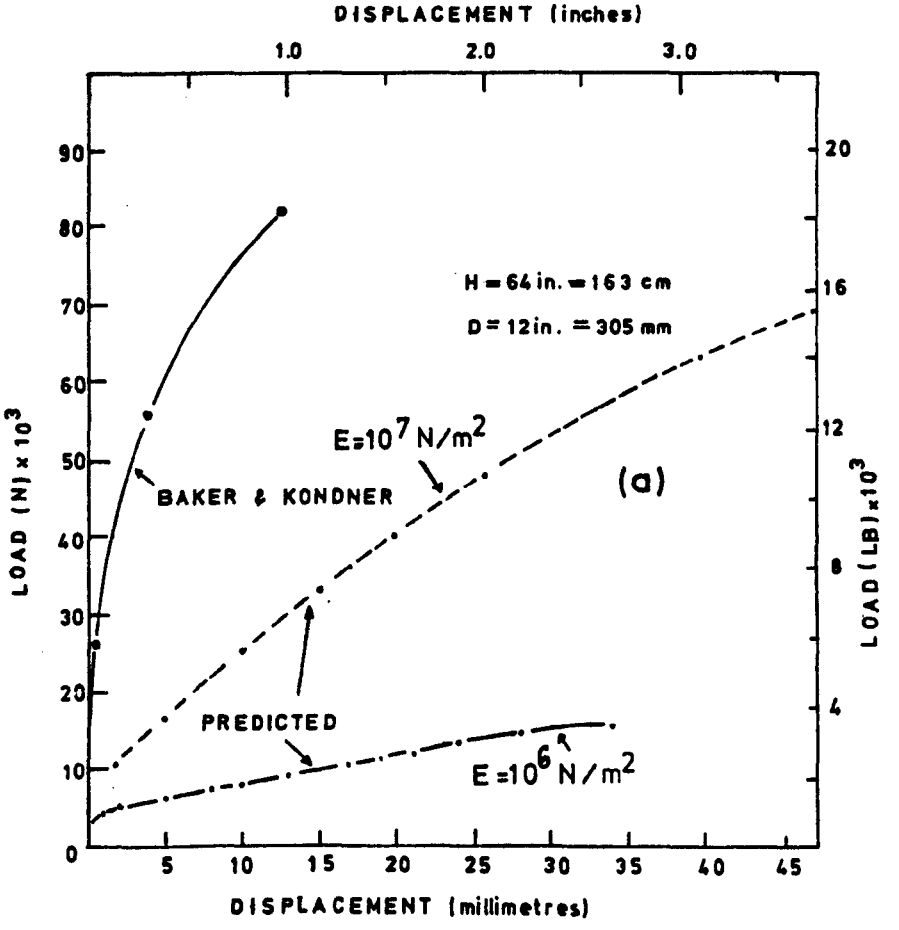
DISPLACEMENT (inches)
1.0 2.0 3.0
H=64 in. = 163 cm
D=12 in. = 305 mm
E=10^7 N/m^2
BAKER & KONDNER
(a)
PREDICTED
E=10^6 N/m^2
LOAD (N) x 10^3
LOAD (LB)x10^3
DISPLACEMENT (millimetres)
5 10 15 20 25 30 35 40 45

Fig. II.4

absolute displacements than the field test ultimate load. The ultimate load calculated using $E = 10^7$ N/m^2, agrees well with the load obtained by Baker and Kondner.

Fig. 11.4 (b) shows the load-displacement curves of the 406mm (16 in.) diameter anchor plate embedded at 348cm (137 in.). The predicted loads are now obtained at smaller absolute displacements than the field test ultimate load. The value of the ultimate load obtained in the field tests is about twice the calculated value with $E = 10^7$ N/m^2.

Baker and Kondner found that the ultimate load of the shallow anchor (D = 305mm, H = 163cm) was higher than the values predicted by their equation, and Balla's theory. They also stated that since the thickness, t, of the field anchor was indeterminate, a direct comparison between the ultimate load of the deep anchor and that predicted by their equation was not justified. In the finite element method the value of t and also the values of the constants in the stress-strain relationship were assumed.

CHAPTER XII

CONCLUSIONS AND SUGGESTIONS

12.1 Summary of conclusions

This thesis has been concerned with a single vertical anchor embedded in dry sand, with particular reference to the influence of such factors as the initial state of the sample and the load-displacement behaviour. From the experimental and theoretical work, a summary of the main conclusions is as follows:-

(1) The initial state of the sample was defined by determining the distribution of density and coefficient of earth pressure at rest. The use of the load-displacement curve, together with the above parameters showed that the repeatability of the sample after 45 minutes of vibration, although reasonable for any time of vibration, was well within the experimental error defined in this research.

(2) Experimental investigation showed that the load-displacement behaviour of the anchor is affected by the method of placing. The "fixed" anchor obtains a larger ultimate load than the "free" anchor, at a smaller absolute displacement.

(3) The load-displacement behaviour of the anchor is not affected by the variation of the constant rate of strain between 0.5mm/min and 29mm/min, but the withdrawal of the anchor at greater constant rates requires further investigation.

(4) In the case of the boundary conditions, the investigation showed that the load-displacement behaviour of the anchor is affected to a rather more significant degree than that so far suggested by previous workers. It is

thought that a general trend could not be obtained, mainly due to the effect of wall friction varying with the distance of the boundaries from the shaft. In some cases, it was found that the anchor behaves as "shallow" although the relative depth was greater than the critical depth.

(5) The diameter of the shaft in any calculations, can be ignored when the ratio of the anchor plate diameter to the anchor shaft diameter is equal to, or greater than four. But if the thickness of the plate is large, a substantial frictional force would be introduced.

(6) Similarly, the entire behaviour of the anchor is affected by the thickness of the plate, when a ratio of anchor plate thickness to anchor plate diameter less than three is employed. For small ratios, a "modulated" load-displacement curve is recorded. As the ratio increases, the ultimate load and the displacement at which this occurs increase.

(7) Both pressure gauges used in this investigation were found to function reasonably well for the measurement of horizontal stresses. The coefficient of earth pressure at rest varies with the density of the sample and also the depth of embedment of the gauge. The values of K_o obtained throughout the investigation, showed that the method of vibration used in this research does not produce an overconsolidated sample, a fact suggested by other researchers.

(8) The load-displacement behaviour of the anchor was found to depend on: the initial state of the sample, the depth and diameter of the anchor plate, as well as the parameters mentioned previously. The following points are clear:-

(i) The rate of change of the load with the displacement, prior to the ultimate load, increases with the depth and density of the sample increasing; but during the post-peak part of the load-displacement curve, the decrease in the rate of change decreases with the depth increasing and density decreasing.

(ii) The relationship between ultimate load and depth, showed that the load increases with the anchor depth, and also the rate of change increases with the anchor plate diameter.

(iii) Similarly, the relationship between ultimate load and the anchor plate diameter, although linear for depths between 30cm and 40cm, shows a non-linear relationship at greater depths, with its rate of change increasing with depth.

(iv) The ultimate load increases with the relative depth, and the rate of change of the relationship increases with the anchor plate diameter, and also with the density of the sample.

(v) The average maximum pressure on the anchor plate decreases with the diameter of the plate increasing, for any depth investigated, and obtains a constant value at about D = 51mm.

(vi) Although the breakout factor is known to increase with the relative depth in shallow anchors, it was found that as regards deep anchors, for each plate diameter this tended to oscillate about a certain value. For any relative depth the breakout factor

decreases with the anchor plate diameter increasing but for D $\geqslant$ 38mm the breakout factor is independent of the relative depth investigated in this work. For plates with D $\geqslant$ 51mm the breakout was found to be about 76 when the anchor plates were embedded at $\frac{H}{D} \geqslant 10$.

(vii) The anchor displacement to ultimate load increases linearly with the relative depth for each anchor plate diameter, but the rate of change of the relationship is independent of the diameter of the plate.

(9) The theoretical investigation showed that the behaviour of the anchor can be investigated using the finite element method. The various parameters affecting the load-displacement behaviour of the anchor were examined. Although the predicted values may not agree well, with the experimental ones, due to the various assumptions made i.e. G and failure criteria, it is considered that the general trends show agreement The following information was obtained:-

(i) The linear analysis can be used to predict the elastic part of the load-displacement curve, provided sensible values of E and ν are used. The rate of change of the load with the displacement increases with both these parameters increasing, i.e. ν and E.

(ii) The non-linear analysis shows substantial agreement with the experimental load-displacement behaviour of the anchor. The post-peak part

of the curve cannot be predicted unless a different method of applying the displacement is used, i.e. iterative method.

(iii) The investigation into the distribution of the load on the anchor plate, showed that the method of applying load in order to predict the displacement may not be accurate. The distribution of the incremental load is not uniform, and varies not only with the size of the incremental displacement but also from increment to increment. The method used in this research, i.e. applying increments of displacement in order to predict the load, seems to be a suitable approach.

(iv) The distribution of the stress on the anchor plate was found to be non-uniform.

(v) The anchor plate thickness and shaft diameter affect the ultimate load of the anchor. The effect of the boundaries on the behaviour of the anchor may be calculated, provided enough elements are used in the sample.

(vi) The displacement zones agree well with experimental ones near the anchor plate, but displacements are also predicted well outside the measured experimental zone. This fact was also observed by McMullan who stated that a minimum (sensible) value of displacement must be used to record the contour of displacement/non-zero displacement.

(vii) The failure zones were also calculated, but their validity cannot be proved due to the lack of

experimental information. Their accuracy may be improved, if smaller elements are used or a triangular shape element is employed.

12.2 Suggestions for further work

Based on the literature survey carried out and the results of the experimental and theoretical investigations, it is considered that more work should be carried out in the following areas:-

(1) Effect of different types of loading in dry sand. Although, e.g. cyclic loading tests may not be of any practical use, their results could help in understanding the behaviour of an anchor in wet sand under the same type of loading.

(2) Stresses in the sample were calculated using the computer program . Experiments could be carried out using pressure gauges, in order to obtain the distribution of stresses while the load-displacement is recorded. A comparison between results would be useful for the theoretical work.

(3) Effect of boundaries on the load-displacement behaviour of the anchor could also be investigated using a pressure gauge. This could be embedded in the sample at different distances from the anchor shaft, and the pressure could be recorded while the anchor is being withdrawn.

(4) Effect of the bottom boundary on the load-displacement curve needs investigation, and this could be done by increasing the distance of the bottom end of the anchor plate from the bottom of the tank, whilst the depth of the anchor is kept

constant.

(5) Withdrawal of the anchor at greater constant rates of strain, than those used in this research, should be investigated to find their effect on the behaviour of the anchor.

(6) It was found, in this research, that the thickness of the plate affects the behaviour of the anchor. Different shapes of anchor footings should be investigated, e.g. a cone fitted to a plate, and varying the thickness of the plate.

(7) Little data is available on safety factors. A design procedure with sufficient safety factors, covering both displacement of foundation and working loads, needs to be established.

(8) Although the finite element method has been shown to be a powerful method in predicting and understanding the behaviour of the anchor, the stress-strain relationship and failure criteria of the soil are their main drawbacks. Considerable work on the stress-strain behaviour of the soil needs to be done. A stress-strain relationship, valid not only in the principal directions, but in any direction has to be developed. Having achieved this, the behaviour of elements during the pullout of the anchor needs to be investigated.

APPENDICES

APPENDIX A

REVIEW OF THEORETICAL WORK

Mors (1959, Ref. 27) considered both the earth weight method and the friction cylinder method, Fig. A.1.

In his earth weight method, Mors modified his original failure surface and neglected the shearing resistance along it. He obtained the equation:-

$$P_m = W = W_2 + W_3$$

Where

$$W_3 = \frac{\pi \gamma H}{6} \left(4R_2^2 + \frac{R_2 D}{2} - \frac{5D^2}{4}\right)$$

$$W_2 = \frac{\pi \gamma D^2 H}{4}$$

Where

R_2 = radius of the failure circle at ground level.

In his friction cylinder method, Mors introduced the passive earth pressure of the soil outside the failure surface. He obtained the following ultimate load equation:-

$$P_m = \pi \gamma DH \left(\frac{D}{4} + \frac{H}{1 + \mathfrak{I}} K_p \tan\phi\right)$$

Where

K_p = the coefficient of passive earth pressure

$\mathfrak{I}$ = function of K_p

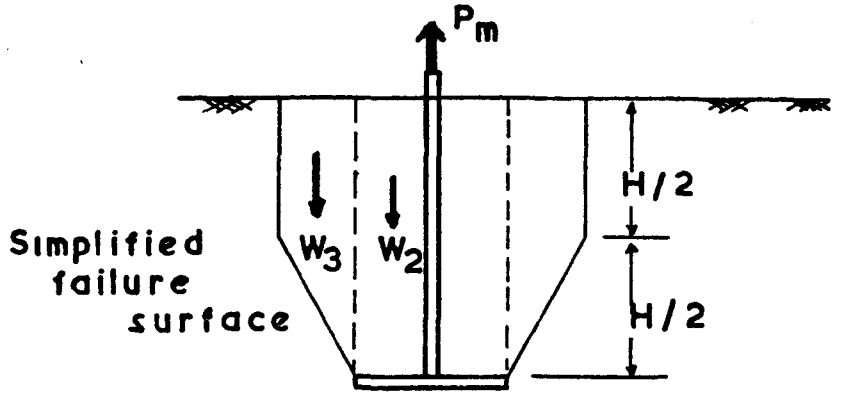

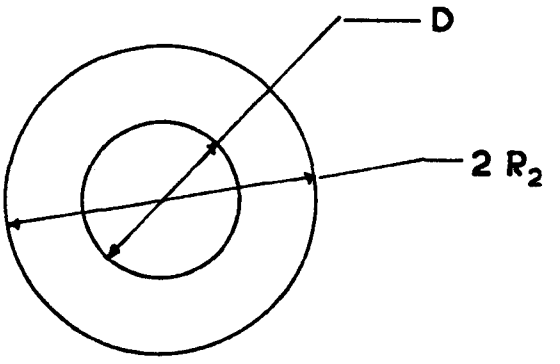

Earth weight

method

(a)

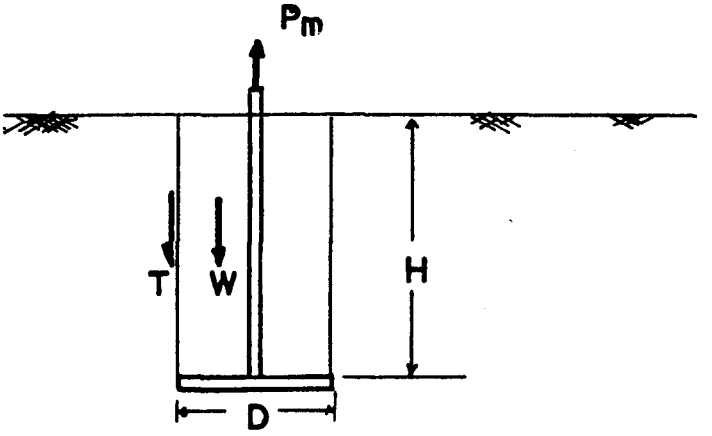

Friction cylinder

method

(b)

Mors' methods

Fig. A.1

Matsuo's (1967, Ref. 28) analysis resembles that of Balla's. He also used Kotter's equation to calculate the total shearing resistance along his three dimensional failure surface, composed of a logarithmic spiral and straight line, Fig. A.2. He gave the ultimate load equation to be:-

$$P_m = W + \gamma (D_2^3 K_3 - V_3) + C_u D_2^2 K_4$$

Where

$$K_3 = \pi \left[(a - 1) (a^2 F_1 + a F_2 + a b F_3 + b F_4 + F_5) + b\right]$$

$$K_4 = \pi \left[(a - 1) (a F_6 + F_7) + b (b \tan \quad + 2)\right]$$

$$a = \frac{X_o}{D_2}, \qquad b = \frac{H_2}{D_2}$$

V_3 = Volume of anchor

F_i = Functions of and where i = 1, 2, 3, ...7

D_2 , a, b, = Found by trial and error

Howat (1969) used both Balla's method and his own failure surface to obtain an equation for the ultimate load. He considered, his failure surface could be approximated by a straight line instead of a curvilinear section, and produced the following ultimate load equation:-

$$P_m = \gamma H^3 \left(F + \frac{C_u F_c}{\gamma H} + F_s\right)$$

Where

F, F_c and F_s = coefficient given in the ranges $\frac{H}{D}$ = 1 to 25 and ϕ = 20^o to 40^o

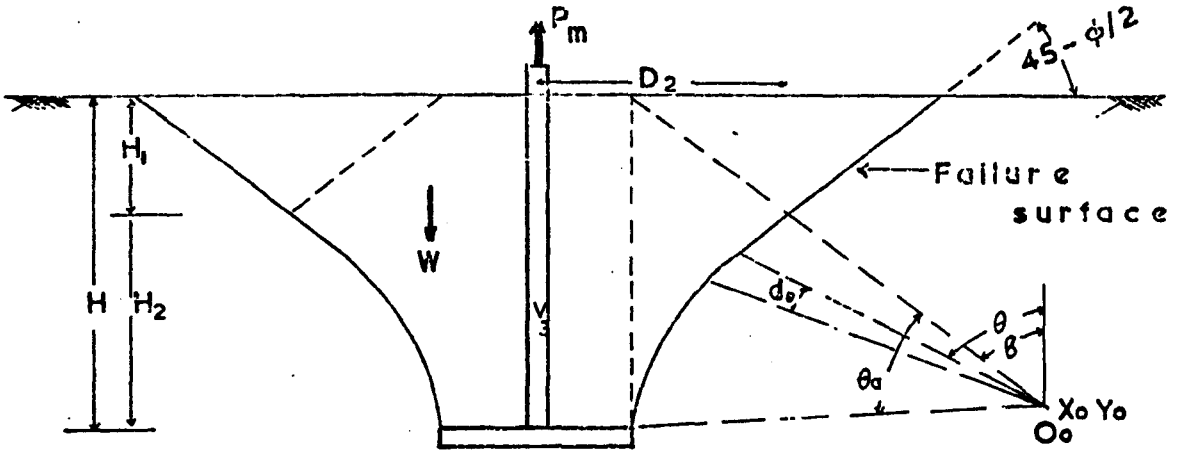

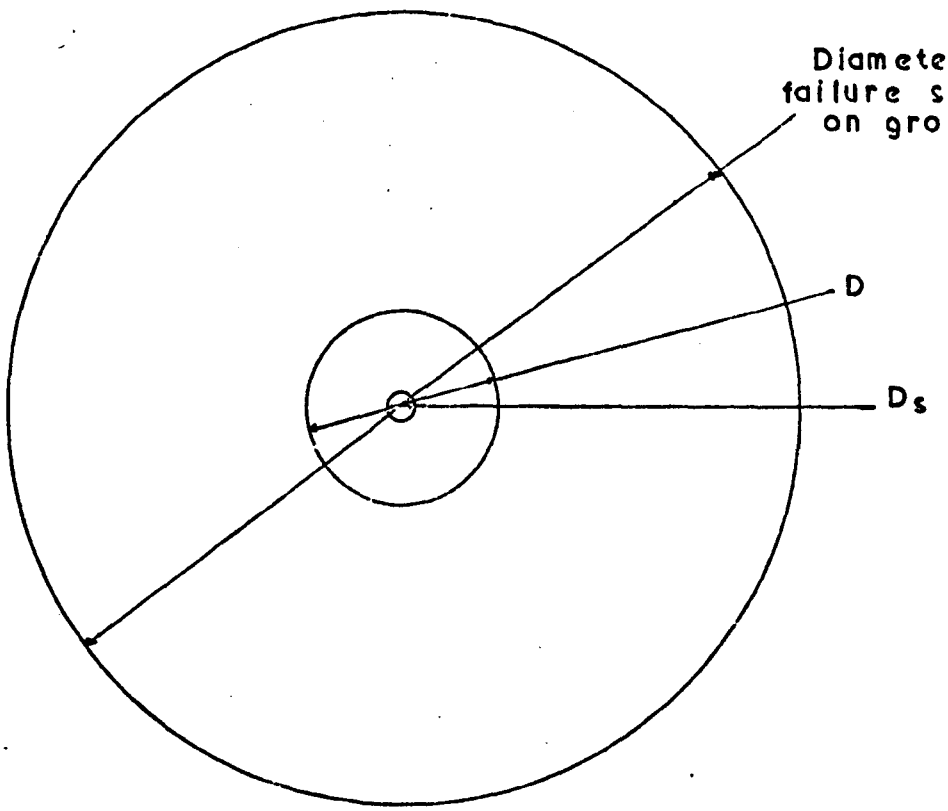

Matsuo's method

Fig. A.2

Mariupol'skii (1965) assumed his failure surface to have the shape shown in Fig. A.3 (a). He based his theory on the two following factors:-

(a) The force acts against gravity.

(b) The soil cannot take tension.

Mariupol'skii gave the ultimate load equation to be:-

$$P_m = W + W_1 + \gamma V + Q$$

Where

V = The volume between failure surface and the cylinder, formed with the anchor plate as its base.

Q = The total cohesive force on the failure surface.

To calculate V and Q, he considered a cylindrical ring of radius r, height z' and thickness dr. He then considered the outer portion of volume V' and obtained the equation:-

$$\gamma V' + Q' = 2 r z' (c + \psi)$$

Where

$2 \pi z' c$ = Vertical cohesion component acting on the ring.

$2 \pi z' \psi$ = Vertical friction component acting on the ring.

Q' = Total cohesive force acting along the lower boundary of volume V'.

c = Specific shear resistance of soil due to cohesion.

ψ = Reduced specific friction resistance in the given cross section of height z' equal to:-

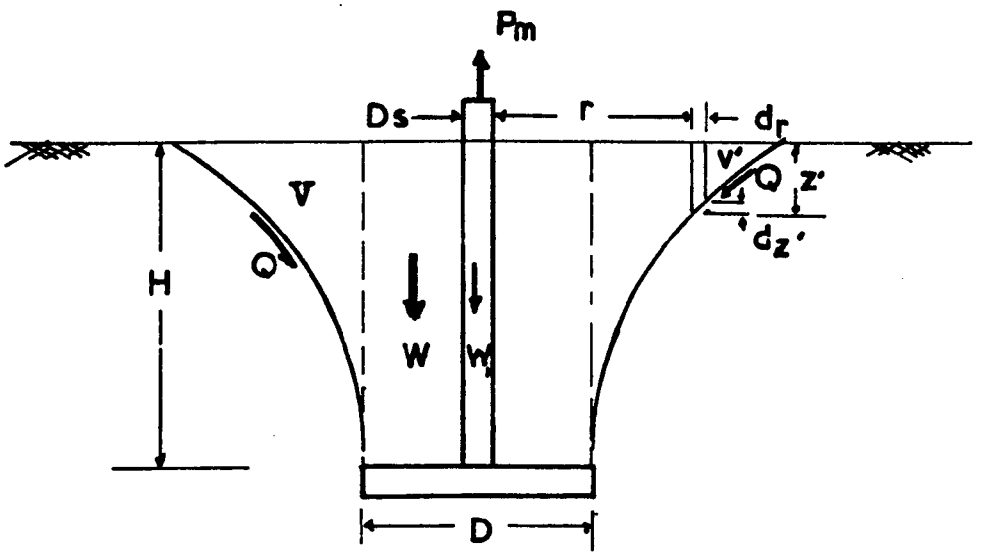

Mariupol'skii's method
(a)

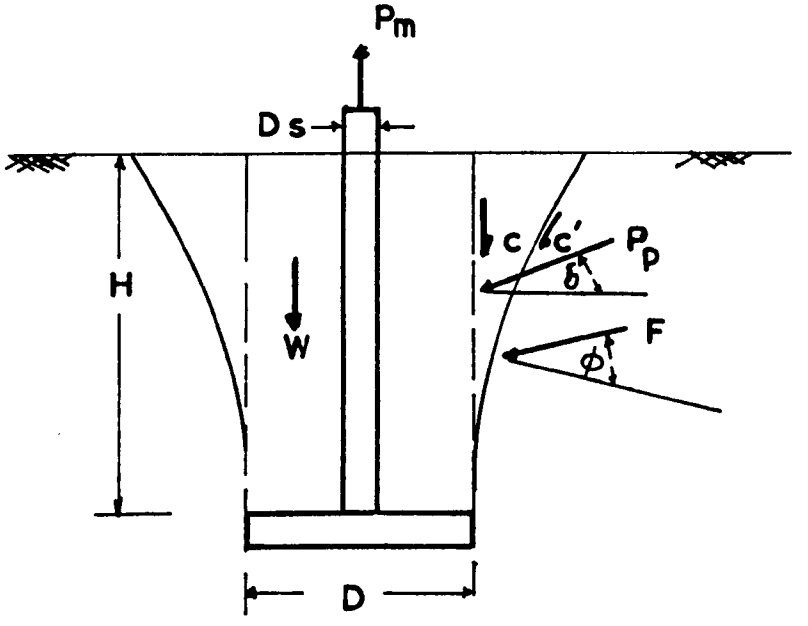

Meyerhof & Adams
theory
(b)

Fig. A.3

$$\psi = \frac{\tan\phi \int_0^{z'} b\, r\, (r, z)\, d\, z}{z'}$$

Where

σ_r = the radial stress at radius r.

In order to calculate σ_r , Mariupol'skii used the following expression without explanation.

$$\sigma_r = \frac{p'}{\tan^2\phi} \cdot \frac{R}{r} \cdot e^{-m(r-R)} \cdot \left(\frac{e^{\left(\frac{mz}{\tan\phi}\right)} - e^{\left(-\frac{mz}{\tan\phi}\right)}}{e^{\left(\frac{mn}{\tan\phi}\right)} - e^{\left(-\frac{mn}{\tan\phi}\right)} - 2} \right)$$

Where

m = constant of integration, express in terms of $\frac{1}{n\,H}$

n = dimensionless function of ϕ

$R = \frac{D}{2}$

p' = average pressure on soil resting against the anchor plate.

Combining his expressions and using his experimental results Mariupol'skii obtained the following equation for the ultimate load of an anchor.

$$P_m = W_1 + \frac{\pi}{4}(D^2 - D_s^2) \quad \frac{\gamma H \left[1 - \left(\frac{D_s}{D}\right)^2 + 2\,K\,\frac{H}{D}\tan\phi\right] + 4\,\frac{c\,H}{D}}{1 - \left(\frac{D_s}{D}\right)^2 - \frac{2\,n\,H}{D}}$$

Where

K = coefficient of lateral pressure

Meyerhof and Adams (1968) by making use of the tests performed by other researchers, developed a general theory for the ultimate load of a shallow anchor. Their assumed failure

surface. shown in Fig. A.3 (b), has approximately the shape of a truncated pyramid. They simplified the problem, due to the difficulty in obtaining the stresses on the failure surface, by replacing the frictional and cohesive components acting on the failure surface with the cohesion and passive earth pressure acting on an assumed vertical failure surface, passing through the edge of the anchor plate. They produced the following equation for the ultimate load:-

$$P_m = 2C + 2P_p \sin\delta + W$$

Where

$C = c_u H$

P_p = total passive earth force

δ = angle of inclination of P_p to the horizontal.

Expressing

$$P_p = \frac{\gamma H^2 K_p}{2 \cos\delta}$$

they obtained the following equation:-

$$P_m = 2c_u H + \gamma H^2 K_p \tan\delta + W$$

Assuming $\delta = \frac{2\phi}{3}$, Meyerhof and Adams plotted $K_p \tan\delta$ against ϕ and found that $K_p \tan\delta$ increased rapidly. By replacing $K_p \tan\delta$ by $K_u \tan\phi$, the equation of the ultimate load became:-

$$P_m = 2c_u H + \gamma H^2 K_u \tan\phi + W$$

The value of K_u was found to be relatively constant for a

wide range of ϕ , and for sand this can be taken to have the value of 0.95.

Trofimenkov and Mariupol'skii(1965) proposed an empirical bearing capacity type formula for calculating the ultimate load of anchor. The equation was expressed as

$$P_m = A_1 \; c_u + A_2 \; \gamma \; H$$

Where

A_1, A_2 = dimensionless coefficients, functions of ϕ

$$A_2 = A_1 \cos\phi + 1$$

From their experimental results, they were able to obtain values for A_1 and A_2, for $\phi = 10^{\circ}$ to $\phi = 40^{\circ}$.

APPENDIX B

SHEAR BOX TEST

Shear box tests were carried out on different states of sand, i.e. loose and dense. The loose sand was obtained by pouring the soil through a funnel and keeping the funnel as low as possible. For the dense sand, a sieve vibrator was used to control the density. Two times of vibration were used, i.e. 2 min. and 5 min.

Fig. B.1 shows the shear stress plotted against the horizontal displacement with a 14.37 Kg. normal load for loose, 2 min. and 5 min. vibration times. Fig. B.2 and Fig. B. 3 also show the same curves with normal loads of 24.37 Kg. and 34.37 Kg. respectively.

The maximum shear stress obtained from each shear stress-displacement curve, was plotted against the vertical stress, Fig. B.4(a). The three straight lines gave the angle of internal friction for the loose sand, 2 min. and 5 min. of vibration to be 31.8^{o}, 40.2^{o} and 45.0^{o} respectively.

To correct the above values of ϕ for dilatancy, the vertical displacement was plotted against the horizontal displacement, Fig. B.5. The slope of the curves, $\frac{dy}{dx}$, at which the maximum shear occurred, Fig. B.1, Fig. B.2 and Fig. B.3 were recorded. These were used to obtain the following expression:-

$$\tau_p - \frac{dy}{dx} \times \text{normal stress}.$$

which was plotted against the normal stress, Fig. B.4 (b). The true angle of internal friction, given by this graph, is about 43.2^{o}.

The correction for the loose sand is negligible and that for the 2 min. vibration would be about 1^{o} since that for the

5 min. was about 1.8^{o}.

Table B.1 gives the density for different states of sand. The values for 5 min. and 10 min. of vibration indicate that the increase in the density is very small i.e. 0.6%.

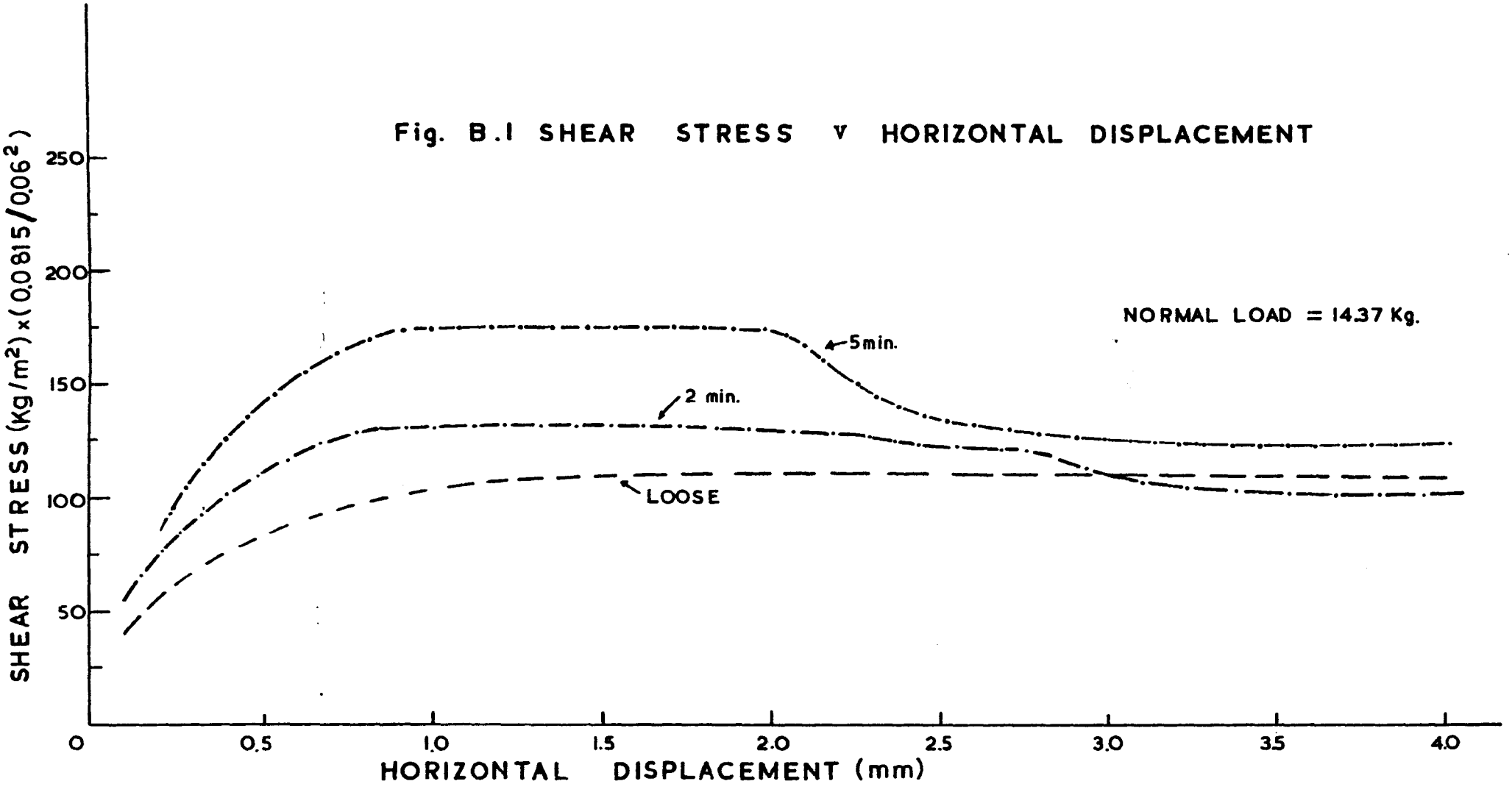
Fig. B.I SHEAR STRESS v HORIZONTAL DISPLACEMENT
SHEAR STRESS (Kg/m²) x (0.0815/0.06²)
250
200
150
100
50
0
0.5
1.0
1.5
2.0
2.5
3.0
3.5
4.0
HORIZONTAL DISPLACEMENT (mm)
NORMAL LOAD = 14.37 Kg.
5min.
2 min.
LOOSE

Fig. B.2 SHEAR STRESS v HORIZONTAL DISPLACEMENT

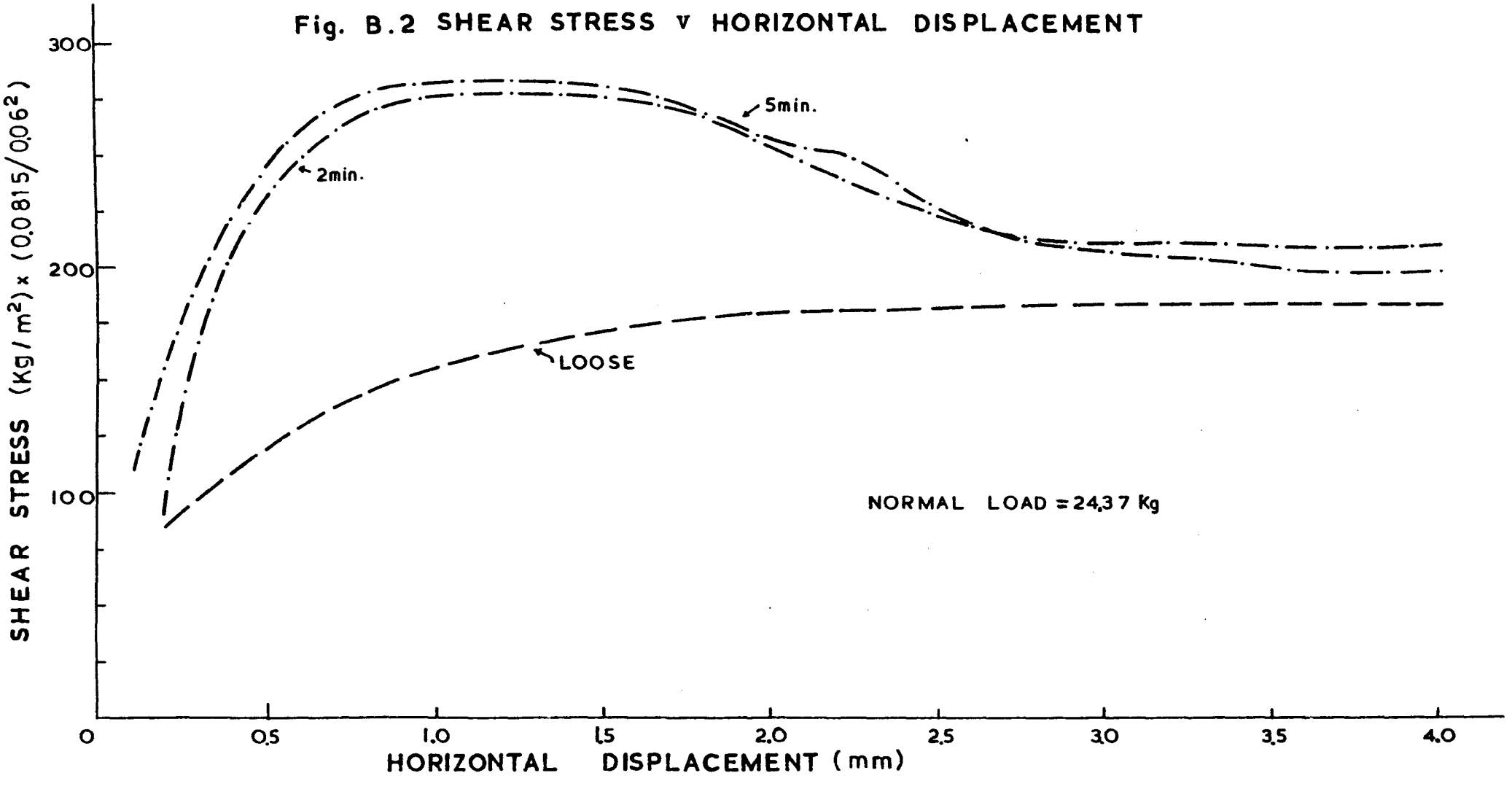

Fig.B.3 SHEAR STRESS v HORIZONTAL DISPLACEMENT

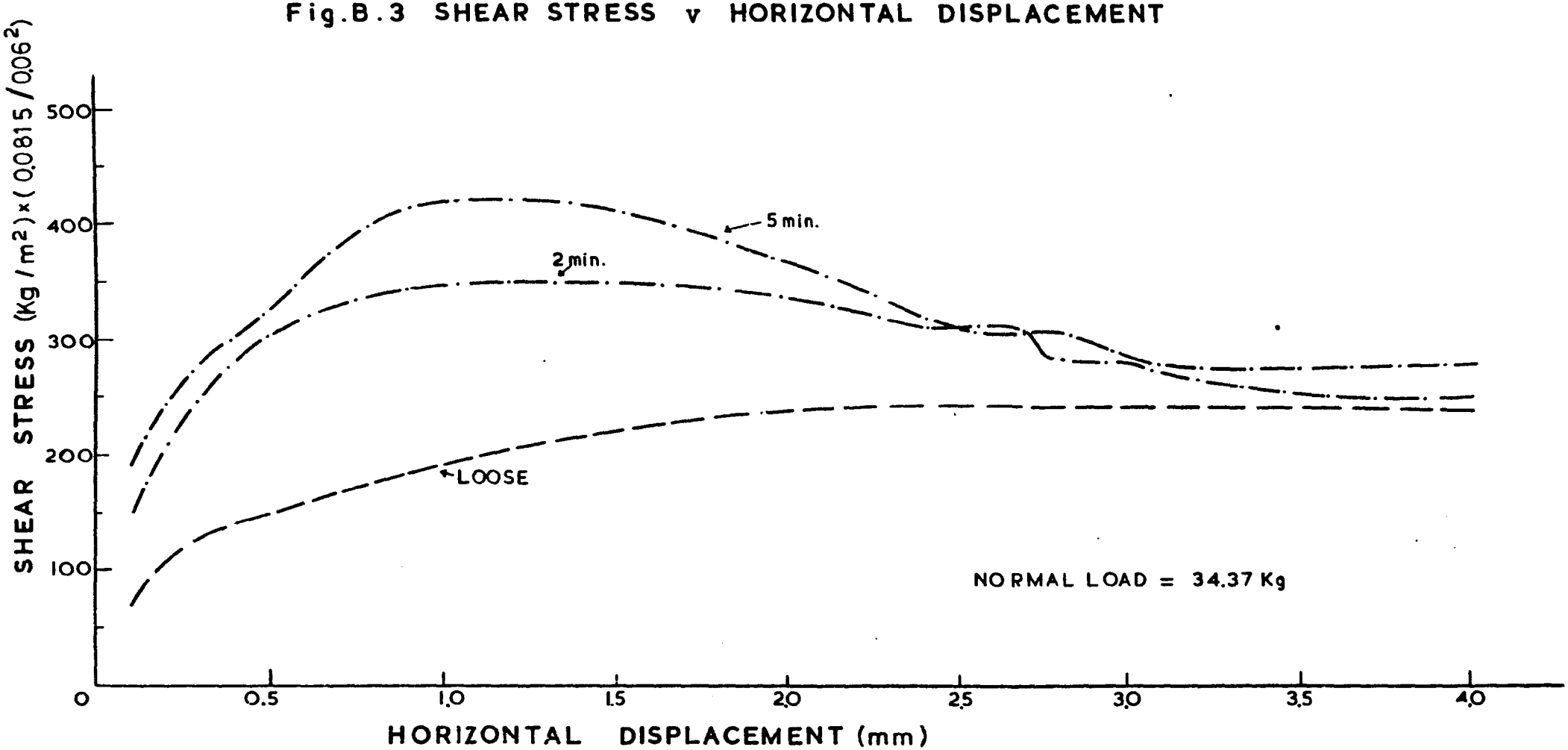

Fig. B.4 SHEAR STRESS v NORMAL STRESS

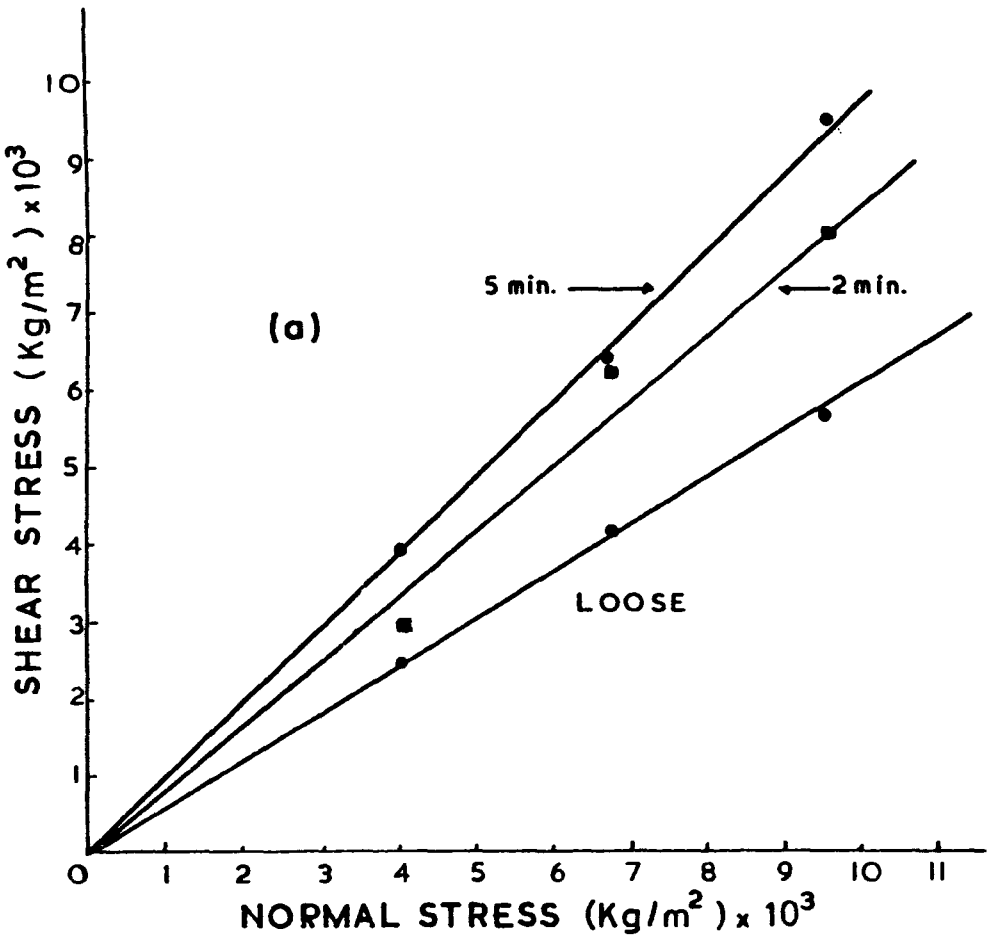

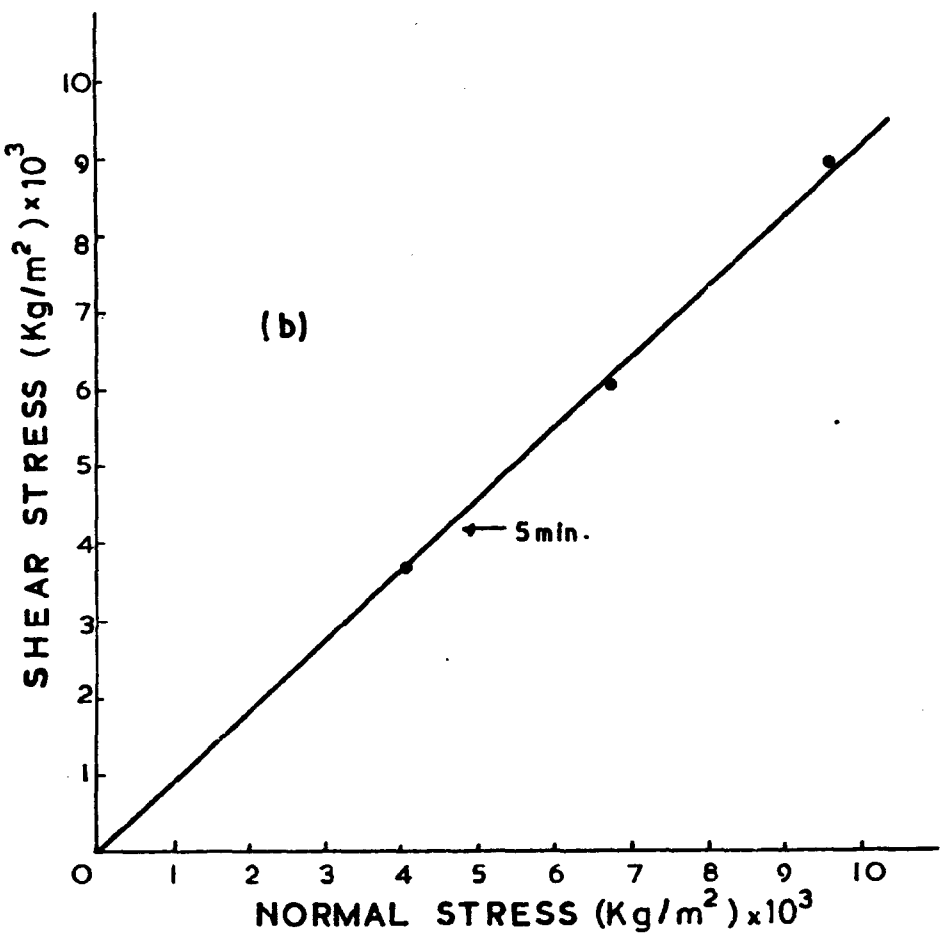

Fig. B.5 HORIZONTAL DISP. v VERTICAL DISP.

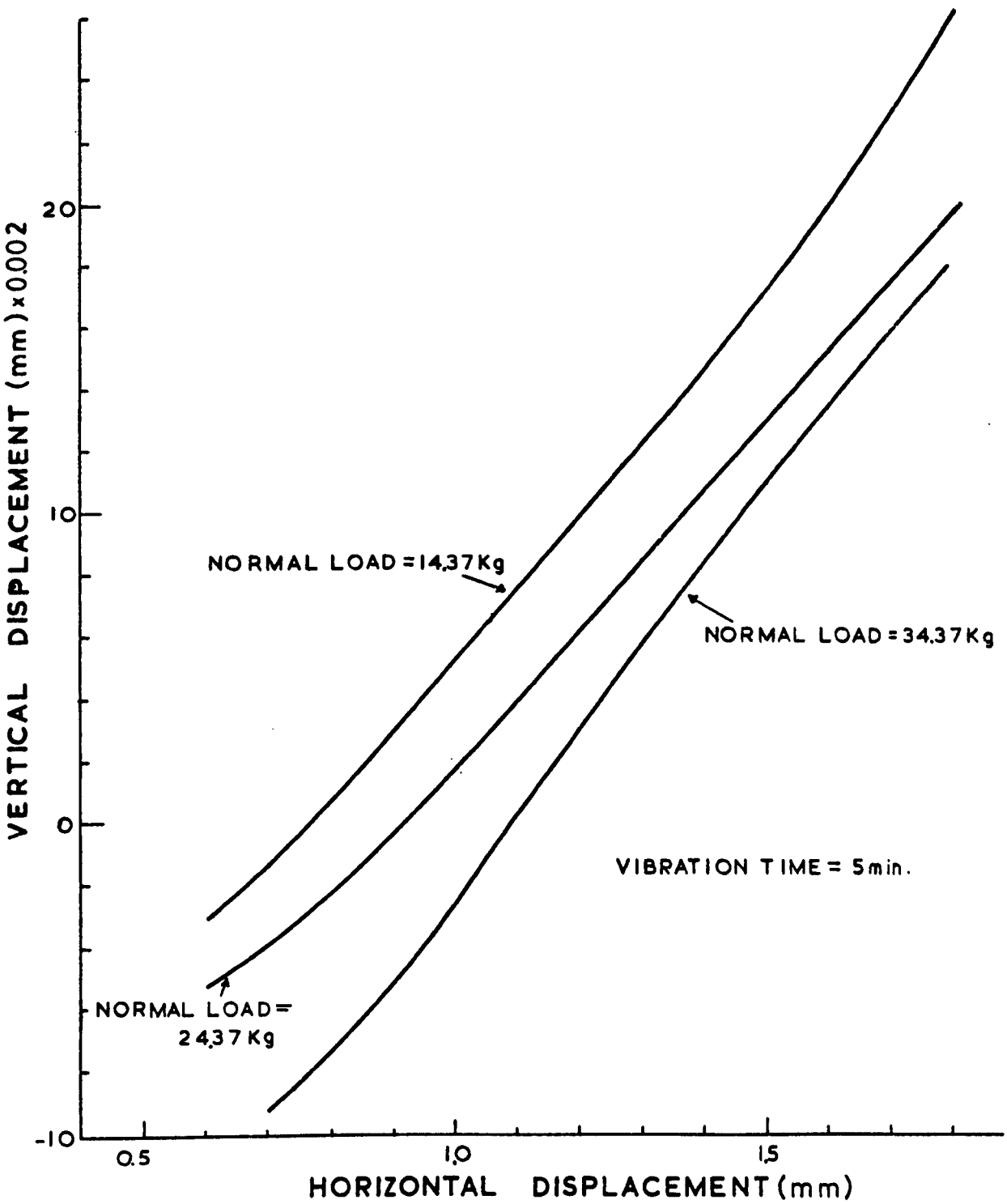

TABLE B.1

DENSITY VARIATION

TIME OF VIBRATION (min)	WEIGHT OF SAMPLE (gr)	DENSITY (gr/cm^3)
Loose	174	1.566
2	186	1.674
5	189	1.701
10	190	1.710

APPENDIX C

VIBRATION FORMULAE

From Simple Harmonic Motion

$$T = \frac{2\pi}{\omega} \qquad (1)$$

$$T = \frac{1}{f} \qquad (2)$$

$$V_m = \omega a \qquad (3)$$

$$A_m = \omega^2 a \qquad (4)$$

Where:-

f = Frequency

ω = Angular velocity

T = Period

a = Amplitude

A_m = Maximum acceleration

V_m = Maximum velocity

Equations (1) and (2) are combined to give

$$\omega = 2\pi f \qquad (5)$$

Both sides of the equation (5) are multiplied by a to obtain:-

$$V_m = 2\pi a f \qquad (6)$$

Equation (4) becomes:-

$$A_m = \frac{V^2_m}{a} \qquad (7)$$

When ω is substituted by $\frac{V_m}{a}$

Equation (7) becomes:-

$$A_m = 2\pi f V_m \qquad (8)$$

When $\frac{V_m}{a}$ is substituted by $2\pi f$ from equation (6), equations, $V_m = 2\pi a f$ and $A_m = 2\pi f V_m$, relate the four parameters, i.e. f, a, V_m and A_m.

APPENDIX D

DETERMINATION OF COEFFICIENT OF EARTH PRESSURE AT REST

A constant power supply, 10 Volts output, was connected to the input terminals of the soil pressure cell (Type 0234, Active diameter = 36 mm, pressure range = 0 - 20 N cm^{-2}). The output terminals of the gauge were connected to the digital voltmeter (shown in Plate 8). The calibration was carried out by inserting the gauge in the glass tube, filled with water; and the two straight lines shown in Fig. D.1 were obtained. Horizontal and vertical readings at various depths of sand were recorded for 45 minutes vibration. The densities were calculated using the following equation:-

$$\omega_{sand} = \frac{H_{water} \times \omega_{water}}{H_{sand}}$$

Where:-

ω_{sand} = unit weight of sand.

ω_{water} = unit weight of water.

H_{sand} = height of sand above the gauge

H_{water} = (increase in the voltage) / slope of the calibration line.

$$H_{water} = \frac{\text{Increase in the voltage}}{(1\,mV/30\,cm)}$$

Table D.1 gives the readings and results obtained with the membrane of the gauge facing upwards.

Fig. D.1 Calibration of gauge

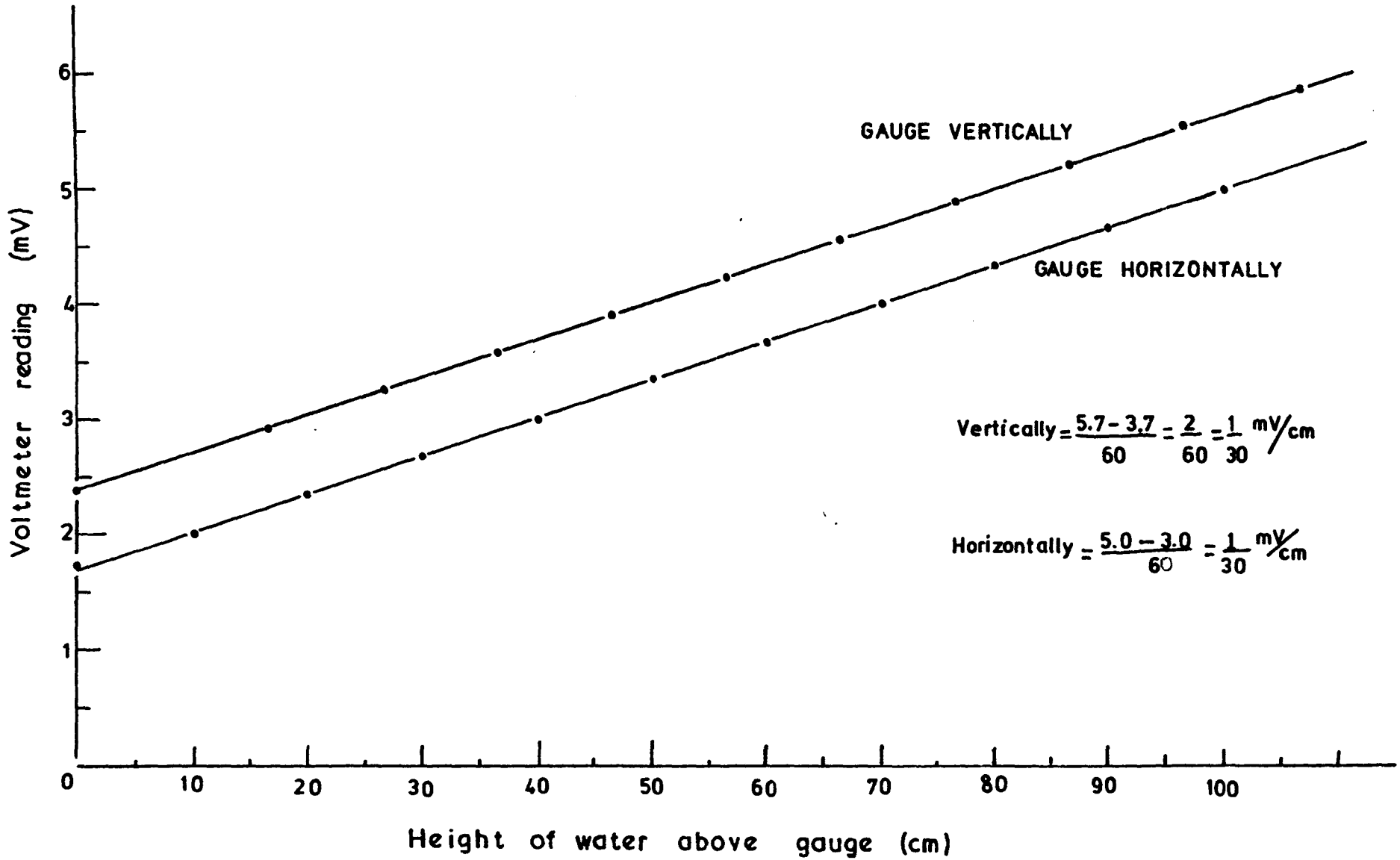

The coefficient of earth pressure at rest, K_o, (See Table D.2) was calculated from the following equation:-

$$K_o = \frac{\omega_{water} \times H_{water}}{\omega'_{sand} \times H_{sand}}$$

Where:-

ω'_{sand} are the values of the unit weight of sand obtained from the density tube.

Table D.1

H_{sand} (cm)	Increase in Voltage (mv)	H_{water} (cm)	Density (gr/cm^3)
34	0.90	27	0.79
46	0.50	15	0.33
56	0.40	12	0.21
71	0.83	59	0.36

Table D.2

H_{sand} (cm)	Increase in Voltage (mv)	H_{water} (cm)	K_o
31	1.30	39	0.74
42	0.80	24	0.34
56	0.50	15	0.16
70	0.60	18	0.153

APPENDIX E

LOAD-DISPLACEMENT CURVES

This appendix includes the load-displacement curves and the graphs of the ultimate load plotted against the relative depth, which have not been presented in Chapter 8.

Four different times of vibration were used for each anchor depth, 10, 20, 30 and 45 minutes. The anchor plate was embedded at four different depths at about 30, 40, 50 and 60 cm.

The following parameters were kept constant:-

(a) Rate of pull-out = 28 mm/min.

(b) Thickness of plate = 102 mm.

(c) Diameter of shaft for 38 mm and 51 mm diameter plate = 6 mm.

Diameter of shaft for 13 mm and 19 mm and 25 mm diameter plate = 5 mm.

Fig. E.1 Load v Displacement

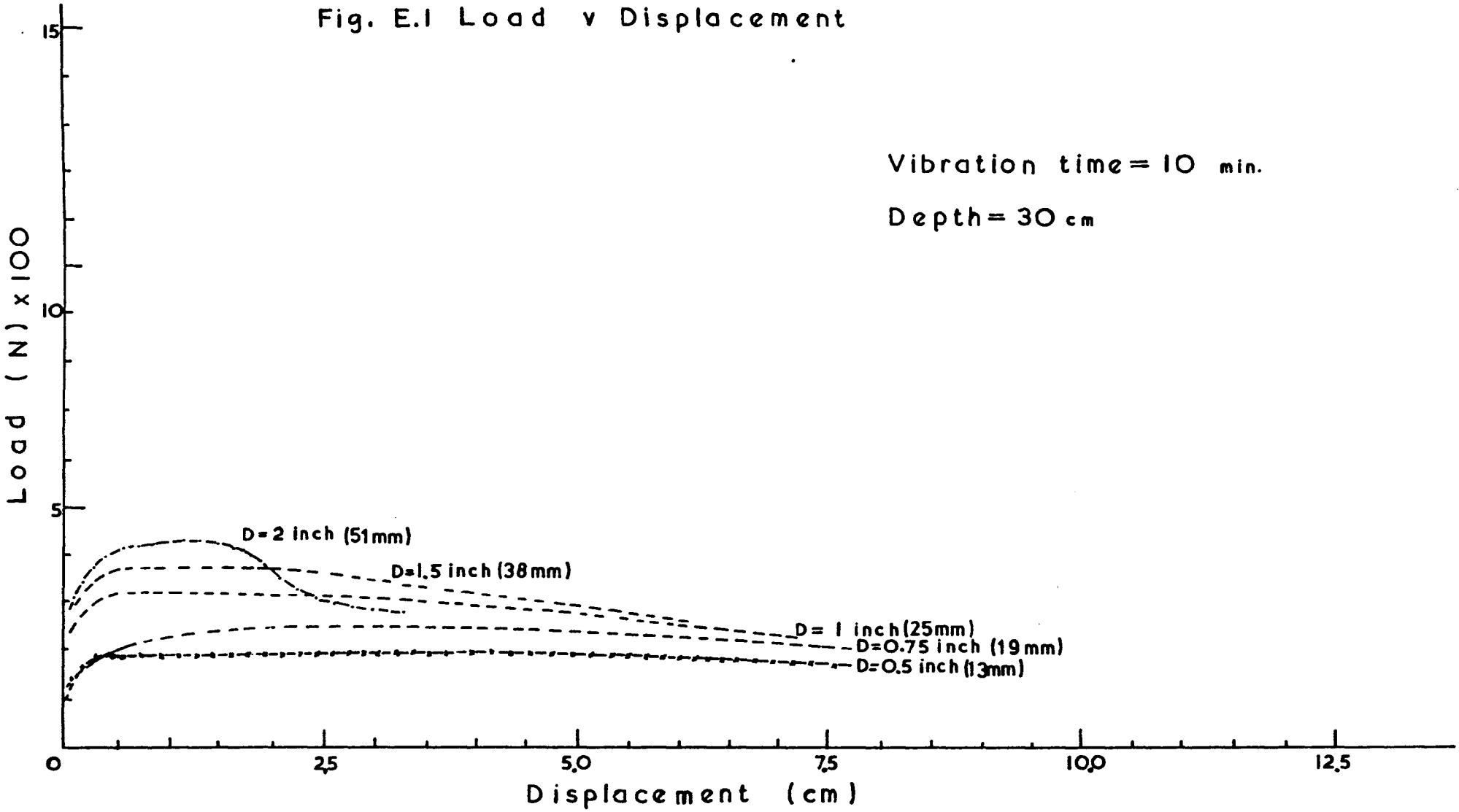

Fig. E.2 Load v Displacement

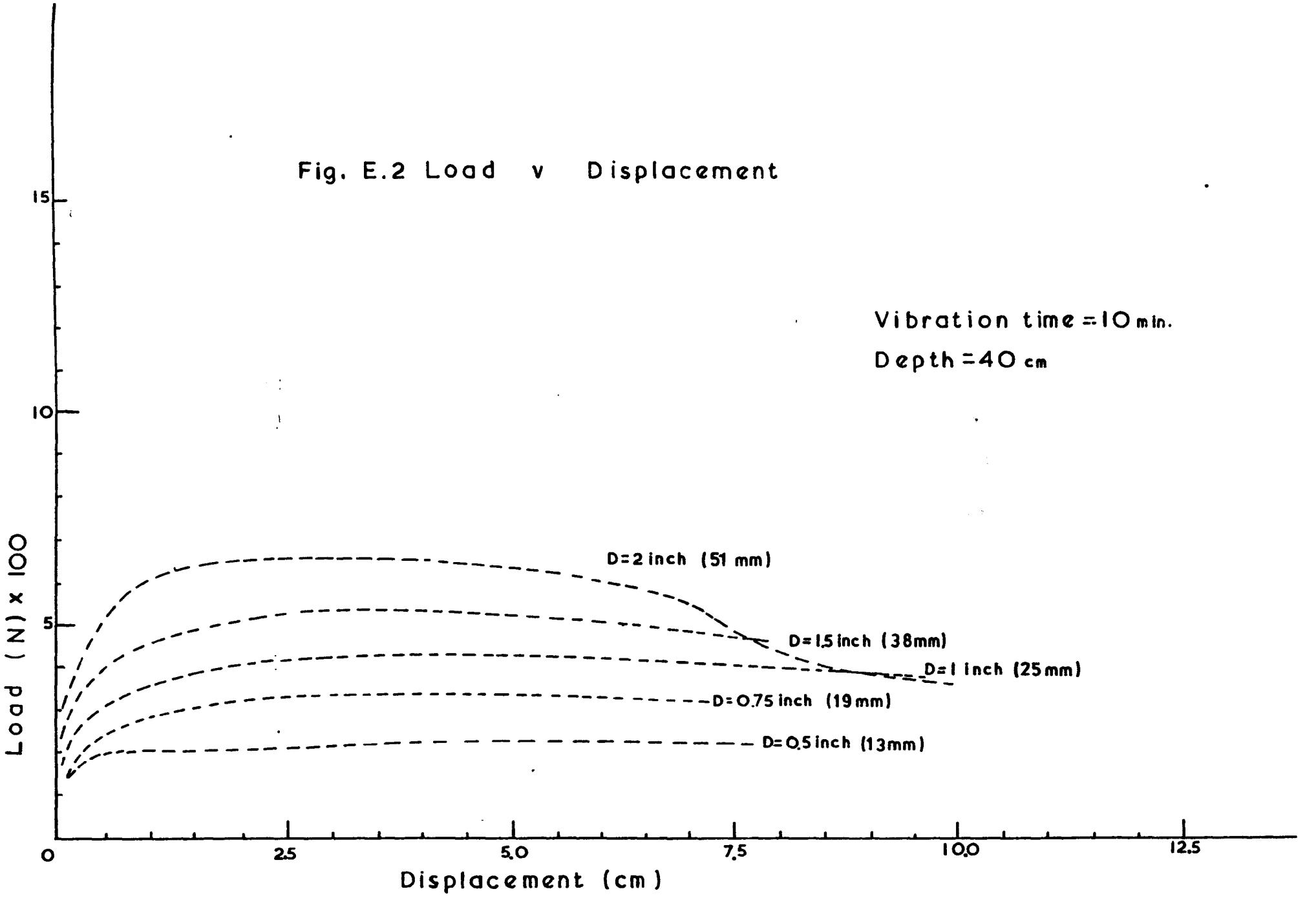

Fig. E.3 Load v Displacement

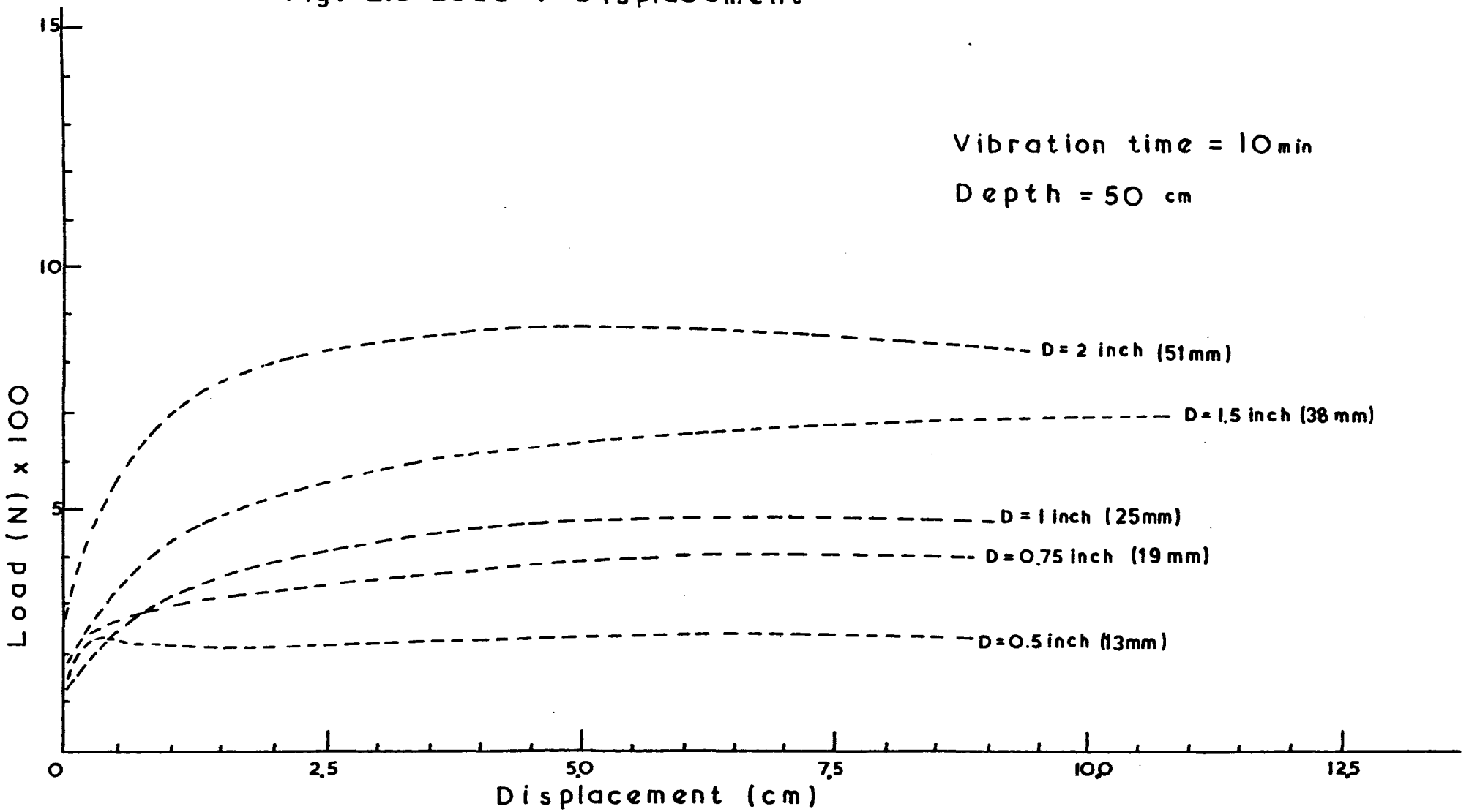

Fig. E.4 Load v Displacement

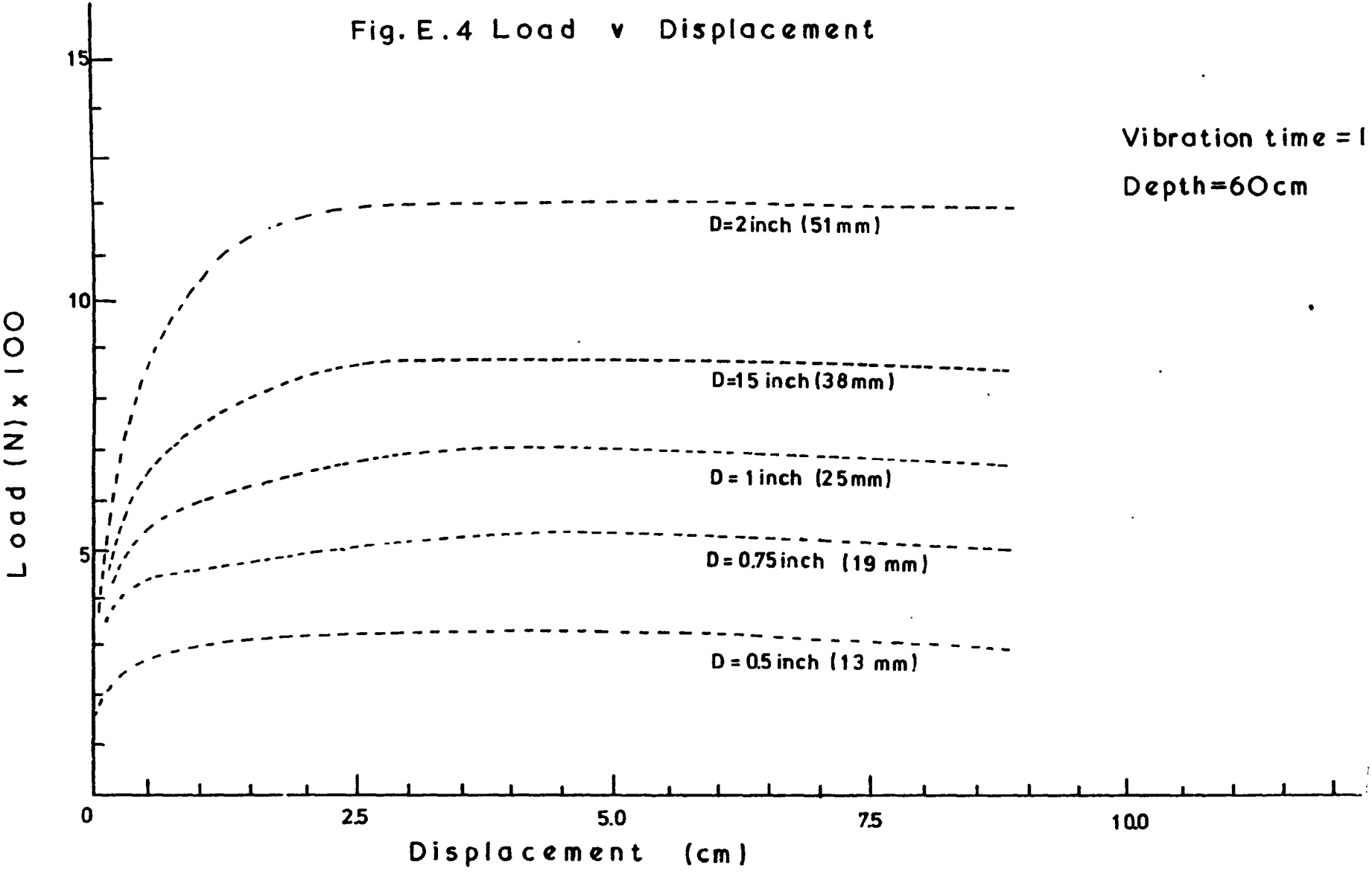

Fig. E.5 P_m V H / D

Vibration time = 10 min.

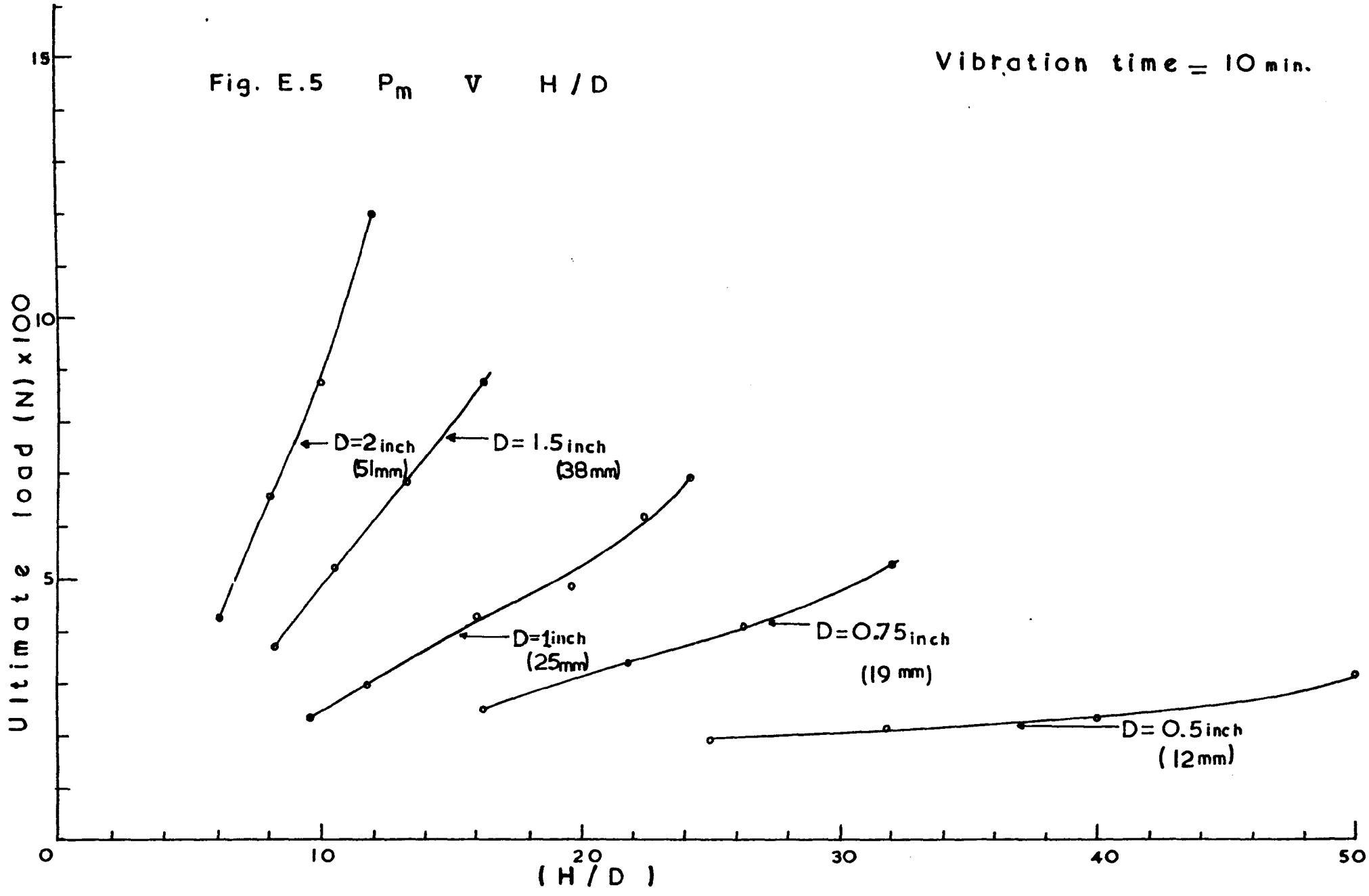

Fig. E.6 Load v Displacement

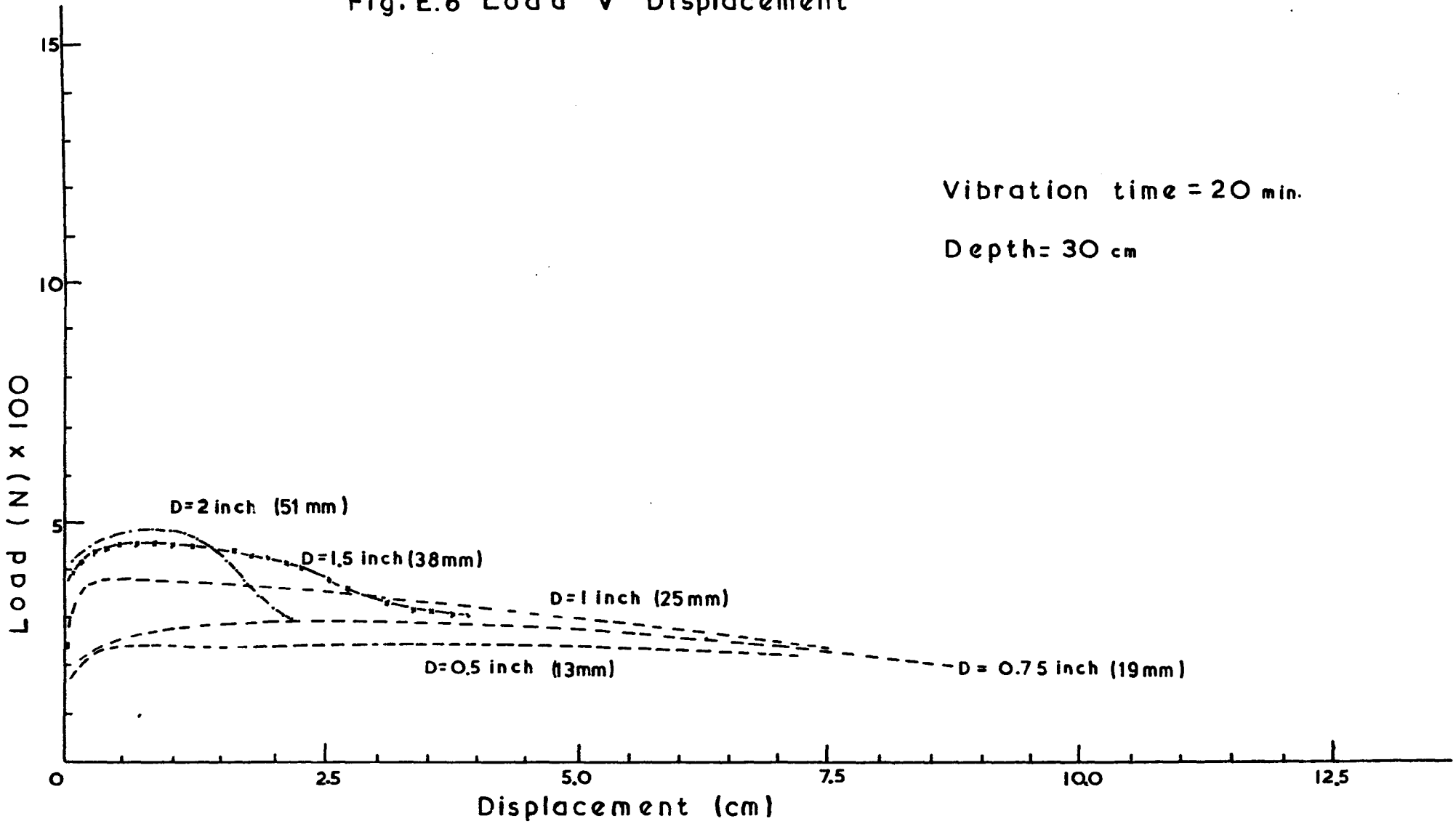

Fig. E.7 Load v Displacement

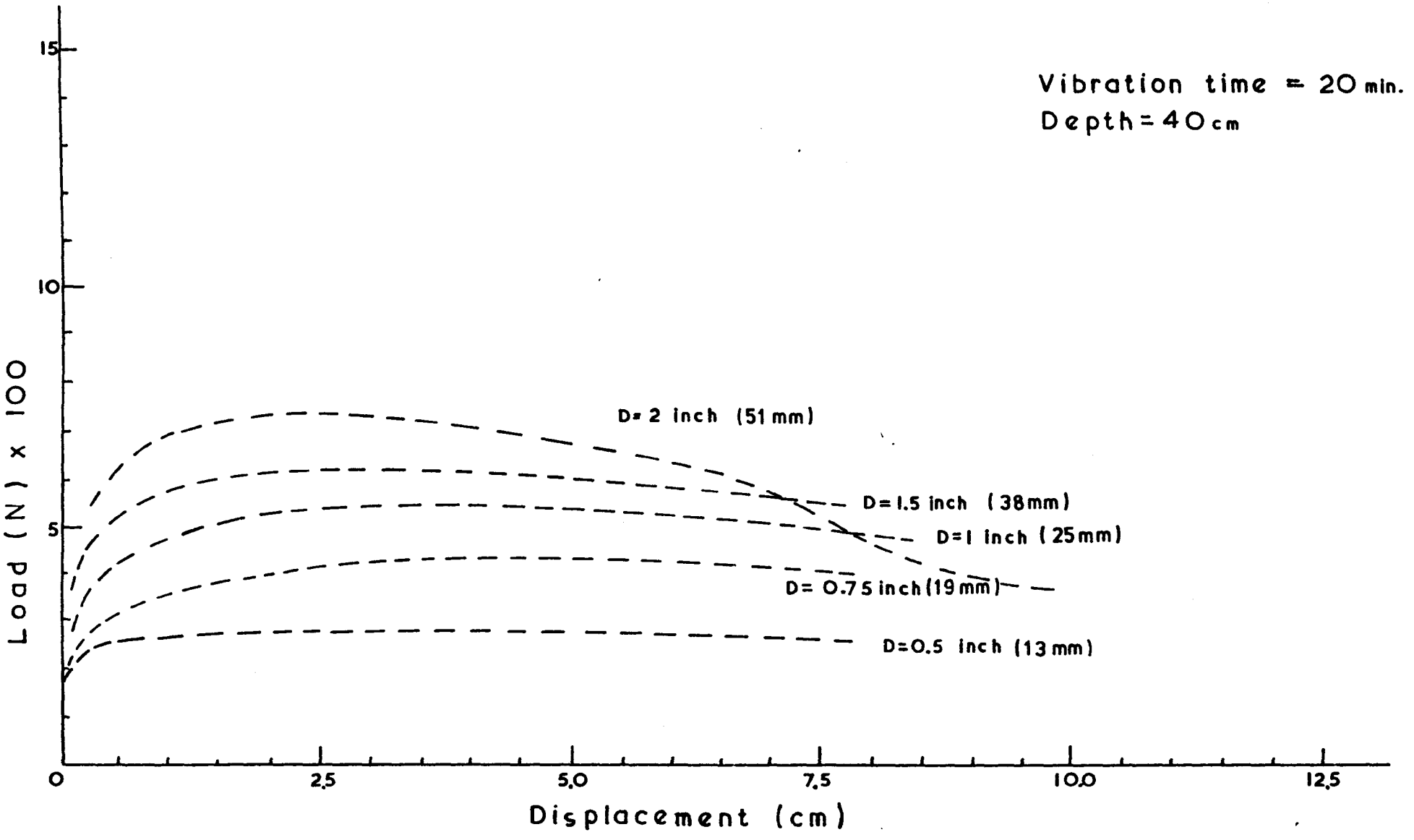

Fig. E.8 Load v Displacement

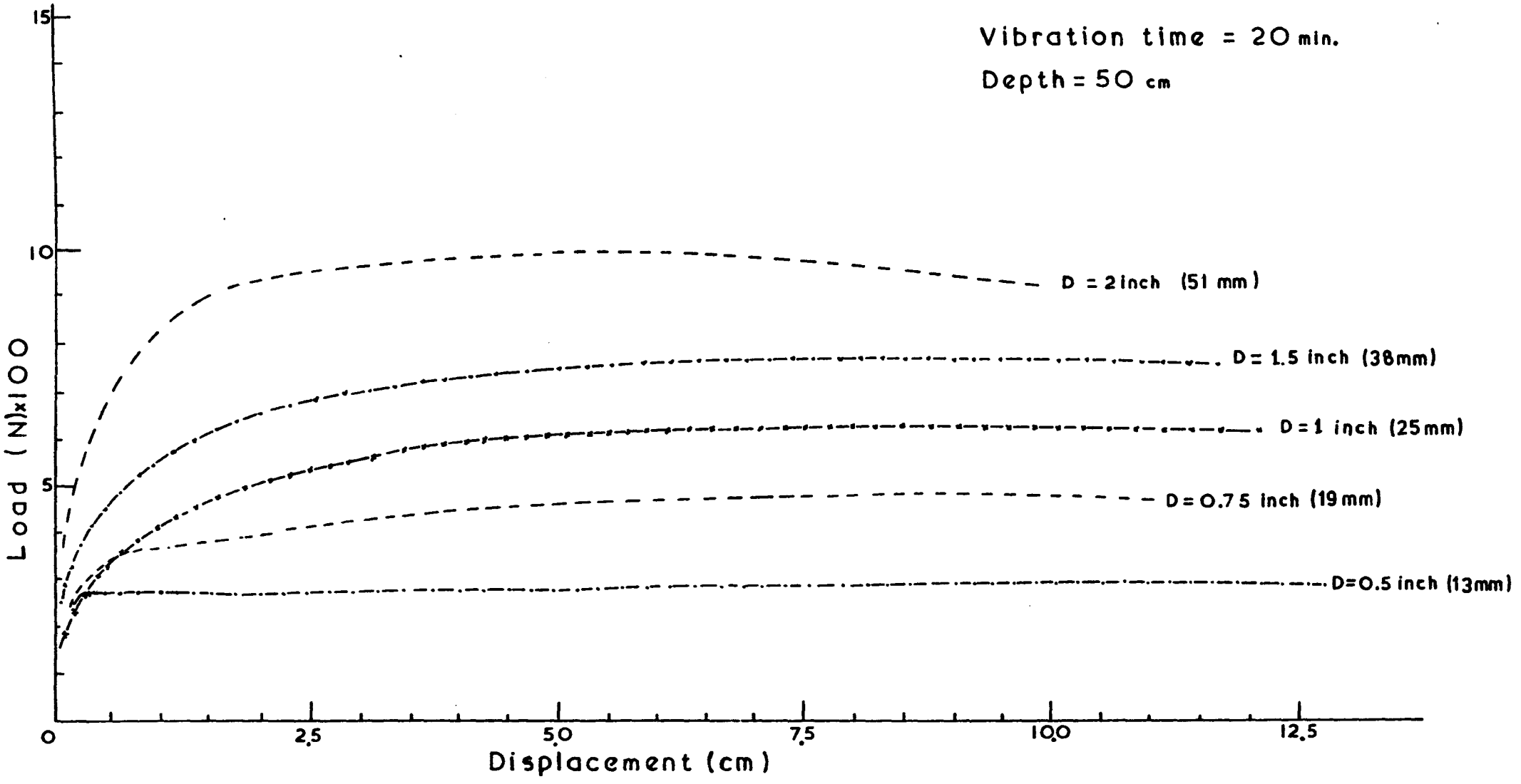

Fig. E.9 Load v Displacement

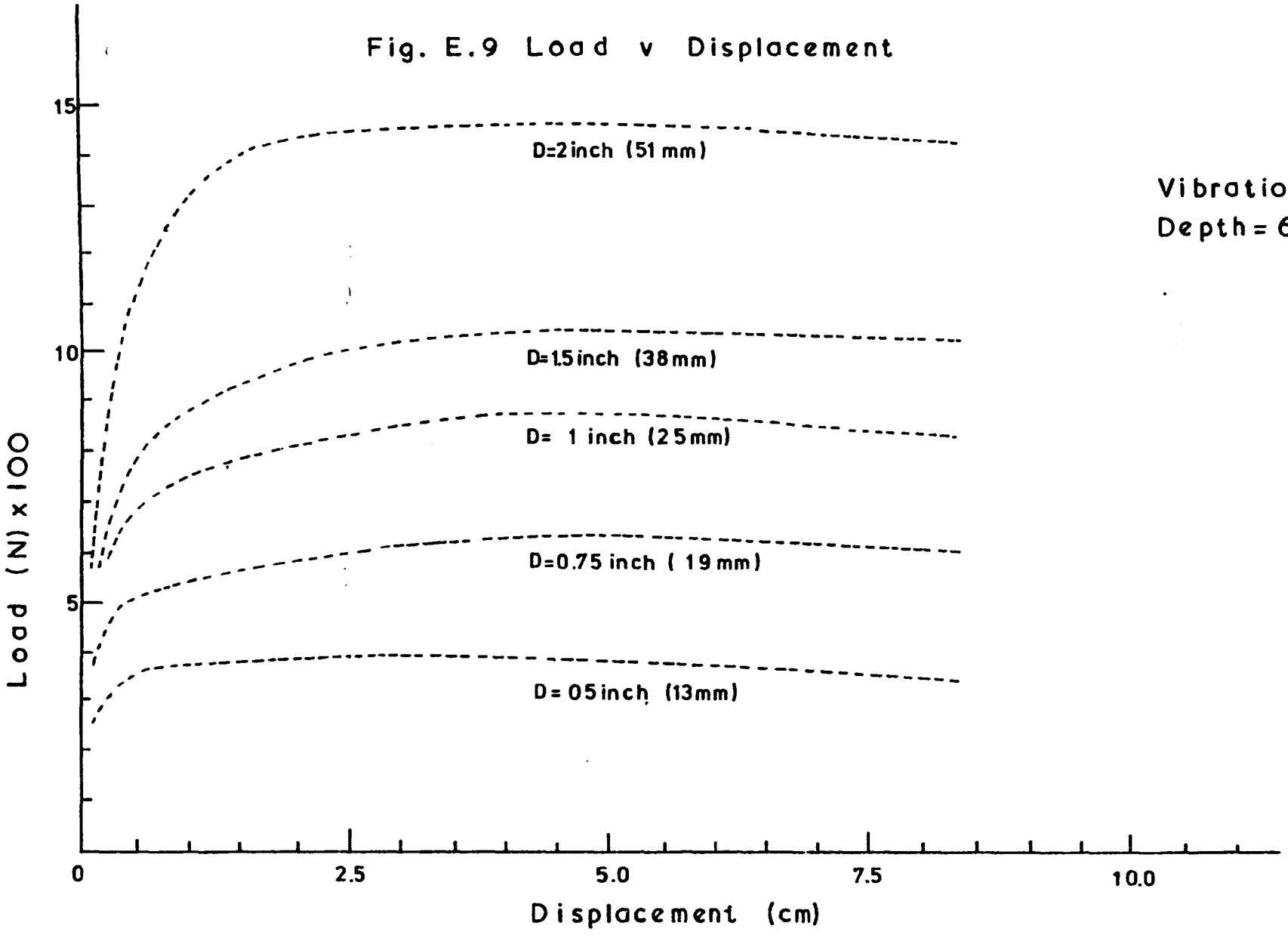

Vibration time=20min.
Depth = 60cm

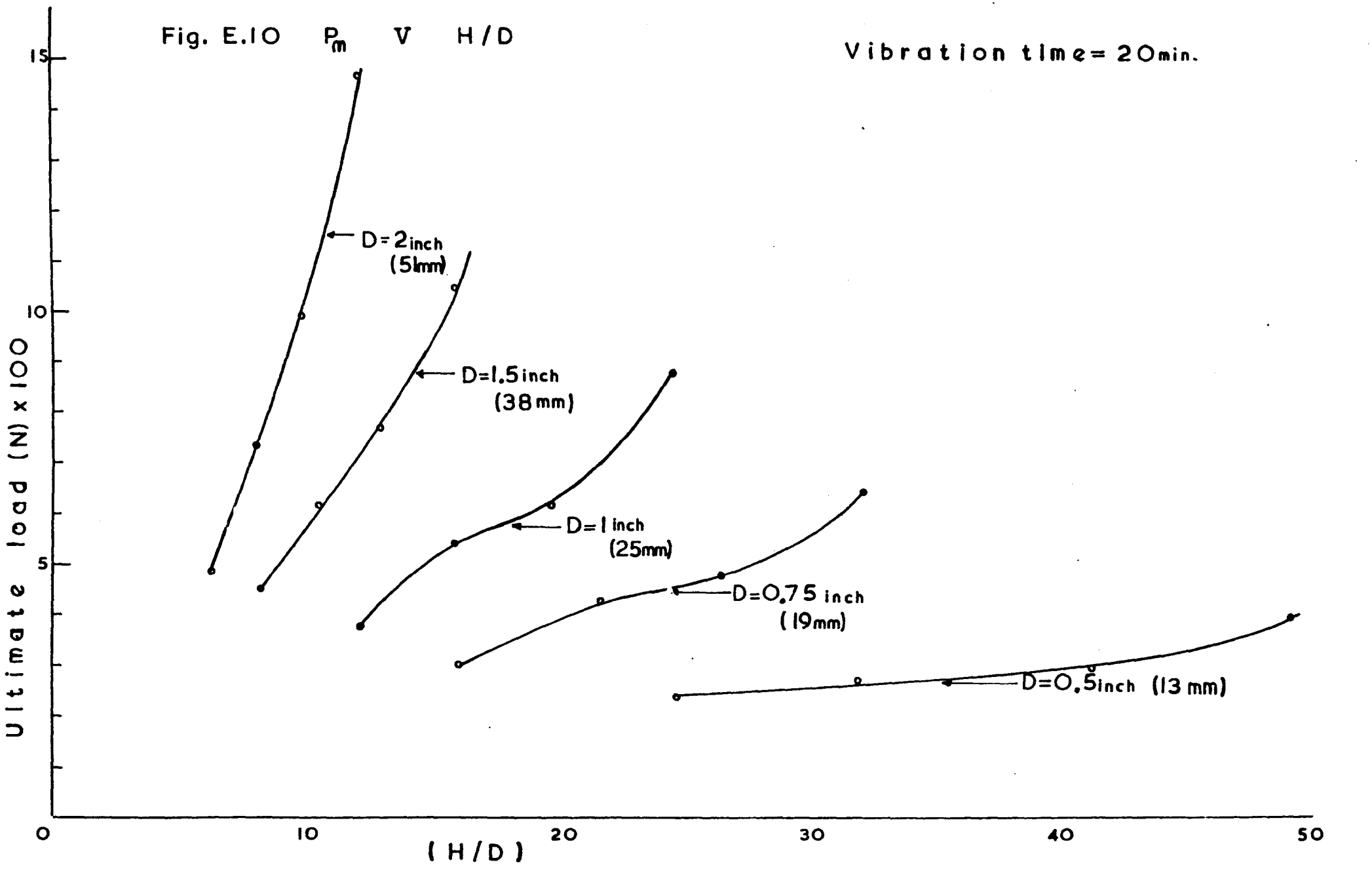
Fig. E.10 P_m V H/D
Vibration time = 20min.
Ultimate load (N) x 100
15
10
5
0
10
20
30
40
50
(H/D)
D = 2inch (51mm)
D = 1.5inch (38mm)
D = 1 inch (25mm)
D = 0.75 inch (19mm)
D = 0.5inch (13 mm)

Fig. E.11 Load v Displacement

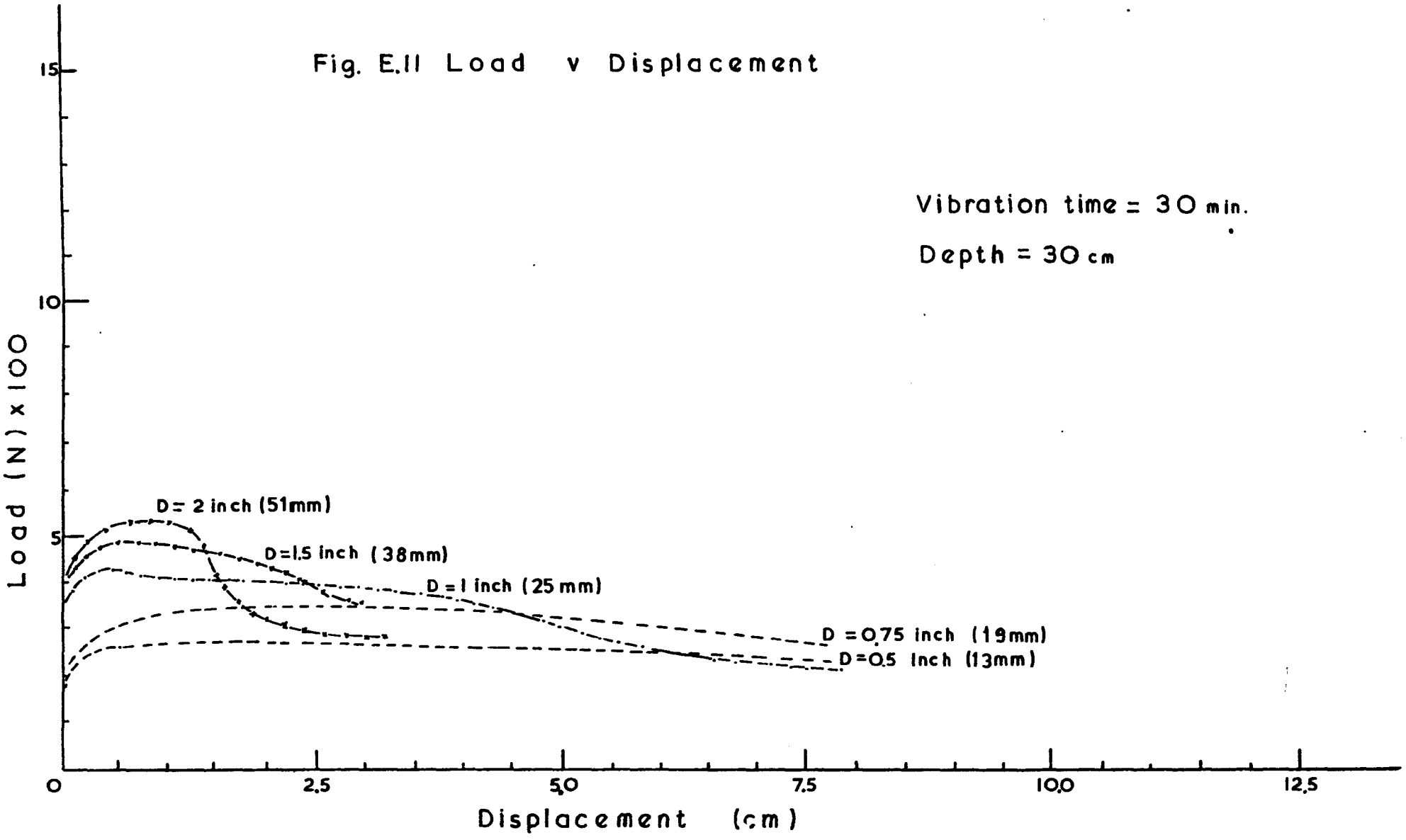

Fig. E.12 Load v Displacement

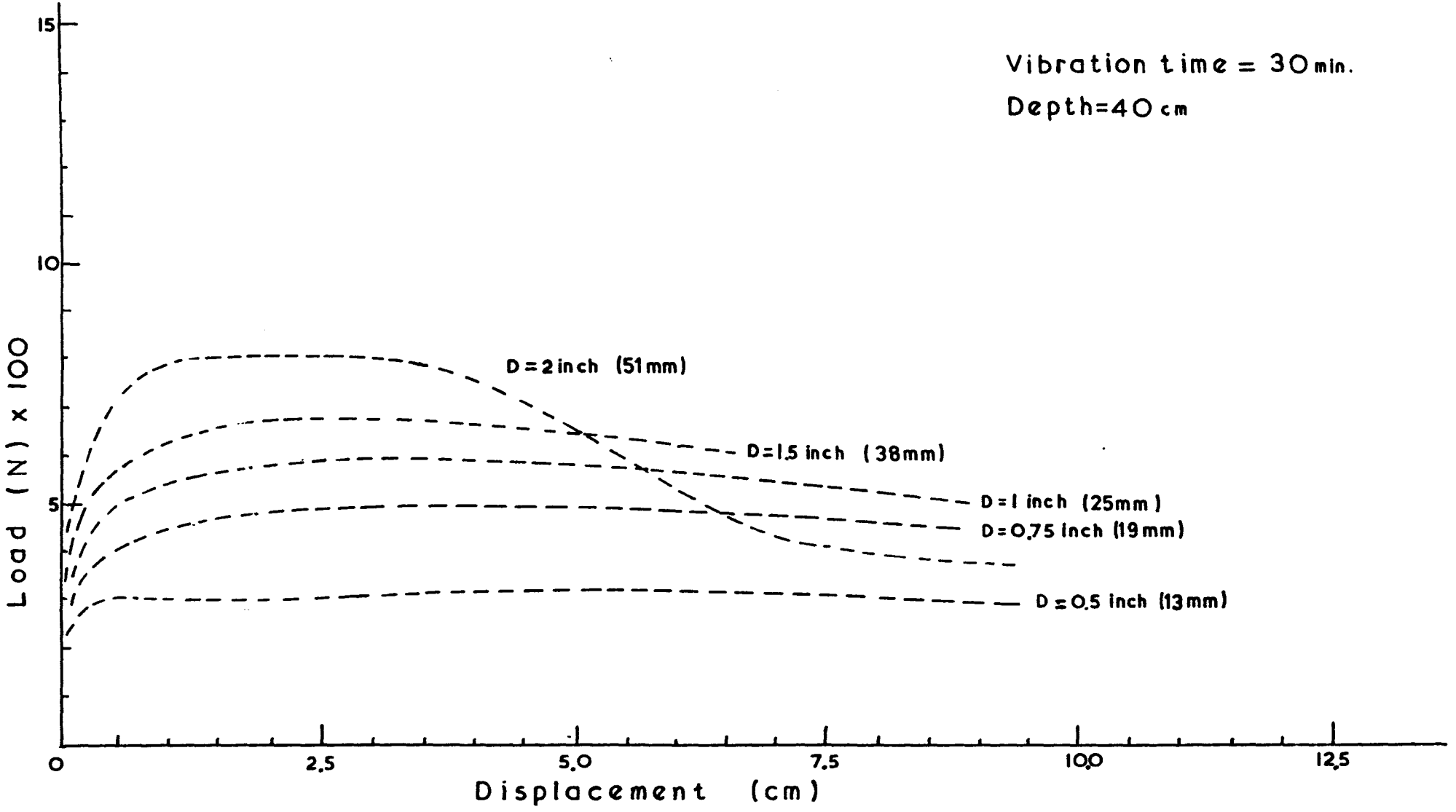

Fig. E.13 Load v Displacement

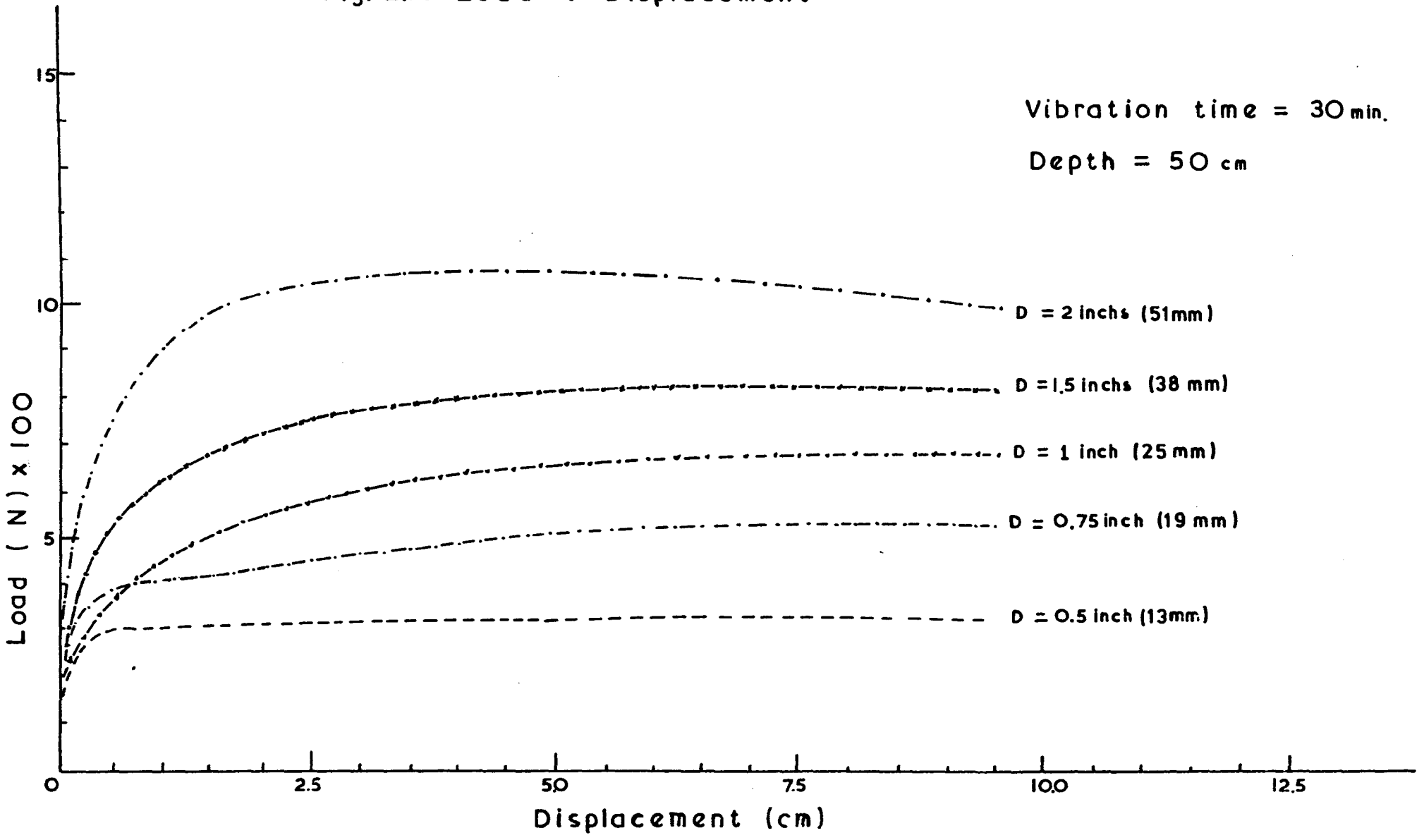

Fig. E.14 Load v Displacement

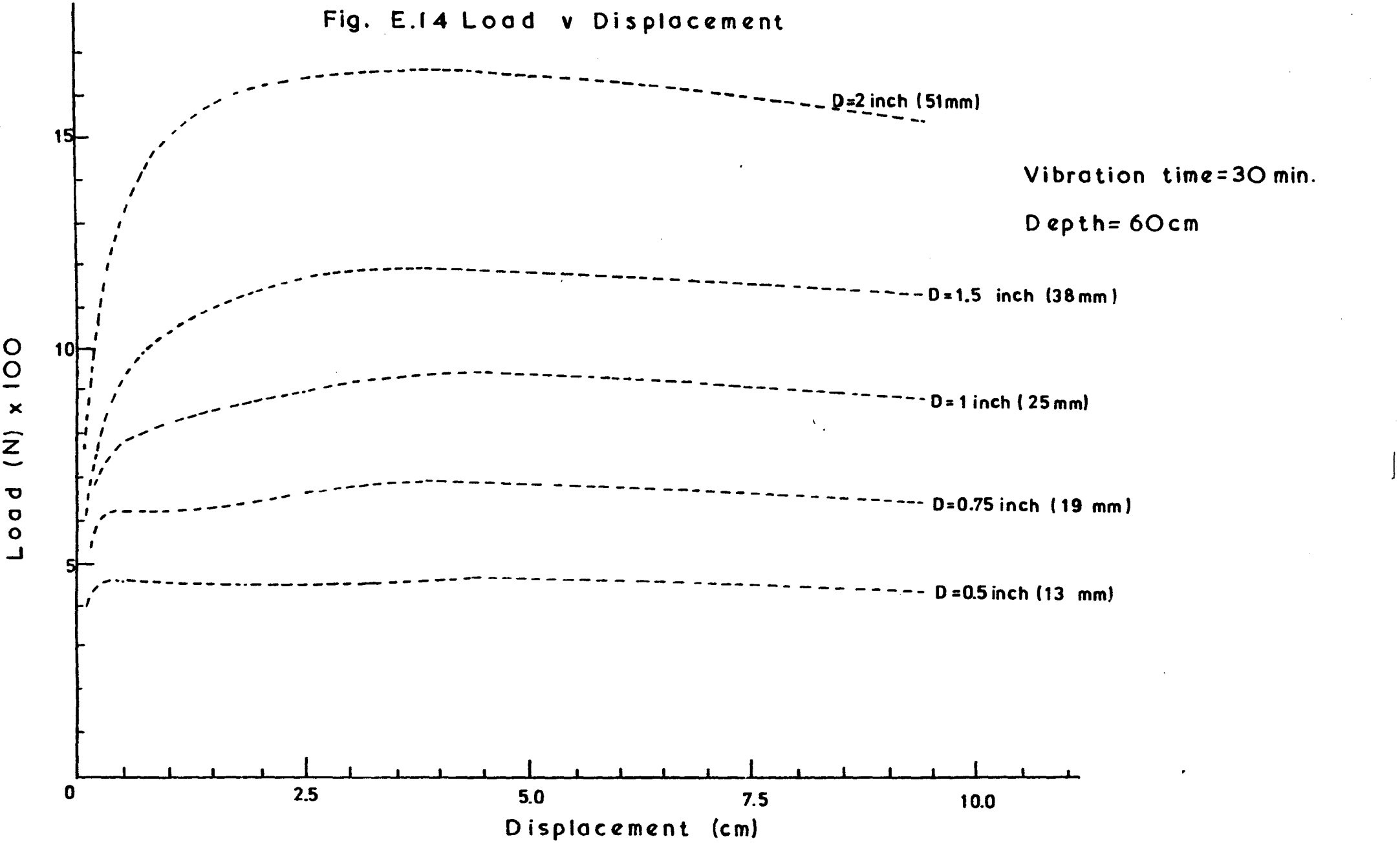

Fig. E.15 Ultimate load v (H/D)

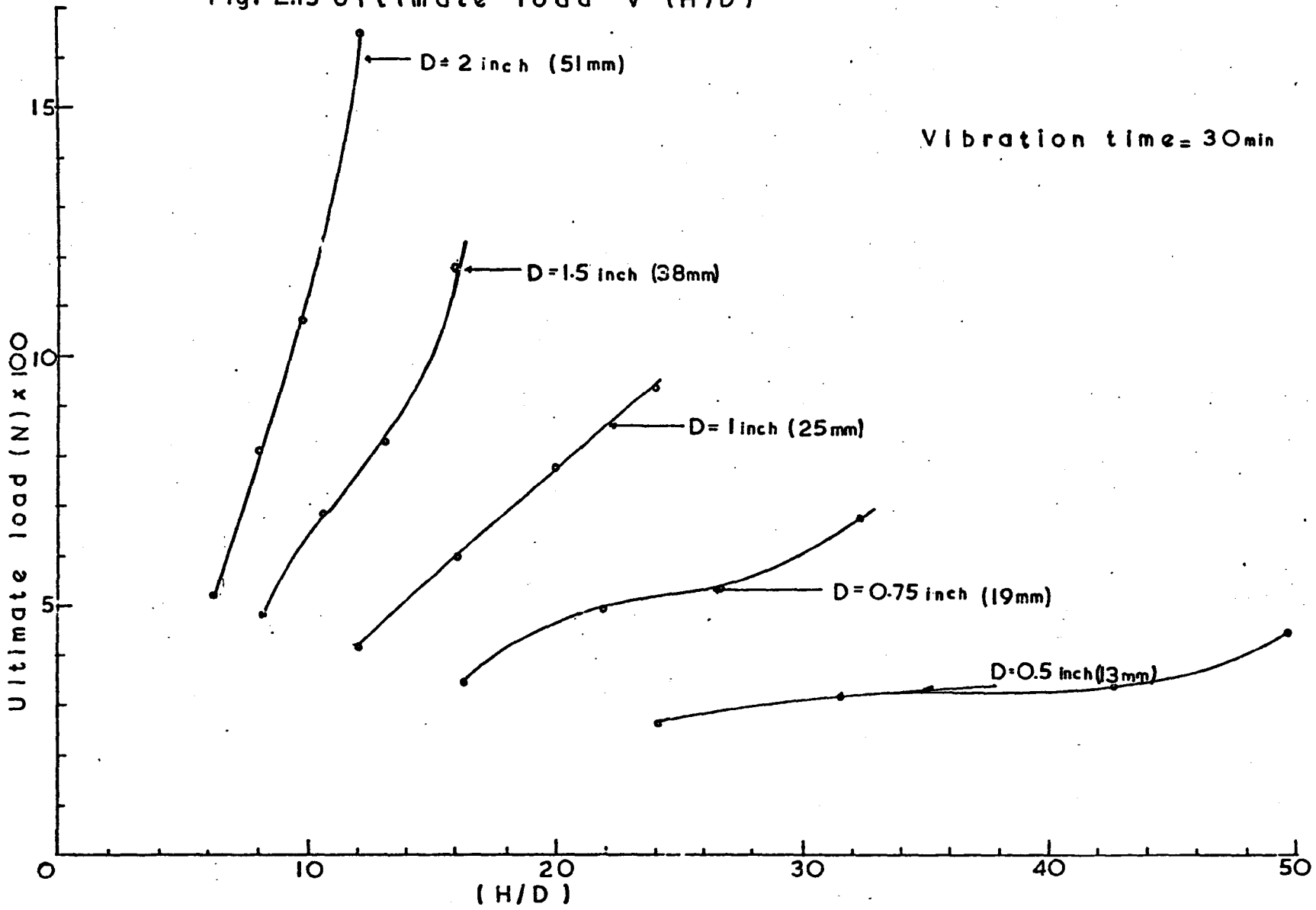

APPENDIX F

INTRODUCTION TO FINITE ELEMENT METHOD

In the finite element method, the body is visualised to be made up of a number of elements interconnected at a discrete number of nodes. If the relationship of force-displacement for each element is known, then the behaviour of the entire body can be studied.

The procedure of solving a problem is as follows:-

(a) The continuum is split into finite elements by imaginary surfaces; an assumption is made about the variation of displacement within the element.

(b) The stiffness matrix and other properties of each element in the continuum are derived.

(c) The "overall stiffness matrix" and the "overall force vector" are assembled.

(d) Using the boundary conditions, the relationship [overall stiffness matrix] {displacment} = {Force} is solved for the displacements.

(e) Using the nodal displacements, the stresses and strains within each element are calculated.

To develop the finite element method, the following assumptions have to be made:-

(a) The displacements within the deformed continuum are linearly related to the forces, i.e. Hooke's law is obeyed; the continuum behaves elastically. For non-linearly elastic

or plastic material, such as soil, appropriate stress-strain relationships are used.

(b) Within a finite element, its geometrical and material properties remain constant

(c) Displacements are small and are linearly related to the strains within the deformed continuum; i.e. continuum is geometrically linear.

The main advantages of the method are:-

(a) Any shape of continuum can be represented by finite elements.

(b) Continuum with variable material properties, can be dealt with by dividing it into elements with different properties

(c) A step by step analysis can be carried out and therefore geometry or properties can be varied between steps.

To obtain the relationship between nodal forces and nodal displacements the principle of the "work done" could be used. The matrix is called the "element stiffness matrix" and is given by the following relationship:-

$$[K_e] = \int_{vol} [H]^T [D] [H] \, dvol$$

Where:-

$$\{\text{Strains}\} = [H] \{\text{nodal displacements}\}$$

$$\{\text{Stresses}\} = [D] \{\text{Strains}\}$$

The "overall stiffness matrix" is assembled by using the

"element stiffness matrices".

The total external force at a point is made up of the nodal forces from each element surrounding that node.

The problem can only be solved if the displacements or the external forces or a combination of these two are known, which are then inserted in the relevant matrices for the solution of the problem.

APPENDIX G

EVALUATION OF MATRIX [S]

$$[L]=\begin{bmatrix} 0 & 1 & 0 & 2 & 0 & 0 & 0 & 0 \\ \frac{1}{2} & 1 & \frac{2}{2} & 2 & 0 & 0 & 0 & 0 \\ 0 & 0 & 0 & 0 & 0 & 0 & 1 & 2 \\ 0 & 0 & 1 & 2 & 0 & 1 & 0 & 2 \end{bmatrix}$$

$$[L]^T=\begin{bmatrix} 0 & \frac{1}{2} & 0 & 0 \\ 1 & 1 & 0 & 0 \\ 0 & \frac{2}{2} & 0 & 1 \\ 2 & 2 & 0 & 2 \\ 0 & 0 & 0 & 0 \\ 0 & 0 & 0 & 1 \\ 0 & 0 & 1 & 0 \\ 0 & 0 & 2 & 2 \end{bmatrix}$$

$$[D]=\begin{bmatrix} D_{11} & D_{12} & D_{13} & 0 \\ D_{21} & D_{22} & D_{23} & 0 \\ D_{31} & D_{32} & D_{33} & 0 \\ 0 & 0 & 0 & D_{44} \end{bmatrix}$$

From the matrices $[L]$, $[L]^T$ and $[D]$, the product of $[L]^T [D] [L]$ is found.

First $[L]^T$ is multiplied by $[D]$ to give the following 8 x 4 matrix:-

$$[L]^T[D] = \begin{bmatrix} \frac{D_{11}}{2} & \frac{D_{21}}{2} & \frac{D_{31}}{2} & 0 \\ D_{11} + D_{21} & D_{12} + D_{22} & D_{13} + D_{23} & 0 \\ \frac{3}{2}D_{21} & \frac{3}{2}D_{22} & \frac{3}{2}D_{23} & D_{44} \\ 2(D_{11} + D_{21}) & 2(D_{12} + D_{22}) & 2(D_{13} + D_{23}) & 2D_{44} \\ 0 & 0 & 0 & 0 \\ 0 & 0 & 0 & D_{44} \\ D_{21} & D_{22} & D_{23} & 0 \\ 2D_{21} & 2D_{22} & 2D_{23} & 2D_{44} \end{bmatrix}$$

The above matrix is multiplied by matrix $[L]$ to give an 8 x 8 matrix, the product of $[L]^T[D][L]$

$$[L]^T[D][L] =$$

$\frac{D_{11}}{r^2}$	$\frac{D_{11}+D_{12}}{r}$	$\frac{z}{r^2}D_{11}$	$\frac{z(D_{11}+D_{12})}{r}$	0	0	$\frac{D_{13}}{r}$	D_{13}
$\frac{(D_{11}+D_{12})}{r}$	$D_{11}+D_{12}+D_{21}+D_{22}$	$\frac{z(D_{11}+D_{12})}{r}$	$z(D_{11}+D_{12}+D_{21}+D_{22})$	0	0	$D_{13}+D_{23}$	$r(D_{13}+D_{23})$
$\frac{z}{r^2}D_{11}$	$z\frac{(D_{11}+D_{12})}{r}$	$\frac{z^2}{r^2}D_{11}+D_{44}$	$\frac{z^2}{r}(D_{11}+D_{12})+rD_{44}$	0	D_{44}	$\frac{z}{r}D_{13}$	$z(D_{23}+D_{44})$
$\frac{z}{r}(D_{11}+D_{12})$	$z(D_{11}+D_{12}+D_{21}+D_{22})$	$\frac{z^2}{r}(D_{11}+D_{12})+rD_{44}$	$z^2(D_{11}+D_{12}+D_{21}+D_{22})$ $+D_{44}r^2$	0	rD_{44}	$z(D_{13}+D_{23})$	$rz(D_{13}+D_{23}+D_{44})$
0	0	0	0	0	0	0	0
0	0	D_{44}	rD_{44}	0	D_{44}	0	zD_{44}
$\frac{D_{31}}{r}$	$D_{31}+D_{32}$	$\frac{z}{r}D_{31}$	$z(D_{31}+D_{32})$	0	0	D_{33}	rD_{33}
D_{31}	$r(D_{31}+D_{32})$	$z(D_{31}+D_{44})$	$zr(D_{31}+D_{32}+D_{44})$	0	zD_{44}	rD_{33}	$r^2D_{33}+z^2D_{44}$

Since the element is cylindrical with thickness x, where:- $x = r_2 - r_1$, and height h, where $h = z_4 - z_1$, the product $[L]^T [D] [L]$ is integrated between the limits shown below:-

Let $[S] = \int [L]^T [D] [L] \; d\,(VOL)$

But $d\,(VOL) = 2\pi r \, d r \, d z$

$\therefore \quad [S] = 2\pi \int_{r_1}^{r_2} \int_{z_1}^{z_4} [L]^T [D] [L] \; r \, d r \, d z$

By multiplying $[L]^T [D] [L]$ first by r and then integrating, an 8 x 8 matrix is obtained.

$$[S] = \begin{bmatrix} S_{11} & S_{12} & S_{13} & S_{14} & 0 & 0 & S_{17} & S_{18} \\ S_{21} & S_{22} & S_{23} & S_{24} & 0 & 0 & S_{27} & S_{28} \\ S_{31} & S_{32} & S_{33} & S_{34} & 0 & S_{36} & S_{37} & S_{38} \\ S_{41} & S_{42} & S_{43} & S_{44} & 0 & S_{46} & S_{47} & S_{48} \\ 0 & 0 & 0 & 0 & 0 & 0 & 0 & 0 \\ 0 & 0 & S_{63} & S_{64} & 0 & S_{66} & 0 & S_{68} \\ S_{71} & S_{72} & S_{73} & S_{74} & 0 & 0 & S_{77} & S_{78} \\ S_{81} & S_{82} & S_{83} & S_{84} & 0 & S_{86} & S_{87} & S_{88} \end{bmatrix}$$

Let $h_1 = z_4 - z_1$ $\quad x_1 = r_4 - r_1$

$h_2 = (z_4^2 - z_1^2)/2$ $\quad x_2 = (r_4^2 - r_1^2)/2$

$h_3 = (z_4^3 - z_1^3)/3$ $\quad x_3 = (r_4^3 - r_1^3)/3$

$h_4 = (z_4^4 - z_1^4)/4$ $\quad x_4 = (r_4^4 - r_1^4)/4$

Then the elements of matrix [S] are as follows:-

$$S_{11} = 2\pi D_{22} \log_e\left(\frac{r_2}{r_1}\right)$$

$$S_{22} = 2\pi h_1 x_2 (D_{11} + D_{12} + D_{21} + D_{22})$$

$$S_{33} = 2\pi \left[h_3 D_{22} \log_e\left(\frac{r_2}{r_1}\right) + h_1 x_2 D_{44}\right]$$

$$S_{44} = 2\pi \left[h_3 x_2 (D_{11} + D_{12} + D_{21} + D_{22}) + h_1 x_4 D_{44}\right]$$

$$S_{66} = 2\pi h_1 x_2 D_{44}$$

$$S_{77} = 2\pi h_2 x_2 D_{33}$$

$$S_{88} = 2\pi \left[h_2 x_4 D_{33} + h_3 x_2 D_{44}\right]$$

$$S_{12} = 2\pi h_1 x_1 (D_{21} + D_{22})$$

$$S_{21} = 2\pi h_1 x_1 (D_{12} + D_{22})$$

$$S_{13} = 2\pi h_2 D_{22} \log_e\left(\frac{r_2}{r_1}\right)$$

$$S_{31} = 2\pi h_2 D_{22} \log_e\left(\frac{r_2}{r_1}\right)$$

$$S_{14} = 2\pi h_2 x_1 (D_{21} + D_{22})$$

$$S_{41} = 2\pi h_2 x_1 (D_{12} + D_{22})$$

$$S_{17} = 2\pi h_1 x_1 D_{23}$$

$$S_{71} = 2\pi h_1 x_1 D_{32}$$

$$S_{18} = 2\pi h_1 x_2 D_{23}$$

$$S_{81} = 2\pi h_1 x_2 D_{32}$$

$$S_{23} = 2\pi h_2 x_1 \ (D_{12} + D_{22})$$

$$S_{32} = 2\pi h_2 x_1 \ (D_{21} + D_{22})$$

$$S_{24} = 2\pi h_2 x_2 \ (D_{11} + D_{12} + D_{21} + D_{22})$$

$$S_{42} = 2\pi h_2 x_2 \ (D_{11} + D_{12} + D_{21} + D_{22})$$

$$S_{27} = 2\pi h_2 x_2 \ (D_{12} + D_{22})$$

$$S_{72} = 2\pi h \ x \ (D_{21} + D_{22})$$

$$S_{28} = 2\pi h_1 x_3 \ (D_{12} + D_{23})$$

$$S_{82} = 2\pi h_1 x_3 \ (D_{21} + D_{32})$$

$$S_{34} = 2\pi \left[h_2 x_1 \ (D_{21} + D_{22}) + h_1 x_2 \ D_{44} \right]$$

$$S_{43} = 2\pi \left[h_2 x_1 \ (D_{12} + D_{22}) + h_1 x_2 \ D_{44} \right]$$

$$S_{36} = 2\pi \ h_1 x_2 \ D_{44}$$

$$S_{63} = 2\pi \ h_1 x_2 \ D_{44}$$

$$S_{37} = 2\pi \ h_2 \ x_1 \ D_{23}$$

$$S_{73} = 2\pi \ h_2 x_1 \ D_{32}$$

$$S_{38} = 2\pi \ h_2 x_2 \ (D_{23} + D_{44})$$

$$S_{83} = 2\pi \ h_2 x_2 \ (D_{32} + D_{44})$$

$$S_{46} = 2\pi \ h_1 x_3 \ D_{44}$$

$$S_{64} = 2\pi \ h_1 x_3 \ D_{44}$$

$$S_{47} = 2\pi \ h_2 x_2 \ (D_{13} + D_{23})$$

$$S_{74} = 2\pi \ h_2 x_2 \ (D_{31} + D_{32})$$

$$S_{48} = 2\pi \ h_2 x_3 \ (D_{13} + D_{23} + D_{44})$$

$$S_{84} = 2\pi \ h_2 x_3 \ (D_{31} + D_{32} + D_{44})$$

$$S_{68} = 2\pi \ h_2 x_2 \ D_{44}$$

$$S_{86} = 2\pi \ h_2 x_2 \ D_{44}$$

$$S_{78} = 2\pi \ h_1 x_3 \ D_{33} \qquad S_{87} = S_{78}$$

APPENDIX H

INVERSION OF [N]

The matrix [N] is inverted to give the matrix [C] . The inversion of [N] is mainly required for saving computer time, which is needed for obtaining more iterations and steps, and also for avoidance of rearranging it so as to obtain the inverse of it. Rearrangement is required due to the element N_{55} being zero. Any attempt to invert [N] using standard computer subroutine will fail.

$$[N] = \begin{bmatrix} 1 & r_1 & z_1 & r_1 z_1 & 0 & 0 & 0 & 0 \\ 0 & 0 & 0 & 0 & 1 & r_1 & z_1 & r_1 z_1 \\ 1 & r_2 & z_2 & r_2 z_2 & 0 & 0 & 0 & 0 \\ 0 & 0 & 0 & 0 & 1 & r_2 & z_2 & r_2 z_2 \\ 1 & r_3 & z_3 & r_3 z_3 & 0 & 0 & 0 & 0 \\ 0 & 0 & 0 & 0 & 1 & r_3 & z_3 & r_3 z_3 \\ 1 & r_4 & z_4 & r_4 z_4 & 0 & 0 & 0 & 0 \\ 0 & 0 & 0 & 0 & 1 & r_4 & z_4 & r_4 z_4 \end{bmatrix}$$

The inverse of $[N]$, which is $[C]$ has the form shown below:-

$$[C] = \begin{bmatrix} C_{11} & 0 & C_{13} & 0 & C_{15} & 0 & C_{17} & 0 \\ C_{21} & 0 & C_{23} & 0 & C_{25} & 0 & C_{27} & 0 \\ C_{31} & 0 & C_{33} & 0 & C_{35} & 0 & C_{37} & 0 \\ C_{41} & 0 & C_{43} & 0 & C_{45} & 0 & C_{47} & 0 \\ 0 & C_{52} & 0 & C_{54} & 0 & C_{56} & 0 & C_{58} \\ 0 & C_{62} & 0 & C_{64} & 0 & C_{66} & 0 & C_{68} \\ 0 & C_{72} & 0 & C_{74} & 0 & C_{76} & 0 & C_{78} \\ 0 & C_{82} & 0 & C_{84} & 0 & C_{86} & 0 & C_{88} \end{bmatrix}$$

But there is a rule between a square matrix and its inverse, which is:-

$$[N]\,[N]^{-1} = [I]$$

Where:-

$[I]$ is a unit matrix.

$$\therefore \quad [N]^{-1} = [C]$$

$$[N]\,[C] = [I]$$

$$[I]=\begin{bmatrix} 1 & 0 & 0 & 0 & 0 & 0 & 0 & 0 \\ 0 & 1 & 0 & 0 & 0 & 0 & 0 & 0 \\ 0 & 0 & 1 & 0 & 0 & 0 & 0 & 0 \\ 0 & 0 & 0 & 1 & 0 & 0 & 0 & 0 \\ 0 & 0 & 0 & 0 & 1 & 0 & 0 & 0 \\ 0 & 0 & 0 & 0 & 0 & 1 & 0 & 0 \\ 0 & 0 & 0 & 0 & 0 & 0 & 1 & 0 \\ 0 & 0 & 0 & 0 & 0 & 0 & 0 & 1 \end{bmatrix}$$

Using the relationship $[N][C] = [I]$, the non-zero elements of matrix $[C]$ were found as follows:-

$$C_{41} = \left[(R_{41}-1)-(R_{31}-1)\frac{Z_{43}}{Z_{33}}\right] \Big/ \left[Z_{44}-\frac{Z_{43}}{Z_{33}}Z_{34}\right]$$

$$C_{31} = \left[R_{31}-1-Z_{34}C_{41}\right] / Z_{33}$$

$$C_{21} = \left[-1-(Y_2Z_2-Y_1Z_1)C_{41}-(Z_2-Z_1)C_{31}\right] \Big/ \left[Y_2-Y_1\right]$$

$$C_{11} = 1-Y_1Z_1C_{41}-Z_1C_{31}-Y_1Z_{21}$$

$$C_{52} = C_{11}$$

$$C_{62} = C_{21}$$

$$C_{72} = C_{31}$$

$$C_{82} = C_{41}$$

$$C_{43} = \left[R_{31}\frac{Z_{43}}{Z_{33}}-R_{41}\right] \Big/ \left[Z_{44}-\frac{Z_{43}}{Z_{33}}Z_{34}\right]$$

$$C_{33} = \left[-R_{31}-Z_{34}C_{43}\right] / Z_{33}$$

$$C_{23} = \left[-1-(Y_2Z_2-Y_1Z_1)C_{43}-(Z_2-Z_1)C_{33}\right] / \left[Y_2-Y_1\right]$$

$$C_{13} = -Y_1Z_1C_{43}-Z_1C_{33}-Y_1Z_{23}$$

$$C_{54} = C_{13}$$

$$C_{64} = C_{23}$$

$$C_{74} = C_{33}$$

$$C_{84} = C_{43}$$

$$C_{45} = -\frac{Z_{43}}{Z_{33}} \Big/ \left[Z_{44}-\frac{Z_{43}}{Z_{33}}Z_{34}\right]$$

$$C_{35} = \left[1-Z_{34}C_{45}\right] / Z_{33}$$

$$C_{25} = \left[-(Y_2Z_2-Y_1Z_1)C_{45}-(Z_2-Z_1)C_{35}\right] \Big/ \left[Y_2-Y_1\right]$$

$$C_{15} = -Y_1Z_1C_{45}-Z_1C_{35}-Y_1C_{25}$$

$$C_{56} = C_{15}$$

$$C_{66} = C_{25}$$

$$C_{76} = C_{35}$$

$$C_{86} = C_{45}$$

$$C_{47} = 1 \Big/ \left[z_{44} - \frac{z_{48}}{z_{88}} z_{84} \right]$$

$$C_{37} = - z_{34} C_{47} / z_{88}$$

$$C_{27} = \left[- (r_2 z_2 - r_1 z_1) C_{47} - (z_2 - z_1) C_{37} \right] / \left[r_2 - r_1 \right]$$

$$C_{17} = - r_1 z_1 C_{47} - z_1 C_{37} - r_1 C_{27}$$

$$C_{58} = C_{17}$$

$$C_{68} = C_{27}$$

$$C_{78} = C_{37}$$

$$C_{88} = C_{47}$$

APPENDIX I

RELOADING STRESS-STRAIN RELATIONSHIP

The reloading portion of the hysteresis loop can be approximately represented by a straight line. By considering the reloading behaviour as linearly elastic, a small error is introduced at the point where the reloading part of the curve meets the main loading curve. The following set of equations, in matrix form, gives the reloading portion of the hysteresis loop:-

$$\{\delta_i\} = \begin{bmatrix} \frac{(\varepsilon_{xxi} - \varepsilon_{xxf})}{(\sigma_{xi} - \sigma_{xf})} & -\frac{(\varepsilon_{xyi} - \varepsilon_{xyf})}{(\sigma_{yi} - \sigma_{yf})} & -\frac{(\varepsilon_{xzi} - \varepsilon_{xzf})}{(\sigma_{zi} - \sigma_{zf})} \\ -\frac{(\varepsilon_{yxi} - \varepsilon_{yxf})}{(\sigma_{xi} - \sigma_{xf})} & \frac{(\varepsilon_{yyi} - \varepsilon_{yyf})}{(\sigma_{yi} - \sigma_{yf})} & -\frac{(\varepsilon_{yzi} - \varepsilon_{yzf})}{(\sigma_{zi} - \sigma_{zf})} \\ -\frac{(\varepsilon_{zxi} - \varepsilon_{zxf})}{(\sigma_{xi} - \sigma_{xf})} & -\frac{(\varepsilon_{zyi} - \varepsilon_{zyf})}{(\sigma_{yi} - \sigma_{yf})} & -\frac{(\varepsilon_{zzi} - \varepsilon_{zzf})}{(\sigma_{zi} - \sigma_{zf})} \end{bmatrix} \{\delta_\sigma\}$$

Where ε_{xyi}, ε_{xyf} etc. are the strains in the x-direction due to the loading in the y-direction at the start and end of the unloading part respectively.

APPENDIX J

```
**********************************************************

        * * * LINEAR  PROGRAM * * *

**********************************************************

 DIMENSION ICOL(169),IDF(169,2),NODES(144,4),IED(144,8),
*COOR(169,2),ZG(144),RG(144),PZ(144),PR(144),PRSO(6),CGE(144),
*C(8,8),CT(8,8),CTS(8,8),SS(8,8),B(4,4),D(4,4),S(8,8),BN(4,8),
*DIS(8),BNC(4,8),STN(4),STS(4),R(4),Z(4),NNPD(6),PD(6),IEP(10),A(27
*8,59),A3(6,278),P3(6),P(278),W(278),P6(278,1),EYM(4),STSI(144,4)
*,PTL(12),PF(12),AMOVE(12)
 EQUIVALENCE(P(1),P6(1,1))
                *** DATA ***
 NSF=1
 NPOIS=6
 NES=4
 NU=59
 NNOD=169
 NCONS=60
 NLAYERS=12
 NSQUARE=12
 NELC=144
 NNODESL=13
 IDIS=6
 NVLC=278
 NOTP=6
 NEP=10
 SPW=1200.0
 NSM=1
 NBS1=NNOD-NNODESL+1
 NLS=NVLC-NOTP+1
 PI=3.141592
```

```
      H=0.9
C        *         *         *         *         *         *         *
      READ(1,10)(EYM(I),I=1,NES)
   10 FORMAT(4F10.1)
      READ(1,11)(PRSO(I),I=1,NPOIS)
   11 FORMAT(6F5.2)
      READ(1,1)(AMOVE(I),I=1,NSM)
    1 FORMAT(F10.5)
      READ(1,2)(IEP(I),I=1,NEP)
    2 FORMAT(5I5)
      READ(1,3)(NNPD(I),I=1,NOTP)
    3 FORMAT(6I5)
      READ(1,4)(ICOL(I),I=1,NNOD)
    4 FORMAT(13I5)
      READ(1,5)(COOR(ICOL(I),1),I=1,NNODESL)
    5 FORMAT(F10.3)
      READ(1,6)(COOR(ICOL(I),2),I=1,NRS1,NNODESL)
    6 FORMAT(F10.3)
                    ****NODES  VS DEGREES OF FREEDOM  ***
      DO 100 I=1,NNOD
      DO 100 J=1,2
  100 IDF(I,J)=1
      DO 101 IC=1,NCONS
      READ(1,9)I,J
    9 FORMAT(2I5)
  101 IDF(I,J)=0
      IK1=1
      DO  102 I=1,NNOD
      DO  102 J=1,2
      IF (IDF(I,J)-1)102,103,103
  103 IDF(I,J)=IK1
      IK1=IK1+1
  102 CONTINUE
C        *         *         *         *         *         *         *
                    ***ELEMENTS  VS  NODES  ***
      DO  104 NL=1,NLAYERS
      DO  104 NB=1,NSQUARE
      NRR=(NL-1)*NSQUARE+NB
```

```
      NRC=(NL-1)*NNODESL+NB
      NRC1=NL*NNODESL+NB
      NODES(NRR,1)=ICOL(NRC)
      NODES(NRR,2)=ICOL(NRC+1)
      NODES(NRR,3)=ICOL(NRC1+1)
      NODES(NRR,4)=ICOL(NRC1)
  104 CONTINUE
C        *          *          *          *          *          *          *
C                   ***ELEMENTS  VS  DEGREES OF FREEDOM  ***
      DO  105 I=1,NELC
      DO 105  J=1,4
      IAA=NODES(I,J)
      JJ=2*(J-1)
      DO  106 K=1,2
      IED(I,JJ+K)=IDF(IAA,K)
  106 CONTINUE
  105 CONTINUE
      WRITE(2,1005)(I,(IED(I,J),J=1,6),I=1,NELC)
 1005 FORMAT(3X,I5,5X,6I10)
C        *          *          *          *          *          *          *
C                   ***NODES  VS   COORDINATES  ***
      DO  107 NL=1,NLAYERS
      DO  107  I=1,NNODESL
      COOR(ICOL(I+NNODESL*NL),1)=COOR(ICOL(I),1)
  107 CONTINUE
      DO  108 I=1,NNODESL-1
      DO  108 NL=1,NLAYERS
      COOR(ICOL(NL*NNODESL+I+1),2)=COOR(ICOL(NL*NNODESL+1),2)
  108 CONTINUE
      WRITE(2,1007)(I,COOR(ICOL(I),1),COOR(ICOL(I),2),I=1,NNOD)
 1007 FORMAT(3X,I5,5X,2F10.5)
C        *          *          *          *          *          *          *
      IAA=1
      IBB=2
      ICC=3
      IDD=4
      DO 8020 IE=1,NES
      ES=EYM(IE)
```

```
      DO 2080 IP=1,NPOIS
      PRS=PRSO(IP)
      DO  109 I=1,NELC
      DO  109 J=1,4
  109 STSI(I,J)=0.0
      DO  110 I=1,NVLC
      DO  110 J=1,NW
  110 A(I,J)=0.0
      DO  111 I=1,NOTP
      DO  111 J=1,NVLC
  111 A3(I,J)=0.0
     *          *          *          *          *          *
                ***ASSEBLE  OF  OVERALL STIFFNESS  ***
      DO  112 K1=1,NELC
      DO  113 L7=1,NEP
      IF(K1.EQ.IEP(L7))GO TO 114
  113 CONTINUE
      GO TO 115
  114 CONTINUE
                ***STIFNESS  IN  SOIL ELEMENTS  PUT  EQUAL  TO ZERO  ***
      DO 116 I=1,8
      DO 116 J=1,8
  116 SS(I,J)=0.0
                ***COORDINATES OF ELEMENT  ***
      CALL CNE(NODES,COOR,K1,IAA,IBB,ICC,IDD,R,Z)
                ***COORDINATES OF  CENTROID  ****
      ZG(K1)=(Z(IDD)+Z(IAA))/2.0
      RG(K1)=(R(IBB)+R(IAA))/2.0
      CGE(K1)=(Z(IDD)+Z(IAA))/2.0
      GO TO 117
  115 CONTINUE
                ***COORDINATES OF ELEMENT  ***
      CALL CNE(NODES,COOR,K1,IAA,IBB,ICC,IDD,R,Z)
                ***COORDINATES OF  CENTROID  ****
      ZG(K1)=(Z(IDD)+Z(IAA))/2.0
      RG(K1)=(R(IBB)+R(IAA))/2.0
      CGE(K1)=(Z(IAA)+Z(IDD))/2.0
      DO 118 I=1,8
```

```
      DO 118 J=1,8
      CTS(I,J)=0.0
      S(I,J)=0.0
      SS(I,J)=0.0
  118 CONTINUE
      CALL CACT(R,Z,IAA,IBB,ICC,IDD,C,CT)
C                     ***MATRIX  [D]  ***
      CALL DMAT(PRS,ES,D)
C                     ***MATRIX  [S]  ***
      CALL SMATR(R,Z,IAA,IBB,ICC,IDD,D,S)
C                     ***TO FIND MATRIX [CTS] =[CT]*[S]  ***
      CALL MMULT(CT,S,CTS,8,8,8,8,8,8)
C                     *** TO FIND MATRIX [SS] =[CTS]*[C] ***
      CALL MMULT(CTS,C,SS,8,8,8,8,8,8)
  117 CONTINUE
      DO  119 I1=1,8
      I2=IED(K1,I1)
      IF(I2.EQ.0) GO TO 119
      IF(I2.GT.NVLC) GO TO 119
      DO  120 J1=1,8
      J2=IED(K1,J1)
      IF(J2.EQ.0)GO TO 120
      IF(J2.GT.NVLC) GO TO 120
      J3=J2-I2*(NW+1)/2
      IF(J3.LE.0.OR.J3.GT.NW)GO TO 120
      A(I2,J3)=A(I2,J3)+SS(I1,J1)
  120 CONTINUE
  119 CONTINUE
      DO  121 I=1,NOTP
      II=NNPD(I)
      NST=IDF(II,2)
      DO  122 J3=1,NW
      J=J3+NST-(NW+1)/2
      AJ(I,J)=A(NST,J3)
  122 CONTINUE
  121 CONTINUE
  112 CONTINUE
        *       *       *       *       *       *       *
```

```
      DO 1231 I=1,NVLC
      I1=(NW+1)/2
      IF(A(I,I1).NE.0.0)GO TO 1231
      DO 1232 J=1,NVLC
      J2=J-I+(NW+1)/2
      IF(J2.LE.0.OR.J2.GT.NW)GO TO 1232
      A(I,J2)=0.0
 1232 CONTINUE
      DO 1233 L=1,NVLC
      J2=I-L+(NW+1)/2
      IF(J2.LE.0.OR.J2.GT.NW)GO TO 1233
      A(L,J2)=0.0
 1233 CONTINUE
      A(I,I1)=1.0E18
 1231 CONTINUE
      DO  123 I=1,NVLC
      P(I)=0.0
  123 W(I)=0.0
C                    ***ELIMINATION OF  ROWS  ****
      DO  124 I=1,NOTP
      II=NNPD(I)
      NST=IDF(II,2)
      P(NST)=AMOVE(NSF)
      DO  125 J=1,NVLC
      J2=J-NST+(NW+1)/2
      IF(J2.GT.NW)GO TO 125
      IF(J2.LE.0)GO TO 125
      A(NST,J2)=0.0
  125 CONTINUE
      J4=(NW+1)/2
      IF(J4.GT.NW)GO TO 124
      IF(J4.LE.0)GO TO 124
      A(NST,J4)=1.0
  124 CONTINUE
C        *           *           *           *           *           *
C                    ***TO CALCULATE DISPLACEMENTS  ***
      CALL MSOLB(A,P6,NVLC,NW,1,1,NVLC,NVLC)
      DO  126 I=1,NVLC
```

```
  126 W(I)=P(I)
      DO 127 I=1,NVLC
  127 P(I)=0.0
C        *          *          *          *          *          *
C                   ***TO CALCULATE LOAD  ****
      CALL MMULT(A3,W,P3,NOTP,NVLC,1,NOTP,NVLC,NOTP)
C        *          *          *          *          *          *
C                   ***TO CALCULATE STRESSES  ***
      DO  128 K1=1,NELC
      DO  129 L7=1,NEP
      IF(K1.EQ.IEP(L7))GO TO 130
  129 CONTINUE
      CALL CNE(NODES,COOR,K1,IAA,IBB,ICC,IDD,R,Z)
      CALL CACT(R,Z,IAA,IBB,ICC,IDD,C,CT)
      DO  131 J=1,8
  131 DIS(J)=0.0
      DO  132 J=1,8
      IF(IED(K1,J).EQ.0)GO TO 133
      DIS(J)=W(IED(K1,J))
      GO TO 132
  133 DIS(J)=0.0
  132 CONTINUE
C                   ***  MATRIX  [BN]  ***
      CALL MBN(ZG,RG,K1,BN)
      DO 134 I=1,4
      DO 134 J=1,8
  134 BNC(I,J)=0.0
C                   ***MATRIX [BNC] =[BN]*[C]  **
      CALL MMULT(BN,C,BNC,4,8,8,4,8,4)
      DO 135 I=1,4
      STN(I)=0.0
  135 STS(I)=0.0
C                   ***MATRIX [STN] =[BNC]*[DIS]  ***
      CALL MMULT(BNC,DIS,STN,4,8,1,4,8,4)
C                   *** MATRIX  [D]  ***
      CALL DMAT(PRS,ES,D)
C                   ***MATRIX  [STS] =[D]*[STN]  ***
      CALL MMULT(D,STN,STS,4,4,1,4,4,4)
```

```
      DO  136 J=1,4
  136 STSI(K1,J)=STS(J)
      GO TO 128
  130 CONTINUE
      DO  137 J=1,4
  137 STSI(K1,J)=0.0
  128 CONTINUE
C        *          *          *          *          *          *
C                    ***TO CALCULATE TOTAL LOAD  ***
      ALOAD=0.0
      DO  138 I=1,NOTP
  138 ALOAD=ALOAD+P3(I)
      WRITE(2,1663)(I,P3(I),I=1,NOTP)
 1663 FORMAT(2X,I3,F12.6)
      WRITE(2,1552)
 1552 FORMAT(/10X,1HW,30X,1HP/)
       WRITE(2,1553)(I,W(I),P(I),I=1,NVLC)
 1553 FORMAT(2X,I3,2F12.6)
      WRITE(2,7890)((STSI(I,J),J=1,4),I=1,NELC)
 7890 FORMAT(3X,4E18.6)
      WRITE(2,6002)ALOAD
 6002 FORMAT(2X,F18.10/)
 2080 CONTINUE
 8020 CONTINUE
      STOP
      END
       * * * * * * * * * * * * * * * * * * * * * * * * * * * * *
              S U B R O U T I N E S
       * * * * * * * * * * * * * * * * * * * * * * * * * * * * *

      SUBROUTINE DMAT(PRS,ES,D)
      REAL D(4,4)
      DO 1 I=1,4
      DO 1 J=1,4
    1 D(I,J)=0.0
      ELS=(PRS*ES)/((1.0+PRS)*(1.0-2.0*PRS))
      GS=ES/(2.0*(1.0+PRS))
      D(1,1)=ELS+2.0*GS
```

```
      D(1,2)=ELS
      D(1,3)=ELS
      D(2,1)=ELS
      D(2,2)=D(1,1)
      D(2,3)=ELS
      D(3,1)=ELS
      D(3,2)=ELS
      D(3,3)=D(1,1)
      D(4,4)=GS
      RETURN
      END
C          *          *          *          *          *          *

      SUBROUTINE CNE(NODES,COOR,K1,IAA,IBB,ICC,IDD,R,Z)
      DIMENSION NODES(144,4),COOR(169,2),R(4),Z(4)
      NW1=NODES(K1,1)
      NW2=NODES(K1,2)
      NW3=NODES(K1,3)
      NW4=NODES(K1,4)
      R(IAA)=COOR(NW1,1)
      Z(IAA)=COOR(NW1,2)
      R(IBB)=COOR(NW2,1)
      Z(IBB)=COOR(NW2,2)
      R(ICC)=COOR(NW3,1)
      Z(ICC)=COOR(NW3,2)
      R(IDD)=COOR(NW4,1)
      Z(IDD)=COOR(NW4,2)
      RETURN
      END
C          *          *          *          *          *          *

      SUBROUTINE CACT(R,Z,IAA,IBB,ICC,IDD,C,CT)
      REAL R(4),Z(4),C(8,8),CT(8,8)
      DO 1 I=1,8
      DO 1 J=1,8
      C(I,J)=0.0
    1 CT(I,J)=0.0
      R31=(R(ICC)-R(IAA))/(R(IBB)-R(IAA))
```

```
      R41=(R(IDD)-R(IAA))/(R(IBB)-R(IAA))
      C33=(Z(ICC)-Z(IAA))-(Z(IBB)-Z(IAA))*R31
      C34=(Z(ICC)*R(ICC)-Z(IAA)*R(IAA))-(Z(IBB)*R(IBB)-Z(IAA)*R(IAA))*R3
     *1
      C43=(Z(IDD)-Z(IAA))-(Z(IBB)-Z(IAA))*R41
      C44=(Z(IDD)*R(IDD)-Z(IAA)*R(IAA))-(Z(IBB)*R(IBB)-Z(IAA)*R(IAA))*R4
     *1
      C(4,1)=(R41-1.0-(R31-1.0)*C43/C33)/(C44-C34*C43/C33)
      C(3,1)=(R31-1.0-C(4,1)*C34)/C33
      C(2,1)=(-1.0-C(4,1)*(R(IBB)*Z(IBB)-R(IAA)*Z(IAA))-C(3,1)*
     *(Z(IBB)-Z(IAA)))/(R(IBB)-R(IAA))
      C(1,1)=1.0-C(4,1)*R(IAA)*Z(IAA)-C(3,1)*Z(IAA)-C(2,1)*R(IAA)
      C(4,3)=(-R41+R31*C43/C33)/(C44-C34*C43/C33)
      C(3,3)=(-R31-C(4,3)*C34)/C33
      C(2,3)=(1.0-C(4,3)*(R(IBB)*Z(IBB)-R(IAA)*Z(IAA))-C(3,3)*(Z(IBB)-Z
     *(IAA)))/(R(IBB)-R(IAA))
      C(1,3)=-C(4,3)*R(IAA)*Z(IAA)-C(3,3)*Z(IAA)-C(2,3)*R(IAA)
      C(4,5)=(-C43/C33)/(C44-C34*C43/C33)
      C(3,5)=(1.0-C(4,5)*C34)/C33
      C(2,5)=(-C(4,5)*(R(IBB)*Z(IBB)-R(IAA)*Z(IAA))-C(3,5)*(Z(IBB)-Z(IAA
     *)))/(R(IBB)-R(IAA))
      C(1,5)=-C(4,5)*R(IAA)*Z(IAA)-C(3,5)*Z(IAA)-C(2,5)*R(IAA)
      C(4,7)=1.0/(C44-C34*C43/C33)
      C(3,7)=-C(4,7)*C34/C33
      C(2,7)=-(C(4,7)*(R(IBB)*Z(IBB)-R(IAA)*Z(IAA))+C(3,7)*(Z(IBB)-Z(IAA
     *)))/(R(IBB)-R(IAA))
      C(1,7)=-C(4,7)*R(IAA)*Z(IAA)-C(3,7)*Z(IAA)-C(2,7)*R(IAA)
      DO 2 J=1,7,2
      DO 2 I=1,4
    2 C(I+4,J+1)=C(I,J)
      DO 3 I=1,8
      DO 3 J=1,8
    3 CT(J,I)=C(I,J)
      RETURN
      END
C          *          *          *          *          *

      SUBROUTINE MBN(ZG,RG,K1,BN)
```

```
      REAL BN(4,8),RG(144),ZG(144)
      DO 1 I=1,4
      DO 1 J=1,8
    1 BN(I,J)=0.0
      BN(1,2)=1.0
      BN(1,4)=ZG(K1)
      BN(2,1)=1.0/RG(K1)
      BN(2,2)=1.0
      BN(2,3)=ZG(K1)/RG(K1)
      BN(2,4)=ZG(K1)
      BN(3,7)=1.0
      BN(3,8)=RG(K1)
      BN(4,3)=1.0
      BN(4,4)=RG(K1)
      BN(4,6)=1.0
      BN(4,8)=ZG(K1)
      RETURN
      END
C          *          *          *          *          *          *

      SUBROUTINE SMATR(R,Z,IAA,IBB,ICC,IDD,D,S)
      REAL R(4),Z(4),D(4,4),S(8,8)
C     TO FORM S=[INT(MT*D*M)]
      PI=3.141592
      Z322=(Z(ICC)*Z(ICC)-Z(IBB)*Z(IBB))/2.0
      Z321=Z(ICC)-Z(IBB)
      Z323=(Z(ICC)**3.0-Z(IBB)**3.0)/3.0
      R211=R(IBB)-R(IAA)
      R212=(R(IBB)*R(IBB)-R(IAA)*R(IAA))/2.0
      R213=(R(IBB)**3.0-R(IAA)**3.0)/3.0
      R214=(R(IBB)**4.0-R(IAA)**4.0)/4.0
      AL21=ALOG(R(IBB)/R(IAA))
      P2=2.0*PI
      S(1,3)=P2*(D(2,2)*Z322*AL21+D(2,4)*R211*Z321)
      S(2,3)=P2*((D(1,2)+D(2,2))*Z322+R211+(D(1,4)+D(2,4))*(R212*Z321))
      S(3,3)=P2*(D(2,2)*Z323*AL21+(D(2,4)+D(4,2))*Z322*R211+D(4,4)*
     *R212*Z321)
      S(4,3)=P2*((D(1,2)+D(2,2))*Z323+R211+(D(1,4)+D(2,4)+D(4,2))*Z322*
```

```
*R212+D(4,4)*Z321*R213)
 S(5,3)=0.0
 S(6,3)=P2*(D(4,2)*Z322*R211+D(4,4)*Z321*R212)
 S(7,3)=P2*(D(3,2)*Z322*R211+D(3,4)*Z321*R212)
 S(8,3)=P2*((D(3,2)+D(4,4))*Z322*R212+D(3,4)*Z321*R213+D(4,2)*Z323*
*R211)
 S(1,4)=P2*((D(2,1)+D(2,2))*Z322*R211+D(2,4)*Z321*R212)
 S(2,4)=P2*((D(1,1)+D(1,2)+D(2,1)+D(2,2))*Z322*R212+(D(1,4)+D(2,4))
**R213*Z321)
 S(3,4)=P2*((D(2,1)+D(2,2))*Z323*R211+(D(4,1)+D(4,2)+D(2,4))*Z322*
*R212+D(4,4)*R213*Z321)
 S(4,4)=P2*((D(1,1)+D(1,2)+D(2,1)+D(2,2))*Z323*R212+(D(1,4)+D(2,4)+
*D(4,1)+D(4,2))*R213*Z322+D(4,4)*R214*Z321)
 S(5,4)=0.0
 S(6,4)=P2*((D(4,1)+D(4,2))*Z322*R212+D(4,4)*R213*Z321)
 S(7,4)=P2*((D(3,1)+D(3,2))*Z322*R212+D(3,4)*R213*Z321)
 S(8,4)=P2*((D(3,1)+D(3,2)+D(4,4))*Z322*R213+D(3,4)*R214*Z321+(D(4,
*1)+D(4,2))*Z323*R212)
 S(1,1)=P2*(D(2,2)*AL21*Z321)
 S(2,1)=P2*((D(1,2)+D(2,2))*R211*Z321)
 S(3,1)=P2*(D(2,2)*AL21*Z322+D(4,2)*R211*Z321)
 S(4,1)=P2*((D(1,2)+D(2,2))*Z322*R211+D(4,2)*Z321*R212)
 S(5,1)=0.0
 S(6,1)=P2*(D(4,2)*R211*Z321)
 S(7,1)=P2*(D(3,2)*R211*Z321)
 S(8,1)=P2*(D(3,2)*R212*Z321+D(4,2)*Z322*R211)
 S(1,2)=P2*((D(2,1)+D(2,2))*R211*Z321)
 S(2,2)=P2*((D(1,1)+D(1,2)+D(2,1)+D(2,2))*R212*Z321)
 S(3,2)=P2*((D(2,1)+D(2,2))*Z322*R211+(D(4,1)+D(4,2))*R212*Z321)
 S(4,2)=P2*((D(1,1)+D(1,2)+D(2,1)+D(2,2))*Z322*R212+(D(4,1)+D(4,2))
**R213*Z321)
 S(5,2)=0.0
 S(6,2)=P2*((D(4,1)+D(4,2))*R212*Z321)
 S(7,2)=P2*((D(3,1)+D(3,2))*R212*Z321)
 S(8,2)=P2*((D(3,1)+D(3,2))*R213*Z321+(D(4,1)+D(4,2))*Z322*R212)
 S(1,5)=0.0
 S(2,5)=0.0
 S(3,5)=0.0
```

```
 S(4,5)=0.0
 S(5,5)=0.0
 S(6,5)=0.0
 S(7,5)=0.0
 S(8,5)=0.0
 S(1,6)=P2*(D(2,4)*R211*Z321)
 S(2,6)=P2*(D(1,4)*D(2,4)*R212*Z321)
 S(3,6)=P2*(D(2,4)*Z322*R211+D(4,4)*R212*Z321)
 S(4,6)=P2*((D(1,4)+D(2,4))*Z322*R212+D(4,4)*R213*Z32
 S(5,6)=0.0
 S(6,6)=P2*(D(4,4)*R212*Z321)
 S(7,6)=P2*(D(3,4)*R212*Z321)
 S(8,6)=P2*(D(3,4)*R213*Z321+D(4,4)*R212*Z322)
 S(1,7)=P2*(D(2,3)*R211*Z321)
 S(2,7)=P2*((D(1,3)+D(2,3))*R212*Z321)
 S(3,7)=P2*(D(2,3)*Z322*R211+D(4,3)*Z321*R212)
 S(4,7)=P2*((D(1,3)+D(2,3))*Z322*R212+D(4,3)*R213*Z321)
 S(5,7)=0.0
 S(6,7)=P2*(D(4,3)*R212*Z321)
 S(7,7)=P2*(D(3,3)*R212*Z321)
 S(8,7)=P2*(D(3,3)*R213*Z321+D(4,3)*R212*Z322)
 S(1,8)=P2*(D(2,3)*R212*Z321+D(2,4)*Z322*R211)
 S(2,8)=P2*((D(1,3)+D(2,3))*R213*Z321+(D(1,4)+D(2,4))*R212*Z322)
 S(3,8)=P2*((D(2,3)+D(4,4))*Z322*R212+D(2,4)*Z323*R211+D(4,3)*R213*
*Z321)
 S(4,8)=P2*((D(1,3)+D(2,3)+D(4,4))*R213*Z322+(D(1,4)+D(2,4))*Z323*
*R212+D(4,3)*R214*Z321)
 S(5,8)=0.0
 S(6,8)=P2*(D(4,3)*R213*Z321+D(4,4)*Z322*R212)
 S(7,8)=P2*(D(3,3)*R213*Z321+D(3,4)*Z322*R212)
 S(8,8)=P2*((D(4,3)+D(3,4))*R213*Z322+D(3,3)*R214*Z321+D(4,4)*R212*
*Z323)
 RETURN
 END
 FINISH
```

```
  ******        ******        ******        ******        ******
  ******        ******        ******        ******        ******
```

APPENDIX K

```
C     ***********************************************************

C           * * * N O N-L I N E A R   P R O G R A M * * *

C     ***********************************************************

      PROGRAM GE03(INPUT,OUTPUT,TAPE1=INPUT,TAPE2=OUTPUT)
      DIMENSION IDF(169,2),NODES(144,4),IED(144,8),COOR(169,2),
     *PO(144),PMZ(144),PMO(144),PMR(144),PRZ(144),ZG(144),RG(144),
     *PZ(144),PR(144),C(8,8),CT(8,8),CTS(8,8),SS(8,8),B(4,4),D(4,4)
     *,R(4),Z(4),CGE(144),NNPO(6),S(8,8),ICOL(169),PTS(144),
     *AMOVE(30),A(278,59),A3(6,278),P(278),W(278),P3(6),P6(278,1)
     *,CEAR(12),SUWS(12),SSAN(144),CKOR(144)
      DIMENSION IW(16)
      DIMENSION BB(4)
      DIMENSION DIS(8),BNC(4,8),BN(4,8),SIN(4),STS(4),CSTRE(144,4),
     *STSI(144,4),DSTRE(144,4),PD(6),PTL(30),PF(30),IEP(10)
      COMMON A
      EQUIVALENCE(P(1),P6(1,1))
      LEVEL 2,A
C                              ************

C                     ****  DATA  ****

      NWV=59
      NW=59
      NNOD=169
      NCONS=60
      NLAYERS=12
      NSQUARE=12
      NELC=144
      NNODESL=13
      IDIS=6
      NVLC=278
```

```
      NOTP=6
      NEP=10
      SPW=1700.0
      NSM=30
      NRS1=NNOD-NNODESL+1
      NLS=NVLC-NOTP+1
      NABOVE=53
      NDOWN=27
      PI=3,141592
      AF2=1470.0
      ACG=9.81
      AK1=45.0
      AK2=1650.0
      FI=43.2
      RAD=PI/180.0
      AKR=(1.0-SIN(FI*RAD))/(1.0+SIN(FI*RAD))
C     AKR=0.19
      AF1=70.0
      AKRES=0.26
      H=0.9
      ARAN=1.0/AKR
      GN=0.0
      ESOIL=1000000.0
      PSOIL=0.4
      READ(1,1)(AMOVE(I),I=1,NSM)
      WRITE(2,1)(AMOVE(I),I=1,NSM)
    1 FORMAT(F10.7)
      READ(1,2)(IEP(I),I=1,NEP)
      WRITE(2,2)(IEP(I),I=1,NEP)
    2 FORMAT(I5)
      READ(1,3)(NNPD(I),I=1,NOTP)
      WRITE(2,3)(NNPD(I),I=1,NOTP)
    3 FORMAT(I5)
      READ(1,4)(ICOL(I),I=1,NNOD)
      WRITE(2,4)(ICOL(I),I=1,NNOD)
    4 FORMAT(13I4)
      READ(1,5)(COOR(ICOL(I),1),I=1,NNODESL)
      WRITE(2,5)(COOR(ICOL(I),1),I=1,NNODESL)
```

```
    5 FORMAT(F10.3)
      READ(1,6)(COOR(ICOL(I),2),I=1,NRS1,NNODESL)
      WRITE(2,6)(COOR(ICOL(I),2),I=1,NRS1,NNODESL)
    6 FORMAT(F10.3)
      WRITE(2,10)AKR,ARAN
   10 FORMAT(2F10.5)
C                              ************
C
C              ****DISTRIBUTION  OF  "K. &  U.W.S.****
      READ(1,8)(CEAR(I),I=1,NLAYERS)
      READ(1,7)(SUWS(I),I=1,NSQUARE)
    8 FORMAT(6F10.5)
    7 FORMAT(6F10.1)
      DO 97 I=1,NLAYERS
      DO 97 J=1,NSQUARE
      II=(I-1)*NSQUARE+J
   97 SSAN(II)=SUWS(I)
      DO 98 I=1,NLAYERS
      DO 98 J=1,NSQUARE
      II=(I-1)*NSQUARE+J
   98 CKOR(II)=CEAR(I)
      WRITE(2,99)(SSAN(I),I=1,NELC)
      WRITE(2,99)(CKOR(I),I=1,NELC)
   99 FORMAT(12F10.5)

C                        ******************
C                   ****  NODES  VS  D.  OF  FREEDOM  ****

      DO 100 I=1,NNOD
      DO 100 J=1,2
      IDF(I,J)=1
  100 CONTINUE
      DO 101 IC=1,NCONS
      READ(1,9)I,J
      WRITE(2,9)I,J
    9 FORMAT(2I5)
      IDF(I,J)=0
  101 CONTINUE
```

```
      IK1=1
      DO 102 I=1,NNOD
      DO 102 J=1,2
      IF (IDF(I,J)-1)102,103,103
  103 IDF(I,J)=IK1
      IK1=IK1+1
  102 CONTINUE
C                                  ***********
C
C                     ****  ELEMENTS  VS  NODES  ****
C
      DO 104 NL=1,NLAYERS
      DO 104 NB=1,NSQUARE
      NRR=(NL-1)*NSQUARE+NB
      NRC=(NL-1)*NNODESL+NB
      NRC1=NL*NNODESL+NB
      NODES(NRR,1)=ICOL(NRC)
      NODES(NRR,2)=ICOL(NRC+1)
      NODES(NRR,3)=ICOL(NRC1+1)
      NODES(NRR,4)=ICOL(NRC1)
  104 CONTINUE
C                                  ***********
C
C                    ****  ELEMENTS  VS  D.  OF  FREEDOM  ****
C
      DO 105 I=1,NELC
      DO 105 J=1,4
      IAA=NODES(I,J)
      J3=2*(J-1)
      DO 106 K=1,2
      IED(I,J3+K)=IDF(IAA,K)
  106 CONTINUE
  105 CONTINUE
C                                  ***********
C
C                     ****  NODES  VS  COORDINATES  ****
```

```
      DO 107 NL=1,NLAYERS
      DO 107  I=1,NNODESL
      COOR(ICOL(I+NNODESL*NL),1)=COOR(ICOL(I),1)
  107 CONTINUE
      IX=NNODESL-1
      IY=NLAYERS+1
      DO 108 I=1,IX
      DO 108 NL=1,IY
      NLL=NL-1
      COOR(ICOL(NLL*NNODESL+I+1),2)=COOR(ICOL(NLL*NNODESL+1),2)
  108 CONTINUE
C                                 ***********
      DO 109 I=1,NSM
      PTL(I)=0.0
      PF(I)=0.0
  109 CONTINUE
      PTE=0.0
      DO 110 I=1,NELC
      PR(I)=0.0
      PO(I)=0.0
      PZ(I)=0.0
      PRZ(I)=0.0
      PMR(I)=0.0
      PMO(I)=0.0
      PMZ(I)=0.0
      PTS(I)=0.0
  110 CONTINUE
C                                 ***********
C
C                     ****INITIAL DIRECTION OF INCREMENTAL STRESS ****
      DO 111 K1=1,NELC
      CSTRE(K1,1)=+0.000001
      CSTRE(K1,2)=-0.00001
      CSTRE(K1,3)=+0.00001
  111 CONTINUE

      IAA=1
```

```
      IBB=2
      ICC=3
      IDD=4


C           **          **          **          **          **          **

      DO 112 NSF=1,NSM

C                     ****  ITERATION  ****

      DO 113 IC1=1,1
      DO 114 I=1,NELC
      DO 114 J=1,4
      STSI(I,J)=0.0
  114 CONTINUE
      DO 115 I=1,NVLC
      DO 115 J=1,NW
  115 A(I,J)=0.0
      DO 116 I=1,NOTP
      DO 116 J=1,NVLC
  116 AS(I,J)=0.0

C                     ****  OVERALL  STIFFNESS MATRIX  ****

      DO 117 K1=1,NELC

      DO 118 L7=1,NEP
      IF(K1.EQ.IEP(L7))GO TO 119
  118 CONTINUE
      IF(IC1.EQ.1.AND.NSF.EQ.1)GO TO 120
C           TO CHECK FAILURE OF ELEMENTS
      IF(PR(K1).LE.0.0.OR.PR(K1).GE.PMR(K1))GO TO 119
      IF(PO(K1).LE.0.0.OR.PO(K1).GE.PMO(K1))GO TO 119
      IF(PZ(K1).LE.0.0.OR.PZ(K1).GE.PMZ(K1))GO TO 119
C     IF(PTS(K1).LE.0.0)GO TO 119
      GO TO 120
  119 CONTINUE
```

```
      DO 121 I=1,8
      DO 121 J=1,8
      SS(I,J)=0.0
  121 CONTINUE
C             COORDINATES  OF  ELEMENT
      CALL CNE(NODES,COOR,NELC,NNOD,K1,IAA,IBB,ICC,IDD,R,Z)
C             COORDINATES  OF  CENTROID
      ZG(K1)=(Z(IDD)+Z(IAA))/2.0
      RG(K1)=(R(IBB)+R(IAA))/2.0
      CGE(K1)=(Z(IDD)+Z(IAA))/2.0
      GO TO 122
  120 CONTINUE
C             COORDINATES  OF  ELEMENT
      CALL CNE(NODES,COOR,NELC,NNOD,K1,IAA,IBB,ICC,IDD,R,Z)
      IF(NSF.NE.1)GO TO 123
      IF(IC1.NE.1)GO TO 123
C             COORDINATES  OF  CENTROID
      ZG(K1)=(Z(IDD)+Z(IAA))/2.0
      RG(K1)=(R(IBB)+R(IAA))/2.0
      CGE(K1)=(Z(IAA)+Z(IDD))/2.0
  123 CONTINUE
      DO 124 I=1,8
      DO 124 J=1,8
      C(I,J)=0.0
      CT(I,J)=0.0
      CTS(I,J)=0.0
      SS(I,J)=0.0
      S(I,J)=0.0
  124 CONTINUE
C             MATRIX  [C]
      CALL CACT(R,Z,IAA,IBB,ICC,IDD,C)
C             MATRIX  [CT]
      DO 126 I=1,8
      DO 126 J=1,8
      CT(J,I)=C(I,J)
  126 CONTINUE
      IF(NSF.NE.1)GO TO 127
      IF(IC1.NE.1)GO TO 127
```

```
      PZ(K1)=0.0
      PR(K1)=0.0
      PO(K1)=0.0
      PRZ(K1)=0.0
      PMZ(K1)=0.0
      PMO(K1)=0.0
      PMR(K1)=0.0
C             INITIAL  STRESSES
      SPW=SSAN(K1)
      AKRES=CKOR(K1)
      PZ(K1)=SPW*ACG*(H-CGE(K1))
      PR(K1)=AKRES*PZ(K1)
      PO(K1)=PR(K1)
      PRZ(K1)=0.0
      PMZ(K1)=ARAN*SQRT(PO(K1)*PR(K1))
      PMO(K1)=ARAN*SQRT(PZ(K1)*PR(K1))
      PMR(K1)=ARAN*SQRT(PZ(K1)*PO(K1))
  127 CONTINUE
      DO 128 I=1,4
      DO 128 J=1,4
      B(I,J)=0.0
      D(I,J)=0.0
  128 CONTINUE
C             STRAIN-STRESS RELATIONSHIP
      CALL BMAT(PR,PO,PZ,PMR,PMO,PMZ,CSTRE,NELC,K1,GN,
     *AK2,AKR,AK1,AF1,AF2,ESOIL,PSOIL,B)
      DO 135 I=1,4
  135 BB(I)=1.0
C             STRESS-STRAIN  RELATIONSHIP
      CALL MSOLVE(B,BB,4,4,2,2)
      DO 136 I=1,4
      DO 136 J=1,4
      D(I,J)=B(I,J)
  136 CONTINUE
C             MATRIX  [S]
      CALL SMATR(R,Z,IAA,IBB,ICC,IDD,D,S)
C             MATRIX  [CTS]
      CALL MMULT(CT,S,CTS,8,8,8,8,8,8)
```

```
C            MATRIX  [SS]       -    ELEMENT  STIFFNESS  MATRIX
      CALL MMULT(CTS,C,SS,8,8,8,8,8,8)
  122 CONTINUE
C     TO FORM OVERALL STIFNESS MATRIX [SM]
      DO 137 I1=1,8
      I2=IED(K1,I1)
      IF(I2.EQ.0) GO TO 137
      IF(I2.GT.NVLC) GO TO 137
      DO 138 J1=1,8
      J2=IED(K1,J1)
      IF(J2.EQ.0)GO TO 138
      IF(J2.GT.NVLC) GO TO 138
      J3=J2-I2+(NW+1)/2
      IF(J3.LE.0.OR.J3.GT.NW)GO TO 138
      A(I2,J3)=A(I2,J3)+SS(I1,J1)
  138 CONTINUE
  137 CONTINUE
  117 CONTINUE
C          **          **          **          **          **          **

      WRITE(2,15)(PR(I),PZ(I),PO(I),PRZ(I),PMR(I),PMZ(I),P
     *MO(I),PYS(I),I=1,NELC)
   15  FORMAT(3X,8F12.2)

C                    ****  TO  GENERATE  [A3]  ****
      DO 139 I=1,NOTP
      II=NNPD(I)
      NST=IDF(II,2)
      DO 140 J3=1,NWV
      J=J3+NST-(NW+1)/2
      IF(J.LE.0.OR.J.GT.NVLC)GO TO 140
      A3(I,J)=A(NST,J3)
  140 CONTINUE
  139 CONTINUE

C                    ****  TO  CHECK DIAGONAL  OF  THE  [A]  ****

      DO 141 I=1,NVLC
```

```
      I1=(NW+1)/2
      IF(A(I,I1).NE.0.0)GO TO 141
      DO 142 J=1,NVLC
      J2=J-I+(NW+1)/2
      IF(J2.LE.0.OR.J2.GT.NW)GO TO 142
      A(I,J2)=0.0
  142 CONTINUE
      DO 143 L=1,NVLC
      J2=I-L+(NW+1)/2
      IF(J2.LE.0.OR.J2.GT.NW)GO TO 143
      A(L,J2)=0.0
  143 CONTINUE
      A(I,I1)=1.0E18
  141 CONTINUE

      DO 144 I=1,NVLC
      P(I)=0.0
  144 W(I)=0.0

C             INSERT  THE  KNOWN  DISPLACEMENTS  IN  LOAD  MATRIX
C             ZERO  THE  CORRESPONDING  ROWS  OF  [A]
C             PUT  1  IN  THE  DIAGONAL  ELEMENTS  OF  THESE  ROWS

      DO 145 I=1,NOTP
      II=NNPD(I)
      NST=IDF(II,2)
      P(NST)=AMOVE(NSF)
      DO 146  J=1,NVLC
      J2=J-NST+(NW+1)/2
      IF(J2.GT.NW)GO TO 146
      IF(J2.LE.0)GO TO 146
      A(NST,J2)=0.0
  146 CONTINUE
      J4=(NW+1)/2
      IF(J4.GT.NW)GO TO 145
      IF(J4.LE.0)GO TO 145
      A(NST,J4)=1.0
  145 CONTINUE
```

```
C                                  **********

C                        ****  TO  CALCULATE  DISPLACEMENTS  ****

      CALL MSOLB(A,P6,NVLC,NW,1,1,NVLC,NVLC)
      DO 149 I=1,NVLC
  149 W(I)=P(I)

      DO 150 I=1,NVLC
  150 P(I)=0.0
C                                  ***********

C                        ****  TO  CALCULATE  LOAD  ****
      CALL MMULT(A3,W,P3,NOTP,NVLC,1,NOTP,NVLC,NOTP)
C                                  ***********

      WRITE(2,1663)(I,P3(I),I=1,NOTP)
 1663 FORMAT(2X,I3,F12.6)



C                        ****  INCREMENTAL STRESSES  ****
      DO 151 K1=1,NELC
      IF(PR(K1).LE.0.0.OR.PR(K1).GE.PMR(K1))GO TO 152
      IF(PO(K1).LE.0.0.OR.PO(K1).GE.PMO(K1))GO TO 152
      IF(PZ(K1).LE.0.0.OR.PZ(K1).GE.PMZ(K1))GO TO 152
C     IF(PTS(K1).LE.0.0)GO TO 152
      CALL CNE(NODES,COOR,NELC,NNOD,K1,IAA,IBB,ICC,IDD,R,Z)
C           MATRIX  [C]
      DO 153 I=1,8
      DO 153 J=1,8
  153 C(I,J)=0.0
      CALL CACT(R,Z,IAA,IBB,ICC,IDD,C)
      DO 155 J=1,8
  155 DIS(J)=0.0
C           DISPLAACEMENT  AT  EACH  NODE  OF  ELEMENT
      DO 156 J=1,8
```

```
      IF(IED(K1,J).EQ.0)GO TO 157
      DIS(J)=W(IED(K1,J))
      GO TO 156
  157 DIS(J)=0.0
  156 CONTINUE
      DO 158 I=1,4
      DO 158 J=1,8
      BNC(I,J)=0.0
      BN(I,J)=0.0
  158 CONTINUE
C             MATRIX  [BN]
      CALL MMBN(ZG,RG,NELC,K1,BN)
      DO 159 I=1,4
      STN(I)=0.0
      STS(I)=0.0
  159 CONTINUE
C             MATRIX  [BNC]
      CALL MMULT(BN,C,BNC,4,8,8,4,8,4)
C             MATRIX  [STN]
      CALL MMULT(BNC,DIS,STN,4,8,1,4,8,4)
      DO 160 I=1,4
      DO 160 J=1,4
      B(I,J)=0.0
      D(I,J)=0.0
  160 CONTINUE
C             STRAIN-SRESS  RELATIONSHIP
      CALL BMAT(PR,PO,PZ,PMR,PMO,PMZ,CSTRE,NELC,K1,GN,
     *AK2,AKR,AK1,AF1,AF2,ESOIL,PSOIL,B)
      DO 161 I=1,4
  161 BB(I)=1.0
C             STESS-STRAIN  RELATIONSHIP
      CALL MSOLVE(B,BB,4,4,2,2)
      DO 162 I=1,4
      DO 162 J=1,4
      D(I,J)=B(I,J)
  162 CONTINUE
C             INCREMENTAL  STRESSES
      CALL MMULT(D,STN,STS,4,4,1,4,4,4)
```

```
      DO 163 J=1,4
  163 STSI(K1,J)=-STS(J)
      GO TO 151
  152 CONTINUE
C             ELEMENT  DOES NOT  EXIST
      DO 165 J=1,4
  165 STSI(K1,J)=0.0
  151 CONTINUE
      IF(IC1.NE.1)GO TO 164
C             FIRST  ITERATION
      DO 167 I=1,NELC
      DO 167 J=1,4
  167 CSTRE(I,J)=0.0
      DO 168 I=1,NELC
      DO 168 J=1,4
  168 CSTRE(I,J)=STSI(I,J)
      GO TO 113
  164 CONTINUE
C             ALL  ITERATIONS  EXEPT  THE FIRST  ONE
      DO 169 I=1,NELC
      DO 169 J=1,4
  169 DSTRE(I,J)=0.0
C             DIFFERENCE  BETWEEN  TWO  CONS.  INCREMENTAL  STRESSES
      DO 170  I=1,NELC
      DO 170  J=1,4
  170 DSTRE(I,J)=STSI(I,J)-CSTRE(I,J)
      DO 171  I=1,NELC
      DO 171 J=1,4
  171 CSTRE(I,J)=0.0
      IF(IC1.LE.2)GO TO 172
C     DO 173 I=1,NELC
C     DO 173 J=1,4
C 173 IF(ABS(DSTRE(I,J)).GT.1.0E-6)GO TO 172
       GO TO 174
  172 CONTINUE
      DO 175 I=1,NELC
      DO 175 J=1,4
  175 CSTRE(I,J)=STSI(I,J)
```

```
  113 CONTINUE
C          **          **          **          **          **          **

  174 CONTINUE
C             TOTAL  STRESSES
      DO 176 I=1,NELC
      DO 176 J=1,4
  176 CSTRE(I,J)=STSI(I,J)
      DO 177 I=1,NELC
      PR(I)=PR(I)+STSI(I,1)
      PO(I)=PO(I)+STSI(I,2)
      PZ(I)=PZ(I)+STSI(I,3)
      PRZ(I)=PRZ(I)+STSI(I,4)
      PMR(I)=0.0
      PMO(I)=0.0
      PMZ(I)=0.0
      PTS(I)=0.0
      IF((PR(I).LE.0.0).OR.(PO(I).LE.0.0).OR.(PZ(I).LE.0.0))GO TO 177
      PMR(I)=ARAN*SQRT(PO(I)*PZ(I))
      PMO(I)=ARAN*SQRT(PR(I)*PZ(I))
      PMZ(I)=ARAN*SQRT(PR(I)*PO(I))
      X11=PR(I)+PZ(I)
      X12=SQRT((PZ(I)-PR(I))*(PZ(I)-PR(I))+4.0*PRZ(I)*PRZ(I))
      PTS(I)=(X11-X12)/2.0
  177 CONTINUE
C             TOTAL  LOAD
      PDS=0.0
      DO 178 I=1,NOTP
      IF(P3(I).GT.1.0E6.OR.P3(I).LT.0.0)GO TO 178
      PDS=PDS+P3(I)
  178 CONTINUE
      PTL(NSF)=PDS
       PTE=PTE+PTL(NSF)
      PF(NSF)=PTE
      WRITE(2,6001)
 6001 FORMAT(/3X,2HPF/)
      WRITE(2,6002)(PF(I),I=1,NSF)
 6002 FORMAT(2X,F20.6)
```

```
      NSF1=NSF-1
      FACTOR=PF(NSF)-PF(NSF1)
      IF(ABS(FACTOR).LE.10.0E-6)GO TO 179
  112 CONTINUE
C          **          **          **          **          **          **

  179 STOP
      END
C      * * * * * * * * * * * * * * * * * * * * * * * * * *
C                    S U B R O U T I N E S
C      * * * * * * * * * * * * * * * * * * * * * * * * * *

      SUBROUTINE CNE(NODES,COOR,NELC,NNOD,K1,IAA,IBB,ICC,
     *IDD,R,Z)
      DIMENSION NODES(NELC,4),COOR(NNOD,2),R(4),Z(4)
      NW1=NODES(K1,1)
      NW2=NODES(K1,2)
      NW3=NODES(K1,3)
      NW4=NODES(K1,4)
      R(IAA)=COOR(NW1,1)
      Z(IAA)=COOR(NW1,2)
      R(IBB)=COOR(NW2,1)
      Z(IBB)=COOR(NW2,2)
      R(ICC)=COOR(NW3,1)
      Z(ICC)=COOR(NW3,2)
      R(IDD)=COOR(NW4,1)
      Z(IDD)=COOR(NW4,2)
      RETURN
      END
C     *     *     *     *     *     *     *     *     *     *     *

      SUBROUTINE CACT(R,Z,IAA,IBB,ICC,IDD,C)
      REAL R(4),Z(4),C(8,8)
      R31=(R(ICC)-R(IAA))/(R(IBB)-R(IAA))
      R41=(R(IDD)-R(IAA))/(R(IBB)-R(IAA))
      C33=(Z(ICC)-Z(IAA))-(Z(IBB)-Z(IAA))*R31
      C34=(Z(ICC)*R(ICC)-Z(IAA)*R(IAA))-(Z(IBB)*R(IBB)-Z(IAA)*R(IAA))*R3
     *1
```

```
      C43=(Z(IDD)-Z(IAA))-(Z(IBB)-Z(IAA))*R41
      C44=(Z(IDD)*R(IDD)-Z(IAA)*R(IAA))-(Z(IBB)*R(IBB)-Z(IAA)*R(IAA))*R4
     *1
      C(4,1)=(R41-1.0-(R31-1.0)*C43/C33)/(C44-C34*C43/C33)
      C(3,1)=(R31-1.0-C(4,1)*C34)/C33
      C(2,1)=(-1.0-C(4,1)*(R(IBB)*Z(IBB)-R(IAA)*Z(IAA))-C(3,1)*
     *(Z(IBB)-Z(IAA)))/(R(IBB)-R(IAA))
      C(1,1)=1.0-C(4,1)*R(IAA)*Z(IAA)-C(3,1)*Z(IAA)-C(2,1)*R(IAA)
      C(4,3)=(-R41+R31*C43/C33)/(C44-C34*C43/C33)
      C(3,3)=(-R31-C(4,3)*C34)/C33
      C(2,3)=(1.0-C(4,3)*(R(IBB)*Z(IBB)-R(IAA)*Z(IAA))-C(3,3)*(Z(IBB)-Z
     *(IAA)))/(R(IBB)-R(IAA))
      C(1,3)=-C(4,3)*R(IAA)*Z(IAA)-C(3,3)*Z(IAA)-C(2,3)*R(IAA)
      C(4,5)=(-C43/C33)/(C44-C34*C43/C33)
      C(3,5)=(1.0-C(4,5)*C34)/C33
      C(2,5)=(-C(4,5)*(R(IBB)*Z(IBB)-R(IAA)*Z(IAA))-C(3,5)*(Z(IBB)-Z(IAA
     *)))/(R(IBB)-R(IAA))
      C(1,5)=-C(4,5)*R(IAA)*Z(IAA)-C(3,5)*Z(IAA)-C(2,5)*R(IAA)
      C(4,7)=1.0/(C44-C34*C43/C33)
      C(3,7)=-C(4,7)*C34/C33
      C(2,7)=-(C(4,7)*(R(IBB)*Z(IBB)-R(IAA)*Z(IAA))*C(3,7)*(Z(IBB)-Z(IAA
     *)))/(R(IBB)-R(IAA))
      C(1,7)=-C(4,7)*R(IAA)*Z(IAA)-C(3,7)*Z(IAA)-C(2,7)*R(IAA)
      DO 1 J=1,7,2
      DO 1 I=1,4
      C(I+4,J+1)=C(I,J)
    1 CONTINUE
      RETURN
      END
C     *     *     *     *     *     *     *     *     *

      SUBROUTINE BMAT(PR,PO,PZ,PMR,PMO,PMZ,CSTRE,NELC,
     *K1,GN,AK2,AKR,AK1,AF1,AF2,ESOIL,PSOIL,B)
      REAL PR(NELC),PO(NELC),PZ(NELC),PMR(NELC),PMO(NELC),
     *PMZ(NELC),CSTRE(NELC,4),B(4,4)
      AR1=PMR(K1)/PR(K1)
      AR2=PMO(K1)/PO(K1)
      AR3=PMZ(K1)/PZ(K1)
```

```
      PROS=SQRT(PR(K1)*PO(K1))
      POZS=SQRT(PO(K1)*PZ(K1))
      PZRS=SQRT(PZ(K1)*PR(K1))
      ER=EXP(-AR1*PR(K1)/POZS)
      EO=EXP(-AR2*PO(K1)/PZRS)
      EZ=EXP(-AR3*PZ(K1)/PROS)
      PZRG=(PZ(K1)/PR(K1))**GN
      PORG=(PO(K1)/PR(K1))**GN
      PZOG=(PZ(K1)/PO(K1))**GN
      PROG=(PR(K1)/PO(K1))**GN
      POZG=(PO(K1)/PZ(K1))**GN
      PRZG=(PR(K1)/PZ(K1))**GN
      IF(CSTRE(K1,1).LT.0.0)GO TO 2
C     LOADING
      B(1,2)=-1.0/((AK2*PR(K1)/PZ(K1))*(PZRS/AKR-PO(K1)))
      B(1,1)=1.0/(AK1*((POZS/AKR)-PR(K1)))
      B(1,3)=-1.0/((AK2*PR(K1)/PO(K1))*(PROS/AKR-PZ(K1)))
      GO TO 3
C     ULOADING
    2 B(1,1)=ER/(AF1*POZS)
      B(1,2)=-EO/(AF2*PZRG*PZRS)
      B(1,3)=-EZ/(AF2*PORG*PROS)
    3 IF(CSTRE(K1,2).LT.0.0)GO TO 4
C     LOADING
      B(2,1)=-1.0/((AK2*PO(K1)/PZ(K1))*(POZS/AKR-PR(K1)))
      B(2,2)=1.0/(AK1*(PZRS/AKR-PO(K1)))
      B(2,3)=-1.0/((AK2*PO(K1)/PR(K1))*(PROS/AKR -PZ(K1)))
      GO TO 5
C     ULOADING
    4 B(2,1)=-ER/(AF2*PZOG*POZS)
      B(2,2)=EO/(AF1*PZRS)
      B(2,3)=-EZ/(AF2*PROG*PROS)
    5 IF(CSTRE(K1,3).LT.0.0)GO TO 6
C     LOADING
      B(3,1)=-1.0/((AK2*PZ(K1)/PO(K1))*(POZS/AKR-PR(K1)))
      B(3,2)=-1.0/((AK2*PZ(K1)/PR(K1))*(PZRS/AKR-PO(K1)))
      B(3,3)=1.0/(AK1*(PROS/AKR-PZ(K1)))
      GO TO 7
```

```
C       ULOADING
      6 B(3,1)=-ER/(AF2*POZG*POZS)
        B(3,2)=-EC/(AF2*PRZG*PZRS)
        B(3,3)=EZ/(AF1*PROS)
      7 CONTINUE
C       ESOIL=(1.0/B(1,1)+1.0/B(3,3))/2.0
C       PSOIL=-(B(1,3)/B(1,1)+B(3,1)/B(3,3))/2.0
        GSOIL=ESOIL/(2.0*(1.0+PSOIL))
        B(4,4)=1.0/GSOIL
        RETURN
        END
C       *     *     *     *     *     *     *     *     *

C       TO FORM S=[INT(MT*D*M)]
        SUBROUTINE SMATR(R,Z,IAA,IBB,ICC,IDD,D,S)
        REAL R(4),Z(4),D(4,4),S(8,8)
        PI=3.141592
        Z322=(Z(ICC)*Z(ICC)-Z(IBB)*Z(IBB))/2.0
        Z321=Z(ICC)-Z(IBB)
        Z323=(Z(ICC)**3-Z(IBB)**3)/3.0
        R211=R(IBB)-R(IAA)
        R212=(R(IBB)*R(IBB)-R(IAA)*R(IAA))/2.0
        R213=(R(IBB)**3-R(IAA)**3)/3.0
        R214=(R(IBB)**4-R(IAA)**4)/4.0
        AL21=ALOG(R(IBB)/R(IAA))
        P2=2.0*PI
        S(1,3)=P2*(D(2,2)*Z322*AL21+D(2,4)*R211*Z321)
        S(2,3)=P2*((D(1,2)+D(2,2))*Z322*R211+(D(1,4)+D(2,4))*(R212*Z321))
        S(3,3)=P2*(D(2,2)*Z323*AL21+(D(2,4)+D(4,2))*Z322*R211+D(4,4)*
       *R212*Z321)
        S(4,3)=P2*((D(1,2)+D(2,2))*Z323*R211+(D(1,4)+D(2,4)+D(4,2))*Z322*
       *R212+D(4,4)*Z321*R213)
        S(5,3)=0.0
        S(6,3)=P2*(D(4,2)*Z322*R211+D(4,4)*Z321*R212)
        S(7,3)=P2*(D(3,2)*Z322*R211+D(3,4)*Z321*R212)
        S(8,3)=P2*((D(3,2)+D(4,4))*Z322*R212+D(3,4)*Z321*R213+D(4,2)*Z323*
       *R211)
        S(1,4)=P2*((D(2,1)+D(2,2))*Z322*R211+D(2,4)*Z321*R212)
```

```
 S(2,4)=P2*((D(1,1)+D(1,2)+D(2,1)+D(2,2))*Z322*R212+(D(1,4)+D(2,4))
**R213*Z321)
 S(3,4)=P2*((D(2,1)+D(2,2))*Z323*R211+(D(4,1)+D(4,2)+D(2,4))*Z322*
*R212+D(4,4)*R213*Z321)
 S(4,4)=P2*((D(1,1)+D(1,2)+D(2,1)+D(2,2))*Z323*R212+(D(1,4)+D(2,4)+
*D(4,1)+D(4,2))*R213*Z322+D(4,4)*R214*Z321)
 S(5,4)=0.0
 S(6,4)=P2*((D(4,1)+D(4,2))*Z322*R212+D(4,4)*R213*Z321)
 S(7,4)=P2*((D(3,1)+D(3,2))*Z322*R212+D(3,4)*R213*Z321)
 S(8,4)=P2*((D(3,1)+D(3,2)+D(4,4))*Z322*R213+D(3,4)*R214*Z321+(D(4,
*1)+D(4,2))*Z323*R212)
 S(1,1)=P2*(D(2,2)*AL21*Z321)
 S(2,1)=P2*((D(1,2)+D(2,2))*R211*Z321)
 S(3,1)=P2*(D(2,2)*AL21*Z322+D(4,2)*R211*Z321)
 S(4,1)=P2*((D(1,2)+D(2,2))*Z322*R211+D(4,2)*Z321*R212)
 S(5,1)=0.0
 S(6,1)=P2*(D(4,2)*R211*Z321)
 S(7,1)=P2*(D(3,2)*R211*Z321)
 S(8,1)=P2*(D(3,2)*R212*Z321+D(4,2)*Z322*R211)
 S(1,2)=P2*((D(2,1)+D(2,2))*R211*Z321)
 S(2,2)=P2*((D(1,1)+D(1,2)+D(2,1)+D(2,2))*R212*Z321)
 S(3,2)=P2*((D(2,1)+D(2,2))*Z322*R211+(D(4,1)+D(4,2))*R212*Z321)
 S(4,2)=P2*((D(1,1)+D(1,2)+D(2,1)+D(2,2))*Z322*R212+(D(4,1)+D(4,2))
**R213*Z321)
 S(5,2)=0.0
 S(6,2)=P2*((D(4,1)+D(4,2))*R212*Z321)
 S(7,2)=P2*((D(3,1)+D(3,2))*R212*Z321)
 S(8,2)=P2*((D(3,1)+D(3,2))*R213*Z321+(D(4,1)+D(4,2))*Z322*R212)
 S(1,5)=0.0
 S(2,5)=0.0
 S(3,5)=0.0
 S(4,5)=0.0
 S(5,5)=0.0
 S(6,5)=0.0
 S(7,5)=0.0
 S(8,5)=0.0
 S(1,6)=P2*(D(2,4)*R211*Z321)
 S(2,6)=P2*(D(1,4)*D(2,4)*R212*Z321)
```

```
      S(3,6)=P2*(D(2,4)*Z322*R211+D(4,4)*R212*Z321)
      S(4,6)=P2*((D(1,4)+D(2,4))*Z322*R212+D(4,6)*R213*Z321)
      S(5,6)=0.0
      S(6,6)=P2*(D(4,4)*R212*Z321)
      S(7,6)=P2*(D(3,4)*R212*Z321)
      S(8,6)=P2*(D(3,4)*R213*Z321+D(4,4)*R212*Z322)
      S(1,7)=P2*(D(2,3)*R211*Z321)
      S(2,7)=P2*((D(1,3)+D(2,3))*R212*Z321)
      S(3,7)=P2*(D(2,3)*Z322*R211+D(4,3)*Z321*R212)
      S(4,7)=P2*((D(1,3)+D(2,3))*Z322*R212+D(4,3)*R213*Z321)
      S(6,7)=P2*(D(4,3)*R212*Z321)
      S(7,7)=P2*(D(3,3)*R212*Z321)
      S(8,7)=P2*(D(3,3)*R213*Z321+D(4,3)*R212*Z322)
      S(1,8)=P2*(D(2,3)*R212*Z321+D(2,4)*Z322*R211)
      S(2,8)=P2*((D(1,3)+D(2,3))*R213*Z321+(D(1,4)+D(2,4))*R212*Z322)
      S(3,8)=P2*((D(2,3)+D(4,4))*Z322*R212+D(2,4)*Z323*R211+D(4,3)*R213*
     *Z321)
      S(4,8)=P2*((D(1,3)+D(2,3)+D(4,4))*R213*Z322+(D(1,4)+D(2,4))*Z323*
     *R212+D(4,3)*R214*Z321)
      S(5,8)=0.0
      S(6,8)=P2*(D(4,3)*R213*Z321+D(4,4)*Z322*R212)
      S(7,8)=P2*(D(3,3)*R213*Z321+D(3,4)*Z322*R212)
      S(8,8)=P2*((D(4,3)+D(3,4))*R213*Z322+D(3,3)*R214*Z321+D(4,4)*R212*
     *Z323)
      RETURN
      END
C     *     *     *     *     *     *     *     *     *

      SUBROUTINE MMBN(ZG,RG,NELC,K1,BN)
      REAL BN(4,8),RG(NELC),ZG(NELC)
      BN(1,2)=1.0
      BN(1,4)=ZG(K1)
      BN(2,1)=1.0/RG(K1)
      BN(2,2)=1.0
      BN(2,3)=ZG(K1)/RG(K1)
      BN(2,4)=ZG(K1)
      BN(3,7)=1.0
      BN(3,8)=RG(K1)
```

```
      BN(4,3)=1.0
      BN(4,4)=RG(K1)
      BN(4,6)=1.0
      BN(4,8)=ZG(K1)
      RETURN
      END
C     *     *     *     *     *     *     *     *     *

      SUBROUTINE MMULT(A,B,C,M,N,L,IA,IB,IC)
      DIMENSION A(IA,N),B(IB,L),C(IC,L)
      DO 51 I=1,M
      DO 51 K=1,L
      SUM=0.0
      DO 52 J=1,N
      D=A(I,J)*B(J,K)
      SUM=SUM+D
   52 CONTINUE
      C(I,K)=SUM
   51 CONTINUE
      RETURN
      END
      *     *     *     *     *     *     *     *     *

      SUBROUTINE MSOLB(A,B,N,NW,NR,NL,IA,IB)
      DIMENSION A(IA,NW),B(IB,NR)
      LEVEL 2,A
      M=(NW+1)/2
      MM1=M-1
      I=N
      DO 14 L1=1,N
      IF(NL)1,4,1
      A(I,M)=1.0/A(I,M)
      J=MM1
      DO 3 L2=1,MM1
      IF(I+J-M)4,4,2
      A(I,J)=A(I,J)*A(I,M)
      J=J-1
      CONTINUE
```

```
4       DO 5 L=1,NR
        B(I,L)=B(I,L)*A(I,M)
5       CONTINUE
        IF(I-1)15,15,6
6       DO 12 K=1,MM1
        I1=I-K
        IF(I1)13,13,7
7       I2=M+K
        IF(NL)8,11,8
8       J=MM1
        DO 10 L2=1,MM1
        IF(I+J-M)11,11,9
9       I3=J+K
        A(I1,I3)=A(I1,I3)-A(I,J)*A(I1,I2)
        J=J-1
10      CONTINUE
11      DO 12 L=1,NR
        B(I1,L)=B(I1,L)-B(I,L)*A(I1,I2)
12      CONTINUE
13      I=I-1
14      CONTINUE
15      DO 19 I=2,N
        J=MM1
        DO 18 L1=1,MM1
        I1=I+J-M
        IF(I1)19,19,16
16      DO 17 L=1,NR
        B(I,L)=B(I,L)-B(I1,L)*A(I,J)
17      CONTINUE
        J=J-1
18      CONTINUE
19      CONTINUE
        RETURN
        END
C       *     *     *     *     *     *     *     *     *

        SUBROUTINE MSOLVE(A,B,N,IA,KONT,OUT)
        DIMENSION A(IA,N),B(N),C(100),IND(100)
```

```
      INTEGER OUT
      M=N
      IF(IA-M) 20,80,80
   20 WRITE(OUT,90) IA,M
   90 FORMAT( 51HOMSOLVE ERROR- THE FIRST DIMENSION OF THE MATRIX IS I3,
     133H BUT THE ORDER OF THE MATRIX IS  I3 ///)
      STOP
   80 IF(KONT.EQ.1.OR.KONT.EQ.2)GO TO 100
      WRITE(OUT,91) KONT
   91 FORMAT(22HOMSOLVE ERROR- KONT IS I3,23H.  IT SHOULD BE 1 OR 2,///)
      STOP
  100 AMAX=0.0
      DO 2 I=1,M
      IND(I)=I
      IF (ABS(A(I,1))-AMAX) 2,2,3
    3 AMAX=ABS(A(I,1))
      I4=I
    2 CONTINUE
      MM=M-1
      DO 111 J=1,MM
      IF (I4-J) 6,6,4
    4 ISTO=IND(J)
      IND(J)=IND(I4)
      IND(I4)=ISTO
      DO 5 K=1,M
      STO=A(I4,K)
      A(I4,K)=A(J,K)
      A(J,K)=STO
    5 CONTINUE
      GO TO (7,6),KONT
    7 STO=B(I4)
      B(I4)=B(J)
      B(J)=STO
    6 AMAX=0.0
      J1=J+1
      IF(A(J,J).EQ.0.0)WRITE(OUT,92) J
   92 FORMAT(34HOMSOLVE ERROR- THE DIAGONAL ON ROW  I3, 9H IS ZERO.
     1 24HYOUR MATRIX IS SINGULAR.  ///)
```

```
      DO 11 I=J1,M
      A(I,J)=A(I,J)/A(J,J)
      DO 10 K=J1,M
      A(I,K)=A(I,K)-A(I,J)*A(J,K)
      IF (K-J1) 14,14,10
   14 IF (ABS(A(I,K))-AMAX) 10,10,17
   17 AMAX=ABS(A(I,K))
      I4=I
   10 CONTINUE
    9 GO TO (12,11),KONT
   12 B(I)=B(I)-A(I,J)*B(J)
   11 CONTINUE
  111 CONTINUE
      IF(A(M,M))94,93,94
   93 WRITE(10,92) M
      STOP
   94 GO TO (19,18),KONT
   19 DO 127 I1=1,M
      I=M+1-I1
      IF (M-I) 327,327,28
   28 I2=I+1
      DO 32 K=I2,M
      B(I)=B(I)-A(I,K)*B(K)
   32 CONTINUE
  327 B(I)=B(I)/A(I,I)
  127 CONTINUE
   18 IF(KONT.EQ.1)RETURN
      DO 140 I1=1,MM
      I=M+1-I1
      I2=I-1
      DO 41 J1=1,I2
      J=I2+1-J1
      J2=J+1
      W1=-A(I,J)
      IF (I2-J2) 141,43,43
   43 DO 42 K=J2,I2
      W1=W1-A(K,J)*C(K)
   42 CONTINUE
```

```
141 C(J)=W1
 41 CONTINUE
    DO 40 K=1,I2
    A(I,K)=C(K)
 40 CONTINUE
140 CONTINUE
    DO 150 I1=1,M
    I=N+1-I1
    I2=I+1
    W=A(I,I)
    IF(W)95,96,95
 96 WRITE(OUT,92) I
    STOP
 95 DO 56 J=1,M
    IF (I-J) 52,53,54
 52 W1=0.0
    GO TO 55
 53 W1=1.0
    GO TO 55
 54 W1=A(I,J)
 55 IF (I1-1) 156,156,57
 57 DO 58 K=I2,M
    W1=W1-A(I,K)*A(K,J)
 58 CONTINUE
156 C(J)=W1
 56 CONTINUE
    DO 50 J=1,M
    A(I,J)=C(J)/W
 50 CONTINUE
150 CONTINUE
    DO 60 I=1,M
 63 IF (IND(I)-I) 61,60,61
 61 J=IND(I)
    DO 62 K=1,M
    STO=A(K,I)
    A(K,I)=A(K,J)
    A(K,J)=STO
 62 CONTINUE
```

```
      ISTO=IND(J)
      IND(J)=J
      IND(I)=ISTO
      GO TO 63
   60 CONTINUE
      RETURN
      END

C      ******      ******      ******      ******      ******
C      ******      ******      ******      ******      ******
```

APPENDIX L

COMPUTER PROGRAMS

The following notation is used in the computer programs:-

DI = Anchor plate diameter in inches.

D_s = Diameter of shaft.

H = Depth of anchor plate.

RD = Relative depth.

FORCE = Ultimate load of anchor.

FV1 = Ultimate load of anchor with F_q = 13.27.

FV2 = Ultimate load of anchor unit F_q = 15.70.

FII = ϕ

PI = π

NP = Number of anchor plates.

NRD = Number of relative depths.

```
C       BAKER  &  KONDNER'S   THEORY
        MASTER ATHENA
        DIMENSION DI(5),D(5),RD(14),H(5,14),FORCE(5,14)
        B=2.54*4.0
        NR=5
        NRD=14
        READ(1,1)(DI(I),I=1,NP)
      1 FORMAT(5F5.2)
        READ(1,2)(RD(J),J=1,NRD)
      2 FORMAT(14F5.1)
        DO 9 I=1,NP
      9 D(I)=2.54*DI(I)
        DO 11 J=1,NP
        DO 11 I=1,NRD
        H(J,I)=RD(I)*D(J)
        X=(D(J)*B*1.7*9.807)/1000.0
        FORCE(J,I)=X*(-150.0*D(J)+(400.0*H(J,I)/9.0))
     11 CONTINUE
        WRITE(2,99)
     99 FORMAT(1H1//////////)
        WRITE(2,100)
    100 FORMAT(27X,3HH/D,47X,8HFORCE(N)/)
        WRITE(2,101)
    101 FORMAT(47X,8HD=12.7MM,7X,8HD=19.0MM,7X,8HD=25.4MM,7X,8HD=38.1MM,
       *7X,8HD=50.4MM/)
        DO 12 J=1,NRD
        WRITE(2,102)RD(J),(FORCE(I,J),I=1,NP)
    102 FORMAT(20X,F10.1,10X,5F15.3)
     12 CONTINUE
        STOP
        END
        FINISH
```

H/D	FORCE(N)				
	D=12.7MM	D=19.0MM	D=25.4MM	D=38.1MM	D=50.4MM
9.0	63.501	153.677	275.203	614.708	1092.814
10.0	80.443	180.997	321.775	723.989	1287.092
11.0	92.586	208.318	370.343	833.271	1481.370
12.0	104.723	235.638	418.912	942.552	1675.648
14.0	129.013	290.279	516.051	1161.115	2064.204
16.0	153.298	344.919	615.190	1379.678	2452.760
20.0	201.867	454.201	807.468	1816.803	3229.872
24.0	250.457	563.482	1001.746	2253.929	4006.985
28.0	299.006	672.764	1196.024	2691.054	4784.097
32.0	347.576	782.045	1390.302	3128.180	5561.209
36.0	396.145	891.326	1584.580	3565.306	6338.321
40.0	444.715	1000.606	1778.858	4002.431	7115.433
46.0	517.569	1164.530	2070.275	4658.120	8281.101
50.0	566.153	1275.811	2264.553	5095.245	9058.214

```
C       MEYERHOF  &  ADAM'S   THEORY
        MASTER ATHENA
        DIMENSION DI(5),D(5),RD(14),VOL(5),WEI(5),H1(5),H(5,14),FORCE(5,14
       *),R1(5),R2(5)
        PI=3.14
        FII=43.2
        FI=(FII*PI)/180.0
        NR=5
        RDA=9.0
        SKU=5.65
        NRD=14
        READ(1,1)(DI(I),I=1,NP)
      1 FORMAT(5F5.2)
        DO 9 I=1,NP
      9 D(I)=2.54*DI(I)
        READ(1,2)(RD(J),J=1,NRD)
      2 FORMAT(14F5.1)
        DO 10 I=1,NP
        DO 10 J=1,NRD
        R1(I)=D(I)/2.0
        H(I,J)=RD(J)*D(I)
        H1(I)=RDA*D(I)
        R2(I)=R1(I)+H1(I)*TAN(FI/3.0)
        VOL(I)=(PI*H1(I)*(R2(I)*R2(I)+R2(I)*R1(I)+R1(I)*R1(I)))/3.0
        WEI(I)=(VOL(I)*1.7*9.07)/1000.0
        CONST=(SKU*PI*1.7*9.807*TAN(FI))/2000.0
        FORCE(I,J)=CONST*D(I)*(2.0*H(I,J)-H1(I))*H1(I)+WEI(I)
     10 CONTINUE
        WRITE(2,99)
     99 FORMAT(1H1//////////)
        WRITE(2,100)
    100 FORMAT(17X,3HH/D,52X,6HFORCE(N)/)
        WRITE(2,101)
    101 FORMAT(37X,8HD=12.7MM,7X,8HD=19.0MM,7X,8HD=25.4MM,7X,8HD=38.1MM,
       *7X,8HD=50.4MM/)
        DO 11 J=1,NRD
```

```
      WRITE(2,102)RD(J),(FORCE(I,J),I=1,NP)
  102 FORMAT(10X,F10.1,20X,5F15.3)
   11 CONTINUE
      STOP
      END
      FINISH
```

H/D	FORCE(N)				
	D=12.7mm	D=19.0mm	D=25.4mm	D=38.1mm	D=50.4mm
9.0	25.784	87.021	206.272	696.167	1650.173
10.0	30.882	104.228	247.059	833.825	1976.474
11.0	35.981	121.435	287.847	971.483	2302.775
12.0	41.079	138.643	328.635	1109.142	2629.076
14.0	51.276	173.057	410.210	1384.458	3281.679
16.0	61.473	207.472	491.785	1659.775	3934.281
20.0	81.867	276.301	654.936	2210.408	5239.486
24.0	102.261	345.130	818.086	2761.041	6544.690
28.0	122.655	413.959	981.237	3311.674	7849.895
32.0	143.048	482.788	1144.387	3862.308	9155.100
36.0	163.442	551.618	1307.538	4412.941	10460.304
40.0	183.836	620.447	1470.689	4963.574	11765.509
46.0	214.427	723.690	1715.414	5789.524	13723.316
50.0	234.821	792.520	1878.565	6340.157	15028.520

```
      VESIC'S THEORY
      MASTER ATHENA
      DIMENSION DI(5),D(5),RD(14),AREA(5),H(5,14),FV1(5,14),FV2(5,14)
      PI=3.14
      NP=5
      NRD=14
      DS=(2.54*3.0)/16.0
      FQ1=13.27
      FQ2=15.70
      READ(1,1)(DI(I),I=1,NP)
    1 FORMAT(5F5.2)
      READ(1,2)(RD(J),J=1,NRD)
    2 FORMAT(14F5.1)
      DO 9 I=1,NP
    9 D(I)=2.54*DI(I)
      DO 11 I=1,NP
   11 AREA(I)=(PI*(D(I)*D(I)-DS*DS))/4.0
      DO 12 J=1,NP
      DO 12 I=1,NRD
      H(J,I)=RD(I)*D(J)
      OVP=(H(J,I)*1.7*9.807)/1000.0
      FV1(J,I)=AREA(J)*OVP*(FQ1+(D(J)/(3.0*2.0*H(J,I))))
      FV2(J,I)=AREA(J)*OVP*(FQ2+(D(J)/(3.0*2.0*H(J,I))))
   12 CONTINUE
      WRITE(2,99)
   99 FORMAT(////////////64X,8HFORCE(N)/)
      WRITE(2,100)
  100 FORMAT(17X,3HH/D,14X,3HFV1,4X,3HFV2,5X,3HFV1,4X,3HFV2,5X,3HFV1,
     *4X,3HFV2,5X,3HFV1,4X,3HFV2,5X,3HFV1,4X,3HFV2)
      WRITE(2,101)
  101 FORMAT(/35X,9HD= 12.7MM,6X,9HD= 19.0MM,6X,9HD= 25.0MM,6X,9HD= 38.0
```

```
   *MM,6X,9HD= 51.0MM/)
    DO 13 J=1,NRD
    WRITE(2,102)RD(J),(FV1(I,J),FV2(I,J),I=1,NP)
102 FORMAT(10X,F10.1,10X,5(2F7.1,1X))
 13 CONTINUE
    STOP
    END
    FINISH
```

	FORCE(N)									
H/D	FV1	FV2	FV1	FV2	FV1	FV2	FV1	FV2	FV1	FV2
	D= 12.7MM		D= 19.0MM		D= 25.0MM		D= 38.0MM		D= 51.0MM	
9.0	2.8	3.3	10.1	12.0	24.7	29.3	85.2	100.8	203.4	240.6
10.0	3.1	3.6	11.3	13.3	27.5	32.5	94.7	112.0	226.0	267.3
11.0	3.4	4.0	12.4	14.7	30.2	35.8	104.1	123.2	248.5	294.0
12.0	3.7	4.3	13.5	16.0	33.0	39.0	113.6	134.4	271.1	320.7
14.0	4.3	5.1	15.8	18.7	38.5	45.5	132.5	156.7	316.2	374.1
16.0	4.9	5.8	18.0	21.3	44.0	52.0	151.4	179.1	361.4	427.5
20.0	6.1	7.2	22.5	26.6	55.0	65.0	189.2	223.8	451.6	534.3
24.0	7.3	8.7	27.0	32.0	65.9	78.0	227.0	268.6	541.9	641.1
28.0	8.6	10.1	31.5	37.3	76.9	91.0	264.9	313.3	632.2	747.9
32.0	9.8	11.6	36.0	42.6	87.9	104.0	302.7	358.1	722.4	854.7
36.0	11.0	13.0	40.5	48.0	98.9	117.0	340.5	402.8	812.7	961.5
40.0	12.2	14.5	45.0	55.3	109.9	130.0	378.3	447.6	903.0	1068.3
46.0	14.1	16.6	51.8	61.3	126.3	149.5	435.0	514.7	1038.4	1228.5
50.0	15.3	18.1	56.3	66.6	137.3	162.5	472.9	559.4	1128.7	1335.3

APPENDIX M

TRIAXIAL TESTS

Triaxial tests were performed in order to determine whether the sample has cohesion. Table M.1 shows the various values of ϕ, obtained using different conditions of sand, i.e. different densities. The shear stress was plotted against the normal stress for the sand with γ = 1.60 gr/cm^3, see Fig. M.1. The figure shows that the sand has no cohesion. The angle of internal friction, ϕ, was plotted against density, γ, see Fig. M.2. The figure shows that the rate of increase of ϕ with γ increases.

TABLE M.1

No.	Cell Pressure (lb/in^2)	$(\sigma_1' - \sigma_3')/2$ (lb/in^2)	$(\sigma_1' + \sigma_3')/2$ (lb/in^2)	ϕ	ε_f (%)	γ (gr/cm^3)
1	25	44.44	69.44	39.8°	6.5	1.64
2	25	46.26	71.27	40.5°	6.0	1.67
3	25	35.13	60.13	35.7°	8.1	1.58
4	10	14.26	24.27	36.0°	10.0	1.58
5	25	53.13	78.15	42.9°	5.5	1.70
6	10	21.10	31.10	42.8°	4.3	1.69

Fig. M.1 Shear stress V Normal stress

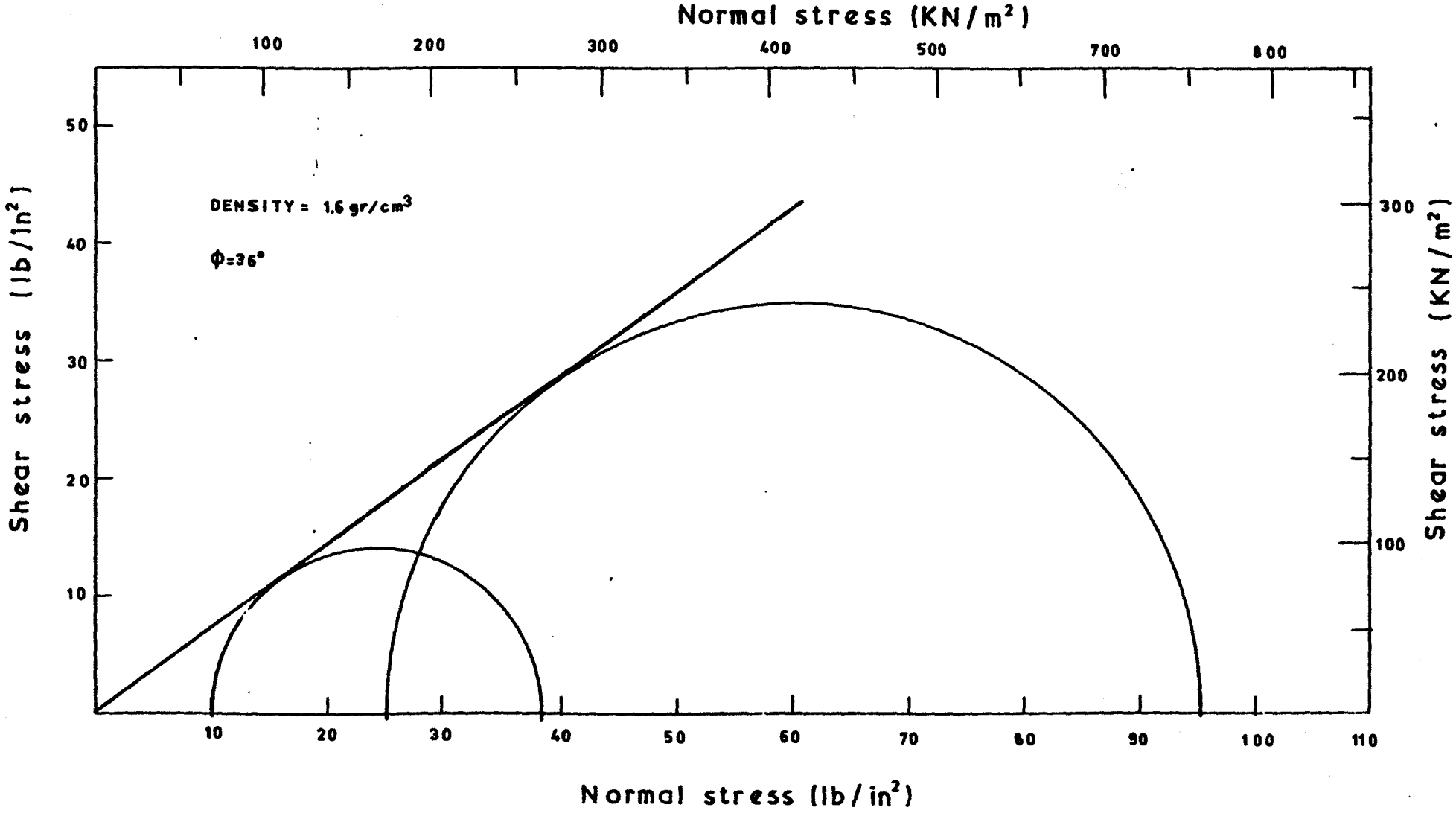

Fig. M.2 Angle of internal friction V Density

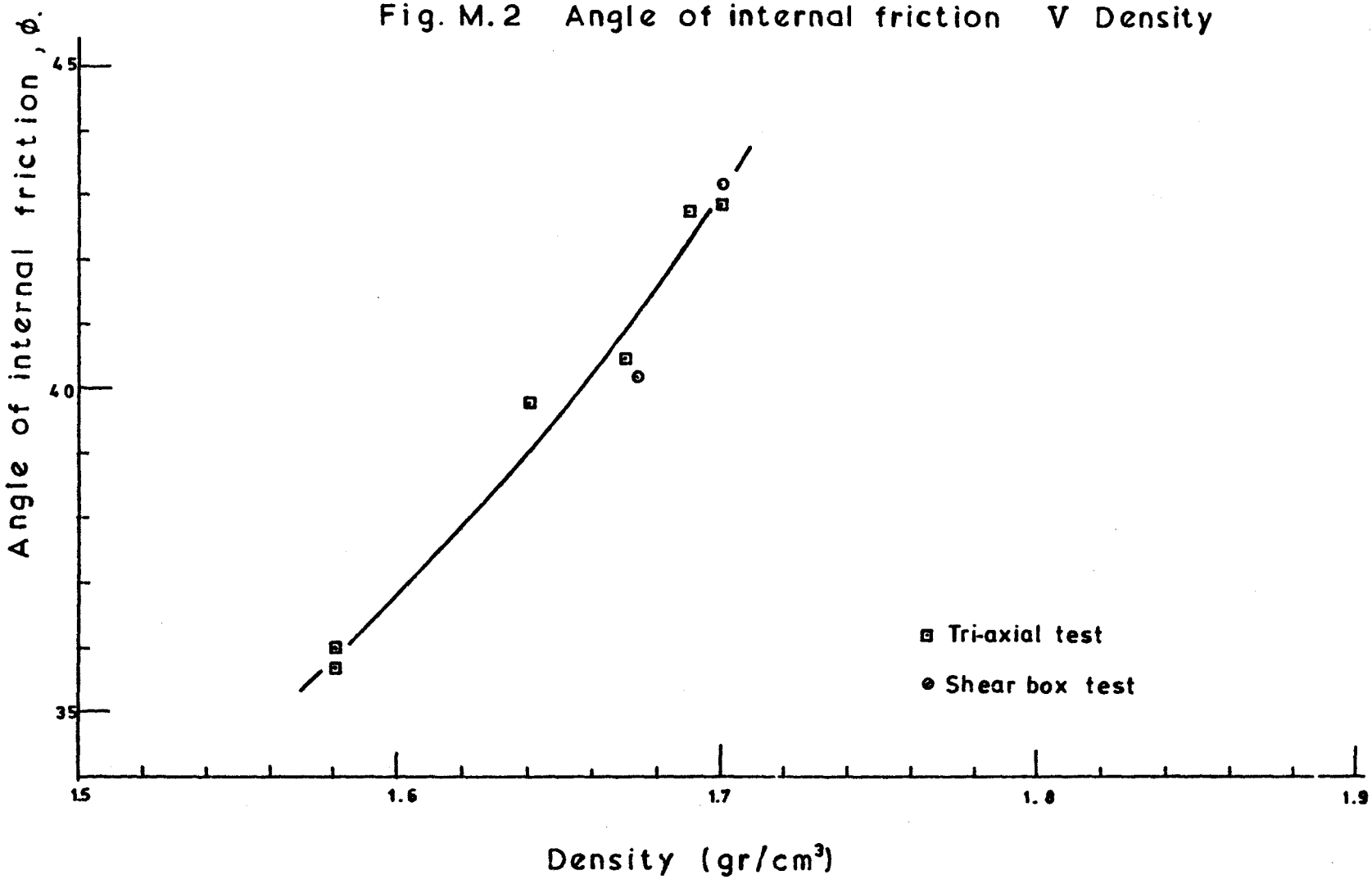

REFERENCES

1. KOLBUSZWESKII, J.J., (1948). An experimental study of the maximum and minimum porosities of sands. 2nd Int. Conf. on Soil Mech. and Fdn. Eng., Rotterdam, 1948, Vol. 1, p.158. - General investigation of the fundamental factors controlling the loose packing of sands. 2nd Int. Conf. on Soil Mech. and Fdn. Eng., Rotterdam, 1948, Vol. VII, pp.47-49.

2. KOLBUSZWESKII, J.J. and JONES, R.H. (1961). The preparation of sand samples for laboratory testing, Proc. of Midlands Soil Mech. Soc., Vol. 4, 1961, pp.107-123.

3. GISBOURNE, R., (1970). The penetration resistance of sands. Ph.D. Thesis, University of Aston, 1970.

4. WALKER, B.P. and WHITAKER, T., (1967). An apparatus for forming uniform beds of sand for model foundation tests. Geotechnique 17, 1967, pp.161-167.

5. JAMES, J.P., (1967). Stress displacement relationship for sand subjected to passive pressure. Ph.D. Thesis, University of Manchester, 1967.

6. BUTTERFIELD, R. and ADRAWES, K.Z., (1970). An air activated sand spreader for forming uniform beds of sand. Geotechnique 20, 1970, pp.97-100.

7. HOWAT, M.D., (1969). The behaviour of earth anchorages in sand. M.Sc. Thesis, University of Bristol.

8. FEDA, J., (1961). Research on the bearing capacity of loose soil. Proc. of 5th Int. Conf. on Soil Mech. and Fdn. Eng., Paris, 1961, Vol. 1, pp.635-642.

9. MOGAMI, T. and KUBO, K., (1953). Behaviour of soil during vibration. Proc. 3rd Int. Conf. on soil Mech. and Fdn. Eng., 1953, Vol. 1, pp.152-155.

10. ALYANAK, J., (1961). Vibration of sand with reference to the minimum Porosity Test. Proc. of Midlands Soil Mech. and Fdn. Eng. Soc., Vol. 4, pp.37-72.

11. SELIG, E.T., (1963). Effect of vibration on density of sand. Proc. 2nd Pan American Conf. on Soil Mech. and Fdn. Eng., Brazil 1963, Vol. 1, pp.129-144.

12. KOLBUSZEWSKII, J.J., (1948). General investigation of the fundamental factors controlling the loose packing of sands. 2nd Int. Conf. on Soil Mech. and Fdn. Eng., Rotterdam, 1948, Vol. 1, p.158.

13. LINGER, D.A., (1963). Effect of vibration on soil properties. Highway Research Record, No. 21, 1963 p.10.

14. YOUD, T.L., (1970). Densification and shear of sand during vibration. Journal of A.S.C.E. Soil Mech. Div., Vol. 96, SM3, pp.363-379.

15. ADAMS, J.I. and HAYES, D.C., (1967). The uplift capacity of shallow foundations. Ontario Hydro Research Quarterly, Vol. 19, No. 1, pp.1-13.

16. ADAMS, J.I., (1969). Grouted anchor transmission tower footings. Ontario Hydro Research Quarterly, Vol.21, No. 3, pp.1-7.

17. MULLER, A.G. and HAEFELI, R., (1953). Tension anchoring in the ground with special reference to foundation problems of overhead lines. Bulletin des Schweizer-cshen Elektrotechnischen Verems, No. 21, p.905.

18. SUTHERLAND, H.B., (1965). Model Studies for shaft raising through cohesionless soils. Proc. of the 6th Int. Conf. on Soil Mech. and Fdn. Eng., Vol. II, pp.410-413.

19. MARIUPL'SKII, L.G., (1965). The bearing capacity of anchor foundations. Osnovaniya, Fundamenty: Mekhanika Gruntor No. 1, 1965.

20. BAKER, W.H. and KONDNER, R.L., (1966). Pullout load capacity of a circular earth anchor buried in sand. Highway Research Record, No. 108, pp.1-10.

21. CRIVELLI, I., (1969). Prestressed VSL Rock and Alluvium Anchors. Brochure, Losinger & Co. SA, Berne, Switzerland - Advances in anchoring. Construction News, October 23, pp.15-17.

22. PRICE, D.J., (1970). Rock bolting systems and their applications. The Consulting Engineer, May, pp.17-23.

23. CARR, R.W., (1970). An experimental investigation of plate anchors in sand. Ph.D. Thesis, University of Sheffield.

24. McMULLAN, D.J., (1975). The behaviour of inclined ground anchors in sand, both singly and in groups. Ph.D. Thesis, University of Bristol, 1975.

25. PARRY-DAVIES, R., (1967). Use of rock anchors in deep excavations. Symp. on Deep Basements, Johannesburg, pp. 23-33.

26. TROFIMENKOV, J.G. and MARIUPOL'SKII, L.G., (1964). Screw piles used for mast and tower foundations. Osnovaniya, Fundamenty Mekhanika Gruntor No. 4, 1964.

27. MORS, H. (1959). Das Verhalten von Mastgrundungen bei Zugbeanspruchung. Die Bautechnik Vol. 10, 1959.

28. MATSUO, M., (1967, 1968). Study on the uplift resistance of footings. Soils and Foundations, Vol. VII, No. 4, pp.18-43 and Vol. VIII, No. 1, pp.1-33.

29. HEALY, K.A., (1971). Pullout resistance of anchors buried in sand. A.S.C.E. Soil Mech. Div., Vol.97, SMII, 1971.

30. GOTRILL, A., (1969). Ground anchoring techniques extended to London Clay, Construction News, March 13, pp.18-19.

31. MEYERHOF, G.G. and Adams, J.I., (1968). The ultimate capacity of foundations. Canadian Geotechnical Journal, Vol. 5, No. 4, pp.225-244.

32. YILMAZ, M., (1971). The behaviour of group anchors in sand. Ph.D. Thesis, University of Sheffield, 1971.

33. ANDERSON, J.K. et al, (1965). The Forth Road Bridge. Published as a separate by Inst. Civil Eng.

34. ADAMS, J. and KLYM, T.W., (1972). A study of anchorages for transmission tower foundation. Canadian Geotechnical Journal, Vol. 9, 1972, pp.89-104.

35. BAUER, K., (1965). The injection Bauer Anchor System. Civil Eng. Journal, Zurich No. 47, November 19, pp.1265-1273.

36. POLAND, G.G., (1960). Anchoring a tunnel in sand. Civil Engineering (A.S.C.E.), March 1960, pp.59-61.

37. JYOEV, L.N., (1956). Experimentalance issledovania ankernych Kreplenui. Gidrotechnitsheskoe Stroitelstro 9.

38. DORR, H., (1924). The bearing capacity of piles. Bautechnik, No. 7.

39. KILLER, J., (1953). Fondations economiques des pylones de lignes Aeriennes. Proc. of the 3rd Int. Conf. on Soil Mech. and Fdn. Eng., Vol. III, pp.265-276.

40. BALLA, A., (1961). The resistance to breaking out of mushroom foundations for pylons. Proc. 5th Int. Conf. on Soil Mech. and Fdn. Eng., Vol. 1, 1961, pp.569-576.

41. TURNER, E.A., (1962). Uplift resistance of transmission tower footings. Journal of the Power Division, Proc. A.S.C.E., Vol. 88 No. PO2.

42. EL-RAYES, M.K., (1965). Behaviour of cohesionless soils under uplift forces. Ph.D. Thesis, University of Glasgow.

43. VESIC, A.S., (1972). Expansion of cavities in infinite soil mass. A.S.C.E., Soil Mech. and Fdn. Division, March 1972.

44. DIAZ, R.F., (1967). Pullout resistance of deeply buried anchors in sand. M.Sc. Thesis, Duke University, Durham, North Carolina.

45. ASHBEE, R.A., (1969). A uniaxial analysis for the use in uplift foundation calculation. Central Electricity Research Laboratories, Lab. Note No. RD/L/R1608.

46. LARNACH, W.J., (1972). The pullout resistance of inclined anchors installed singly and in groups in sand. Ground Engineering, Vol. 5, No. 4, 1972, pp.14-17.

47. HANNA, T.H., (1970). Land anchorage systems. Symposium at MEXE, April 1970.

48. BEMBEN, S.M. and KUPFERMAN, (1969). The vertical holding capacity of marine anchor flukes subjected to static and cyclic loading. Offshore Technology Conference, Houston, TX, Vol. 1, Paper No. 2185, May 1975, pp.363-374.

49. BRIGGS A., (1960). Strutted sheet piles excavations in cohesionless material. M.Sc. Thesis University of Manchester, England, 1960.

50. DURELLI, A.J. and RILEY, W.F., (1961). Performance of embedded pressure gauges under static and dynamic loadings. Symposium on Soil Dynamics, ASTM, 64th Annual Meeting, June 1961.

51. DANIEL, W.T., (1957). Stress-strain characteristics of granular material, Engineering, July 12, 1957.

52. EDWARDS, D. (1974). Part III project at Queen Mary College, University of London.

53. DANIEL, W.T., HARVEY, R.C. and BURLEY, E., (1975). Non-linear characteristics of engineering soils. Journal of Materials Science 10, 1975, pp.1616-1625.

54. HARVEY, R.C. and BURLEY, E., (1975). On the behaviour and expendiency of ground anchors. Civil Eng. February 1975.

55. DANIEL, W.T., HARVEY, R.C. and BURLEY, E., (1976). Stress-strain characteristics of particulate material under the condition of no lateral strain. Journal of Materials Science 11, 1976, pp.689-695.

56. HARVEY, R.C. and BURLEY, E., (1973). The behaviour of inclined anchors in cohesionless sand. Ground Eng., Sept. 1973, Vol. 6, No. 3, pp.48-55.

57. HARVEY, R.C., BURLEY, E. and DANIEL, W.T., (1974). Cavitation in semi-infinite granular media. Civil Engineering, No. 812, March 1974, pp.52-55.

58. BURLEY, E., HARVEY, R.G. and DANIEL, A.W.T., (1974). Axial stress-strain characteristics of sand. Proc. Paper 10504, Proc. A.S.C.E., Journal of Geotechnical Eng. Division, May 1974.

59. KANAYAN, A.S., (1966). Experimental investigation of the stability of bases of anchor foundations. Osnovaniya, Fundamenty i Mekhanika Gruntor No. 1, 1965.

60. NATH B., (1974). Fundamentals of Finite Elements for Engineers. The Athlone Press of the University of London, 1974.

61. LARNACH, W.J., (1973). The behaviour of grouped inclined anchors in sand. Ground Engineering, Vol.61, No.6 1973 pp.34-38.

62. ROSCOE, K.H., (1968). Soil and model tests. Journal of Strain Analysis, Vol. 3, No. 1, pp.57-64.

63. SIMITH, G.N., (1971). An Introduction to Matrix and Finite Element Methods in Civil Engineering. Applied Science Publishers Ltd., London, 1971.

64. GIRIJAVALLABHAN, C.V,, and REECE, L.G., (1968). Finite-element method for problems in soil mechanics. Journal of Soil Mech. and Fdn. Div., Proc. A.S.C.E., Vol. 94, No. SM2, pp.473-495.

65. LITTLEJOHN, G.S., (1970). Soil Anchors. Ground Engineering, Proceedings of Conference, I.C.E, 1970, pp.33-44.

66. LITTLEJOHN, G.S., (1968). Recent developments in ground anchor construction. Ground Engineering, Vol. I, No. 3, May 1968, pp.32-36.

67. LITTLEJOHN, G.S., (1970). Anchorages in Soils - Some Empirical Design Rules. Supplement on Ground Anchors. The Consulting Engineer, May 1970.

68. LITTLEJOHN, G.S., (1973). Ground Anchors Today - A Forward. Ground Engineering, 6 (6), 1973, pp.20-23.

69. HANNA, T.H., SPARKS, R. and YILMAZ, M., (1972). Anchor behaviour in sand. Journal of Soil Mech. and Fdn. Div., Proc. A.S.C.E., Vol. 98, No. SM11, November, 1972.

70. KALAJIAN, E.H., (1971). The vertical holding capacity of marine anchors in sand, subjected to cyclic and static loading. Ph.D. Thesis, University of Massachusetts (1971).